THE EXPLORATION OF LEWIS ACIDITY AND FLUOROPHILICITY OF GERMANIUM COMPOUNDS AND THEIR APPLICATIONS IN C-F BOND ACTIVATION

By

ARDALAN HAYATIFAR

Bachelor of Science in Chemistry.
Shahid Beheshti University
Tehran, Iran
2013

Master of Science in Nanochemistry.
Iran University of Science and Technology
Tehran, Iran
2015

Submitted to the Faculty of the
Graduate College of
Oklahoma State University
in partial fulfillment of
the requirements for
the Degree of
DOCTOR OF PHILOSOPHY
July, 2021

THE EXPLORATION OF LEWIS ACIDITY AND FLUOROPHILICITY OF GERMANIUM COMPOUNDS AND THEIR APPLICATIONS IN C-F BOND ACTIVATION

Dissertation Approved:

Dr. Charles S. Weinert

Dissertation Advisor

Dr. Allen W. Apblett

Dr. Richard A. Bunce

Dr. Christopher J. Fennell

Dr. Natascha Riedinger

ACKNOWLEDGMENTS

This journey would not have been possible without the friends and mentors in the US and Iran. I thank all the people who made it possible for me to finish my doctoral studies.

I would like to thank my advisor, Prof. C. S. Weinert for providing an environment for research full of support, professionalism, trust, and freedom. I cannot imagine a better mentorship, and I owe my growth as a chemist to you. Your passion for Chemistry and your devotion to teaching and service to the community as a scientist/teacher are inspirational for me.

I thank my committee members for providing support and advice during my years at OSU. I would like to especially thank Dr. C. J. Fennell for guidance in computational Chemistry and helping with calculations in Chapter IV of this dissertation.

I love to thank all my lab members and undergraduate research assistants. Dr. Floyd Shumaker, thanks for being a mentor, role model, and brother from day one. In hard times, you kept reminding me that *tomorrow the birds will sing*, and you always believed in me. You have taught me many lessons in the lab and life. Probably the most important one is to always look *inside*. Miguel Leal, thanks for being a loyal brother in happy and sad moments. Without your patience and kindness, these whole years would not have been tolerable. Dr. Sangeetha Komanduri, thank you for setting an example of hard work and the courage to pursue dreams.

Acknowledgments reflect the views of the author and are not endorsed by committee members or Oklahoma State University.

Thanks to our new lab members, Thad Stancil and Vanessa Fortney, the undergraduate research colleagues: Emily Elifritz, Molly Bloom, and Kaitlyn Pixley.

I would like to thank the OSU Chemistry department: Dr. A. Iob for his support and guidance in teaching, Mr. Ed Wright, the NMR staff, and Dr. Jacobs.

My dear friend Dr. Jon Day, I am so thankful for you. I enjoyed our discussions and I have always learned so much from your wisdom and intelligence.

I love to thank my families far from home: Dear Andersons, Jim, Gaye, David, Cindy, and Carol, and Bud Blossom. I am so thankful for all your love and support. Eric Brinkman, my first friend in the US who taught me what it means to be a man and how "the heart of man plans his way...". Thanks for being a brother and a very dear friend. I love to thank Tim and Valerie Brinkman for loving me like their son and grandpa Peter and grandma Priscilla Lovell for supporting and loving me like a grandkid.

My dear old friends in Iran: Sina Khodabandelou and Mahrad Rahimi, thanks for being with me and staying with me, and inspiring me at every step of this journey. Faramarz Moattar, I am forever thankful for your friendship and your wisdom, and your kind words.

I would love to thank my family. My mom and dad, Ardeshir and Fereshteh Hayatifar, I love you, and I owe everything to you. It is an honor for me to be your son. Baba, I am finishing what you started. Maman thanks for trusting me and investing all your life in me lovingly and sacrificially. My dear brother Amirhossein, you have always been there for me and tolerated me with love. My in-laws, Hadi, Mansoureh, and Soroush Aghakhaninejad for loving me like their new son.

Finally, I would like to thank my dear wife, Sarah. I am so honored that the universe gave you to me as a gift. Love you!

Acknowledgments reflect the views of the author and are not endorsed by committee members or Oklahoma State University.

To Sarah

Name: ARDALAN HAYATIFAR

Date of Degree: JULY, 2021

Title of Study: THE EXPLORATION OF LEWIS ACIDITY AND FLUOROPHILICITY OF GERMANIUM COMPOUNDS AND THEIR APPLICATIONS IN C-F BOND ACTIVATION

Major Field: CHEMISTRY

Abstract: The elusive branched fluoro-oligogermane $(Ph_3Ge)_3GeF$ which is the only crystallographically characterized Ge-F containing compound with unsupported Ge-Ge bonds, was successfully synthesized and its chemical/electrochemical properties studied by NMR, UV-Vis spectroscopy, CV, DPV, and DFT calculations. The key to access $(Ph_3Ge)_3GeF$ is the germylium intermediate $(Ph_3Ge)_3Ge^+$ that is a strong Lewis acid and is able to activate the C−X bond in CH_2X_2 (X=Cl, Br, I).

The potential of germyliums as Lewis acids is explored in hydrodefluorination reactions. In a transition-metal-free approach, the germylium $[Ph_3Ge]^+$ generated from Ph_3GeH and a catalytic amount of $[Ph_3C][B(C_6F_5)_4]$ is able to convert aryl and aliphatic acid fluorides directly to their corresponding aldehydes without decarbonylation. The catalyst is also capable of performing the hydrodefluorination of aliphatic organofluorines.

In the early attempts at C−F amination of organofluorines, it was observed that germanium amides Ph_3GeNR_2 exhibit a frustrated-Lewis pair-type reactivity. However, when germanium amides Ph_3GeNR_2 (R=TMS, Me, ^{i}Pr) are reacted with acyl fluorides, it results in the direct amidation reactions to form important tertiary amides. Experimental and computational studies suggest a σ-bond metathesis pathway for this reaction.

TABLE OF CONTENTS

Chapter Page

LIST OF TABLES

Table Page

LIST OF FIGURES

Figure Page

Figure Page

Figure Page

Figure Page

Figure Page

LIST OF SCHEMES

Scheme Page

Scheme Page

ABBREVIATIONS

ACS	American Chemical Society
AIBN	Azobisisobutyronitrile
BCF	Tris(pentafluorophenyl)borane $B(C_6F_5)_3$
BDE	Bond Dissociation Energy
bpy	2,2′-Bipyridine
BSA	Bis(trimethylsilyl)acetamide
Bu	Butyl
CDC	Centers for Disease Control and Prevention
CV	Cyclic Voltammetry
Cy	Cyclohexyl
DCC	Dicyclohexylcarbodiimide
DFT	Density Functional Theory
DPV	Differential Pulse Voltammetry
EPR	Electron Paramagnetic Resonance
Et	Ethyl
FIA	Fluoride Ion Affinity
FLP	Frustrated Lewis Pair
GC-MS	Gas Chromatography-Mass Spectrometry
HDF	Hydrodefluorination
HFIP	Hexafluoroisopropanol
hfcc	Hyperfine Coupling Constant
HMPT	Hexamethylphosphoramide

HOMO	Highest Occupied Molecular Orbital
HRAM-MS	High Resolution Accurate Mass Spectrometry
^{i}Pr	*iso*-propyl
IRC	Intrinsic Reaction Coordinate
LUMO	Lowest Unoccupied Molecular Orbital
Me	Methyl
Mes	Mesityl
NBO	Natural Bond Orbital
^{n}Bu	n-Butyl
NMR	Nuclear Magnetic Resonance
NTf	Triflimide
ORTEP	Oak Ridge Thermal-Ellipsoid Plot
PFAS	Per- or Poly- Fluorinated Alkanes
PFOS	Per-Fluoro-Octane Sulfonate
Ph	Phenyl
phen	1,10-Phenanthroline
SOMO	Singly Occupied Molecular Orbital
TASF	Tris(dimethylamino)sulfonium Difluorotrimethylsilicate
TBAF	Tetrabutylammonium Fluoride
TDDFT	Time-Dependent Density Functional Theory
THF	Tetrahydrofuran
TMS	Trimethylsilyl
TPFC	Tris(pentafluorophenyl)-corrole
trip	2,4,6-Triisopropylphenyl
UV	Ultra Violet
WBI	Wiberg Bond Indices
WCA	Weakly Coordinating Anion

NOMENCLATURE

SYMBOLS	**UNITS/VALUE**	**DESCRIPTION**
λ_{max}	nm, Å	Absorbance maxima
ϵ	$Lmol^{-1}\,cm^{-1}$	Molar absorptivity
ω	degrees °	Dihedral Angle
$\Delta\nu_{1/2}$	Hertz	Half width at half maximum for a peak
I	-	Nuclear Spin
^{1}H	-	Hydrogen Isotope for Proton NMR
$\{^{1}H\}$	-	Proton Decoupled
^{11}B	-	Isotope for Boron NMR
^{13}C	-	Isotope for Carbon NMR
^{19}F	-	Isotope for Fluorine NMR
BDE	$kcal.mol^{-1}$	Bond Dissociation Energy
a	mT	Hyperfine Coupling Constant
g	2.00232	Proportionality Factor
ee	%	Enantiomeric Excess

CHAPTER I

Introduction

1.1 Introduction - Germanium

Main-group elements are the elements in the periodic table that fill their s and p shells to fulfill their electron configurations. The elements in the s block are metals and their chemistry is consistent with ionic models and the elements in the p block mostly form covalent compounds.

Germanium was initially predicted 1871 by Mendeleev as "eka-silicon". Germanium is named in honor of Germany by C. A. Winkler who discovered it in 1886 while analyzing the mineral argyrodite Ag_8GeS_6.[1] Germanium is a metalloid and forms gray-white brittle crystals.

Table 1.1 summarizes some properties of germanium in group 14. Going down the group, both the covalent and metallic radius increase. Along with the decrease in the first ionization energy from C. to Pb, the metallic character of the elements increases down the group. In the solids of the elements in group 14, the band gap decreases down the group. The band gap is the distance between the valence band consisting of filled sp^3 orbitals, and the conduction band that is formed by the anti-bonding sp^3 orbitals.[2,3]

Table 1.1: Properties of group 14 elements

Element	C	Si	Ge	Sn	Pb
First ionization energy ($kJ.mol^{-1}$)	1090	786	762	707	716
Band gap (eV)	6.0	1.10	0.67	0.08	0

Catenation is the ability to form element-element bonds and group 14 is the most important group for elements with this ability. While carbon is probably the best catenator among all elements, as shown in Table 1.2, the element-element bond energy decreases going down the group. As a result, the tendency to form bonds decreases from carbon to lead.[2]

Table 1.2: Element-element bond energies in group 14 ($kJ.mol^{-1}$)

C–C	Si–Si	Ge–Ge	Sn–Sn	Pb–Pb
348	326	186	150	87

Unlike hydrocarbons that can form a variety of structures with different chain lengths and ring sizes, the longest hydrosilane only contains seven silicon atoms with the formula of Si_7H_{16}. The longest fully-characterized oligogermane was synthesized by the hydrogermolysis reaction and is the hexagermane $^{i}Pr_3Ge(GePh_2)_4Ge^{i}Pr_3$.[4]

In Table 1.3 it is shown that the element-O and element-F bond energies decrease down group 14 indicating that while Si and C are oxo- and fluoro-philic, Ge, Sn, and Pb have a *soft* character.

Table 1.3: Element-O/F bond energies in group 14 ($kJ.mol^{-1}$)

C–O	Si–O	Ge–O	C–F	Si–F	Ge–F
360	466	350	486	584	466

The element-O bond energy is consistent with the high reactivity of silanes with water and their violent hydrolysis, because the Si–O bond is stronger than Si–Si and Si–H bonds. Element-H bonds unlike those in hydrocarbons are a functional group in the heavier elements of group 14. Table 1.4 summarizes the element-hydrogen bond energies in group 14.[2]

Germanium can adopt the +2 and +4 oxidation states. There are five isotopes of germanium ^{70}Ge, ^{72}Ge, ^{73}Ge, ^{74}Ge, and ^{76}Ge with relative abundances of 21.2, 27.7, 7.7, 35.9 and 7.5% respectively.[5] The only NMR-active isotope is ^{73}Ge with the spin

Table 1.4: Element-H bond energies in group 14 ($kJ.mol^{-1}$)

C–H	Si–H	Ge–H	Sn–H	Pb–H
412	318	288	250	<157

of 9/2 and the receptivity of 0.617 relative to ^{13}C. The high quadrupole moment of this isotope results in broad signals in its NMR spectra.[6]

Organogermanium compounds can be accessed using different synthetic methods. The first organogermanium compound was synthesized by Winkler in 1886 by alkylating a Ge halide $GeBr_4$ using Et_2Zn to yield tetra-alkyl Et_4Ge. Other methods include using Grignard reagents, organolithium reagents, direct synthesis using alkyl halides and germanium in the presence of a copper catalyst at 300 °C, and the addition of germanium hydrides to carbon-carbon multiple bonds.[7]

1.1.1 Oligogermanes

Germanium catenates, also known as oligogermanes, are heavier analogues of hydrocarbons. The first oligogermane $Ph_3GeGePh_3$ was synthesized by the reductive coupling of Ph_3GeBr using sodium and was reported in 1925.[8] Scheme 1.1 shows several routes for Ge–Ge bond formation. The reaction of Grignard reagents with germanium halides can form *per*-phenylated chains.[9] Several tri- and tetra-germanes were prepared by reacting organo-alkaline metal (Li, Na, K) germanium compounds and germanium halides.[10–12]

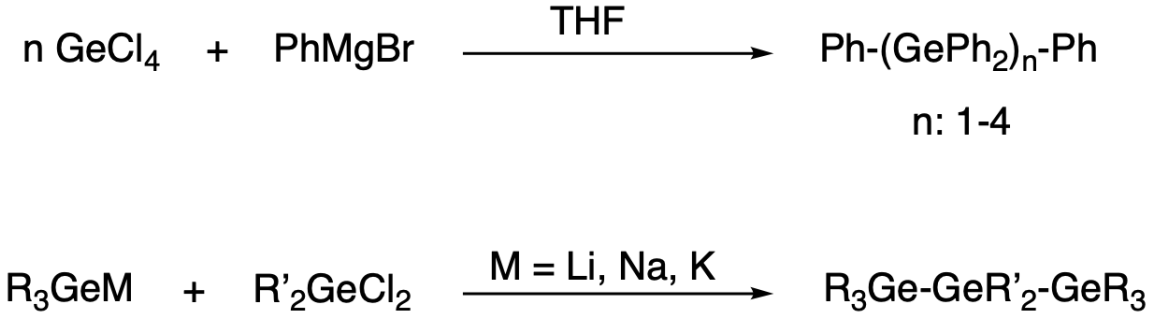

Scheme 1.1: Classic approaches to Ge–Ge bond formation

While the aforementioned methods are synthetically useful, they suffer from low selectivities, often have low yields, and require the handling of very reactive reagents. A cleaner approach to oligogermanes is by hydrogermolysis reaction in which a germanium hydride reacts with a germanium amide to form the Ge–Ge bond. This method will be discussed extensively in Chapter II.

CHAPTER II

Synthesis of the Elusive Branched Fluoro-oligogermane $(Ph_3Ge)_3GeF$

2.1 Introduction - Branched Oligogermanes

2.1.1 σ-Delocalization in Oligogermanes

Oligogermanes are the heavier analogues of hydrocarbons. Like hydrocarbons, oligogermanes can adopt linear, cyclic and branched geometries. One of the main differences in the bonding descriptions between these two groups is that, in organic compounds, electrons in σ orbitals of the C−C bonds are considered to be localized and the delocalization of electrons is mainly associated with mobility of π electrons that are in $2p_z$ orbitals, perpendicular to the plane of the molecule.[13] Some observations point to the fact that this is not the case in heavier E−E (E = Si, Ge, Pb) analogues. For example, linear polystannane oligomers ($R(SnR_2)_nR$) (R = alkyl or aryl) that are the tin congeners of saturated hydrocarbons ($H(CH_2)_nH$), have absorption maxima that are low in energy and their λ_{max} undergoes a bathochromic shift as the chain gets longer. Thus the electronic spectra of oligostannes shows a close resemblance to unsaturated conjugated polyenes.[14]

The same effect is also observed in polysilanes and permethylated oligosilanes $Me(SiMe_2)_nMe$ (n = 2-6), when the oxidation potential of the polysilane changes and the λ_{max} and ϵ both increase as the length of the chain gets longer.[15,16]

The previously mentioned unusual properties in oligo- and polymers of heavier group 14 elements (Si, Ge, Sn) are attributed to σ-bond electron delocalization. σ-

delocalization arises from an effective overlap between sp^3 hybridized orbitals on the germanium atoms in the catenate, and is due to the diffuse nature of the 4s and 4p atomic orbitals of germanium. Figure 2.1 shows that the delocalized electrons which take part in σ-delocalization, also constitute Ge – Ge σ bonds and are located in the HOMO of the molecule. It can also be seen that the LUMO mainly consists of the σ^* orbitals of the Ge – Ge bonds.

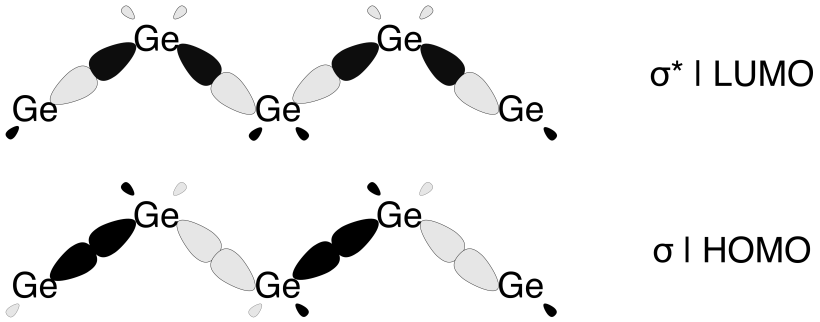

Figure 2.1: Representation of the HOMO and LUMO of a germanium catenate (Adapted from Ref.[17])

2.1.1.1 Effect of Chain Length on σ-Delocalization

The $\sigma \longrightarrow \sigma^*$ transition of saturated alkanes C_nH_{2n+2} is in the far UV region and does not change by much even when the chain length increases.[18] On the other hand, other group 14 catenates such as oligogermanes, polysilanes and polystannanes have a much different electronic absorption pattern. Table 2.1 summarizes the absorbance maxima of a series of isopropyl-capped germanium catenates and as can be seen, the λ_{max} undergoes a red shift as the number of germanium atoms increases in the chain.[19,20]

The aforementioned UV absorption characteristics of oligogermanes and other group 14 catenates illustrate how λ_{max} is strongly dependent on the chain length. Other studies indicate that this dependence is not limited to chain length, and specifically the absorption maxima of oligogermanes changes with temperature (thermochromism) and also with substituents on the germanium backbone.[21] This phe-

Table 2.1: Absorbance maxima of a series of isopropyl capped polygermane $^{i}Pr_3Ge-(GePh_2)_n-Ge^{i}Pr_3$ (n = 0 - 4)

Oligogermane	λ_{max} (nm)†
$^{i}Pr_3Ge-Ge^{i}Pr_3$	231
$^{i}Pr_3Ge-GePh_2-Ge^{i}Pr_3$	242
$^{i}Pr_3Ge-(GePh_2)_2-Ge^{i}Pr_3$	273
$^{i}Pr_3Ge-(GePh_2)_3-Ge^{i}Pr_3$	300
$^{i}Pr_3Ge-(GePh_2)_4-Ge^{i}Pr_3$	310

† In CH_2Cl_2

nomenon is consistent with the delocalization of HOMO electrons across all the germanium atoms in the chain σ-delocalization.[17,22,23]

2.1.1.2 Effect of Substituents on σ-Delocalization

Weinert *et al.* have systematically studied the effect of different substituents on the HOMO-LUMO gap and on the electronic absorption and electrochemical properties of a variety of oligogermanes with different chain lengths. In cases having both alkyl and aryl substituents, electron donating groups can only act as inductive donors, and electron donation causes a destabilization of the DFT calculated HOMO energy, thus leading to an increase in the λ_{max} and a decrease in the oxidation potentials, which were measured by CV. Table 2.2 summarizes these results and it can be seen that phenyl-substituted oligogermanes are easier to oxidize than the alkyl-substituted species. It is noteworthy to mention that the same electrochemical effect is observed in polysilanes as well.[15,24]

Table 2.2: Effect of substituents on the absorption/electrochemical properties and the HOMO energy of digermanes

Digermane	λ_{max} (nm)	E_{ox} (mV)	HOMO (eV)
$Ph_3Ge-GePh_3$	240	1576	-5.45
$^{i}Pr_3Ge-GePh_3$	235	1635	-5.56
$Et_3Ge-GePh_3$	231	1587	-5.46
$Bu_3Ge-GePh_3$	232	1588	-5.38

2.1.1.3 Effect of Conformation on σ-Delocalization

Extensive studies on the effect of oligogermane conformation on the efficiency of σ-delocalization have been carried out. For example, in case of the hexagermane $^{i}Pr_3Ge(GePh_2)_4Ge^{i}Pr_3$, TDDFT calculations and variable-temperature UV-Vis spectroscopy both point to the trans-coplanar conformer to be the thermodynamically most stable conformer, among all other possible conformations than can be formed by rotating about the five Ge−Ge bonds. As shown in Table (2.3), the λ_{max} of the hexagermane undergoes a bathochromic shift as the temperature increases.[25]

Table 2.3: Absorbance maxima of $^{i}Pr_3Ge(GePh_2)_4Ge^{i}Pr_3$ in toluene in varying temperatures

Temperature (K)	λ_{max} (nm)
278	309
288	310
298	310
308	311
318	312
328	312
338	313
348	313
358	314

Generally any conformer in which the overlap between sp^3 orbitals are maximized will have a higher degree of σ-delocalization. Using conformationally constrained oligosilanes it is observed that when the dihedral angle is closer to all anti ($\omega = 180°$), the system will be at its most conjugated form and a cisoid form ($\omega \approx 0 - 60°$) will disrupt the σ-delocalization by suppressing electron conjugation.[26–30]

2.1.1.4 Effect of the Branching on σ-Delocalization

Branched structures are possible in germanium catenates having more than 3 germanium atoms and in some cases a germanium atom can be replaced with another element, such as silicon. UV-Vis and electrochemical studies show that branched

oligogermanes have different properties compared to their linear analogues. The substituents can both electronically and sterically cause change in the absorption properties of branched oligogermanes.

Figure 2.2 shows several branched oligogermanes $(R_3Ge)_3-Ge-R'$, in which R and R′ can be alkyl or aryl groups. The branching usually has a disruptive effect of on σ delocalization, because it can decrease the effective overlap of sp^3 orbitals. Also the degree of catenation has a more profound effect on the electronic absorption properties than the variations of substituents.[31] For example, in the case of tetragermanes, the branched tetragermane **2** has a higher energy $\sigma \longrightarrow \sigma^*$ transition (λ_{max} = 256 nm), compared to its linear analogue Ge_4Ph_{10} (λ_{max} = 282 nm). Simultaneously, the branched pentagermane **4** (λ_{max} = 250 nm) has a lower degree of σ-delocalization compared to its linear analogue Ge_5Ph_{12} (λ_{max} = 295 nm).[21,32,33]

The substituents can alter the geometry of the germanium-germanium backbone of oligogermanes sterically and can cause noticeable changes in their electronic properties. Along with sterics, the substituents can also influence σ-delocalization electronically. For example, it is anticipated that the π-acceptor phenyl ligands will decrease the HOMO-LUMO gap of oligogermanes by donating the σ-electrons in their π^*-orbitals to the Ge–Ge σ-orbital. In **2**, substituting phenyl with a hydrogen decreases the conjugation, and as the number of alky substituents increase, from **2a** to **3** in the germanium-based skeleton the HOMO-LUMO energy gap increases. σ-delocalization can be influenced by the extent of hyperconjugation in a molecule as well. From **4** to **4d**, as the the number of methyl groups increase, compared to more donating groups such as $-SiR_3$ (R = Ph, ^{i}Pr) in **4a** and **4c** or $-GePh_3$ in **4** the λ_{max} undergoes a blue shift. The more σ-donating isopropyl groups in **4c** compared to less strong hyper-conjugative donor methyl groups in **4d** also increase the amount of electron delocalization. Replacing germanium atoms with silicon does seem to affect the electronic absorption properties in longer oligogermanes **5-5e** and shorter branched

oligogermanes **6-6a**.[21,31,32,34–36]

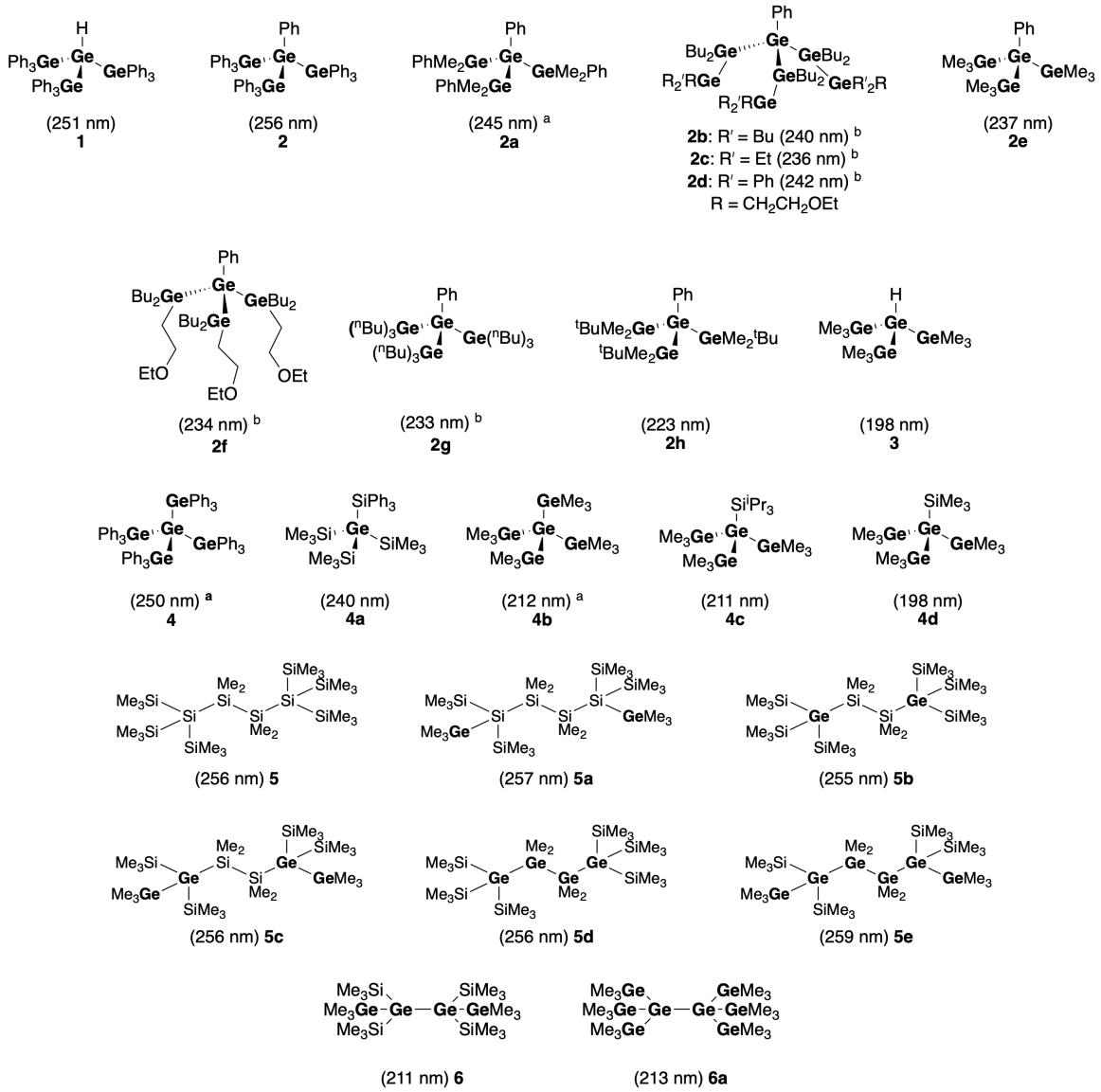

Figure 2.2: In parentheses, reported λ_{max} (nm) of several branched acyclic oligogermanes (^{a} in CH_2Cl_2 and ^{b} in hexane)

2.1.2 Synthesis of Branched Oligogermanes

Compared to linear germanium catenates, branched oligogermanes are somewhat rare. One of the earliest methods for synthesizing them was by using nucelophilic metallated germanium compounds and reacting them with germanium electrophiles. Scheme 2.1 shows three equivalents of Ph_3GeLi can add to GeI_2.[37] In another example, Et_3GeLi

generated *in situ* can react with GeI_2 and MeI to form **7**.[38] An important feature of these nucleophilic synthetic pathways is that, the germanium nucleophile cannot add four times to the germanium electrophile, due to steric hindrance.

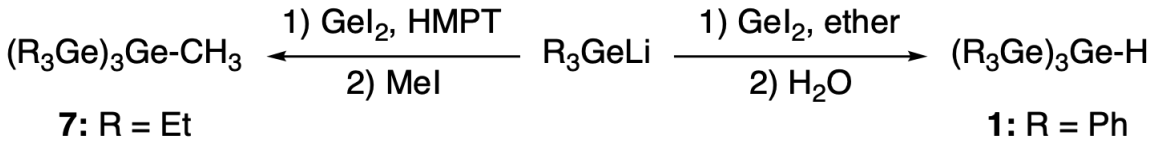

Scheme 2.1: Synthesis of branched oligogermanes from R_3GeLi precursors

Another method to make heterostructures containing both silicon and germanium is to start off by using branched polysilanes. Scheme 2.2 shows how by using KO^tBu a silicon anion can be formed (Step 1) which can react with a germanium electrophile in Step 2 to form a branched oligogermane.[34] More variety can also be introduced into this class of compounds resulting from Lewis acid-induced rearrangements in the synthesized heterostructures. This method is also known as "shuttling" germanium into polysilanes and is suggested to be a cascade of rearrangement reactions that starts by the formation of a germylium cation via methyl group abstraction.[39] Utilizing these rearrangements in tandem with the electrophilic addition of germanium halides yields a diverse array of branched oligogermanes.[40]

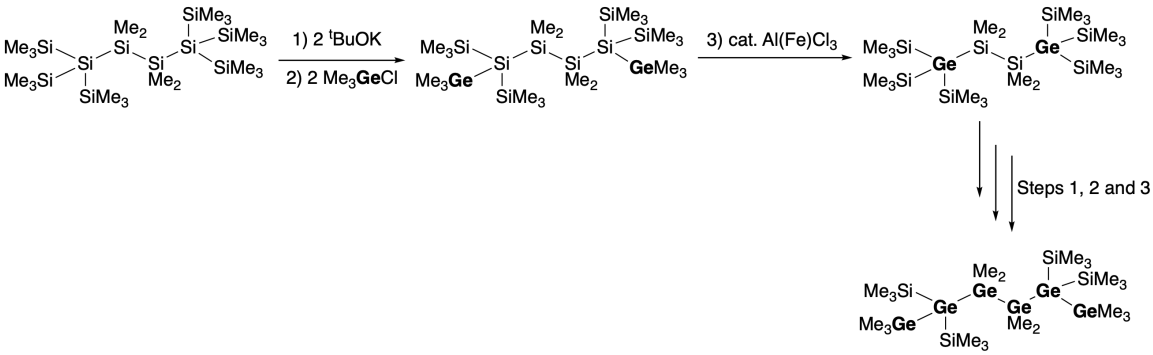

Scheme 2.2: Synthesis of branched oligogermanes from polysilane precursors

Hydrogermolysis, formerly known as "hydrogenolytic fission", of germanium-nitrogen bonds by germanium hydrides is a powerful synthetic tool for the preparation of compounds with Ge–Ge bonds.[41] In this approach, a germylamine (also referred to as a

germanium amide) R_3Ge-NR_2' (R′= Et, Me) and a germanium hydride (or germane) R_3Ge-H are used to construct Ge–Ge bonds.

Early reports of hydrogermolysis type reactions were in fact used for Ge–Sn bond formations (Scheme 2.3-A).[41] Earlier rate studies of the hydrostannolysis reaction (Scheme 2.3-B) suggest that the reaction proceeds via an ionic mechanism, mainly because the rates of the reactions were unaffected when a radical initiator (i.e., AIBN) or inhibitor (i.e, galvinoxyl) was added to the reaction. More importantly, the rate of the reaction is significantly enhanced when the polarity of the solvent increases and when electron-donating groups are attached to the tin amine **8a-e**. The influence of the basicity of the metal amine on the rate of the reaction also sheds light on why tin amines generally react faster than germanium amines. This diminished reactivity is attributed to a more powerful $p_\pi - d_\pi$ interaction[1] in the Ge–N bond compared to the Sn–N bond, in metal amines.[41]

[1]This is an antiquated theory that is no longer considered valid. Please see Chapter IV.

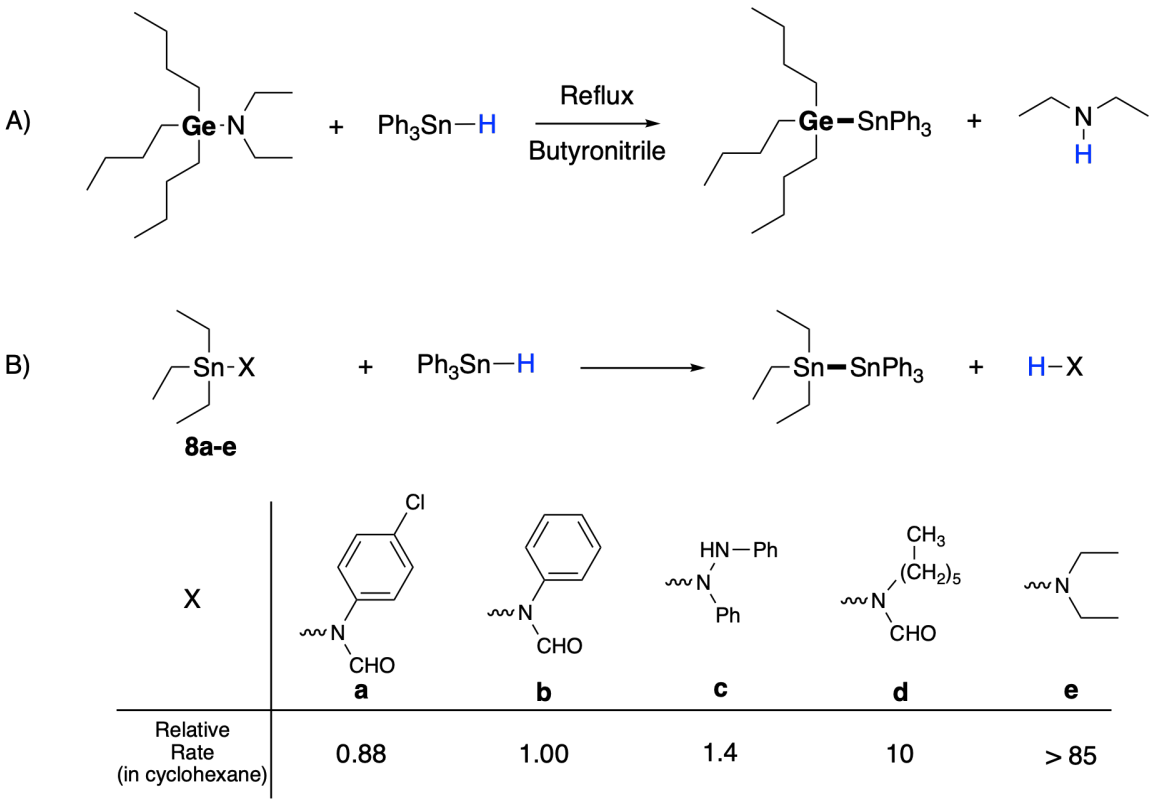

Scheme 2.3: Hydrometalolysis reactions to make A) Ge–Sn and B) Sn–Sn bonds

These observations suggest that it is also very likely that hydrogermolysis reactions in solvents other than acetonitrile proceed through a polar mechanism and they involve a rate-determining step in which the protonation of the germanium amine by the germanium hydride occurs [2]. [42,43]

The very first attempt to put to use the hydrogermolysis reaction for Ge–Ge bond formation was achieved with a relatively protic germane and an electron-donating group present on the germanium amine. Scheme 2.4 shows the formation of a digermane with Et_2NH as the by-product in hot hexane. Though this version of hydrogermolysis was groundbreaking it suffers from several limitations. The synthesis of electron-withdrawing substituted germanium hydride limits the diversity of the germanium catenates that can be formed. Also due to its low volatility the amine

[2]Perhaps the term "hydride" is a bit misleading when the hydrogen atom is actually acting to be protic.

by-product (Et_2NH), has the potential of reacting with the germanium hydride.[44]

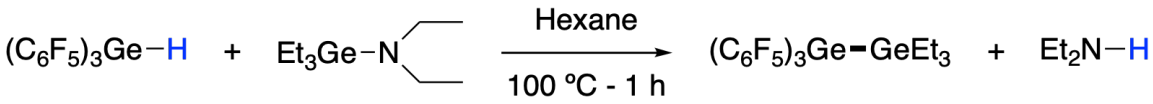

Scheme 2.4: Hydrogermolysis reactions to form Ge−Ge bond, using a more acidic germanium hydride

In 2006, our group presented a new synthetic methodology for Ge−Ge bond formation from germanium amine and germanium hydride precursors. Several attempts were carried out to perform the reaction at room temperature or higher temperatures and in different solvents, such as benzene and toluene, all of which were unsuccessful for the the formation of the Ge−Ge bond. However, the reactions were successful using acetonitrile as the solvent. NMR studies showed that the reaction in Scheme 2.5, involved in the formation of an α-nitrile **9** species as an intermediate, which then reacted with the germanium hydride to form the Ge−Ge bond and regenerate a molecule of acetonitrile. There are several other remarks of this reaction that are of note. The role of acetonitrile in the reaction is still enigmatic because although it seems it is not consumed in the course of reaction (like a catalyst), the reaction only works when the stoichiometry of CH_3CN is in large excess. In the case of hydrostannolysis, it was observed that the amine by-product consumed the tin hydride, and the in hydrogermolysis the key to circumvent this problem was found to be using germanium amines with NMe_2 groups that form a volatile amine ($H-NMe_2$) by-product.[41,45]

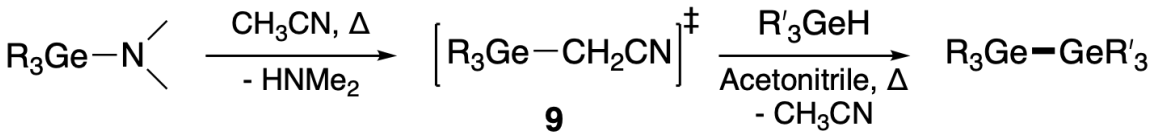

Scheme 2.5: Hydrogermolysis reaction involving α-nitrile intermediates

The hydrogermolysis reaction has been a highly useful tool for synthesizing discrete linear and branched oligogermanes. It has also allowed the generation of a

library of compounds having different functional groups. One similarity of the hydrogermolysis reaction to metal-based synthetic methods that is worthy of mention is that a germanium amine cannot add four times to germanium hydride (i.e., GeH_4) because of the steric hindrance. Scheme 2.6 shows that the hydrogermolysis reaction of GeH_4 and Ph_3GeNMe_2 will not result in the *per*phenylated neo-pentane analogue **4**, but instead only results in the formation of **1**. This apparent limitation is actually useful and it opens the door for the preparation of branched tetragermanes with a hydride functionality.[46]

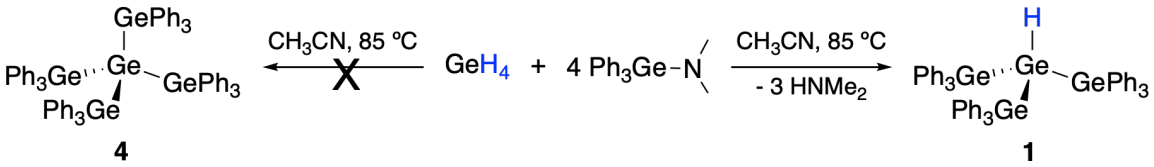

Scheme 2.6: Hydrogermolysis reactions for making branched $(Ph_3Ge)_3Ge-H$

2.1.3 Overview

There has been great interest in single molecule based electronics and significant efforts have been directed towards making molecular wires using purely organic compounds, such as in polyacetylene or carbon-bridged oligo(phenylene vinylene). Organic-based wires are generally limited to short chains, because the electron transfer process is easily disrupted as the poly-ene gets longer and more flexible. This makes conductive organic polymers require linker groups that make them rigid and flat.[47–49]

One way to tune organic wires is by the incorporation of metals. A variety of transition-metal based organic wires containing terpyridine ligands and iron(II), ruthenium(II), or cobalt(II) centers have been reported.[50] In another example, metal wires with the formula $R-(C\equiv C)_n-ML_m-(C\equiv C)_n-R$, that are poly-ynes doped with metals are noteworthy. In metal based systems, the conductivity is mainly dependent on the HOMO energy level which can be tuned by the interactions with the metal center. However, examples of conductive polymers are limited to few metals.[51]

The unique feature of σ-delocalization in main-group elements makes them good candidates for use as molecular wires. Direct and predictable structure-property relationships exist in oligogermanes and the electronic properties can be fine-tuned by changing the length of the chain and/or altering the substituents. As seen earlier (Figure 2.2), by systematically varying parameters such as chain length, substituents, and degree of branching, electronic properties of oligogermanes can be engineered and this opens up an avenue to utilizing them in single-molecule conductors.

It is important to obtain branched oligogermanes in high yields by reproducible methods that do not rely on harsh conditions that are not complicated. The hydrogermolysis reaction is a useful tool for making oligogermanes having different geometries and lengths. In this chapter, the focus will be on a series of oligogermanes containing halogen substituents $(Ph_3Ge)_3Ge{-}X$ (X = F, Cl, Br, I), and how changing the halide will affect the chemical and electrochemical properties, as well as the stability of this series.

2.2 Results and Discussion

2.2.1 Synthesis of $(Ph_3Ge)_3GeX\,(X = H, Cl, Br, I)$

In an earlier study in our group $(Ph_3Ge)_3GeH$ **1** was synthesized using the hydrogermolysis reaction using germane gas GeH_4 and triphenyl germanium amine **10** (Ph_3GeNMe_2). Unlike in saturated hydrocarbons where the C−H bond is considered to be inert and its activation can be a synthetic challenge, the Ge−H bond in germanium hydrides is considered to be a functional group. The primary goal from this reaction was to synthesize the heavier neopentane analogue $(Ph_3Ge)_4Ge$ **4**, via the hydrogermolysis reaction. However, all attempts were unsuccessful because of steric limitations. The hydrogermolysis reaction only occur three times with GeH_4 and this limitation resulted in the isolation of **1** in all trials (Scheme 2.6).[52]

Scheme 2.7 shows other failed attempts to make **4**. Even when **1** is isolated and then reacted separately with **10**, the reaction does not yield **4**. Moreover, when **1** is converted to branched amine **11** ($(Ph_3Ge)_3Ge-NMe_2$), and this is reacted with Ph_3GeH, it again does not result in the formation of **4** and instead it results in the formation of unidentified products, along with pyrimidine, acrylonitrile and **12** ($Ph_3GeGePh_3$).[52]

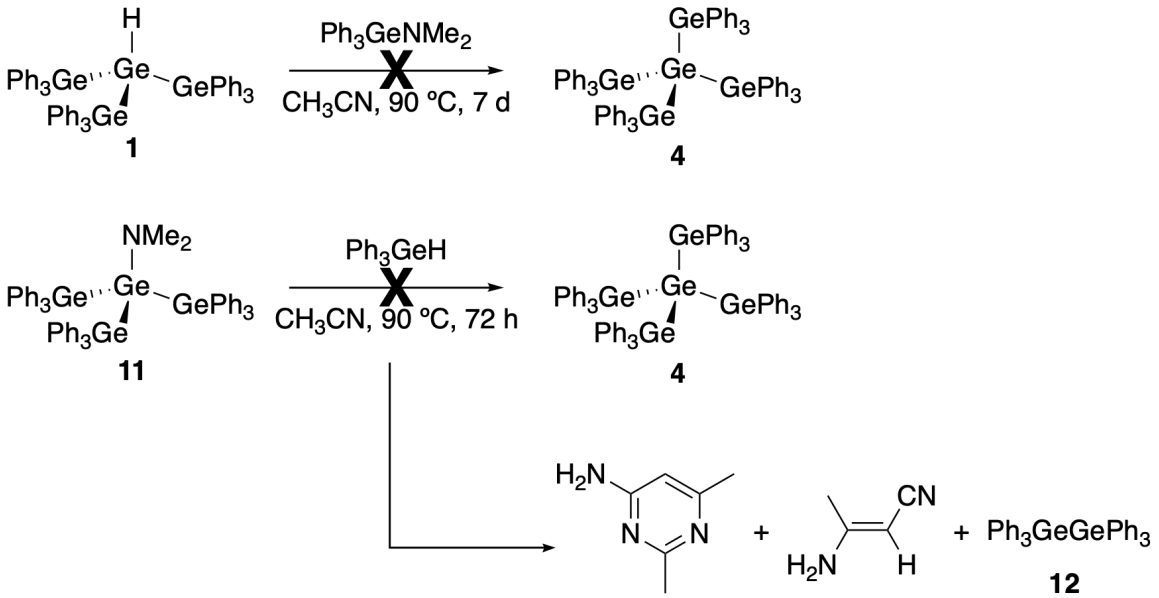

Scheme 2.7: Attempted syntheses of $(Ph_3Ge)_4Ge$ by hydrogermolysis reactions

Suitable crystals for X-ray of **1** were obtained by recrystallization from hot benzene. Figure 2.3 shows the ORTEP diagram of **1**. The bond distances between three peripheral germanium atoms and the central Ge atom have an average value of 2.4310(5) Å, which is similar to the Ge−Ge bond distances in linear oligogermanes, such as Ph_3GeGeR_3 (R = Me, 2.418(1) Å;[53] R = Et, 2.4253(7) Å;[45] R=^{n}Bu, 2.421(8) Å[45]). The Ge−Ge bond distances in **1** are shorter compared to the bonds in $(Ph_3Ge)_3GePh$ **2** where the average Ge−Ge bond length is 2.469(4) Å.[21] The Ge−H bond distance in **1** (1.45(3) Å) is relatively similar to the Ge−H distance in Ph_3GeH (1.50(5) Å).[52,54]

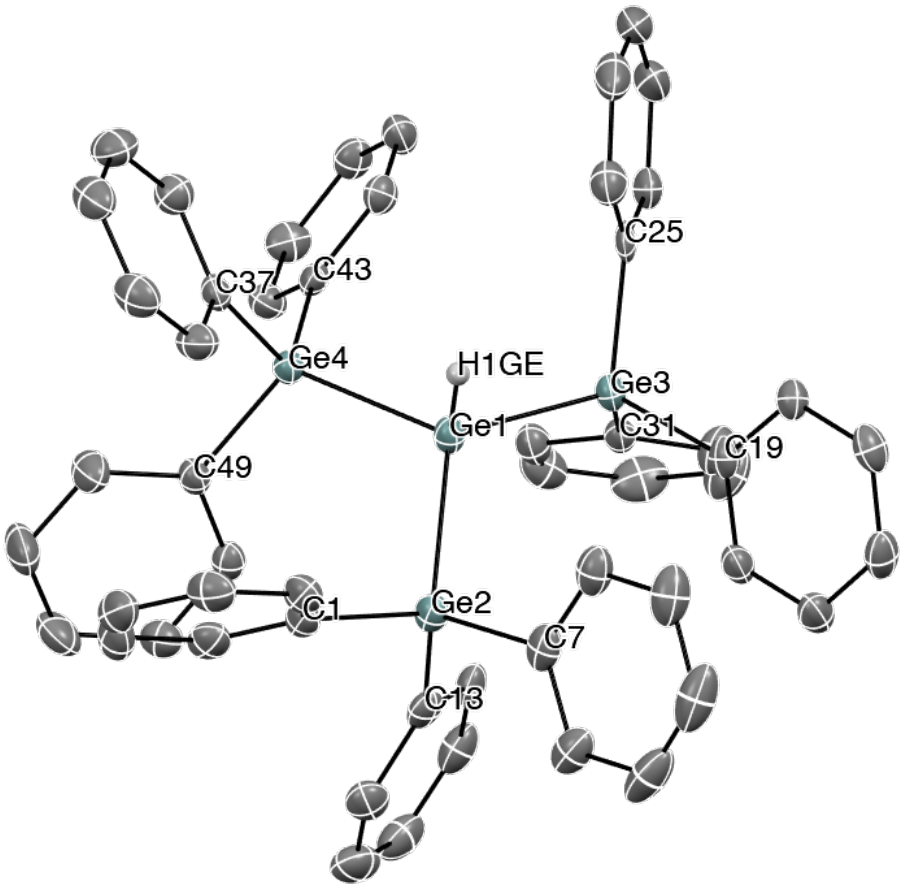

Figure 2.3: ORTEP diagram of $(Ph_3Ge)_3GeH$, drawn at the 50% probability level

The ^{1}H-NMR spectrum of **1** (Figure 2.4) shows the resonance for the Ge−H at δ 4.58 ppm, which is more deshielded than the Ge−H in $(Me_3Ge)_3GeH$ **3**, where the resonance is observed at δ 2.81 ppm. This downfield shift in **1** can be attributed to the inductive electron donation in **3** and a higher degree of anisotropy effects from the phenyl rings in **1**.[52]

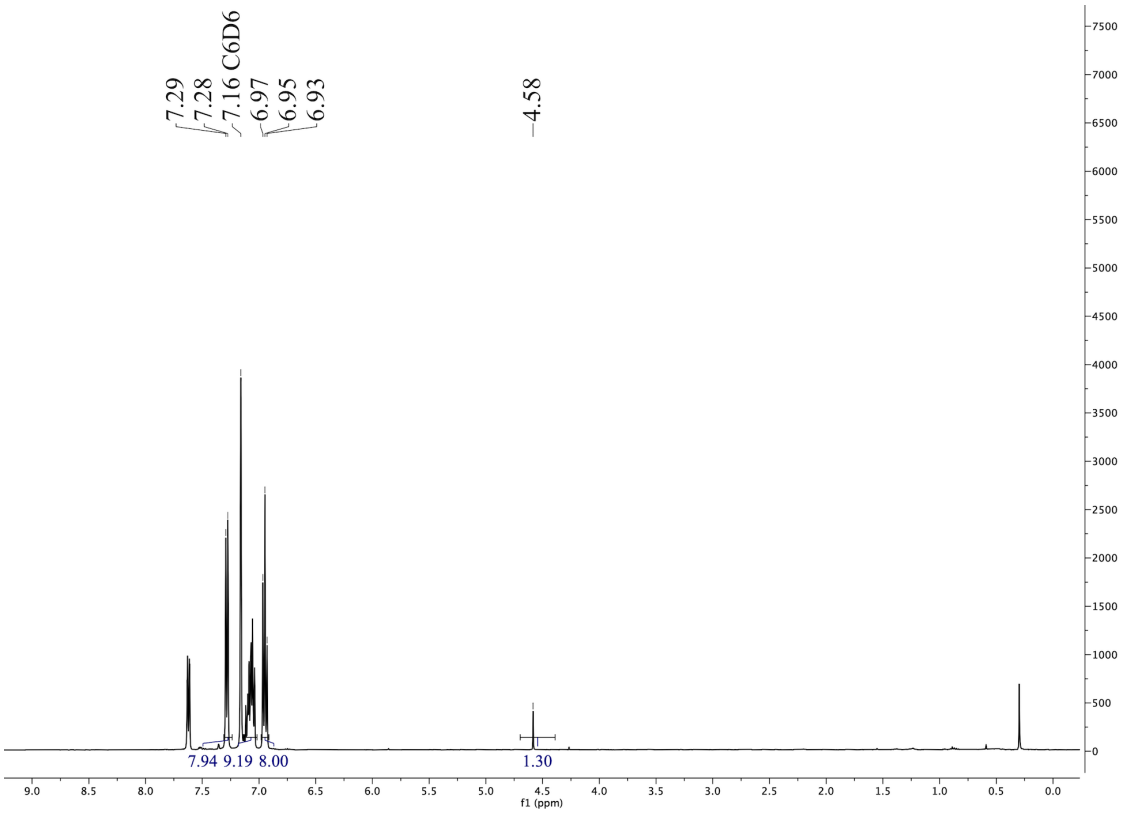

Figure 2.4: ^{1}H-NMR (400 MHz, C_6D_6) spectrum of **1**

Attempts to observe the $^{1}J_{\mathrm{Ge-H}}$ in ^{1}H-NMR spectrum of **1** were unsuccessful. On the contrary, when GeH_4 gas was condensed in a J. Young tube, the ^{1}H-NMR spectrum in C_6D_6 (Figure 2.5) shows the coupling between the NMR active ^{73}Ge isotope (I = 9/2) with an abundance of 8% in the form of a dectet with a Ge−H coupling constant of 98 Hz. The central signal at 3.06 ppm arises from all other isotopic species of germanium. This $^{1}J_{\mathrm{Ge-H}}$ is much smaller in GeH_4 than in **1** and is in agreement with previously reported values (100 Hz).[52,55]

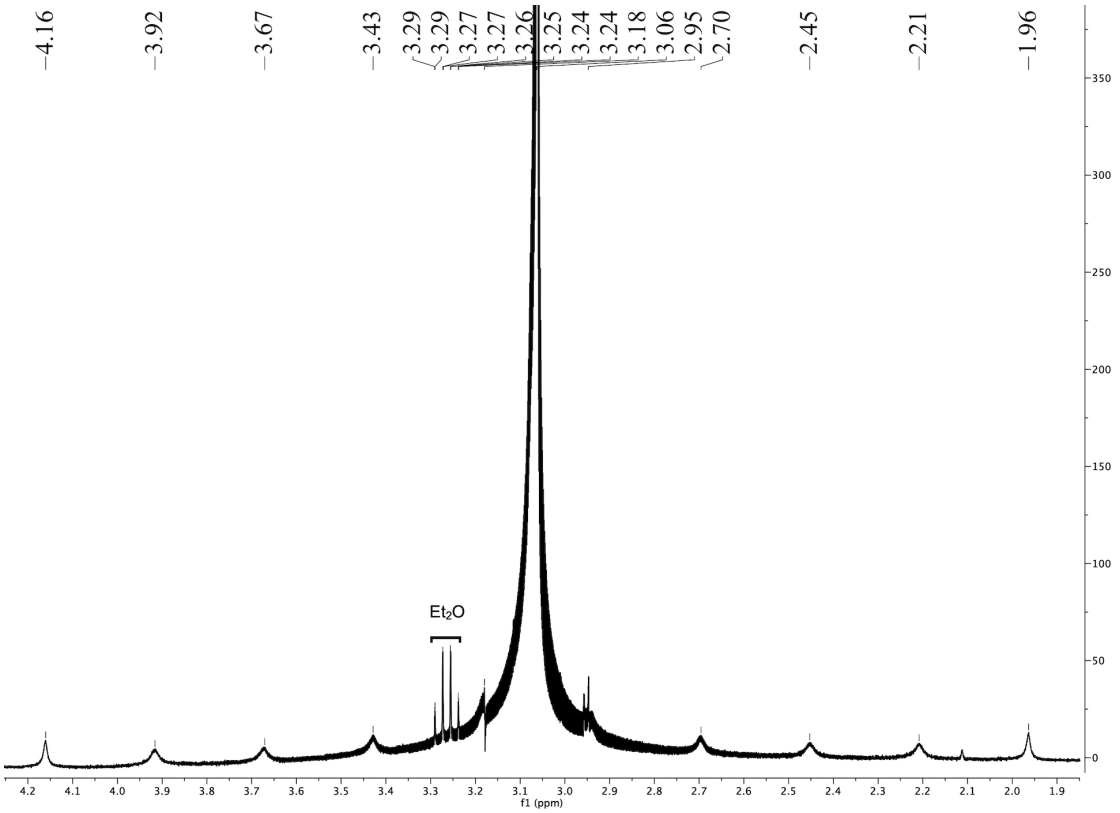

Figure 2.5: ^{1}H-NMR (400 MHz, C_6D_6) spectrum of GeH_4

After synthesizing **1** in high yields the focus became the isolation of the branched germanium cation **13** ($(Ph_3Ge)_3Ge^+$). Starting with **1**, it was rationalized that by using a hydride abstracting reagent such as tritylium hexafluorophosphate $[CPh_3][PF_6]$, the cation [**13**][PF_6] would be formed. In order to be able to use tritylium hexafluorophosphate the solvent of choice needed to be polar, and when the reaction was attempted in dichloromethane (Scheme 2.8), [**13**][PF_6] could not be isolated. Instead the crystals that formed after the reaction was stirred for 36 hours were found to be the chloro- branched oligogermane **14** ($(Ph_3Ge)_3Ge-Cl$). The formation of Ph_3C-H during the course of the reaction was observed in the ^{1}H-NMR spectrum of the reaction mixture with a resonance at δ 5.51 ppm and was further proved with X-ray crystallography. The formation of Ph_3C-H indicates that **13** is generated during the reaction which then abstracts a chlorine atom from the solvent (CH_2Cl_2) to form **14**.[52] In order to further examine these results, the reac-

tion of **1** with $[CPh_3][PF_6]$, was also tried in CH_2Br_2 and CH_2I_2 solvents and **15** ($(Ph_3Ge)_3Ge-Br$) and **16** ($(Ph_3Ge)_3Ge-I$) branched oligogermanes were isolated.[52]

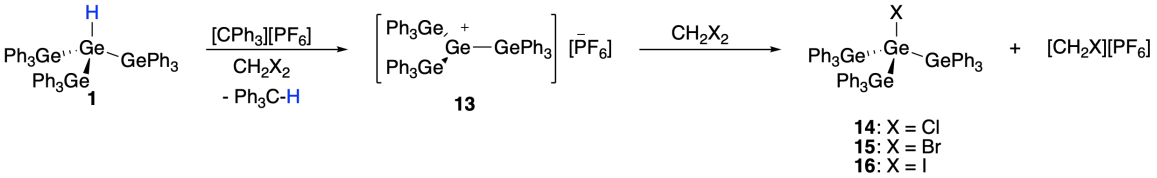

Scheme 2.8: The synthesis of $(Ph_3Ge)_3GeX$ (X = Cl, Br, I) from **1**

2.2.2 Attempted Syntheses of $(Ph_3Ge)_3GeF$

The synthesis of the fluorinated branched oligogermane **17** ($(Ph_3Ge)GeF$) proved to be a much more challenging task. In almost all attempts the reactive branched germylium **13**.[WCA] was formed *in situ*, and then was reacted with a fluorine source.

It was originally anticipated that **13**.[WCA] will react with difluoromethane in a similar fashion to the previous reactions with CH_2X_2 (X = Cl, Br, I). When **1** was reacted with $[CPh_3][B(C_6F_5)_4]$ and then CH_2F_2 was added to the mixture, no Ge–F bond formation was observed (Scheme 2.9).

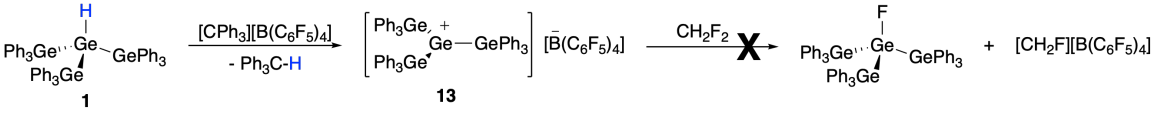

Scheme 2.9: Attempted synthesis of $(Ph_3Ge)_3GeF$ by CH_2F_2

The ^{19}F-NMR spectrum of the reaction mixture (Figure 2.6) after the work-up only contained the signals for $[B(C_6F_5)_4]^-$. This suggested that germylium **13**.[WCA] is not Lewis acidic enough to abstract a fluorine atom from CH_2F_2 and this reaction is not thermodynamically favored because a very unstable carbocation $[CH_2F][WCA]$ must be formed.

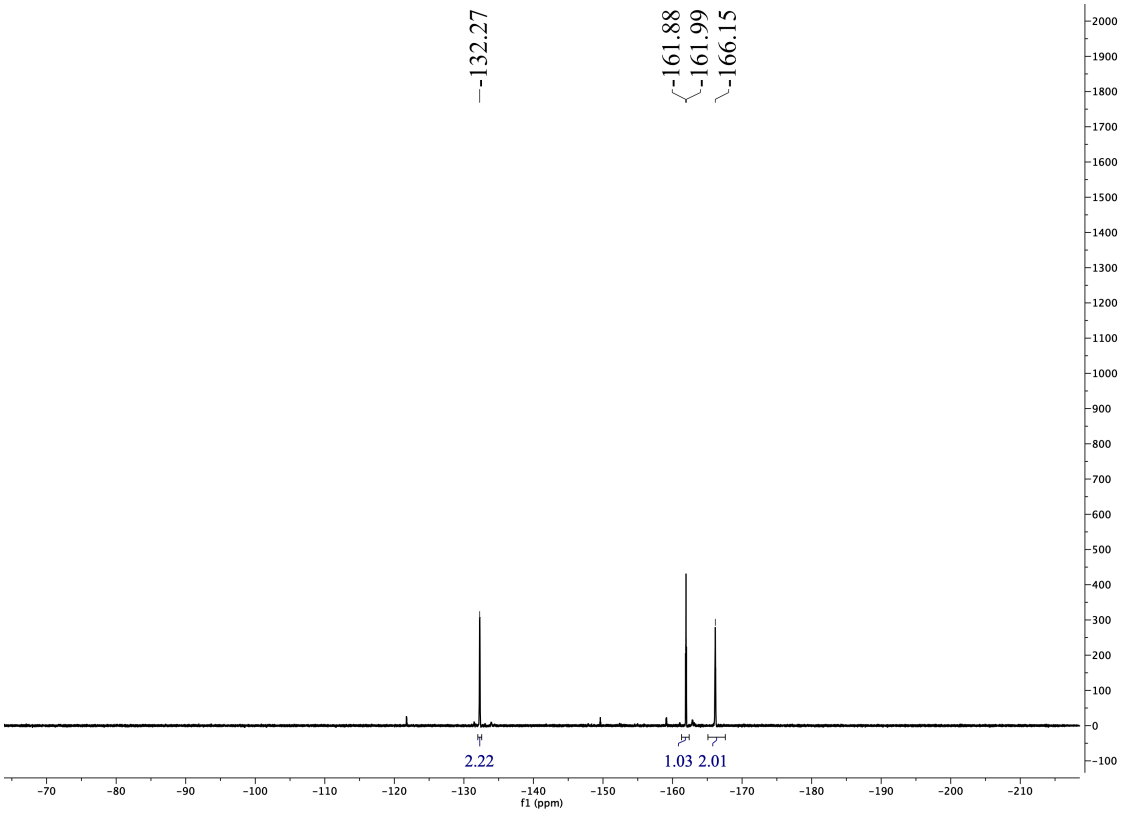

Figure 2.6: ^{19}F-NMR (376 MHz, C_6D_6) spectrum of the reaction mixture of **13**.[$B(C_6F_5)_4$] and CH_2F_2

Scheme 2.10 shows another attempt to obtain **17** using **14** and AgF. This approach seems to be able to make **17** in very low yields. When AgF was added to the reaction black precipitates were formed and an intractable mixture resulted.

14 **17**

Scheme 2.10: Attempted synthesis of $(Ph_3Ge)_3GeF$ from $(Ph_3Ge)_3GeCl$

The crude ^{19}F-NMR spectrum of the reaction mixture (Figure 2.7) shows the minimal formation of **17** with the signal at δ -194.68 ppm. The sharp signal at -202.40 ppm corresponds to the major product **18** (Ph_3GeF).

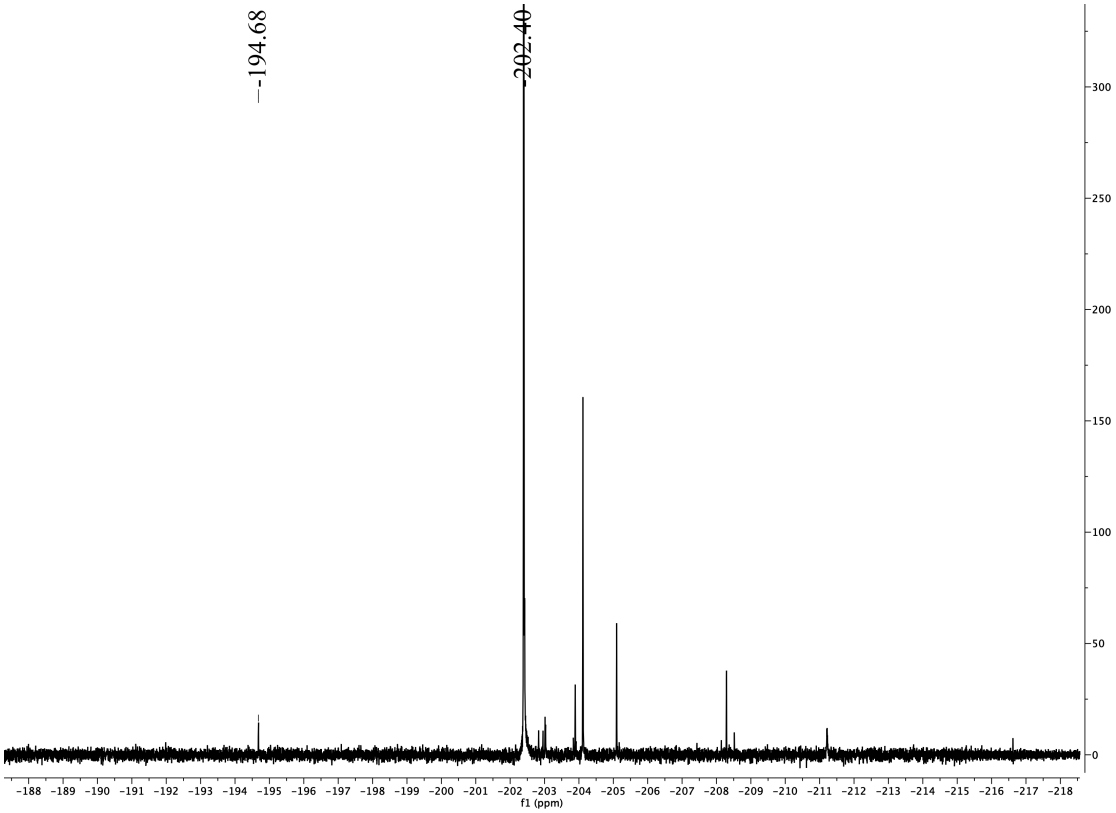

Figure 2.7: Crude ^{19}F-NMR (376 MHz, C_6D_6) spectrum of the reaction mixture of $(Ph_3Ge)_3GeCl$ and AgF

When the reaction mixture was filtered thru celite and solvent was removed *in vacuo*, needle-like crystals were formed that were identified to be Ph_3GeF by ^{19}F-NMR spectroscopy (Figure 2.8). This suggested that **17** was not stable and can degrade to Ph_3GeF in solution.

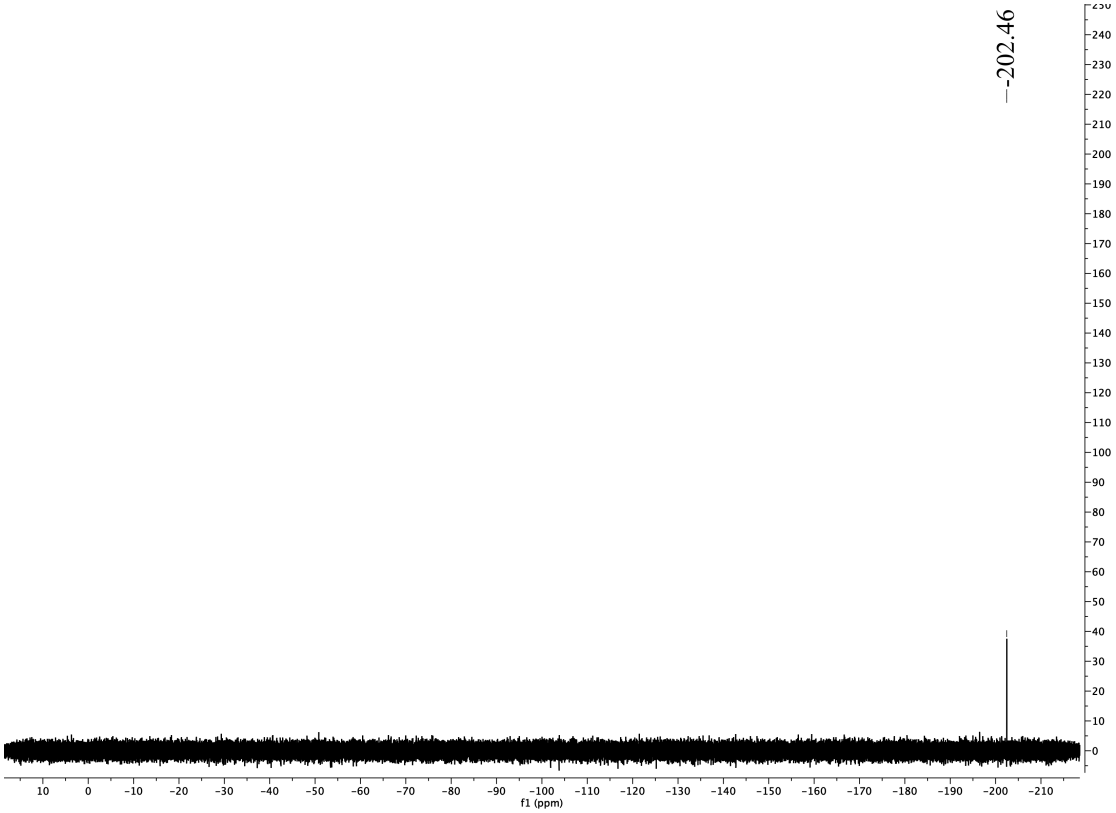

Figure 2.8: ^{19}F-NMR (376 MHz, C_6D_6) spectrum of the reaction of $(Ph_3Ge)_3GeCl$ and AgF after work-up

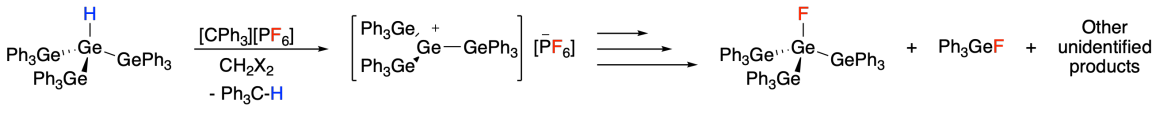

Scheme 2.11: Attempted isolation of $(Ph_3Ge)_3Ge^+$ with WCA = PF_6^-

Attempts that relied on the isolation and using the branched germylium**13**.$[PF_6]$ were unfruitful (Scheme 2.11). When **1** was reacted with $[CPh_3][PF_6]$ and the reaction mixture analyzed, signals that corresponded to Ge–F containing compounds emerged in the ^{19}F-NMR spectrum of the mixture along with other unidentified products. Figure 2.9 shows the signals for **17**, **18** and $[CPh_3][PF_6]$ at -125.58 ppm. This lead to the conclusion that $[PF_6]^-$ is not a good enough WCA to stabilize **13** and using any other fluorine source would be redundant with this WCA since it reacts with the gerymylium. So the focus was then put on a WCA that cannot act as a fluorine

source and $[B(C_6F_5)_4]^-$ was chosen.

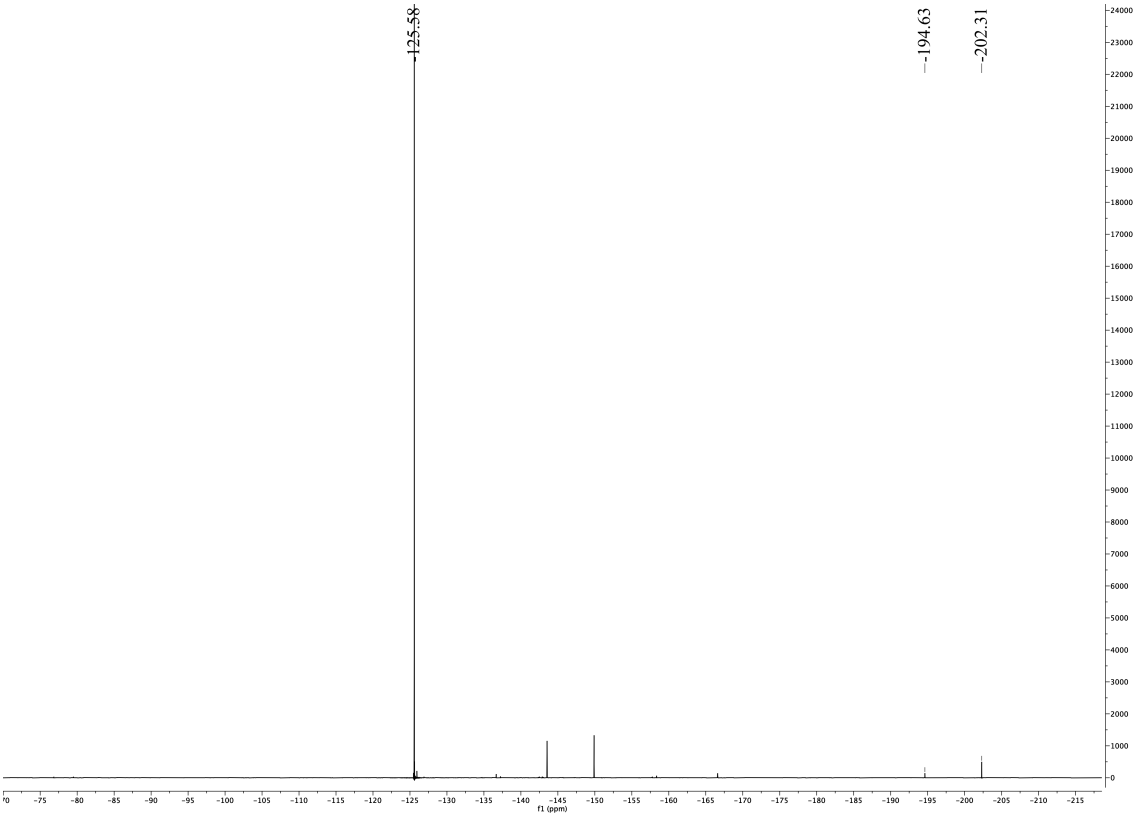

Figure 2.9: ^{19}F-NMR (376 MHz, C_6D_6) spectrum of the reaction of the attempted isolation of $(Ph_3Ge)_3Ge^+.[PF_6]$

As shown in Scheme 2.12, when **13**.$[B(C_6F_5)_4]$ was reacted with XeF_2 in benzene, no signals suggesting the formation of **17** and **18** were observed and an intractable reaction mixture resulted.

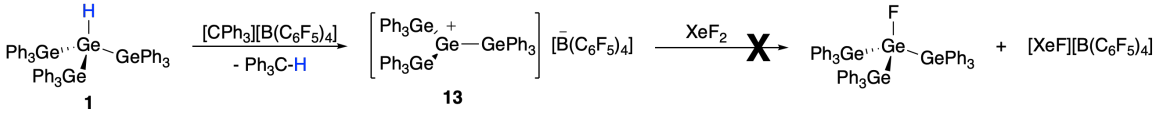

Scheme 2.12: Attempted synthesis of $(Ph_3Ge)_3GeF$ by XeF_2, (WCA = $[B(C_6F_5)_4]$)

The ^{19}F-NMR spectrum of the reaction mixture (Figure 2.10) shows a distinct peak at -113.44 ppm and suggests the degradation of $[B(C_6F_5)_4]^-$.

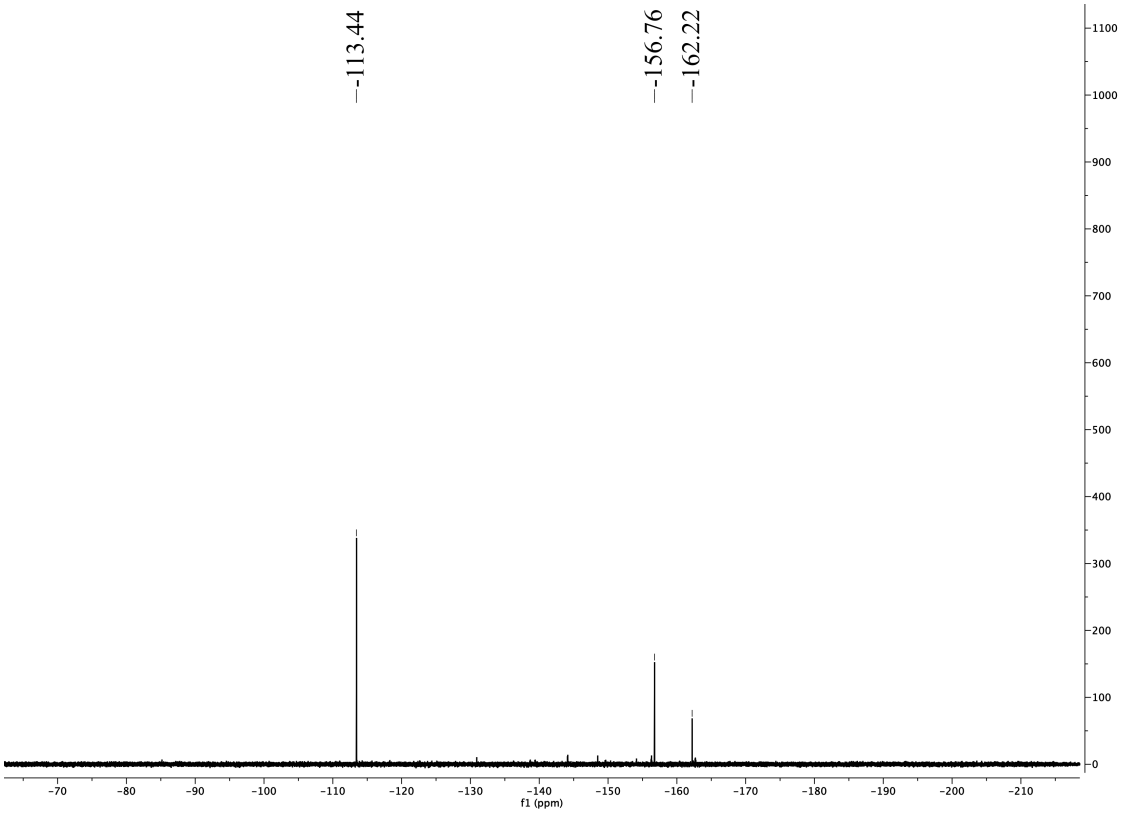

Figure 2.10: ^{19}F-NMR (376 MHz, C_6D_6) spectrum of the reaction mixture of **13**.[$B(C_6F_5)_4$] and XeF_2

When the WCA was changed and **13**.[$SnCl_5$] was reacted with XeF_2 (Scheme 2.13) the reaction lead to the formation of **18** to a small extent.

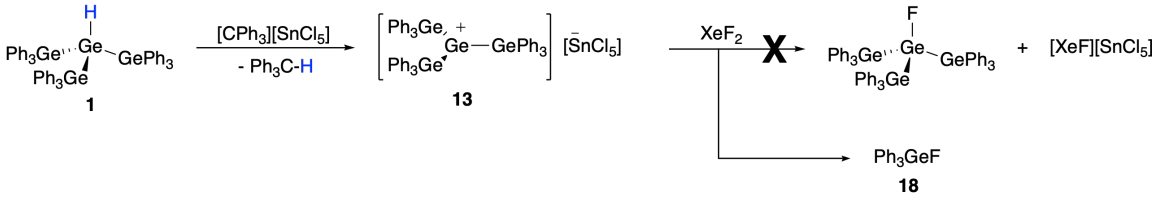

Scheme 2.13: Attempted synthesis of $(Ph_3Ge)_3GeF$ by XeF_2, (WCA = [$SnCl_5$])

Figure 2.11 shows the signal corresponding to Ph_3GeF at -202.40 ppm and again the distinct signal at -113.42 ppm is observed. The signal at -113.4 ppm in the ^{19}F-NMR spectra of both of these cases matches very closely with a standard sample of fluorobenzene in C_6D_6 at -112.84 ppm and other reported value of -113.6 ppm.[56] However the pathway to the formation of fluorobenzene is not clear.

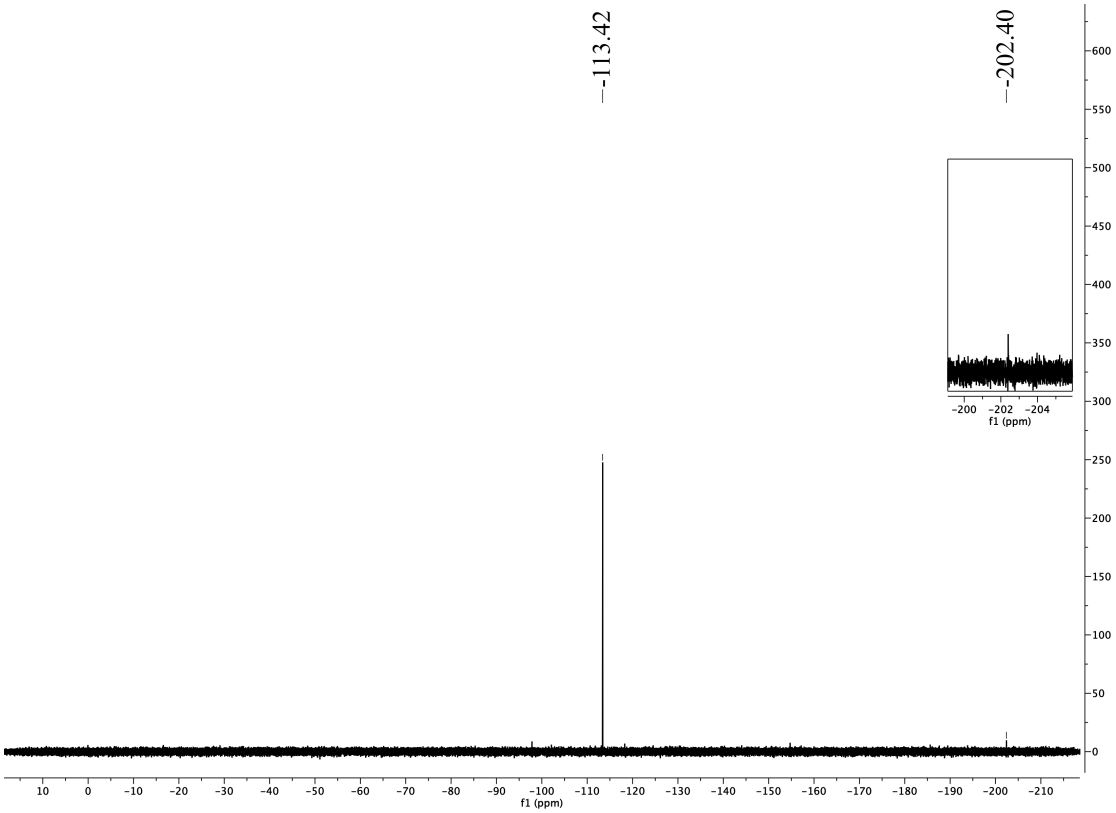

Figure 2.11: ^{19}F-NMR (376 MHz, C_6D_6) spectrum of the reaction mixture of **13**.[$SnCl_5$] and XeF_2

Scheme 2.14 shows the attempted synthesis of **17** using another F^- source. When **13**.[$B(C_6F_5)_4$] was reacted with [$(Me_2N)_3S$][Me_3SiF_2] (TAS-F) in benzene, a complex reaction mixture resulted. When the volatiles were removed *in vacuo* colorless crystals resulted that were shown to be [$(Me_2N)_3S$][$B(C_6F_5)_4$] by X-ray analysis.

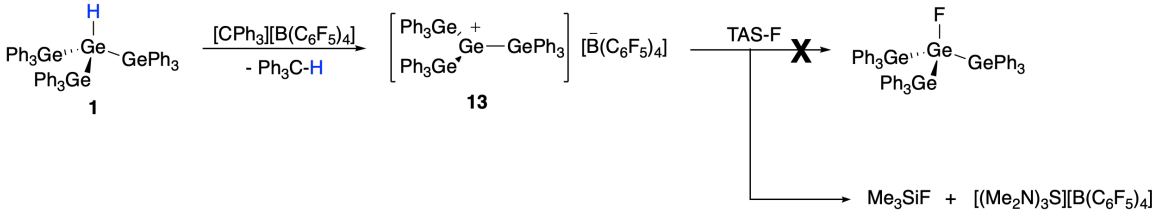

Scheme 2.14: Attempted synthesis of $(Ph_3Ge)_3GeF$ by TAS-F, (WCA = $[B(C_6F_5)_4]^-$)

2.2.3 Synthesis of $(Ph_3Ge)_3GeF$

After numerous attempts it was concluded that **13**.[WCA] was not a stable species, probably due to its very high Lewis acidity. It was theorized that if a suitable WCA can act as both an anion and an *in situ* fluorine source, $(Ph_3Ge)_3GeF$ might be synthesized successfully. A similar reaction (Scheme 2.15) was recently reported where $[CPh_3][BF_4]$ was used to convert another germanium hydride (TPFC)Ge–H (TPFC = tris(pentafluorophenyl)corrole) to (TPFC)Ge–F.[57]

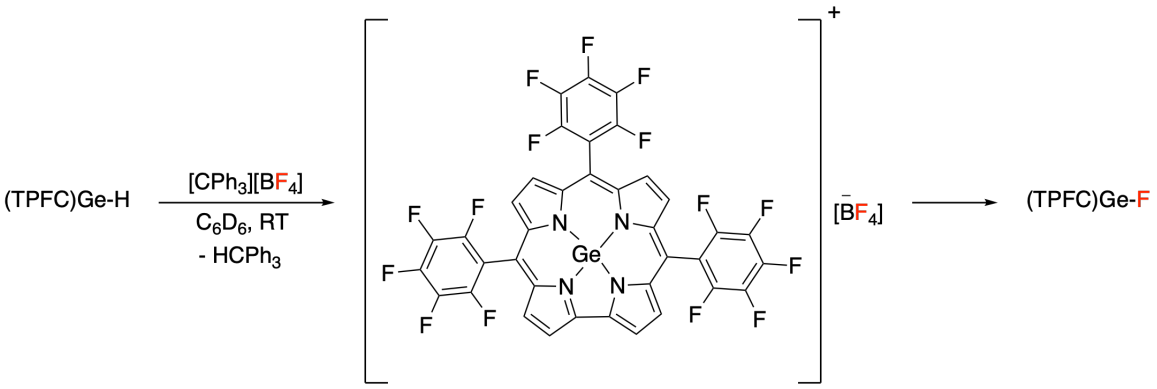

Scheme 2.15: Use of $[BF_4]$ as a WCA and a F^- source to make (TPFC)Ge–F

The oligogermane $(Ph_3Ge)_3GeF$ **17** was successfully synthesized when **1** was reacted with $[CPh_3][BF_4]$ in benzene at room temperature (Scheme 2.16).

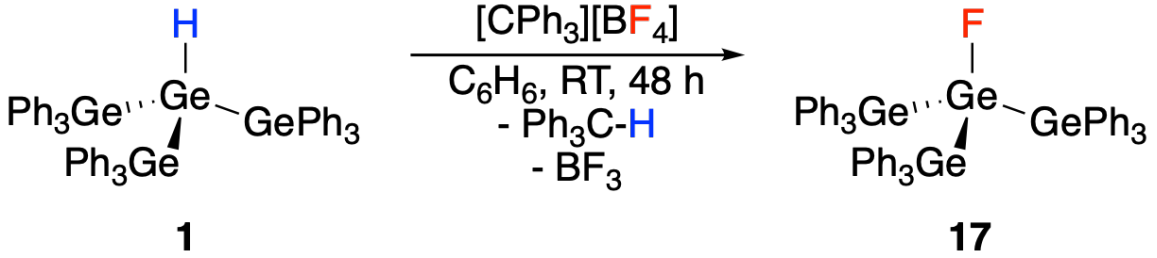

1 **17**

Scheme 2.16: Successful synthesis of $(Ph_3Ge)_3GeF$ by $[CPh_3][BF_4]$

The ^{19}F-NMR spectrum of the reaction mixture (Figure 2.12) shows two different compounds signals at -202.32 ppm and -194.64 ppm with a ratio of 5.7:1. The upfield signal is due to Ph_3GeF and the other peak is assigned to **17**.[58,59]

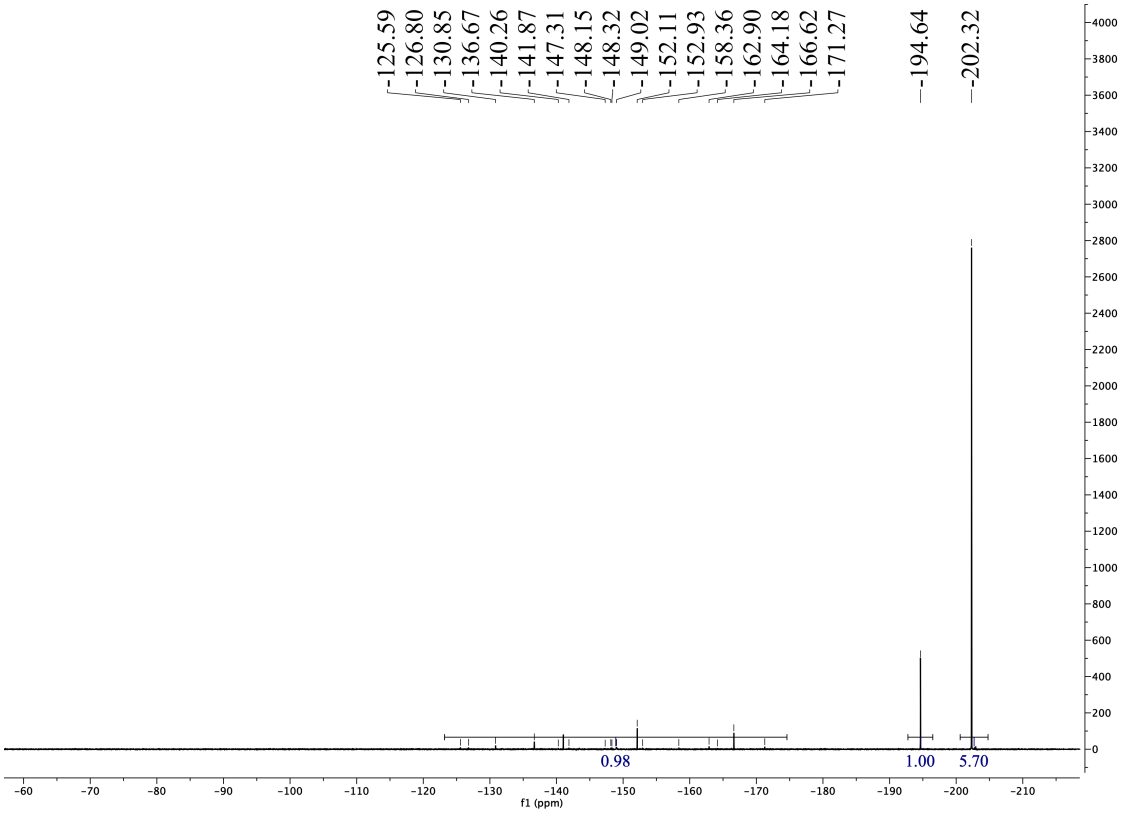

Figure 2.12: ^{19}F-NMR (376 MHz, C_6D_6) spectrum of the reaction of **1** and $[CPh_3][BF_4]$

The presence of Ph_3GeF in the reaction mixture was also shown in the ^{13}C-NMR spectrum of the reaction mixture (Figure 2.13), where the signals at δ 134.6, 134.5, 130.8, and 128.9 ppm correspond to Ph_3GeF.

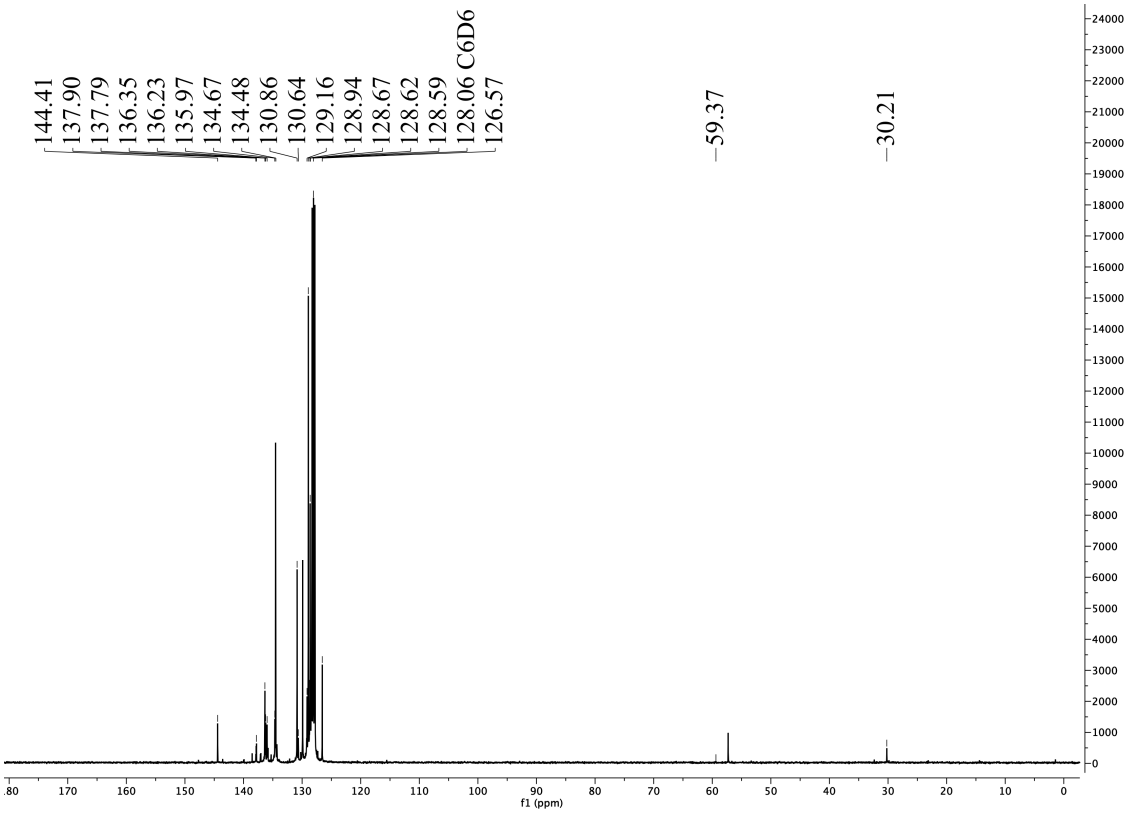

Figure 2.13: ^{13}C-NMR (101 MHz, C_6D_6) spectrum of the reaction of **1** and $[CPh_3][BF_4]$

The formation of Ph_3GeF along with **17** highlights the fact that the germylium intermediate **13**.[WCA] is not stable in solution, and this instability is thought to be the source of other unidentified products in the crude reaction mixture. Upon removal of the solvent *in vacuo* a light brown solid resulted that was not crystalline but contained a small amount of needle-like crystals. The pure form of **17** was obtained by the addition of hexane to a toluene mixture of the crude product and letting it evaporate slowly to 1/3 of the original volume, where colorless crystals of pure **17** were obtained.

2.2.4 Properties of $(Ph_3Ge)_3GeF$

Crystals of **17** that were suitable for X-ray crystallography were grown by the slow evaporation of a toluene solution of pure **17**. Figure 2.14 shows the ORTEP diagram

of **17**.C_6H_6. This structure is disordered and 39% of the time a chlorine atom is present in place of the fluorine atom. The source of this disorder is identified to be the presence of trace amounts of Cl^- in the reaction mixture from earlier steps of the synthesis of Ph_3GeNMe_2 from Ph_3GeCl and $LiNMe_2$. After the formation of the cationic intermediate **13**.[WCA] a chlorine atom was abstracted and resulted in the formation of **14** ($(Ph_3Ge)GeCl$). This disorder happened to a very small extent and occurred in the X-ray studies because only a small fraction of the reaction product yielded suitable crystals. In addition, **14** was not present in the bulk of the product and was not observed by ^1H and ^{13}C-NMR and elemental analysis. Non-disordered crystals of **17** could not be acquired despite several attempts.

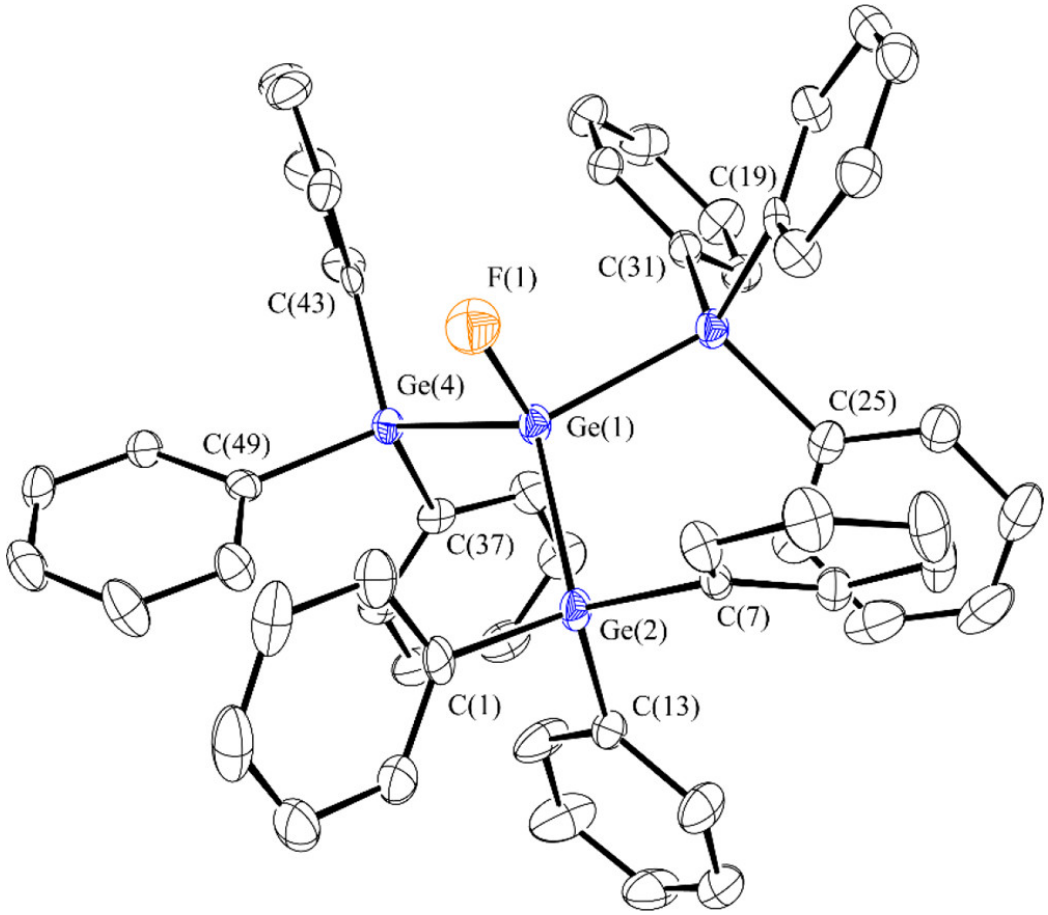

Figure 2.14: ORTEP diagram of $(Ph_3Ge)_3GeF.C_6H_6$, drawn at the 50% probability level. Disordered Cl atom and the solvent molecule are not shown for clarity

The Ge_4 skeleton of **17**.C_6H_6 is isostructural with those of other branched oligogermane halides (**14-16**).[52] The average Ge−Ge bond distance in **17**.C_6H_6 is 2.4699(8) Å and shows that the halide atom does not change the average Ge−Ge bond distance because the value for **17** is very close to the values of those in **14-16** that are 2.4636(7), 2.4698(4), and 2.4689(6) Å, respectively. The Ge−Ge−Ge bond angle in **17**.C_6H_6 is slightly more acute than in **14** (101.34(4)°), **15** (101.38(2)°), and **16** (100.80(2)°).

Table 2.4 summarizes selected bond distances and angles for **17**. Compared to **14** which has reported Ge−Cl bond distance values of 2.230(1) and 2.215(2) Å,[46] in the distorted portion of **17** that contains $(Ph_3Ge)_3GeCl$, the Ge−Cl bond is shorter (2.192(1) Å).

Table 2.4: Selected crystallographic data for **17**

Bond Distance (Å)			Bond Angle (degree)
Ge(1)-Ge(2)	2.4751(8)	F(1)-Ge(1)-Ge(2)	103.3(6)
Ge(1)-Ge(3)	2.4708(8)	F(1)-Ge(1)-Ge(3)	104.2(6)
Ge(1)-Ge(4)	2.4637(8)	F(1)-Ge(1)-Ge(4)	102.1(5)
Ge(1)-F(1)	1.801(1)	Ge(2)-Ge(1)-Ge(3)	111.89(3)
Ge(1)-Cl(1)	2.192(1)	Ge(2)-Ge(1)-Ge(4)	118.82(3)
Ge(2)-C(1)	1.946(5)	Ge(3)-Ge(1)-Ge(4)	114.16(3)
Ge(2)-C(7)	1.961(5)	C(1)-Ge(2)-C(7)	107.0(2)
Ge(2)-C(13)	1.925(6)	C(1)-Ge(2)-C(13)	109.4(2)
Ge(3)-C(19)	1.964(5)	C(7)-Ge(2)-C(13)	111.2(2)
Ge(3)-C(25)	1.946(5)	C(19)-Ge(3)-C(25)	107.8(2)
Ge(3)-C(31)	1.950(5)	C(19)-Ge(3)-C(31)	109.1(2)
Ge(4)-C(37)	1.942(5)	C(25)-Ge(3)-C(31)	107.7(2)
Ge(4)-C(43)	1.953(5)	C(37)-Ge(4)-C(43)	109.6(2)
Ge(4)-C(49)	1.956(5)	C(37)-Ge(4)-C(49)	108.4(2)
		C(43)-Ge(4)-C(49)	104.6(2)

The space group of the crystal lattice of **17** is $P2_1/n$ and is different compared to the space group of the reported two forms of **14** which is $P2_1$. A survey of the Cambridge Crystallographic database indicates structures containing Ge−F are somewhat rare as there are approximately only 30 hits. However, the Ge−F bond distance in **17** (1.801(1) Å) is in the range of other reported values.[57–80]

The Ge–F bond distance in **17** is slightly longer than that in Ph_3GeF, which is 1.749(2) Å, but is comparable to other compounds that have Ge–F bonds. The reported Ge–F bond values range from 1.629(3) Å in (o-$Mes_2C_6H_3$)$_2$Ge(H)–F,[69] to 1.839(2) Å in (3-^{t}Bu–6-(OMe)C_6H_3)$_3$CGeF_3,[76] and 1.867(2) Å in the hypervalent germanium anion (4-methyl-1,4-diazonia- cyclohex-1-yl)methylgermanate.[61] The only other compound that has been reported that has both Ge–F and Ge–Ge bonds (Figure 2.15) was synthesized by Power *et al.*[60] In this cationic compound the Ge–Ge bond is supported by two silver atoms and the Ge–F bond distance is 1.795(5) Å. This reveals **17** to be the only crystallographically characterized example of a compound that has both Ge–Ge and Ge–F bonds present, where the Ge–Ge bond is not supported by another atom.

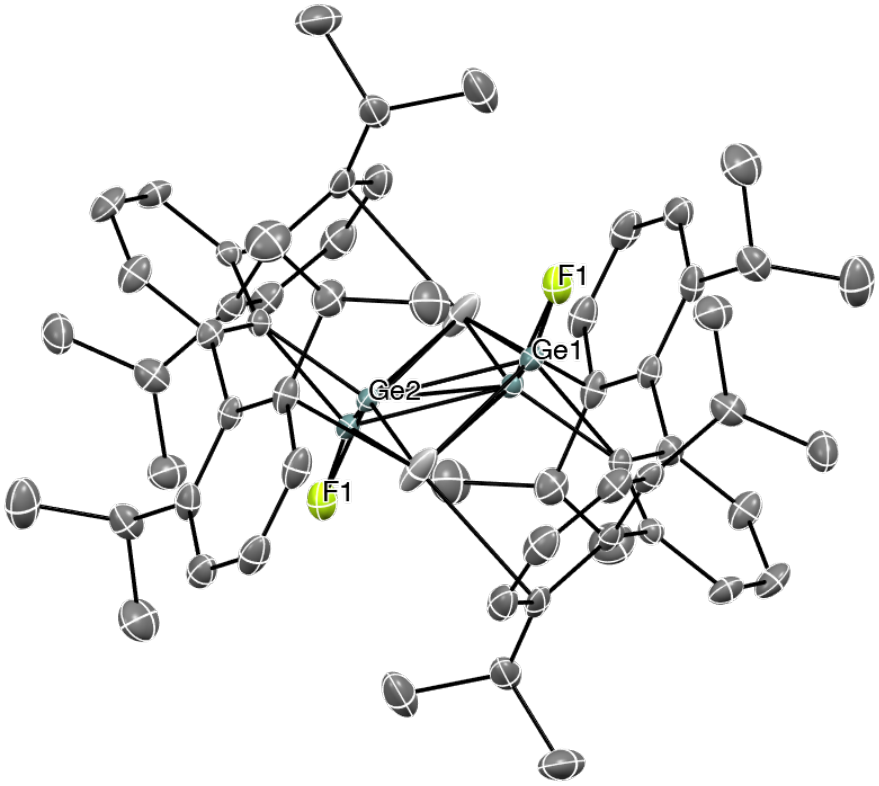

Figure 2.15: ORTEP diagram of the only other reported compound that has Ge–Ge and Ge–F bonds (both of the disordered core arrangements are shown.)

To investigate the electrochemical properties of **17**, CV and DPV studies were conducted in dichloromethane solvent using $[^nBu_4N][PF_6]$ as the supporting electrolyte. Figure 2.16 shows the CV and DPV of **17**, which contain an irreversible oxidation peak at 1725 mV in the CV and at 1680 mV in the DPV. The oxidation potential measured by CV decreases in the series for $(Ph_3Ge)_3Ge–X$ (X = F **17**, Cl **14**, Br **15**, I **16**) due to the decrease of the electronegativity of the halogen atom. As the oxidation potentials are 1668, 1656 and 1643 mV for **14**, **15** and **16**, respectively.[46]

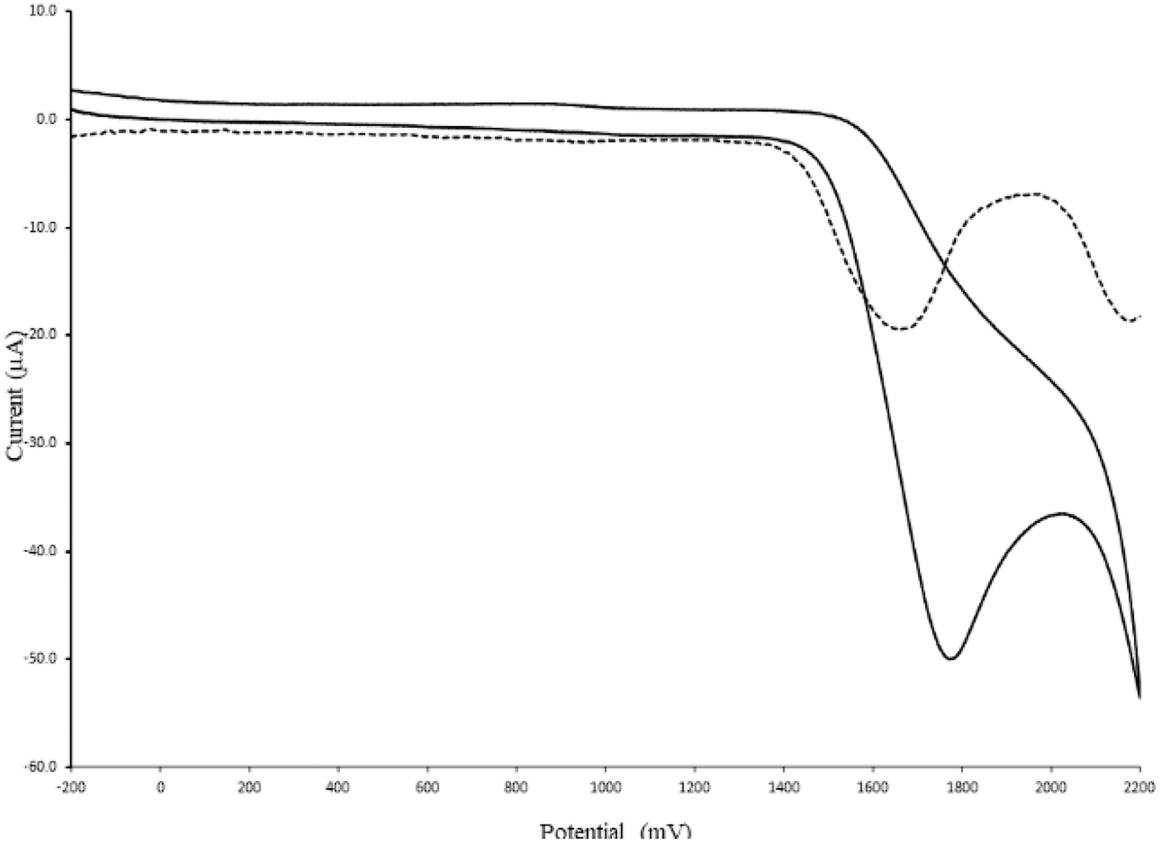

Figure 2.16: CV and DPV of **17** in CH_2Cl_2 solvent using 0.1 M $[^nBu_4N][PF_6]$ as the supporting electrolyte

The electronic properties of **17** were studied by UV-Vis spectroscopy and unlike **14**, **15**, and **16** that show we distinct absorbance maxima at 245, 264 and 271 nm, respectively, **17** is a shoulder at 240 nm. As expected, electronegative fluorine atom causes a blue shift in the absorbance maxima compared to the other branched halides.[46]

In order to better understand the experimental data, DFT calculations were performed on **17**. The energy and shapes of the frontier molecular orbitals of **17** in Figure 2.17 show that the HOMO of **17** is mainly localized on fluorine and the phenyl rings and is not localized much on the Ge_4 skeleton. The LUMO of **17** is mainly distributed on the four germanium atoms and has some presence on the phenyl rings and fluorine atom. The general features of the HOMO and LUMO of **17** closely resemble the frontier orbitals in **14** that are also shown in Figure 2.17.[46]

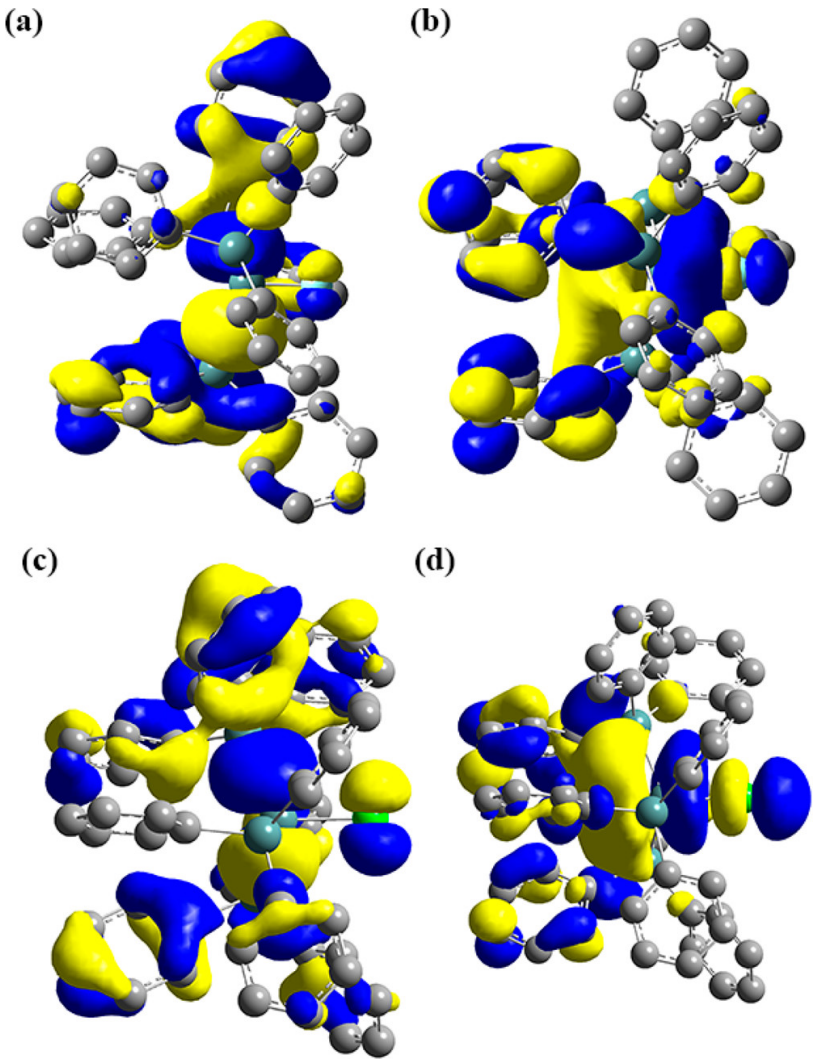

Figure 2.17: Frontier molecular orbitals of a) HOMO, b) LUMO of $(Ph_3Ge)_3GeF$ (**17**) and c) HOMO, d) LUMO of $(Ph_3Ge)_3GeCl$

The HOMO-LUMO gap of **17** calculated by DFT was compared to the computational results for the other experimental data. Because the absolute value of the HOMO and LUMO energies are sensitive to the calculation parameters used, such as the basis set or the number of orbitals involved or their diffuseness, sometimes the calculated ordering of the HOMO-LUMO gaps can be irregular. Table 2.5 shows the DFT calculation results for **14-17**.

Table 2.5: DFT calculations data for **14-17**[46]

Compound	HOMO (eV)	LUMO (eV)	HOMO-LUMO gap (eV)	HOMO-LUMO gap (nm)	λ_{max} (nm)	E_{ox} (mV)
$(Ph_3Ge)_3GeF$	-5.958	-0.850	5.108	242.7	240	1725
$(Ph_3Ge)_3GeCl$	-6.069	-0.990	5.079	244.1	245	1668
$(Ph_3Ge)_3GeBr$	-6.050	-0.950	5.100	243.1	264	1656
$(Ph_3Ge)_3GeI$	-5.997	-1.315	4.682	264.8	271	1643

It was expected that the fluorine atom would stabilize the HOMO and increase the HOMO-LUMO gap of **17** compared to the rest of the series. This trend was supported by the increasing trends observed in the energy for λ_{max} and the oxidation potentials observed in the CV and DPV. However the HOMO energy of **17** was calculated to be -5.95 eV, and therefore, **17** had the highest calculated HOMO in the series. This irregularity did not agree with the experimental results and was attributed to the fact that the 2p orbital of fluorine in **17** was significantly contracted, and thus had a smaller contribution to the HOMO, while, in **14-16** the 2p orbitals were larger and had greater contributions to the HOMO.

Pure **17** can be obtained by successive recrystallizations from toluene and hexane solutions. ^{1}H-NMR spectrum of **17** (Figure 2.18) shows three signals in the aromatic region for the phenyl rings at 6.9, 7.0, and 7.3 ppm. ^{13}C-NMR (Figure 2.19) of pure **17** contains four peaks corresponding to carbons of the phenyl rings at 127.9, 128.6, 136.2, and 136.3 ppm. The ^{19}F-NMR spectrum of **17** (Figure 2.20) shows a signal at -194.70 ppm which is shifted downfield compared to the signal of Ph_3GeF observed at -202.40 ppm.

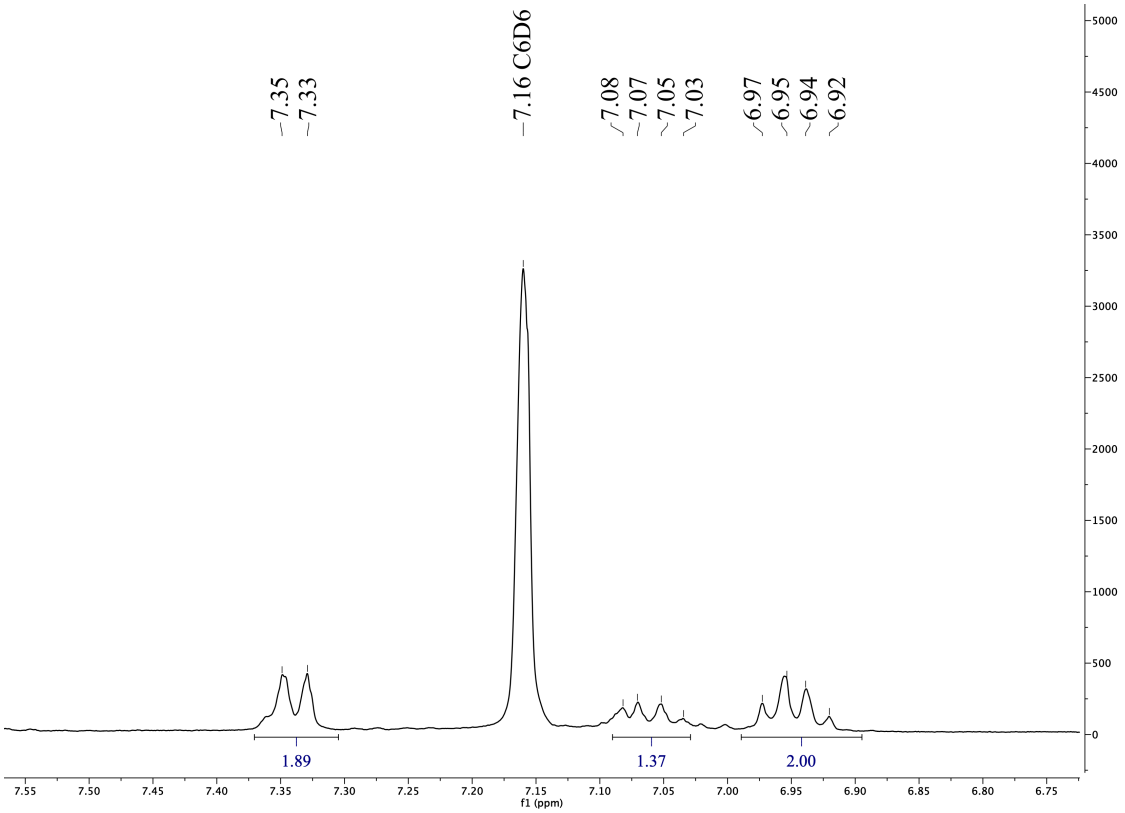

Figure 2.18: ^{1}H-NMR (400 MHz, C_6D_6) spectrum of **17**

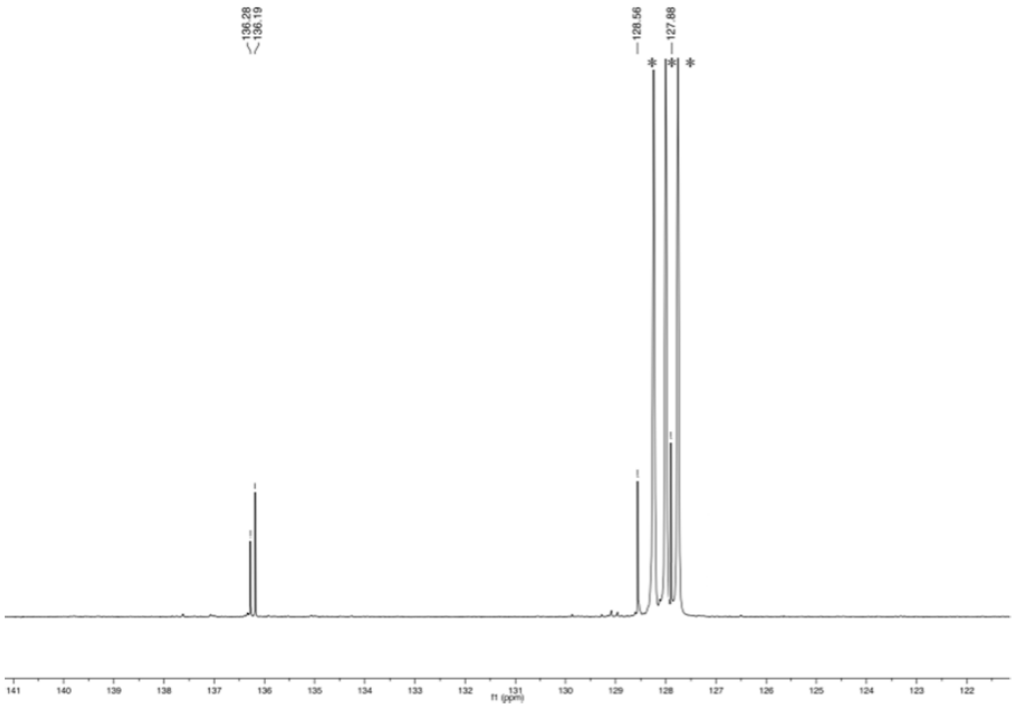

Figure 2.19: ^{13}C-NMR (101 MHz, C_6D_6) spectrum of **17**

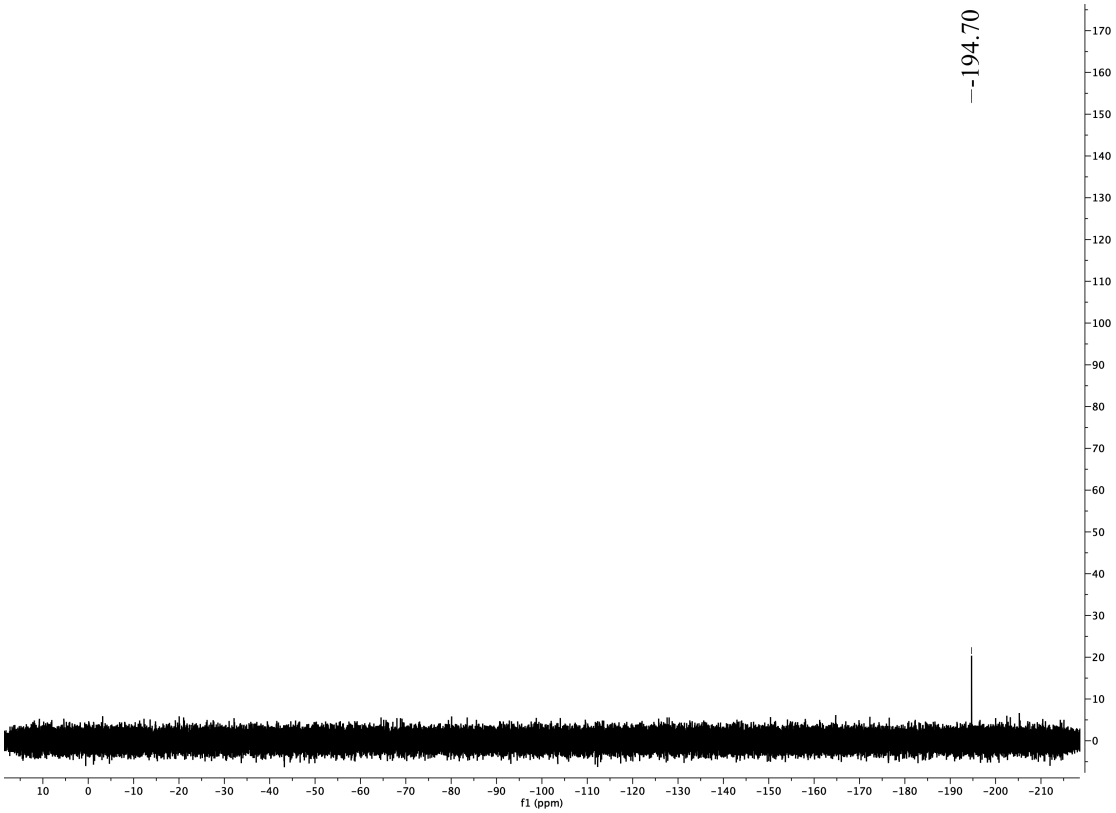

Figure 2.20: ^{19}F-NMR (376 MHz, C_6D_6) spectrum of **17**

In order to investigate the presence of hydrogen bonding in **17**, variable temperature ^{19}F-NMR experiments were conducted. A pure sample of **17** dissolved in toluene-d_8 was prepared and the ^{19}F-NMR spectrum was obtained in the temperature range 60 to -60 °C. Table 2.6 summarizes the results and as can be seen in Figure 2.21, the signal for fluorine atom gets broader and shifts downfield from -194.94 ppm to -193.16 ppm as the temperature decreases. This increase in shielding at higher temperatures is attributed to the more effective anisotropic shielding effects of the neighboring phenyl rings at higher temperatures.

Table 2.6: Variable Temperature ^{19}F-NMR Spectral Data for **17**

Temperature (°C)	δ (ppm)	$\Delta_{1/2}$ (Hz)
-60	-193.16	28
-40	-193.92	16
-20	-194.41	8
0	-194.73	8
20	-194.89	6
40	-194.94	6
60	-194.94	6

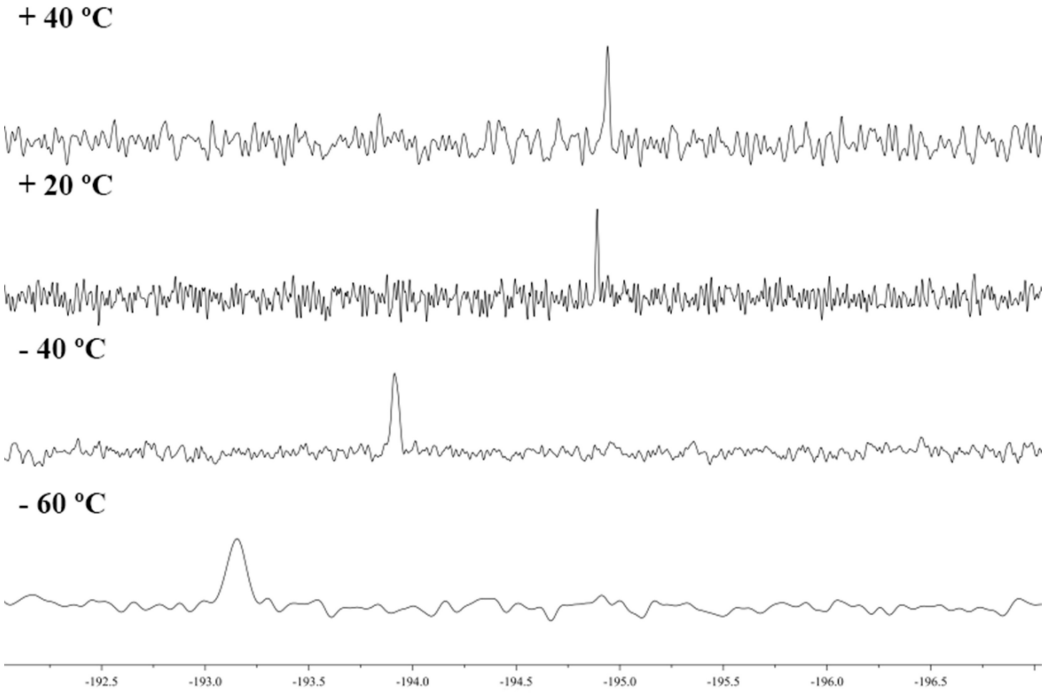

Figure 2.21: Expansion of the variable temperature ^{19}F-NMR (376 MHz, C_7D_8) spectrum of **17**

2.2.5 Isolation of $[(Ph_3Ge)_3Ge^+].[WCA]$

All attempts to isolate **13**.WCA were unsuccessful and different WCAs such as $[CHB_{11}H_{11}]$ or $[B(C_6F_5)_4]$ did not yield the desired compound. One the most common methods for making germylium ions is by using a hydride transfer reaction, also known as Bartlett-Condon-Schneider reaction.[81] In this reaction, a hydride R_3GeH is reacted with a very strong Lewis acid (CPh_3) to form neutral $H-CPh_3$ and the cation

(R_3Ge^+.WCA). Scheme 2.17 shows how this method is used to isolate a 4-coordinate germylium.[?]

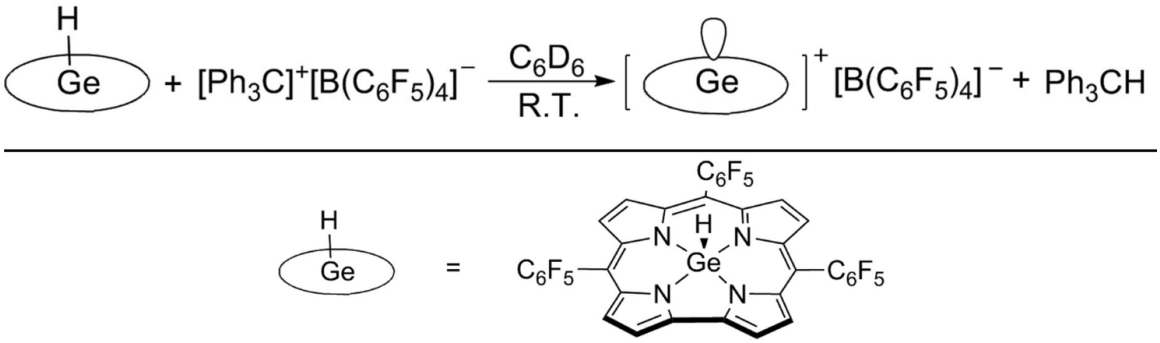

Scheme 2.17: A 4-coordinate germanium ion synthesized by hydride abstraction

In one attempt, $(Ph_3Ge)_3GeH$ **1** was dissolved in toluene and after the addition of $[CPh_3][B(C_6F_5)_4]$, the solution was heated until all the solids were dissolved and then was let to cool down to room temperature slowly. The resulting crystals from this procedure were found to be tetraphenylgermane Ph_4Ge. In other experiments, a variety of other WCAs, such as $[PF_6]^-$ or coordinating solvents like acetonitrile were used and none resulted in isolation of the target cation.

It was determined that most common WCAs were not weakly-coordinating enough to stabilize the branched cation **13** and usually one step in the degradation of the cation was the donation of a halide anion from the WCA to the germylium ion. Among the few reported examples of isolated germylium ion $[B(C_6F_5)_4]^-$ was shown to be a good choice for the WCA. But again, when isolation of **13** was focused on using $[CPh_3][B(C_6F_5)_4]$ using different conditions, all attempts failed. When **1** is reacted with $[CPh_3][B(C_6F_5)_4]$ in benzene, a biphasic liquid mixture resulted. A benzene layer is formed on the top and a dark orange oily layer at the bottom. This bottom layer is proposed to be **13**.$[B(C_6F_5)_4]$ which is an ionic liquid. Attempts to stabilize this ionic liquid with more donating solvents such as THF, or using shorter reaction times were also not fruitful and resulted in crystals that were determined to be $HCPh_3$ by X-ray crystallography.

Another method to access germylium ions is by reacting a germanium halide (R_3Ge-X (X= Cl, Br)) with a suitable reagent to facilitate the heterolytic cleavage of Ge−X bond. Other attempts were focused on using a different class of WCAs known as alkoxy aluminates ($Al(OR^F)_4$). Scheme 2.18 shows the steps used to prepare [Li][$Al(HFIP)_4$] **19** and [CPh_3][$Al(HFIP)_4$] **20** salts. A modified method used by Krossing *et al.* was used to obtain **19**.[82] Purified lithium aluminum hydride ($LiAlH_4$) and HFIP are refluxed in a Schlenk tube to form **19**.

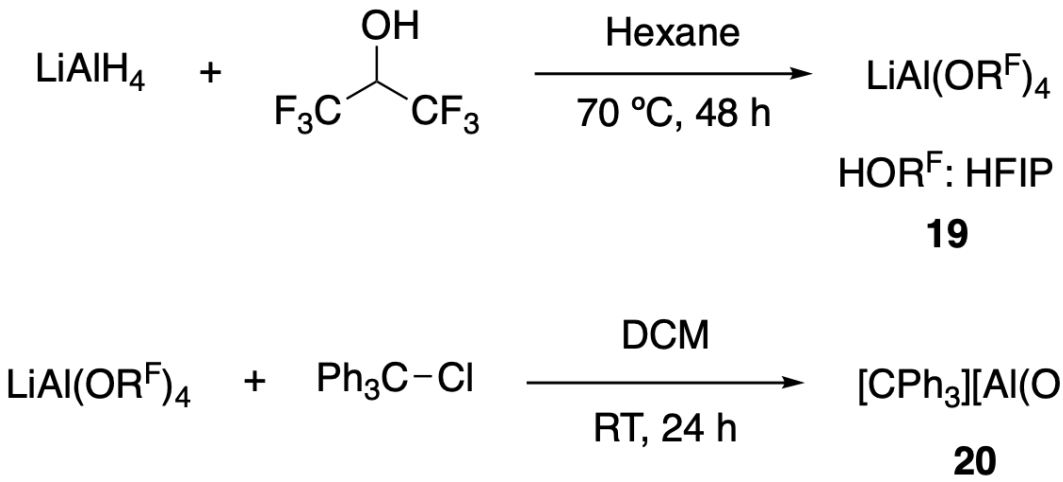

Scheme 2.18: Syntheses of alkoxy aluminates based WCAs

Figure 2.22 shows the ^{1}H-NMR spectrum of **19**. After the addition of 5% THF to $CDCl_3$, the heptet signal at 4.21 ppm that results from coupling of the two $-CF_3$ groups becomes visible. The ^{19}F-NMR spectrum in Figure 2.23 shows a singlet signal at -75.92 ppm for the $-CF_3$ groups of **19**. The key to access high purity **19** is the prior purification of $LiAlH_4$. The purification involves in dissolving the commercial $LiAlH_4$ in diethyl ether and filtering the solution to remove impurities.

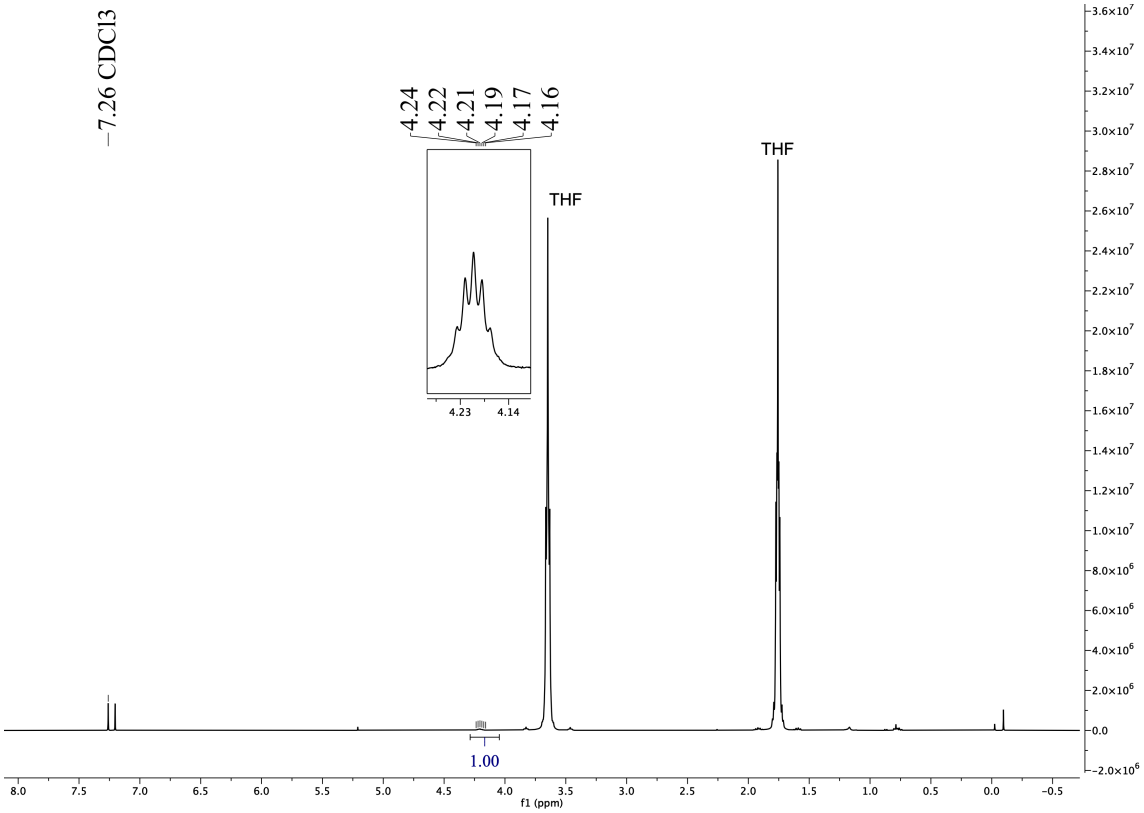

Figure 2.22: ^{1}H-NMR (400 MHz, $CDCl_3$ – 5 % THF) spectrum of **19**

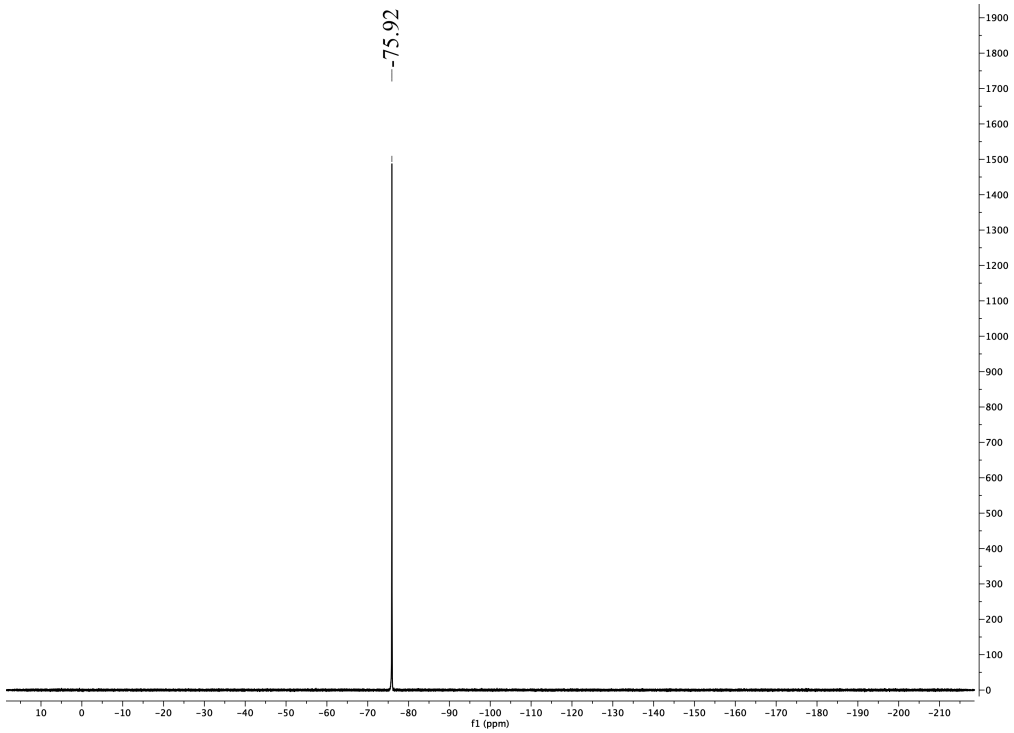

Figure 2.23: ^{19}F-NMR (376 MHz, $CDCl_3$ – 5 % THF) spectrum of **19**

Compound **20** was obtained by reacting **19** with Ph_3CCl in dichloromethane solution at ambient temperature.[83] Figure 2.24 shows the ^{1}H-NMR spectrum for **20**. The signal at 4.35 ppm is due to the C−H in the alkoxide and lower field signals (7-8 ppm) are due to the tritylium phenyl protons. The $\{^1H\}$-^{19}F-NMR spectrum of **20** (Figure 2.25) shows a singlet peak at -76.94 ppm which becomes a doublet when it is proton-coupled (Figure 2.26).

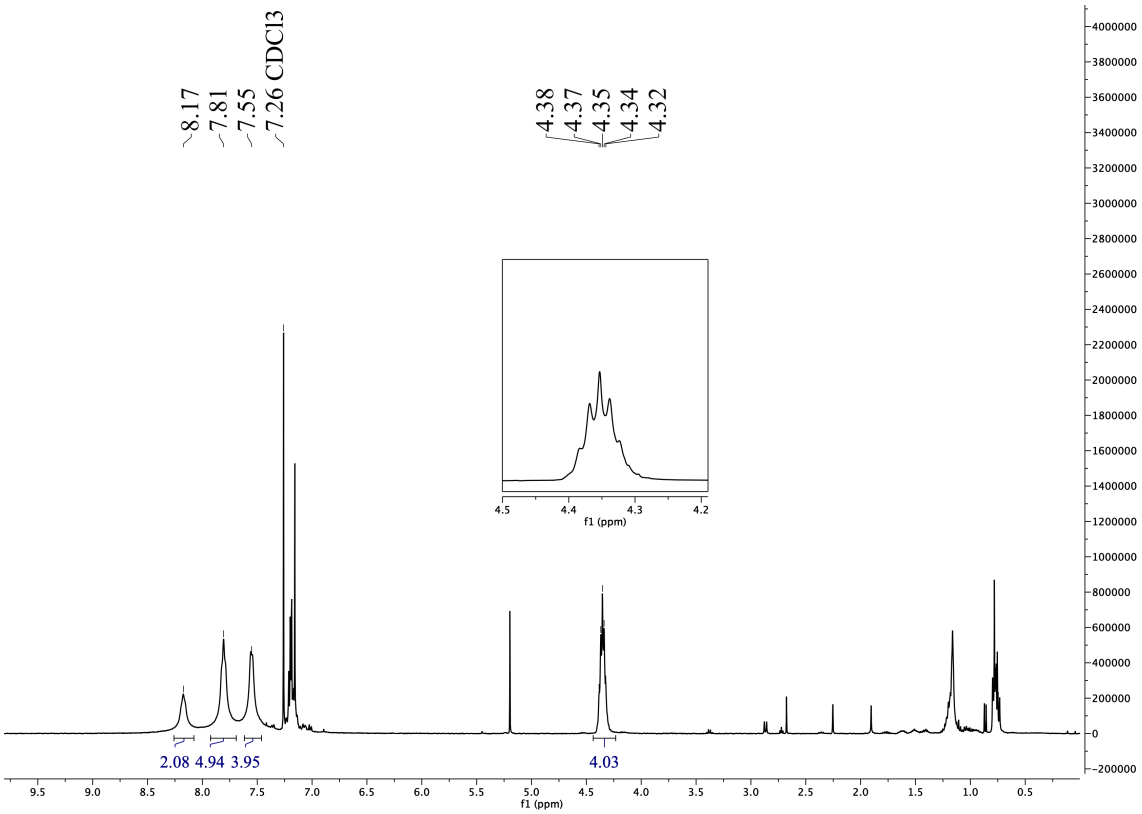

Figure 2.24: ^{1}H-NMR (400 MHz, $CDCl_3$ – 5 % THF) spectrum of **20**

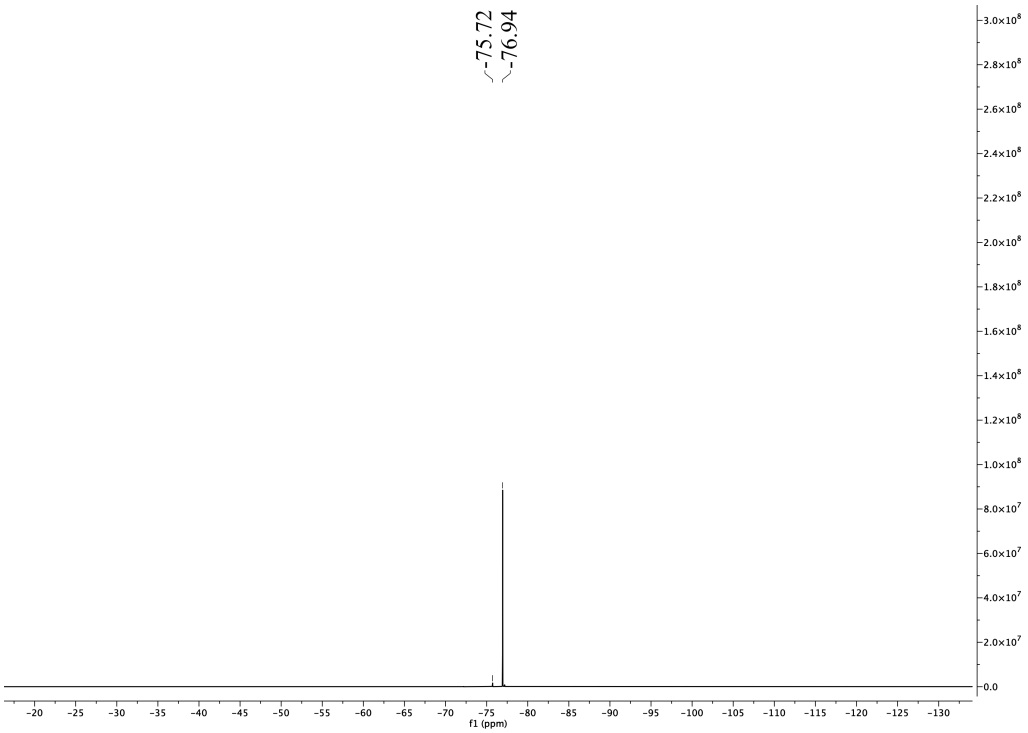

Figure 2.25: ^{19}F-NMR (376 MHz, $CDCl_3$ – 5 % THF) spectrum of **20**

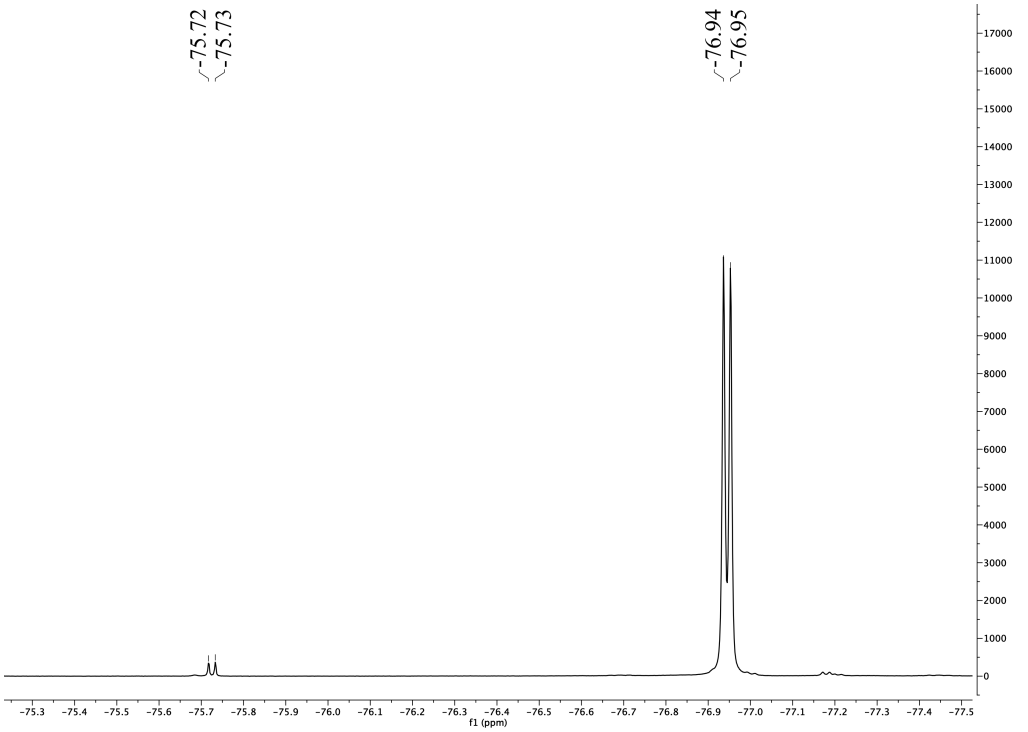

Figure 2.26: $\{^1$H$\}$-^{19}F-NMR (376 MHz, $CDCl_3$ – 5 % THF) spectrum of **20**

In an attempt to isolate **13**.Al(HFIP)$_4$, **1** was reacted with **20** in a benzene solution at room temperature for 30 minutes. The conversion was confirmed by observation of the resonance of Ph_3CH in the ^{1}H-NMR spectrum of the reaction mixture at 5.42 ppm. The ^{19}F-NMR spectrum of the reaction (Figure 2.27) shows four different doublet fluorine signals for $-CF_3$ groups on HFIP, but unfortunately suitable crystals for further analysis could not be obtained.

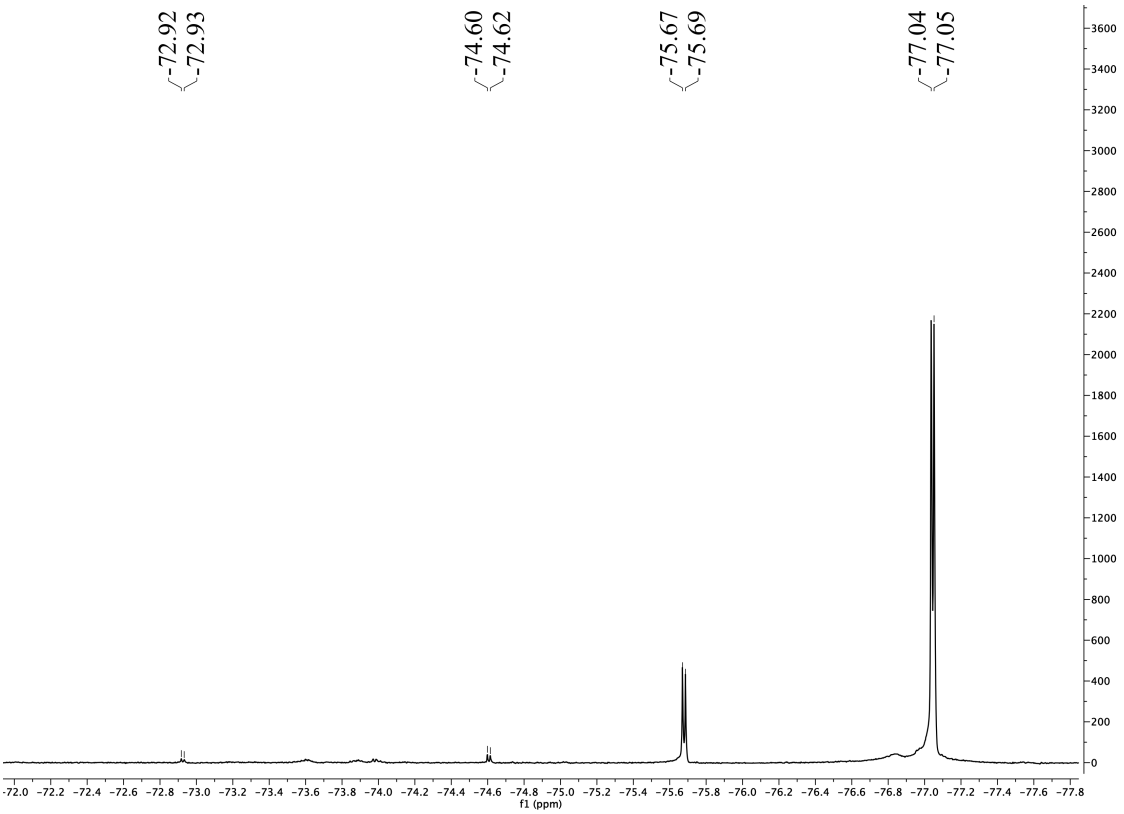

Figure 2.27: ^{19}F-NMR (376 MHz, C_6D_6) spectrum of the attempted reaction to isolate **13**.Al(HFIP)$_4$

2.2.6 Stability of [$(Ph_3Ge)_3Ge^+$].[WCA] in Solution

After numerous repeated attempts, NMR and crystallographic data suggest that **13**.WCA is very unstable in solution and can undergo rearrangements. The recent study by Fu *et al.*, shows that germylium ions can react as electrophiles in Friedel-Crafts reactions or in small molecule activation reactions (Scheme 2.19).[57]

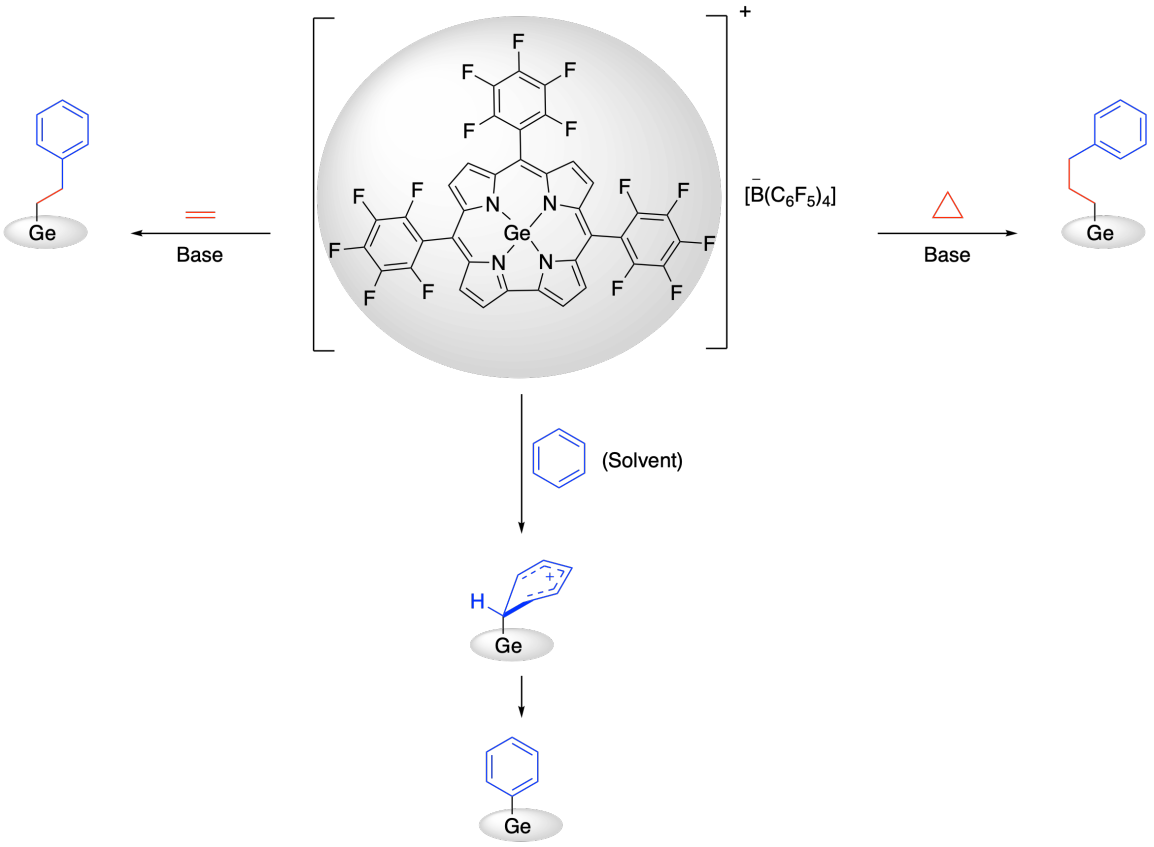

Scheme 2.19: Electrophilic reactivity of a 4-coordinate germylium in a Friedel-Crafts reaction with the solvent (benzene) and small molecules

Obtaining crystals of Ph_4Ge several times in attempts to isolate the germylium ion suggested that **13**.WCA can rearrange and reacts with benzene in a similar fashion to that shown in Scheme 2.19. Other hints that point to the possibility of rearrangements are also explainable. It can be expected that since the **13** cation is a tertiary cation it should be relatively stable. Furthermore, X-ray data by Schnepf *et al.* show that the shortening in the Ge–C bond in Ar_3Ge^+ suggests the interaction between the empty $4p_z$ orbital of the germanium cation and the π electrons of phenyl substituents. Scheme 2.20 shows the possible resonance forms for Ph_3Ge^+.[84]

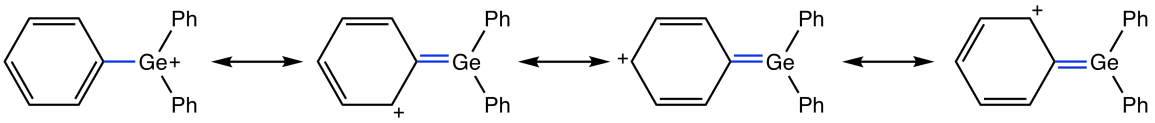

Scheme 2.20: Resonance forms of cation Ph_3Ge^+

In order to assess the stability of **13**.BF_4 in solution a series of timed ^{19}F-NMR experiments were conducted in benzene-d_6 of the reaction in Scheme 2.21. Figure 2.28 shows the ^{19}F-NMR spectrum of the reaction mixture in one hour intervals and that was continued to a total of four days measurements. The signal at -125.60 corresponds to the $[CPh_3][BF_4]$ salt and diminishes over time. This in fact is in line with the observations that $[BF_4]^-$ anion is not a good WCA and will lose F^- during the reaction. The signal at -202.35 ppm is for Ph_3GeF **18** and surprisingly is the first and most abundant compound observed in the solution. Later it will be discussed that the reason for this might be that there are more ways for the formation of **18** then there are for **17**. The signal observed at -194.65 is due to the branched fluoride tetragermane **17**.

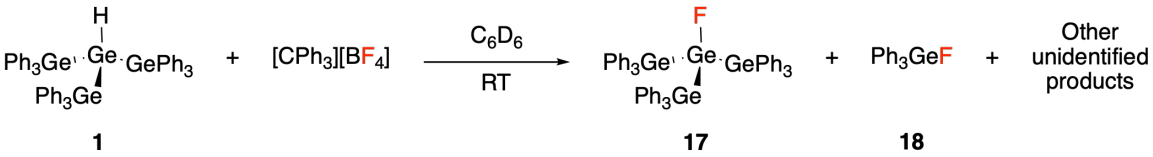

Scheme 2.21: Synthesis of **13**.BF_4 for studying its stability in benzene

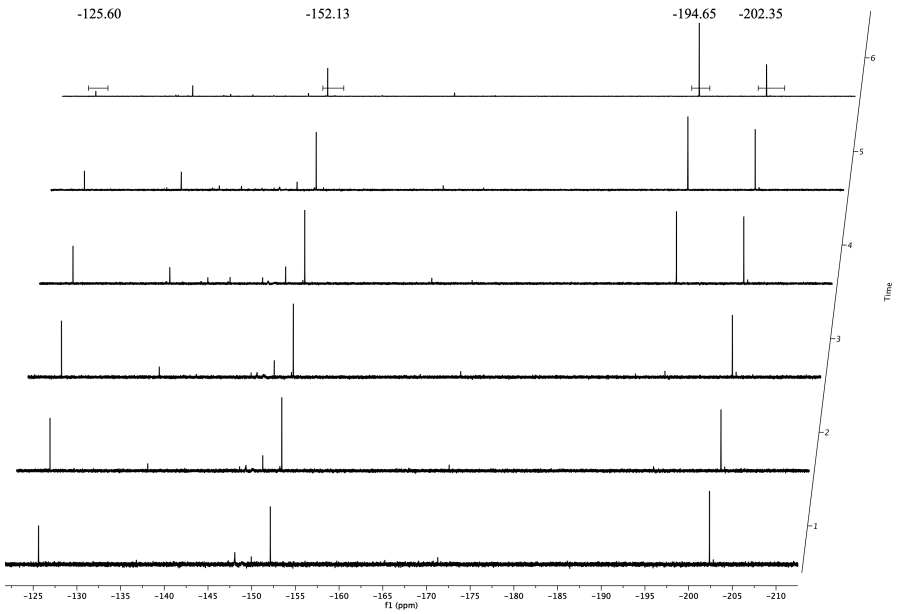

Figure 2.28: The series of timed ^{19}F-NMR (376 MHz, C_6D_6) spectra of the reaction in Scheme 2.21

Figure 2.29 shows several possible aggregates that can be formed in the course of the reaction. In the presence of excess fluoride ion, **18** has the ability to form hypervalent species like **13a**. It has also been suggested that germyliums can form aggregates to stabilize themselves in solution by forming bridged species with present hydride or fluoride species **13a-d**.[59,85,86]

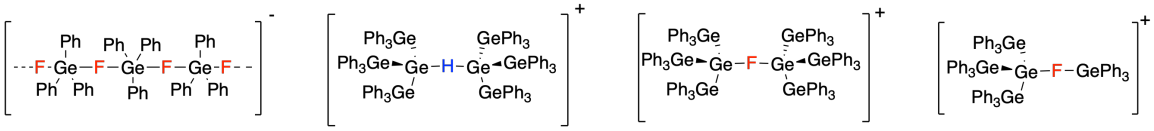

Figure 2.29: Possible aggregates in the reaction of **1** and $[CPh_3][BF_4]$

Figure 2.30 illustrates the ^{19}F-NMR spectrum of the reaction mixture before and after adding D_2O. It was postulated that D_2O would break the aggregates and exchange with fluorine containing compounds in the solution. Upon the addition of D_2O to the reaction mixture, many signals including the supposed signal for **13a** and $[CPh_3][BF_4]$ disappear by either reacting or exchanging with water. However, the signals corresponding to **17** and **18** remain sharp. The signals at -136.66 ppm and -198.17 ppm are unidentified.

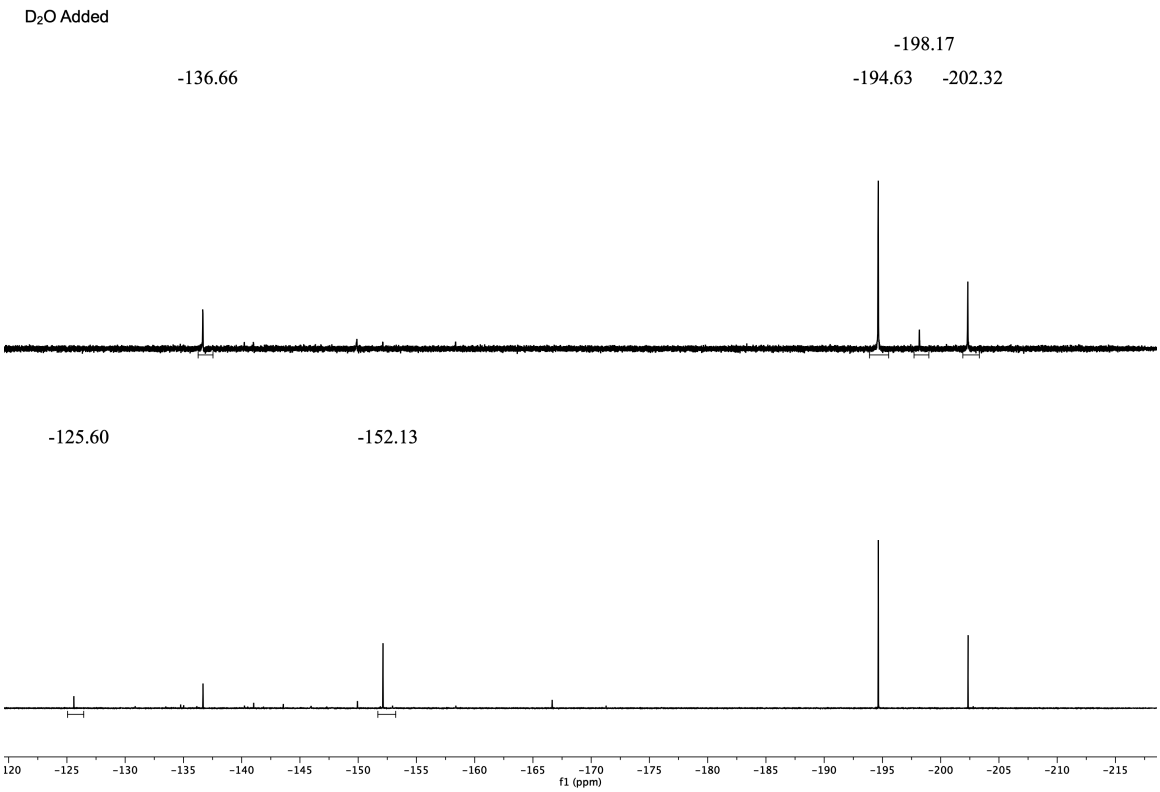

Figure 2.30: ^{19}F-NMR (376 MHz, C_6D_6) spectrum of the reaction, before (bottom) and after (top) adding D_2O

2.2.7 Proposed Degradation Mechanism of 13.BF_4

Spectroscopic and crystal structures data suggest that the cation **13**.BF_4 has the capability of undergoing Friedel-Crafts reaction with benzene. This also strongly suggested the consistent formation of Ph_4Ge crystals in the mixture. While this was discussed in Scheme 2.19, this electrophilic character of germylium ions is not limited to 4-coordinate ones that were prepared by Fang *et al.*[57]

These data also suggest that the germylium intermediate **13**.BF_4 rearranges and at some point produces simpler and theoretically more stable non-branched germylium ions such as Ph_3Ge^+. This behavior is supported by the immediate formation of Ph_3GeF that is clearly visible by ^{19}F-NMR spectroscopy. Muller *et al.* have also demonstrated that the branched germylium ions shown in Scheme 2.22, that bear different substituents, react with the solvent toluene to form Wheland intermediates.[87]

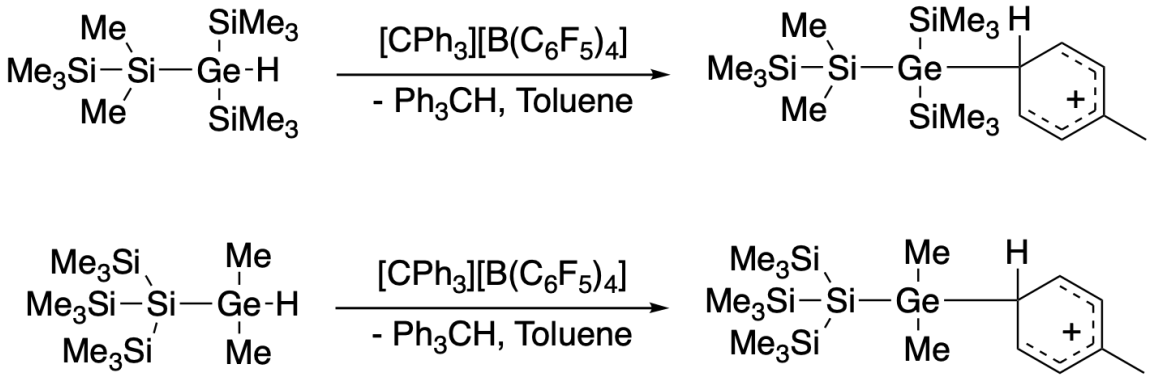

Scheme 2.22: Formation of germyl toluenium ions from the reaction of germyliums and toluene

Scheme 2.23 shows a cascade of proposed reactions that describe the decomposition of **13**.BF_4 in solution. At first **13**.BF_4 is formed and after abstracting a fluorine atom from its counter anion forms **17**. Tertiary **13**.BF_4 then might undergo a rearrangement to form a germylene **21** and the cation Ph_3Ge^+. This cation can then abstract a fluorine atom from $[BF_4]^-$ to form Ph_3GeF, or it can react with benzene to form the Wheland intermediate **22**. It is proposed that germylene **21** can act as a base that converts the Wheland intermediate into Ph_4Ge. The cation formed by the germylene **21a** can abstract a fluorine atom from $[BF_4]^-$ to form **21b** or rearrange again to form the germylene **23** and Ph_3Ge^+. These same steps can then occur to form **23a** and **23b**. In the last step, the **23a** cation rearranges to form germylene (H_2Ge:) **24** which forms the cation **24a** and H_3GeF **24b**.

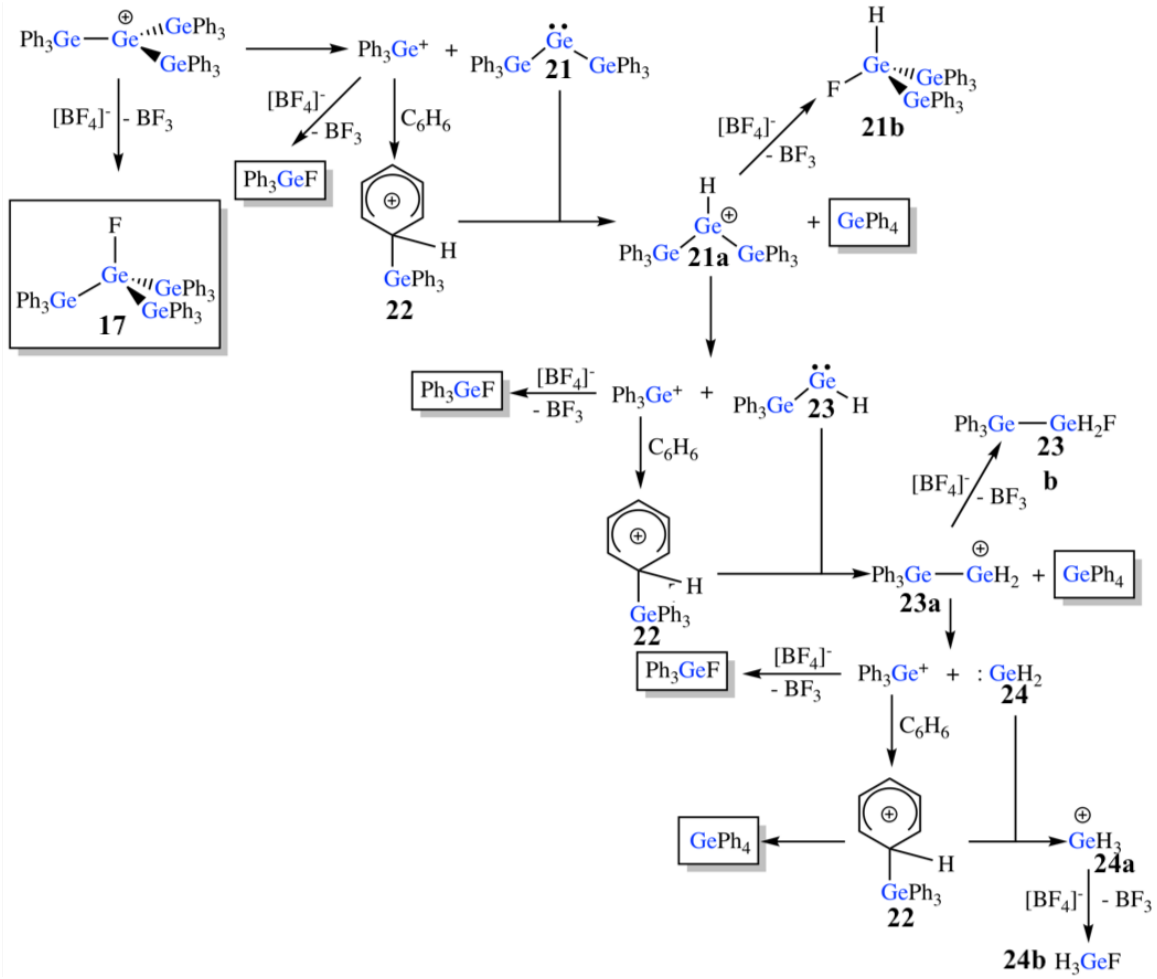

Scheme 2.23: Proposed degradation mechanism of **13**.BF_4 in solution

As summarized in Scheme 2.24, it is indicated that in each step, Ph_4Ge is formed which is consistent with its crystals being prevalent in the reaction mixture product. Germylium ions tend to undergo cleavage of Ge−Ge bonds to form the more stable (by resonance) Ph_3Ge^+ cation. This hypothesis was also tested with other linear branched hydrides. Thus there are three proposed possible pathways to form Ph_3GeF and Ph_4Ge, but only one that leads to formation of $(Ph_3Ge)_3GeF$. This might explain the formation of significant amounts of Ph_3GeF in this reaction.

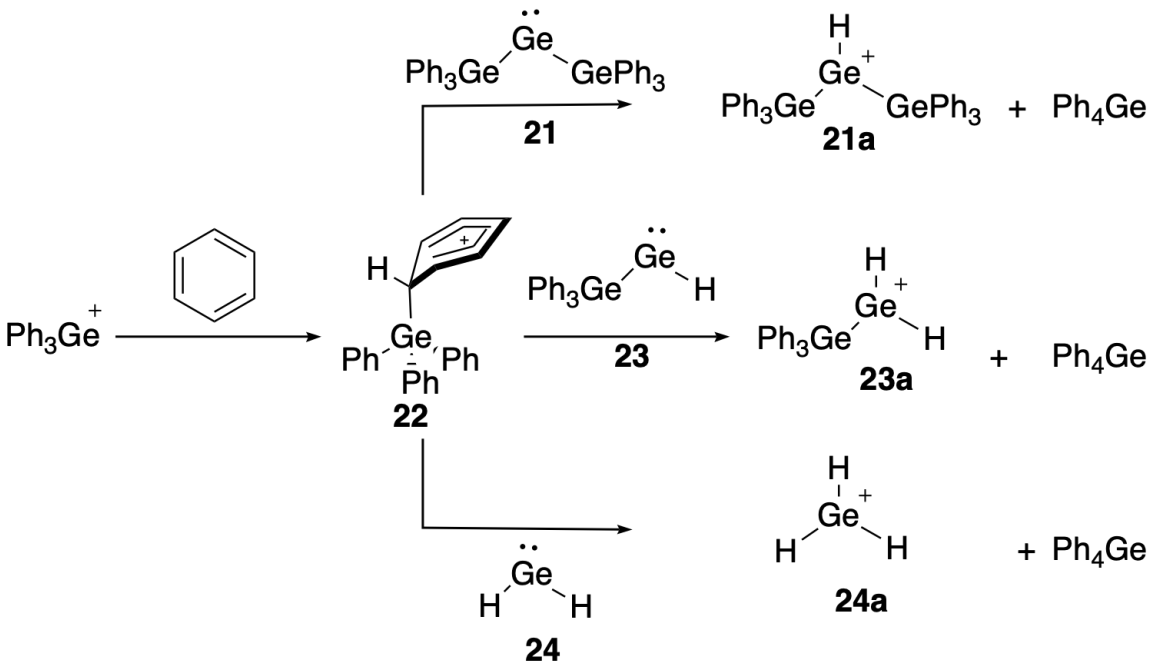

Scheme 2.24: Summary of the key reactions in the proposed degradation mechanism

When the 1,3-dihydrotrigermane H−$(GePh_2)_3$−H and 1,4-dihydrotetragermane dihydride H−$(GePh_2)_4$−H were reacted with $[CPh_3][BF_4]$ in benzene. Both compounds underwent deprotonation that was confirmed by the presence of $HCPh_3$ indicated by a signal at 5.41 ppm in the H-NMR spectra. Figure 2.31 shows the ^{19}F-NMR spectrum for the reaction of 1,3-dihydrotrigermane, in which five fluorine signals are observed at -130.91, -143.39, -148.95, -166.71 and -203.02 ppm. In Figure 2.32, the ^{19}F-NMR spectrum for the reaction of 1,4-dihydrotetragermane again five signals appear in the spectrum at -149.5, -164.2, -166.6, -176.3, -202.3 ppm. Interestingly both reactions result in the formation of Ph_3GeF indicated by the signals at -202.3 ppm, and there are common features such as peaks at -149 and -166 ppm in both spectra. This suggests that the breaking of Ge−Ge bonds upon the formation of a germylium ion can also occur in linear oligogermanes and the degradation will form Ph_3GeF as a by-product.

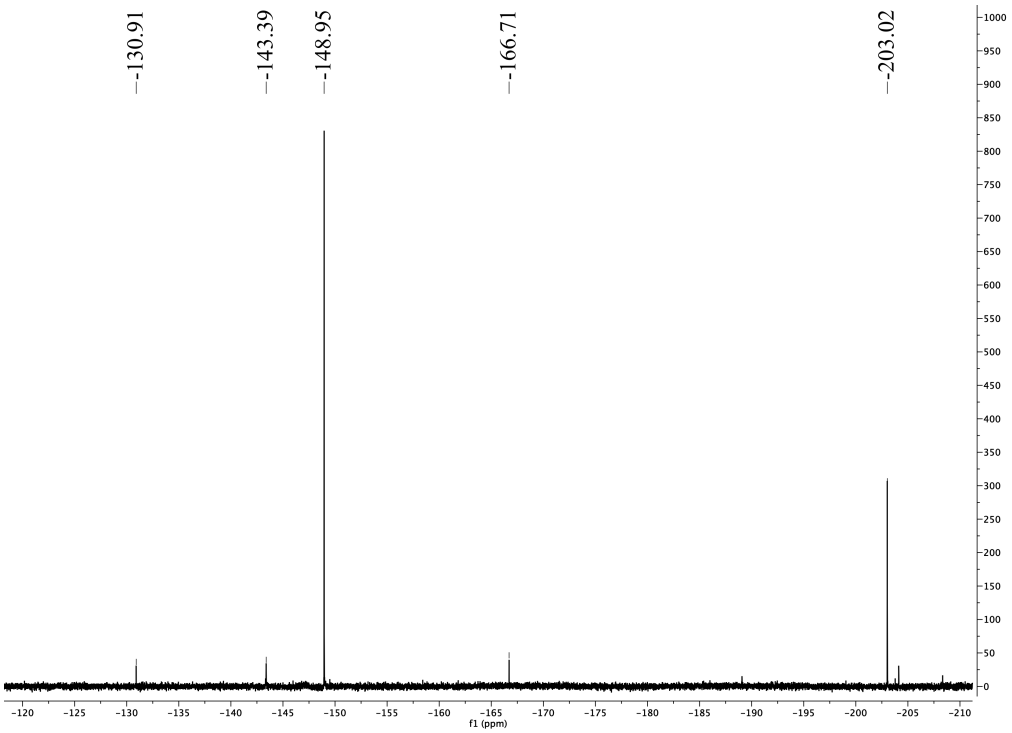

Figure 2.31: ^{19}F-NMR (376 MHz, C_6D_6) spectrum of the reaction of 1,3-trigermane dihydride and $[CPh_3][BF_4]$

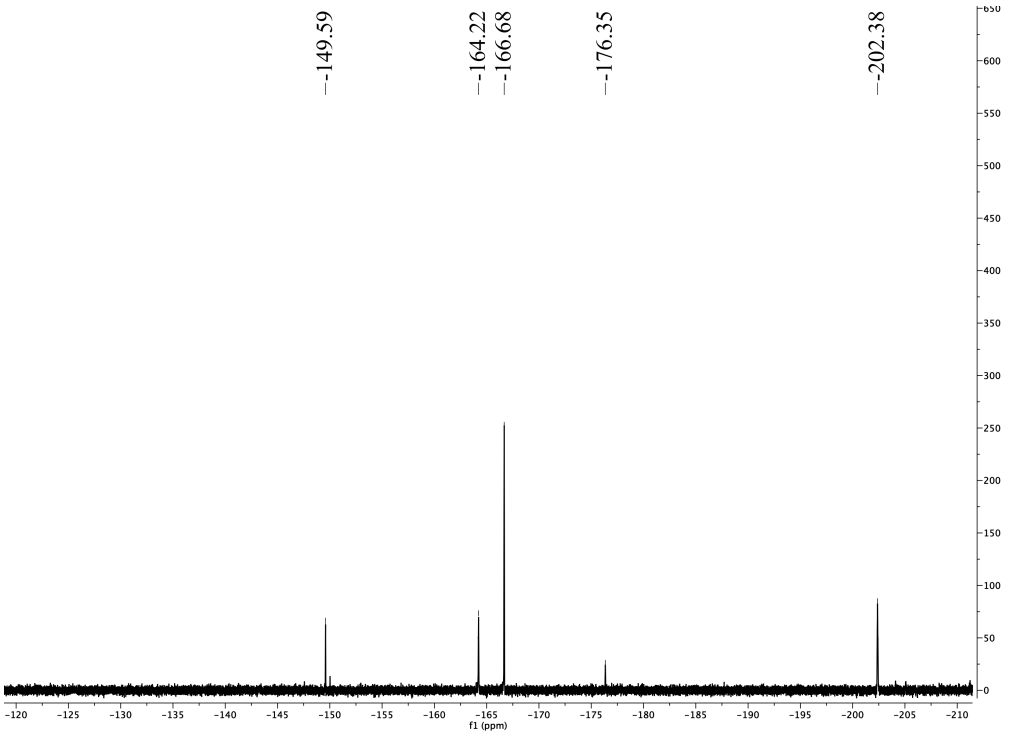

Figure 2.32: ^{19}F-NMR (376 MHz, C_6D_6) spectrum of the reaction of 1,4-tetragermane dihydride and $[CPh_3][BF_4]$

To gain more insight regarding the Lewis acidity and the stability of the cation in **13**.WCA, other reactions were also carried out. One of the questions was to see whether the high FIA of **13**.WCA only happens when $[BF_4]^-$ is the anion which is in the proximity of the Lewis acidic germylium center. To test this, as shown in Scheme 2.25, **13.B(C_6F_5)$_4$** was first synthesized and then was immediately reacted with $LiBF_4$ in a benzene-THF mixture.

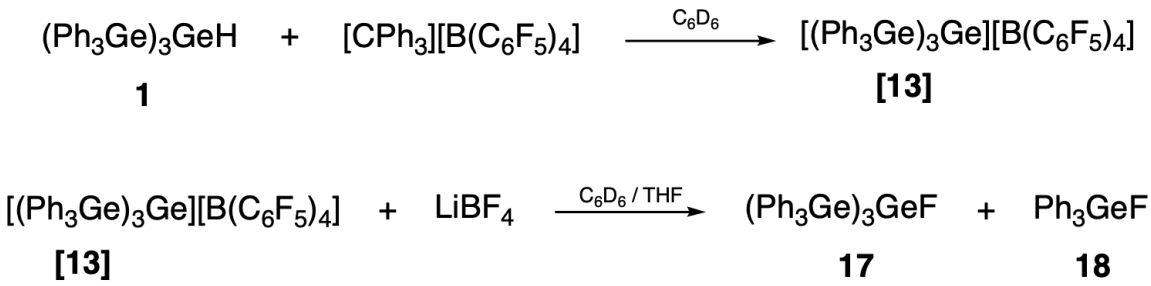

Scheme 2.25: Reaction of **13**.B(C_6F_5)$_4$ and $LiBF_4$

Figure 2.33 shows the ^{19}F-NMR spectra of the reaction mixture at different time intervals. Right after the addition of $LiBF_4$, the dominant compound in the solution is **18** and **17** only forms slightly. This suggests that **13.B(C_6F_5)$_4$** is not a stable cation and is a strong enough Lewis acid to abstract a fluoride atom from $LiBF_4$. The signals at -132, -163 and -167 correspond to the $[B(C_6F_5)_4]^-$ anion. THF had to be used to help transfer $LiBF_4$ to the reaction, so it was used again when $[CPh_3][BF_4]$ was used. When **1** and $[CPh_3][BF_4]$ were reacted in the presence of THF the ^{19}F-NMR (Figure 2.34) indicates the exclusive formation of **18**.

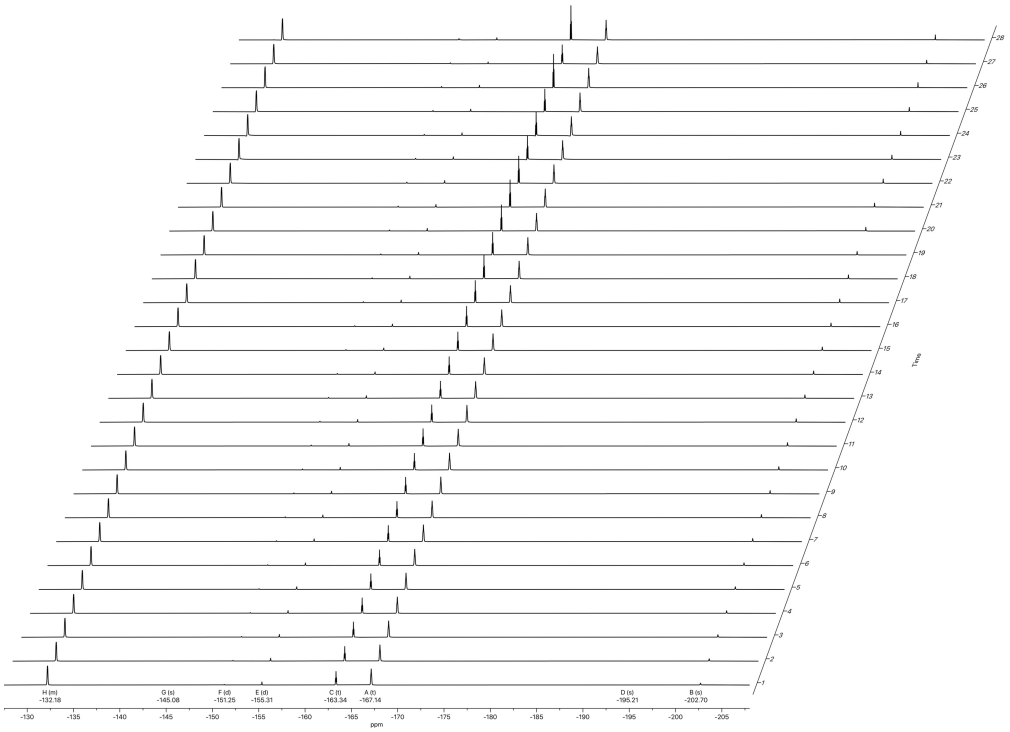

Figure 2.33: ^{19}F-NMR (376 MHz, C_6D_6) spectrum of the reaction of **13**.$B(C_6F_5)_4$ and $LiBF_4$

.

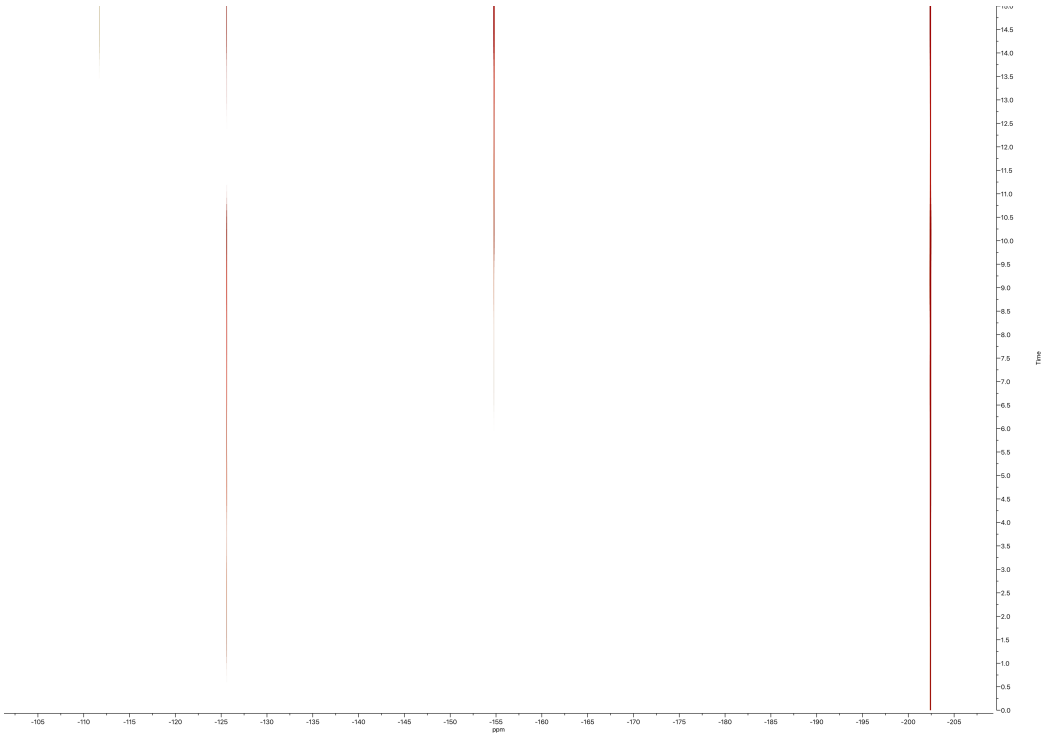

Figure 2.34: ^{19}F-NMR (376 MHz, C_6D_6) spectrum of the formation of **13**.BF_4 in THF

The presence of THF in the reaction mixture was initially thought to be stabilizing by donating electron density to the germylium ion. In contrast, it lead to the exclusive formation of **18** instead of **17**. The reaction shown in Scheme 2.25 was attempted using another WCA. When **13**.$SnCl_5$ was reacted with $LiBF_4$ it did not result in the formation of any fluorinated compounds as no signals were observed in the ^{19}F-NMR spectrum of the reaction mixture over time. It is anticipated that having $SnCl_5$ as the WCA causes **13** to react completely with its WCA to form **14** ($(Ph_3Ge)_3GeCl$) by abstracting a Cl^- from $SnCl_5{}^-$.

It has been elaborately shown that Lewis acids such as BCF ($B(C_6F_5)_3$) are able to form silylium cations from silicon hydrides in solution.[88] To see if **1** is basic enough to form **13**.BCF in solution, the experiment in Scheme 2.26 was conducted. The ^{19}F-NMR spectra of the reaction mixture shows no conversion of Ge−H to Ge−F even after the addition of $LiBF_4$ to the reaction mixture. It also does not indicate any reactions between $LiBF_4$ and BCF to form F−(BCF) anion. It can be concluded that branched hydride **1** is not forming a partially positive germanium center and if there is any equilibrium occurring similar to that shown in Scheme 2.26, it lies to the left.

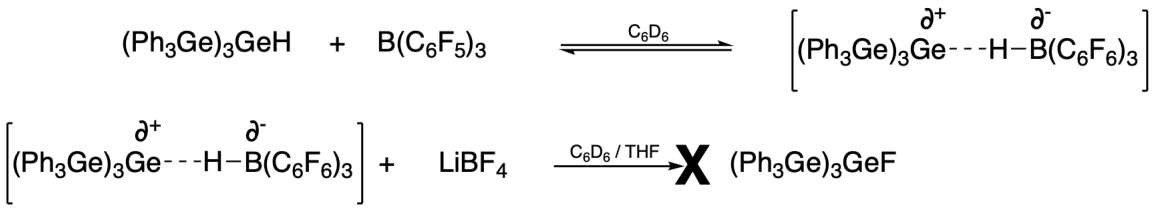

Scheme 2.26: Reaction of **1** with BCF and then $LiBF_4$

2.2.8 ^{73}Ge-NMR Study of $(Ph_3Ge)_3Ge-F$

The only NMR-active isotope of germanium is ^{73}Ge. Its having a large quadrupole moment (I = 9/2) leads to very broad lines especially if the germanium is in an asymmetric environment. Though the natural abundance of ^{73}Ge (7.76 %) is seven times higher than ^{13}C, concentrated samples are required to overcome complications caused by its low resonance frequency 17.4 MHz at a field strength of 11.74 T (^{1}H = 500 MHz).[89]

Many germanium compounds have been studied by ^{73}Ge-NMR and their resonances are referenced to Me_4Ge. The chemical shift for compounds that contain a single germanium atom can vary depending on the environment ranging from 31 ppm for $GeCl_4$ to -1086 ppm for GeI_4 and, intermediate chemical shifts can be observed such as that at -234.3 ppm in $MesGeH_3$. The coordination number of germanium can also affect its chemical shift. For example, hexacoordinate germanium complexes such as $GeCl_4$ (bpy) and $GeCl_4$ (phen) are shielded and have resonances at -313.7 and 319.4 ppm respectively. The upfield shift also occurs in the case of germanium anions, such as the hypervalent $[Ge(NCS)_6]^{2-}$ that shows a germanium signal at -442.5 ppm.[89]

^{73}Ge-NMR of several oligogermanes have been studied by our group. Table 2.7 summarizes the ^{73}Ge-NMR data for these compounds. It can be seen that for an oligogermane with the formula of $(R_3Ge_{peripheral})_3Ge_{central}-R'$ ($R' \neq$ Halides), the signal for central germanium shows up at a higher field compared to peripheral germanium atoms. The presence of H^- or another germanium group ($-GeR''$) will cause a strong shielding effect on the signals compared to when a R' is a phenyl group.[31]

The ^{1}H-coupled ^{73}Ge-NMR spectrum of **1** (Figure 2.35) was measured in benzene and it contains two signals for the central germanium atom and the peripheral germanium atoms. The sharp signal at δ -56 ppm ($\Delta\nu_{1/2}$ = 35 Hz) is assigned to the three peripheral Ph_3Ge- groups and the doublet peak at δ -311 ppm ($\Delta\nu_{1/2}$ = 210

Table 2.7: ^{73}Ge-NMR data for some branched oligogermanes

Compound	δ ($Ge_{peripheral}$) (ppm)	δ ($Ge_{central}$) (ppm)
$(Me_3Ge)_3GePh$ **2e**	-45	-188
$(Me_2{}^tBuGe)_3GePh$ **2h**	n/o†	-207
$(Me_2PhGe)_3GePh$ **2a**	n/o	-204
$(^nBu_3Ge)_3GePh$ **2g**	-33	-195
$(Ph_3Ge)_3GePh$ **2**	n/o	-202
$(Ph_3Ge)_3GeH$ **1**	-56	-311
$(Me_3Ge)_4Ge$ **4b**	-38	-339

† n/o: not observed

Hz) is for the central germanium atom. The coupling constant for this peak is found to be 191 Hz which is approximately twice that observed in aryl germanes that do not contain Ge–Ge bonds ($ArGeH_3$, Ar_2GeH_2, Ph_3GeH), and have $^1J_{Ge-H}$ in the range of 95-98 Hz.[52,90]

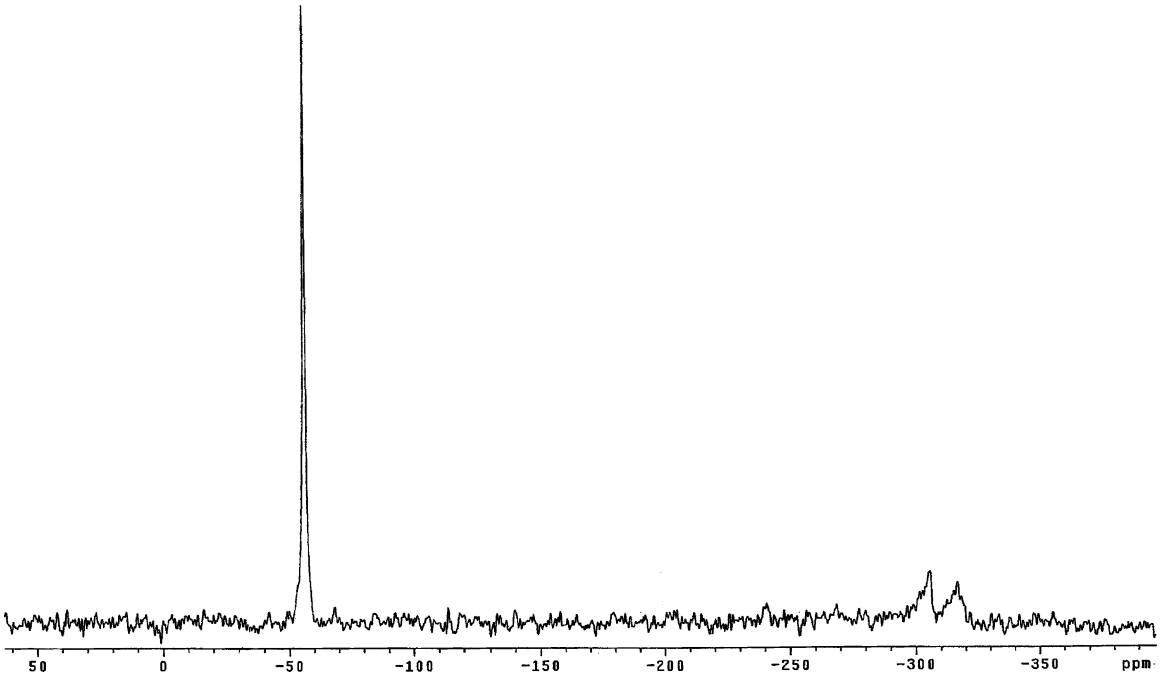

Figure 2.35: ^{1}H-coupled ^{73}Ge-NMR (17.43 MHz, C_6D_6) spectrum of **1**, referenced to $GeMe_4$

To our knowledge, ^{73}Ge-NMR spectra of compounds containing Ge–F bonds have not been reported and the findings that are available are limited to determining $^1J_{Ge-F}$ using ^{19}F-NMR spectroscopy. The $^1J_{Ge-F}$ coupling constant for inorganic

compounds was reported to be 178.5 Hz in GeF_4 and 98 Hz for the $[NH_4]_2[GeF_6]$ anion.[91] The ^{73}Ge-NMR spectrum of **17** in benzene (Figure 2.36) shows a sharp signal at -32.19 ppm for peripheral germanium atoms. This signal is slightly deshielded compared to the compounds in Table 2.7 due to the presence of fluorine. The signal for central germanium of **17** appears as a very broad signal at -322.65 ppm. Surprisingly, the fluorine is causing the peak to shift upfield in contrast to the Ge−H signal of **1** that was observed as a doublet at -311 ppm. The splitting of Ge−F into a doublet in **17** was not observed in any of our attempted ^{73}Ge and ^{19}F-NMR experiments. Acquiring the ^{73}Ge-NMR spectrum of Ph_3GeF was also attempted but no signal was observed. Also when concentrated samples were prepared and were studied by ^{19}F-NMR, the fluorine signal in Ph_3GeF did not show any coupling between germanium and fluorine.

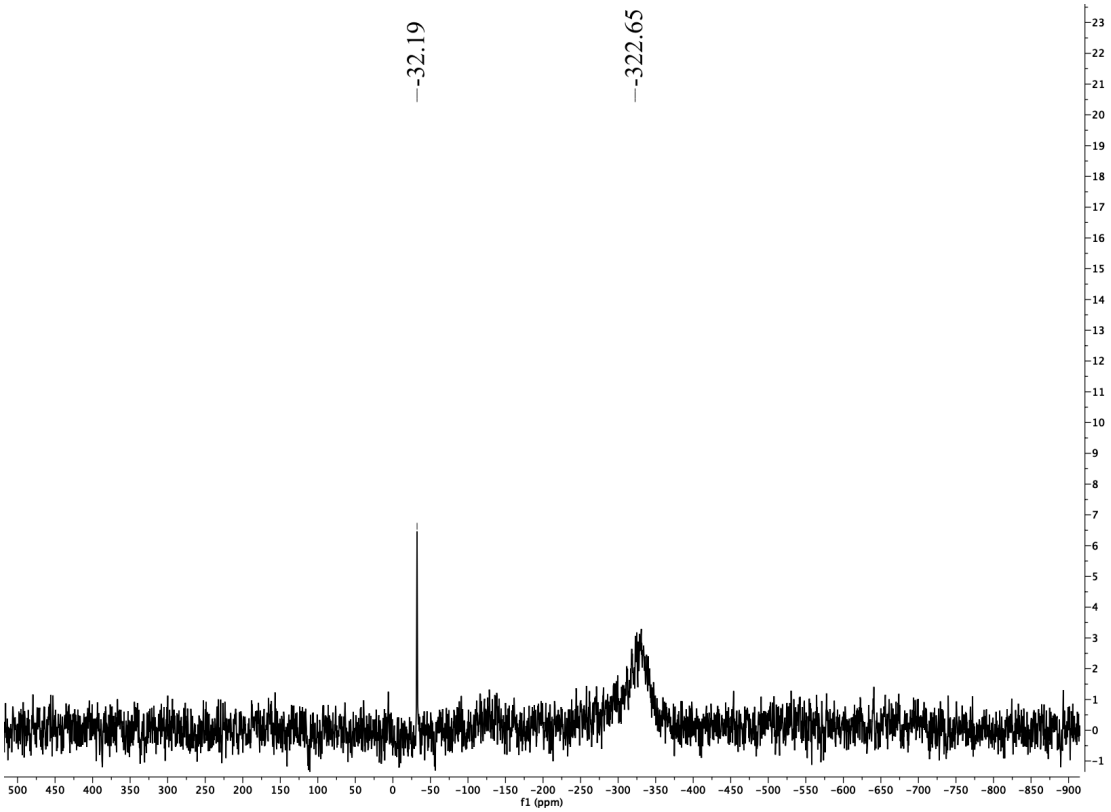

Figure 2.36: ^{1}H-coupled ^{73}Ge-NMR (17.43 MHz, C_6D_6) spectrum of **17**, referenced to $GeMe_4$

2.3 Conclusions

The branched germanium fluoride $(Ph_3Ge)_3GeF$ **17** was successfully synthesized from the branched germanium hydride $(Ph_3Ge)_3GeH$ **1** through a hydride abstraction reaction using $[CPh_3][BF_4]$. Results show that due to its high Lewis acidity, the cationic intermediate $(Ph_3Ge)_3Ge^+$.WCA (**13**.WCA) can undergo a variety of reactions, and in order to access **17** it was essential for the fluorine source to be the WCA itself. Compound **17** was fully characterized and is unique in several aspects. It is the only crystallographically characterized compound that has an unsupported Ge−Ge bond and a Ge−F bond. The electronic properties of **17** studied by UV-Vis spectroscopy along with electrochemical studies using CV and DPV show that among other branched halides (**14-16**), **17** has a larger HOMO-LUMO gap and is harder to oxidize.

Finding a reproducible method to access **17** proved to be difficult but the attempts in finding a successful synthesis for this species paved the way for investigating the potential of germyliums in C−F activation reactions.

2.4 Experimental

2.4.1 General Considerations

Unless otherwise stated, all manipulations were performed with dry, oxygen-free solvents using standard Schlenk techniques and in a glovebox with N_2 atmosphere. Solvents were dried by a Glass Contour solvent purification system. The reagents $[Ph_3C][BF_4]$, $[Ph_3C][B(C_6F_5)_4]$, $[Ph_3C][PF_6]$, XeF_2, CH_2F_2, $[(Me_2N)_3S][Me_3SiF_2]$, and AgF were purchased from Aldrich and were used without any purification. Solution NMR spectroscopy was performed a Bruker Avance III spectrometer operating at 400.00 MHz (^{1}H), 376.31 (^{19}F), or 100.57 (^{13}C) MHz. Variable-temperature ^{19}F-NMR studies were performed using a Agilent INOVA 400 spectrometer operating at 376.31

MHz. UV-Vis spectroscopy studies were conducted in CH_2Cl_2 using an Ocean Optics Red Tide USB650UV spectrometer. Electrochemical experiments (CV and DPV) are performed in CH_2Cl_2 solutions with $[Bu_4N][PF_6]$ as the supporting electrolyte, using a glassy carbon working electrode, a platinum wire counter electrode, and a Ag/AgCl reference electrode, and DigiIvy DY2312 potentiostat. Elemental analysis data were collected by Galbraith Laboratories.

^{73}Ge-NMR spectra were recorded using solutions of **17** in benzene-d_6 on a Varian INOVA 500 MHz spectrometer using a 10 mm low gamma broad-band probe at 17.43 MHz using the Carr-Purcell-Meiboom-Gill (CPMG) pulse sequence.[92,93] All spectra were referenced to $GeMe_4$.

For the X-ray crystal structure determination of **17**, diffraction intensity data were collected with a Siemens P4/CCD diffractometer. Crystallographic data for the X-ray analysis of **17** are shown in the Table 2.8. The crystal-to- detector distance was set to 60 mm, and the exposure time was 20 s per frame with a scan width of 0.5°. The data were integrated using the Bruker SAINT software. Solution by direct methods (SIR-2004) produced a complete heavy-atom phasing model that was consistent with the proposed structures. All non-hydrogen atoms were refined anisotropically by full-matrix least-squares (SHELXL-97). All hydrogen atoms were placed using a riding model. Their positions were constrained relative to their parent atom using the appropriate HFIX command in SHELXL-97. A global RIGU command was used to stabilize the refinement of the thermal ellipsoids and accounts for the substantial number of restraints employed.[94]

Computational studies were performed using Gaussian 03.[95] All energy calculations, optimizations and frequency calculations were done using a hybrid DFT method that included Becke's three-parameter nonlocal exchange function[96] with the correlation functional of Lee-Yang-Parr, B3LYP.[97] 6-31G* was used as the basis set[98] for all elements and geometry optimizations were performed without any

constraints. To confirm the minima of the optimized geometries, frequency calculations were performed at a lower level of theory. Time-dependent DFT studies were also conducted using Gaussian 03 to calculate the possible electronic transitions and oscillator strengths.

2.4.2 Synthesis of Ph_3GeNMe_2

In a 100 mL Schlenk flask, Ph_3GeCl (3 g, 8.83 mmol, 1 equiv) was dissolved in benzene. $LiNMe_2$ (0.54 g, 10.60 mmol, 1.2 equiv.) was slowly added to the benzene solution and the mixture was stirred overnight. The reaction mixture was filtered through celite and solvent was removed *in vacuo* to yield Ph_3GeNMe_2 as white-yellow solid (2.80 g, 91%). ^{1}H-NMR (400 MHz, C_6D_6) δ 7.68 - 7.63 (m, 6H), 7.18 - 7.16 (m, 3H), 7.13 (dd, J = 2.6, 1.2 Hz, 6H), 2.72 (s, 6H) ppm.

2.4.3 Synthesis of $(Ph_3Ge)_3GeH$ 1

In a Schlenk tube, Ph_3GeNMe_2 (4.95 g, 14.22 mmol) was suspended in acetonitrile. Germane gas GeH_4 was added via its condensation by cooling the Schlenk tube using a liquid nitrogen bath. The mixture was allowed to warm to room temperature and then was heated at 90 °C with stirring overnight. After that the reaction mixture was cooled to room temperature. Upon cooling **1** precipitates out of solution as a white solid. Solvent is decanted and solids are further dried *in vacuo* to yield **1**. Spectral data matched the reported values.[52]

2.4.4 Synthesis of $(Ph_3Ge)_3GeF$ 17

In a Schlenk flask, **1** (0.37 g, 0.37 mmol) was dissolved in benzene (10 mL). When $[Ph_3C][BF_4]$ (0.39 g, 1.2 mmol) was added to the mixture it produced a yellow solution. The reaction mixture was stirred at room temperature for 2 days and volatiles were removed *in vacuo*. The resulting light brown residue was washed with hexane

(3 × 15 mL) to remove the formed Ph_3CH. To get pure **17**, the reaction mixture was dissolved in toluene (5 mL) in a vial and it was layered with hexane (15 mL). The resulting mixture was allowed to evaporate slowly to ∼ 8 mL at which time pure crystals of **17** were formed on the walls of the vial. The solution was decanted and crystals were then washed with hexane (3 × 15 mL) to yield **17** as colorless crystals (0.24 g, 65%). ^{1}H-NMR (400 MHz, C_6D_6) δ 7.33 (d, J = 7.6 Hz, 18H, o-C_6H_5), 7.07-7.03 (m, 18H, m-C_6H_5), 6.95 (t, J = 6.8 Hz, 9H, p-C_6H_5) ppm. ^{13}C-NMR (101 MHz, C_6D_6) δ 136.3 (ipso-C_6H_5), 136.2 (o-C_6H_5), 128.5 (m-C_6H_5), 127.9 (p-C_6H_5) ppm. ^{19}F-NMR (376 MHz, C_6D_6) δ -194.72 (Ge−F) ppm. UV-vis (CH_2Cl_2, 25 °C): 240 nm (sh). Anal. calcd for $C_{54}H_{45}FGe_4$: C, 64.61; H, 4.52. Found: C, 64.68; H, 4.57.

2.4.5 Attempted Synthesis of 17 Using $[Ph_3C][B(C_6F_5)_4]$ and XeF_2

To a Schlenk tube, containing a solution of **1** (0.290 g, 0.294 mmol) in toluene, $[Ph_3C][B(C_6F_5)_4]$ (0.326 g, 0.353 mmol) was added slowly. The reaction mixture was stirred overnight at 85 °C. After that, the Schlenk tube was opened in the glove box and XeF_2 (0.060 g, 0.35 mmol) was added. The reaction mixture was again heated to 85 °C for 24 hours. Volatiles were removed *in vacuo* and the solids were washed with hexane (4×10 mL) and solids were filtered through celite using benzene to remove $[XeF][B(C_6F_5)_4]$. The solvent was removed *in vacuo* to yield a colorless oil that contained an intractable mixture of products by ^{19}F, ^{13}C and ^{1}H-NMR.

2.4.6 Attempted Synthesis of 17 Using $[Ph_3C][B(C_6F_5)_4]$ and $[(Me_2N)_3S][Me_3SiF_2]$

To a Schlenk tube, containing solution of **1** (0.453 g, 0.460 mmol) in toluene, $[Ph_3C][B(C_6F_5)_4]$ (0.430 g, 0.465 mmol) was added slowly. The reaction mixture was stirred overnight at 85 °C. After that, the Schlenk tube was opened in the glove box and

$[(Me_2N)_3S][Me_3SiF_2]$ (0.130 g, 0.472 mmol) was added. The reaction mixture was again heated to 85 °C for 24 hours. Volatiles were removed *in vacuo* and the solids were washed with hexane (5×10 mL) and solids were filtered through celite using benzene to remove $[XeF][B(C_6F_5)_4]$. The solvent was removed *in vacuo* to yield a colorless solid. Solids were recrystallized in toluene and crystals were grown at -35 °C that turned out to be $[(Me_2N)_3S][B(C_6F_5)_4]$ by X-ray analysis. The supernatant of the reaction mixture contained an intractable mixture of products by ^{19}F, ^{13}C and ^{1}H-NMR.

2.4.7 Attempted Synthesis of 17 Using $[Ph_3C][B(C_6F_5)_4]$ and CH_2F_2

To a Schlenk tube, containing a solution of **1** (0.657 g, 0.667 mmol) in toluene, $[Ph_3C][B(C_6F_5)_4]$ (0.625 g, 0.678 mmol) was added slowly. The reaction mixture was stirred overnight at 85 °C. After that, the reaction mixture was allowed to cool to room temperature and volatiles were removed *in vacuo*. The Schlenk tube was cooled to -78 °C using a liquid nitrogen bath and CH_2F_2 (13.67 g, 0.262 mol) was introduced to the reaction under static vacuum. The Schlenk tube was sealed and was stirred at -78 °C for 5 hours, after which time the reaction was warmed to room temperature and the volatiles were removed *in vacuo* to yield a light brown solid that contained an intractable mixture of products by ^{19}F, ^{13}C and ^{1}H-NMR.

2.4.8 Crystallographic Data for $(Ph_3Ge)_3GeF{\cdot}C_6H_6$

Table 2.8: Crystallographic data for $(Ph_3Ge)_3GeF$ **17**·C_6H_6

Empirical formula	$C_{60}H_{51}Cl_{0.39}F_{0.61}Ge_4$
Formula weight	1085.15
Temperature (K)	100.0
Wavelength (Å)	0.71073
Crystal system	Monoclinic
Space group	$P2_1/n$
a (Å)	13.4929(8)
b (Å)	21.780(1)
c (Å)	17.724(1)
α (°)	90
β (°)	108.916(2)
γ (°)	90
V, (Å^3)	4927.2(5)
Z	4
ρ (g.cm^{-1})	1.463
Absorption coefficient (mm^{-1})	2.471
F(000)	2199
Crystal size (mm^3)	0.3 × 0.1 × 0.07
Theta range for data collection	2.458 to 25.375
Index ranges	-16 ≤ h ≤16
	-26 ≤ k ≤ 22
	-21 ≤ l ≤21
Reflections collected	19102
Independent reflections	8802 (R_{int} = 0.0586)
Completeness to θ	97.5
Absorption correction	Semi-empirical from equivalents
Refinement method	Full-matrix least squares on F^2
Data/restraints/parameters	8802/521/589
Goodness-of-fit on F^2	0.948
Final R indices (I<2σ(I))	
R_1	0.0500
wR_2	0.1026
Final R indices (all data)	
R_1	0.0957
wR_2	0.1101
Largest diff. peak and hole (e Å^3)	0.705 and - 0.973

CHAPTER III

Transition Metal-Free HDF of Acid Fluorides and Organofluorines by Ph_3GeH Promoted by Catalytic $[Ph_3C][B(C_6F_5)_4]$

3.1 Introduction - Germylium Ions

As was presented in Chapter II, germanium cations also known as germylium ions are trivalent germanium compounds R_3Ge^+.WCA that are ideally isolated cations that have a WCA as their counter-anion. There are several reports of germyliums that are synthesized using Ge(II) germylene species that will not be the focus in this chapter.

Branched germylium $(Ph_3Ge)_3Ge^+$.WCA behaves as a strong Lewis acid and is a very fluorophilic species. It also shows a great potential for the activation of C–X bonds in CH_2X_2 (X = Cl, Br, I) and in reacting as an electrophile in Friedel-Crafts reactions with benzene. These simple but applicable characteristics led us to study the application of a simpler and easy-to-make germylium ion $[Ph_3Ge][B(C_6F_5)_4]$ **1** for main-group-element based hydrodefluorination reactions of aliphatic C–F containing compounds and acyl fluorides.[85]

3.1.1 Germylium Ions

After the discovery of the first carbocation, which is the trityl cation Ph_3C^+ in 1901,[99] there has been a century of efforts directed at isolating and characterizing heavier group 14 cations. Germylium ions were known to exist in vapor phase in the 70s[100] but it was not until 1997 that the first crystallography characterized isolated germylium ion was realized.

Unlike carbon, germanium having an extended coordination sphere is more reluctant to π-conjugation and its cation is larger in size. This will make the isolation of germylium species in the condensed phase a significant challenge.[101] Steric and electronic effects are the keys for isolating a stable germylium ion and this will involve the vital roles of WCAs and solvents for stabilizing germylium.[102]

Figure 3.1 shows the dates that first isolated germylium ions were discovered. The first isolated germylium ion **2a** was synthesized by Sekiguchi *et al.*[103] and was stable enough to be isolated because the cation is stabilized by steric effects and delocalization by resonance.

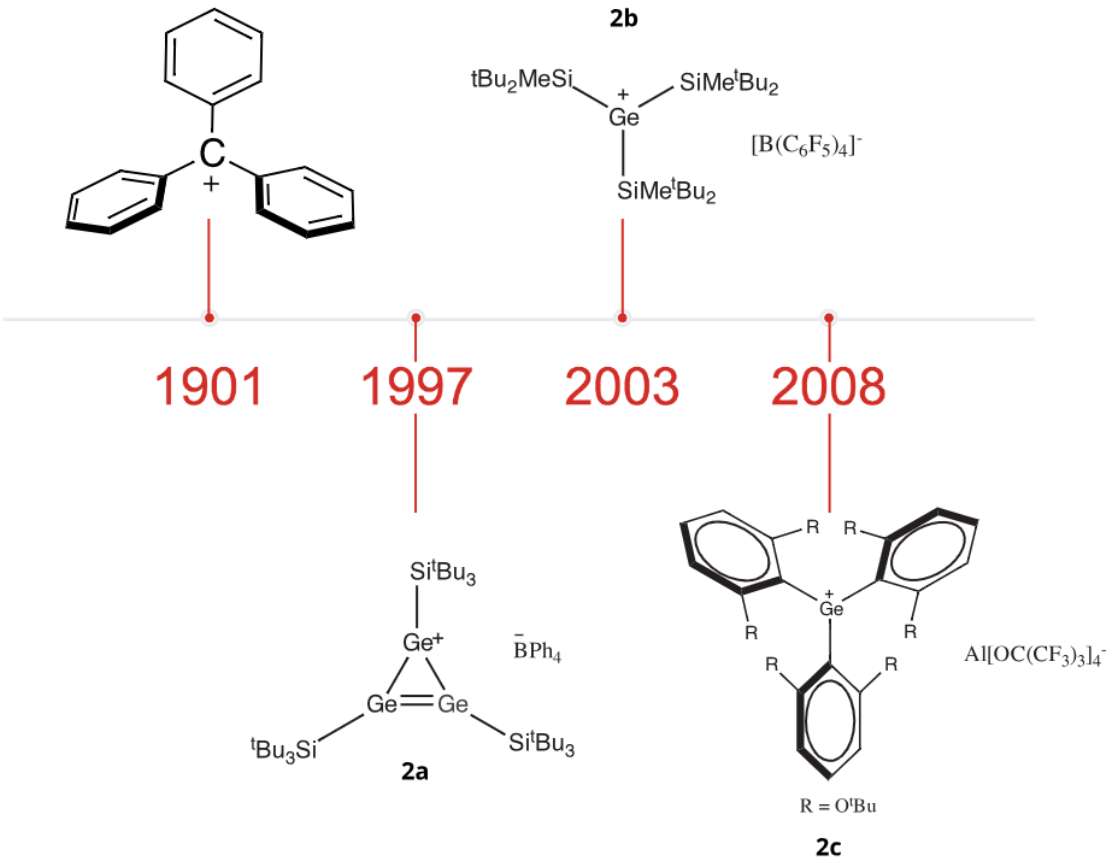

Figure 3.1: Timeline of the discovery of germylium ions. Examples that are stabilized by **2a**-delocalization of the positive charge due to resonance, **2b**-steric effects and **2c**-a weakly-coordinating anion

In 2003, the first example of free germylium ion **2b** was synthesized by the same group and is not stabilized by any conjugation with π bonds but is solely stabilized by bulky ($^{t}Bu_2MeSi$)- groups.[104] Later in 2008, Schnepf *et al.* prepared another free germylium ion that was stabilized by one of the least basic reported WCAs.[105] The latter example highlighted the role of the WCA in isolating free germylium ions.

It is evident from the few examples of free germylium ions that they are very hard to isolate and due to their tremendous electrophilicity, they are very reactive. Another strategy to isolate germyliums is to delocalize the positive charge via homoaromaticity. Sekiguchi *et. al* prepared **2d**, after their success in preparing the aromatically stabilized germylium **2a**. Cation **2d**, shown in Figure 3.2, is a non-classical cyclopropenium ion-like compound where the cation is stabilized by the intramolecular coordination of a C=C double bond though space.[106] Compound **2e** is another example of π-stabilized germylium. The quantum calculations of this norbornyl cation indicate it will have a symmetrically bridged structure.[107]

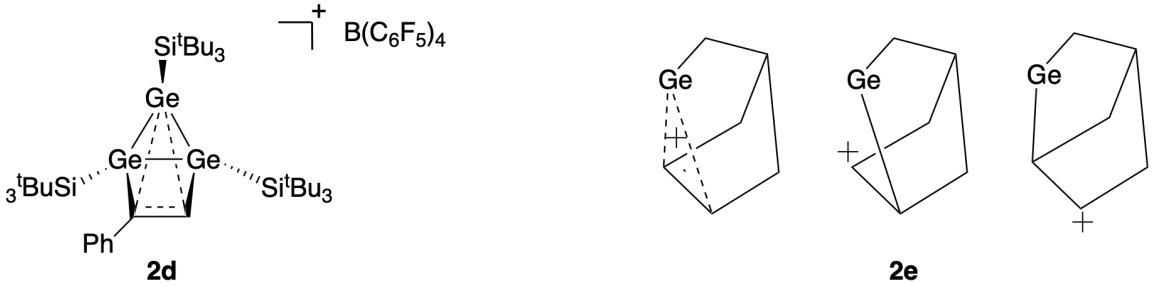

Figure 3.2: Examples of π-stabilized germylium

Due to the high reactivity of germylium ions complexed germylium ions are more common. These type of cations usually are formed when the WCA does not function as an ideal weakly-coordinating counter anion, and acts as a Lewis base with the cation. This will result in close contacts between Ge^+ and atoms on the WCA. X-Ray data (Figure 3.3) show that in Et_3Ge^+ in **2f**, the bromine atom of the carborane anion is in close contact with the germanium atom.[108] In case of Me_3Ge^+ **2g**, hydrogen atoms of methyl groups on the methylated carborane show hydridic character and

these interact with the Ge^+ atom.[109]

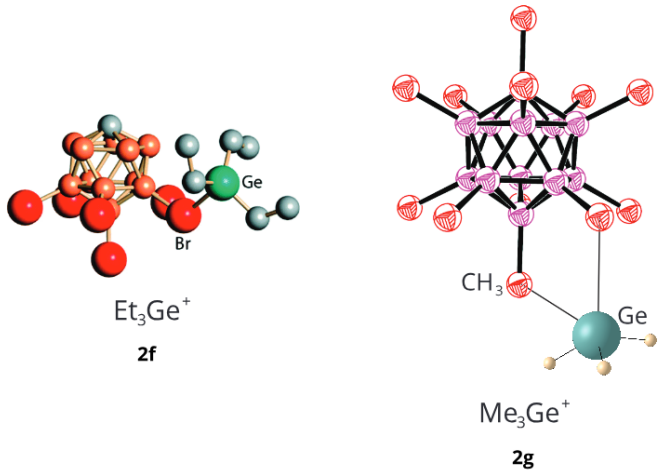

Figure 3.3: Examples of close-contact-stabilized germyliums

Another class of complexed germylium ions are those that are stabilized by three-center-two-electron-bond interactions. In this case two scenarios are important to note. In example **2h** (Figure 3.4) , the germylium center is stabilized intramolecularly by another germanium hydride (R_3Ge-H) and the hydrogen acts as a Lewis base.[110] The X-ray data suggest a symmetric structure but the Lewis description of the bonding shows more than one resonance form. In **2i**, however, the same interaction happens intermolecularly. The importance of this type of interaction will be discussed later, as one of the prevalent aggregates in the synthesis of germylium ions in solution are bridged species like **2i**.[108]

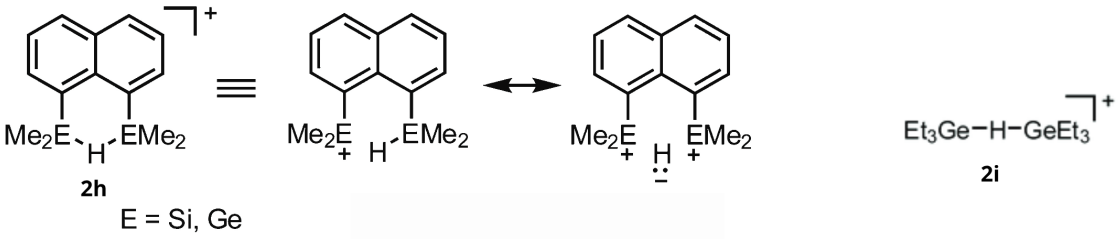

Figure 3.4: Examples of three-center-two-electron bond stabilized germyliums

As discussed in Chapter II, germylium ions have a high propensity to form Wheland intermediates in benzene solvent. This is reactivity is not limited to the solvent molecules and can happen intramolecularly. Scheme 3.1 shows when a deactivated solvent such as $C_6H_4F_2$ is used, the electrophilic germylium exhibits two close contacts to one of the trip substituents attached to the phenyl ring (**2j**).[111]

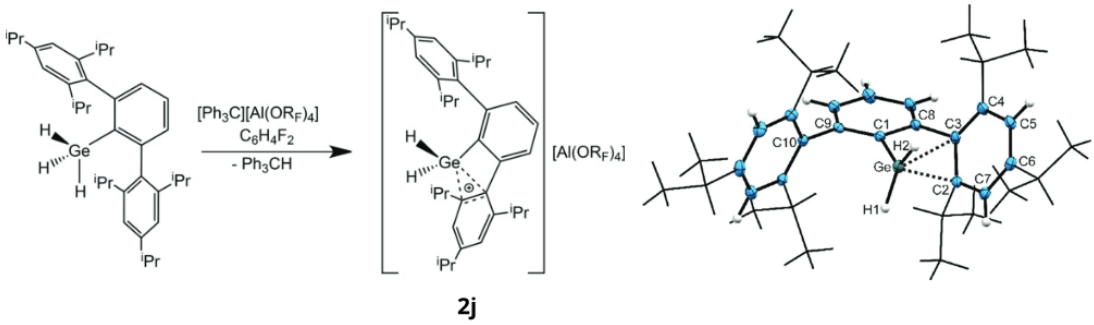

Scheme 3.1: An example of substituent-stabilized germylium

3.1.1.1 The Role of Solvents and WCAs

For the synthesis of free germylium ions it is vital to use a solvent that is weakly coordinating such as dichloromethane or benzene. Although this minimizes interactions, it does not guarantee that there will be no reactions between germylium ions and Lewis basic solvents.

Although the concept of WCAs was introduced years[112] after the discovery of the first carbocations, as was shown earlier, the counter-anion for all isolated cations is a WCA. The critical function of a WCA is to replace a few strong Coulombic interactions with many very weak interactions. WCAs are basically large "spectator anions" and because of their size will have a lower cation-anion interaction energy.[113] It can be certainly stated that one of the most important factors in the stability of a germylium ion is its WCA. Although absolute non-coordination does not occur,[114] an ideal WCA is a very weak Lewis base and nucleophile, is chemically stable with respect to the very powerful oxidizing germylium center, and delocalizes the negative charge

over the skeleton of the anion. A good example of such WCAs are perfluorinated alkoxy aluminates $[Al(OR^F)_4]$, in which the C–F moieties decrease the Van der Waals forces by making the WCA less polarizable.[105]

3.1.2 Synthesis of Germylium Ions

Heterolytic cleavage of Ge–X Bond (X = Cl, Br, I) has been a frequently used method for preparing free germyliums. The halide abstracting reagent can be a strong Lewis acid such as a silylium ion, paired with a WCA (Scheme 3.2). Silver can cause the heterolytic cleavage of Ge–Br bond to form germylium ions as well[105,106] (Scheme 3.3).

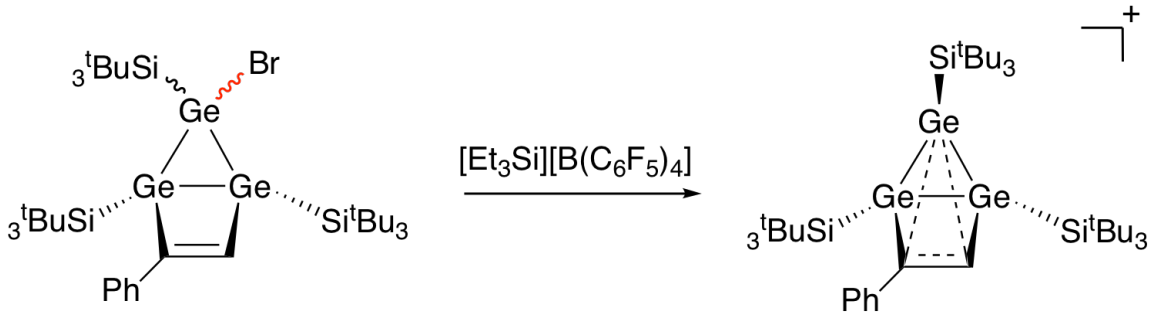

Scheme 3.2: Synthesis of germylium ions by halide abstraction using $Et_3Si.WCA$

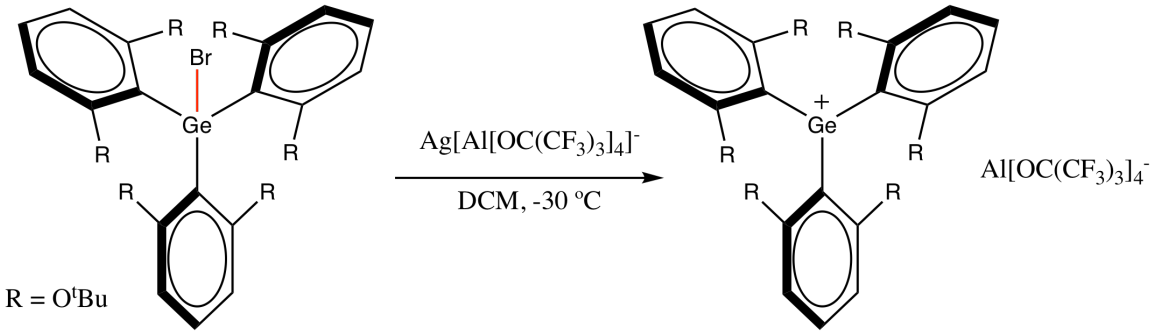

Scheme 3.3: Synthesis of germylium ions by halide abstraction using Ag.WCA

Germanium radicals can undergo a reversible one-electron oxidation with a hydride abstracting reagent to form the corresponding germylium ion. Sekiguchi *et al.* have shown that the germylium ion in Scheme 3.4 can be reduced back to its precursor radical using ^{t}BuLi.[104,115]

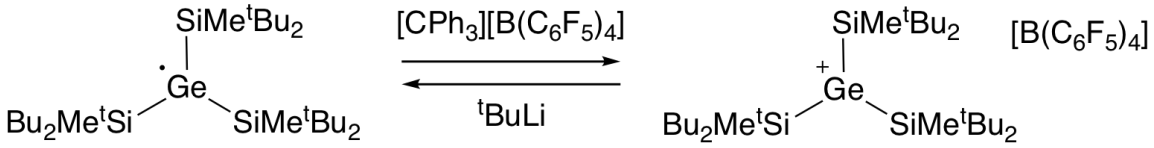

Scheme 3.4: Synthesis of a germylium by oxidation of a germanium radical

The homolytic cleavage of other bonds such as a Ge–Si bond has also been useful in preparing germylium ions. In the example shown in Scheme 3.5, it is suggested that the precursor undergoes a one-electron oxidation by the trityl cation and will then release a ^{t}Bu$_3$Si$^\bullet$ radical to form the germylium ion.[116]

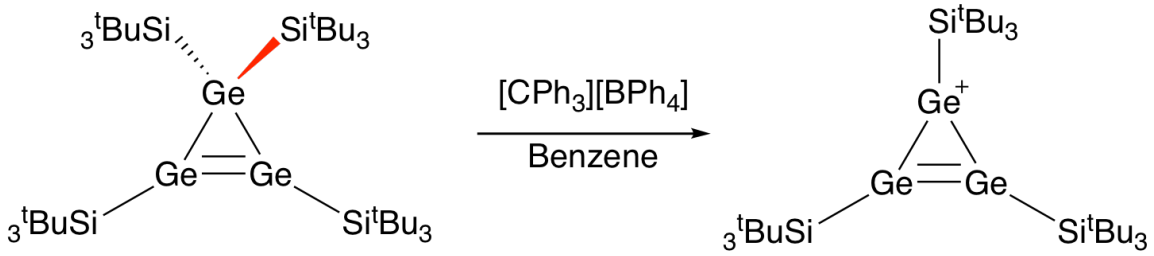

Scheme 3.5: Synthesis of a germylium ion by oxidative cleavage of a Ge–Si bond

Unlike in hydrocarbons where C–H bonds are considered to be inert, Ge–H bonds in germanium hydrides are functional groups. One of the more widely used methods to access germylium ions from these hydrides is by using the Bartlett–Condon–Schneider hydride transfer reaction.[81] For this method to access a free germylium ion it is necessary that the WCAs used be as least Lewis basic as possible. Although this approach is very common for *in situ* formation of complexed germylium ions. Scheme 3.6 shows an example of a tetra-coordinated germylium ion **2k** that was synthesized using this method. Interestingly if the WCA, B(C$_6$F$_5$)$_4$ is switched to BF$_4$ in [CPh$_3$][WCA], the intermediate germylium will abstract a fluorine to form a Ge–F bond.[117]

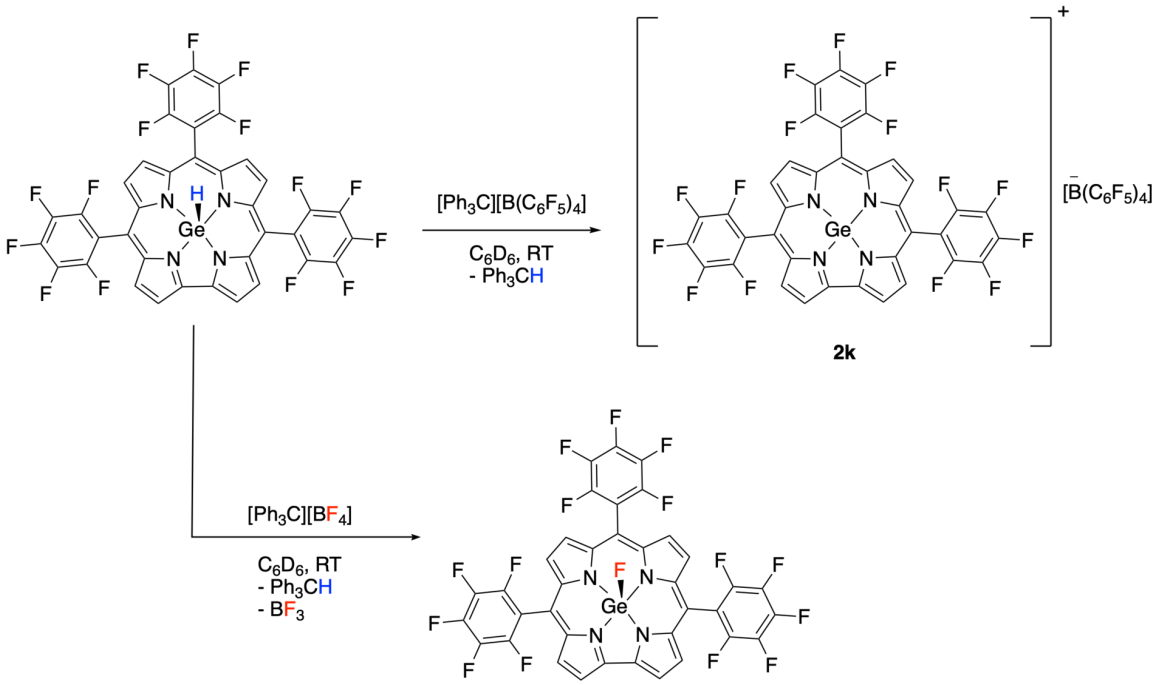

Scheme 3.6: Synthesis of a tetra-coordinated germylium ion by a hydride transfer reaction

Cations of Si, Ge, and Sn have also been made by using the corresponding hydride precursors and a Lewis acid. For example using BCF and R_3SnH (R = Bu or Me), tin cations were synthesized and characterized by ^{119}Sn-NMR spectroscopy and have chemical shifts that are characteristic of tri-coordinated tin species.[118] BCF has also been used as a catalyst for generating silylium ions and H−BCF in the hydrosilation reactions of carbonyl groups.[88]

Though this method is not reported to be useful for the preparation of a free germylium ion or an isolated adduct, the study by Gevorgyan *et al.* shown in Scheme 3.7 indicates that the *trans*-hydrogermylation of alkynes proceeds through a germanium cation and *trans* stereoselectivity arises, from the formation of the bulky $HB(C_6F_5)_3$ hydride.[119]

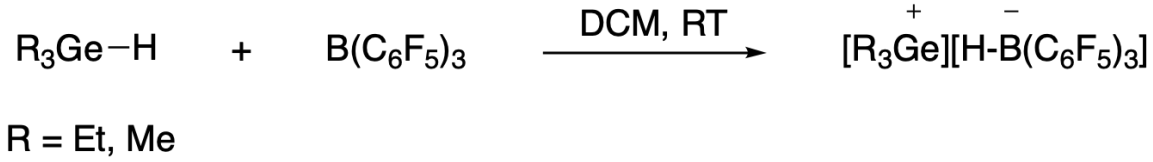

Scheme 3.7: Synthesis germylium ions using BCF

3.1.3 Reactivity and Applications of Germylium Ions

Germylium ions behave as strong electrophiles. X-ray crystallography and computational results suggest sp^2 hybridization for a tri-coordinate germylium ion, in which the positive charge is mainly localized in the empty $4p$ orbital of germanium.[104,105] A recent study by Fang *et al.* however, shows that the hybridization of germylium ions can be tuned by changing the coordination environment around the cationic germanium center. Calculations show that tetra-coordinated germylium **2k** ($[(TPFC)Ge]^+$) adopts *sp* hybridization. As shown in Scheme 2.19 in the presence of a base, **2k** can react with ethylene in benzene to quantitatively form (TPFC)Ge$-CH_2CH_2C_6H_5$ at room temperature. In a similar reaction the the σ C$-$C bond of cyclopropane can also be activated by **2k** to form (TPFC)Ge$-CH_2CH_2CH_2C_6H_5$.[117]

In the presence of Lewis bases the expected fate of a germylium is to form a Lewis acid-base adduct. However when **2k** is reacted with NEt_3 in benzene two products are formed. As shown in Scheme 3.8, in the C$-$N activation pathway, triethylamine first coordinates to the germanium of **2k** and then another NEt_3 molecule acts as a nucleophile to form **3a** and $[NEt_4]^+$.[120]

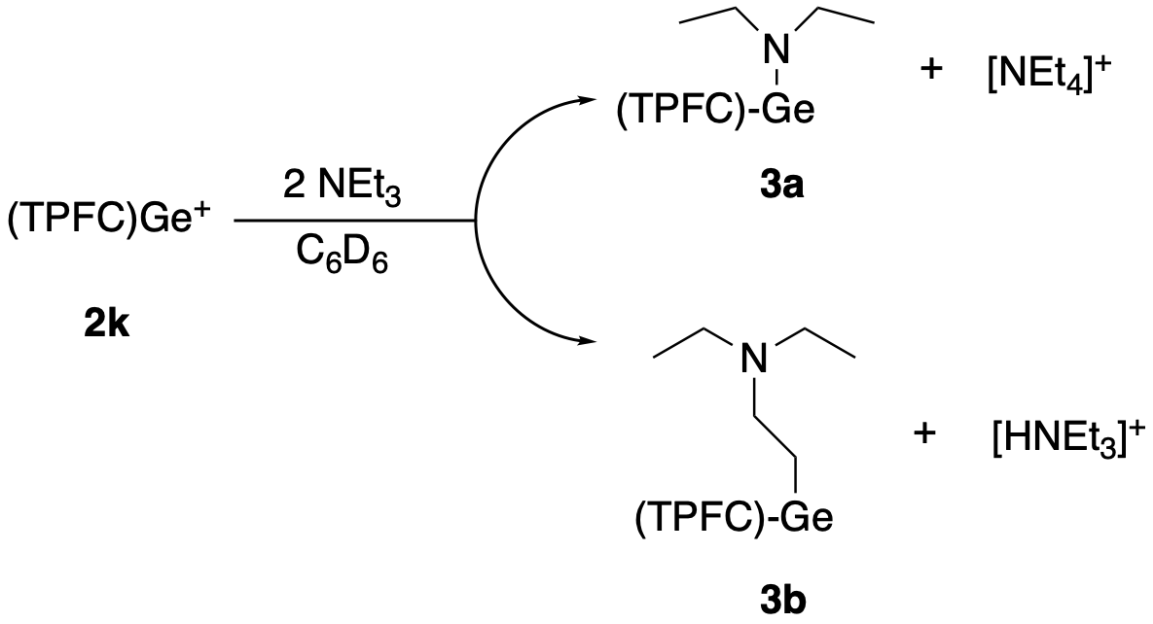

Scheme 3.8: C−H and C−N activation of tertiary amines by a germylium

The determination of the crystal structure of **3b**.H^+, along with DFT calculations suggest that **3b** is the result of the C−H activation of NEt_3. For this product to form, the β-C−H bond of NEt_3 breaks to form Ge−C and N−H bonds respectively. Afterwards, another NEt_3 acts as a base and deprotonates **3b**.H^+ to form **3b** and $[HNEt_3]^+$.[120]

The reports of utilizing germylium ions in chemical transformations are less common than using germanium radicals that are considered to be the key intermediates in important reactions such as hydrogermylations of double and triple bonds. The only reported example of an ionic hydrogermylation is shown in Scheme 3.9, where an *in situ* formed germylium ion (as discussed in Scheme 3.7) forms trans hydrogermylation products upon reaction with an alkyne. These hydrogermylation reactions are catalyzed by BCF and are conducted in dichloromethane solvent at room temperature.[119]

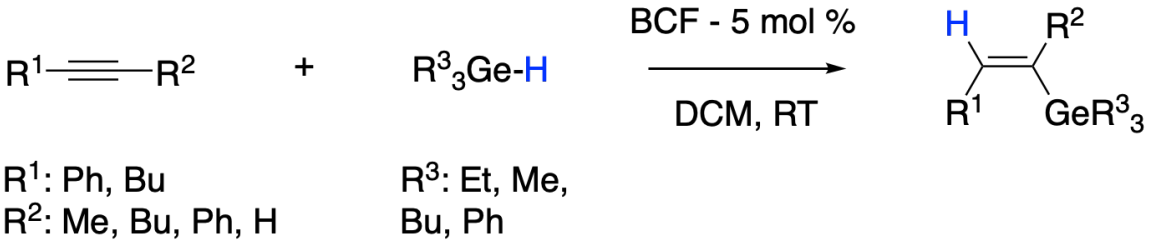

Scheme 3.9: *Trans*-hydrogermylation of alkynes by germylium ions

3.1.4 Main-group Element Based C–F Activation

The C–F bond is the strongest single bond between carbon to another element (105 kcal.mol^{-1}, 400±50 kJ.mol^{-1}).[121] The presence of C–F bonds in many pharmaceuticals and pollutants make efforts directed at its formation and activation worthwhile. Due to its inertness, activating C–F bonds and replacing the fluorine atom with other elements is an important synthetic goal. Replacing a F atom with a H atom, a process known as hydrodefluorination, is the simplest transformation of the C–F bonds. General strategies for C–F activation are summarized in Scheme 3.10.

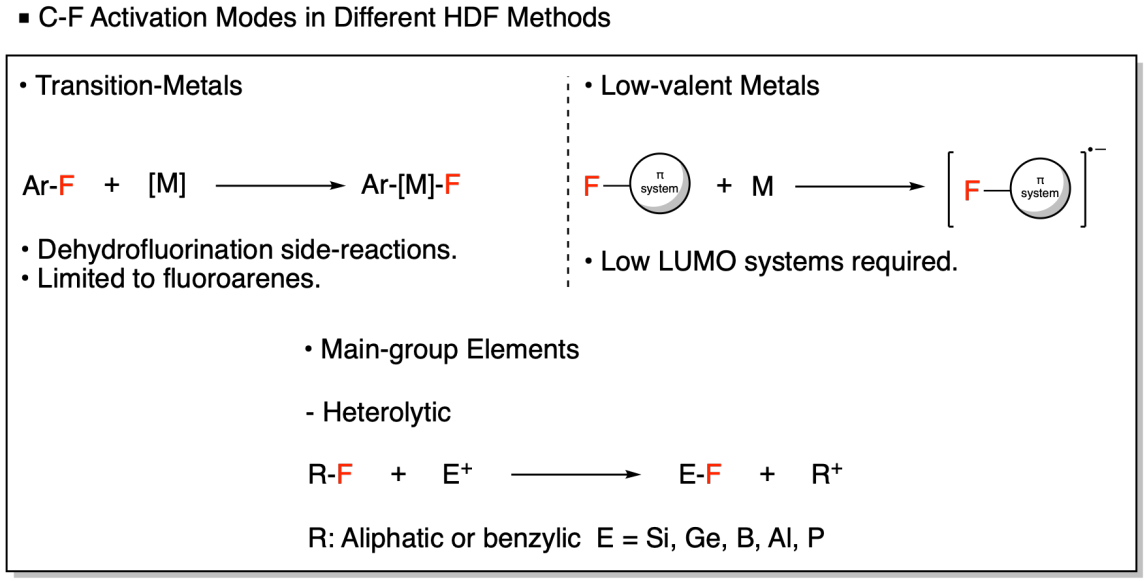

Scheme 3.10: Different C–F bond activation strategies

By using transition-metals C–F bonds can be broken heterolytically. These approaches mainly depend on an oxidative-addition step of a C–F bond to the metal

center. Thus, this method is limited to fluoroarenes and the formed HDF products can also compete with the C−F bonds in side-reactions that occur in C−H activation. Low-valent metals can act as reductants for C−F bonds. This method works with the formation of radical-anion intermediates, and C−F-containing substrates that have LUMO, that are low in energy. This makes this method limited to fluoroarenes.[122]

In main-group element based approaches to C−F bond activation, a main-group Lewis acid (R_3Ge^+) first abstracts a F^- to form a carbocation (Scheme 3.11). Next, the carbocation abstracts a hydride from the germanium hydride to form the HDF product and the Lewis acid catalyst. The stability of the carbocation intermediate formed is the most important step in main-group element based HDF. And for any HDF method to work the high BDE of the C−F bond must be compensated. In main-group elements based HDF the driving force is the formation of strong E−F (E = Ge, Si, B, Al, ...) bonds.[121,122]

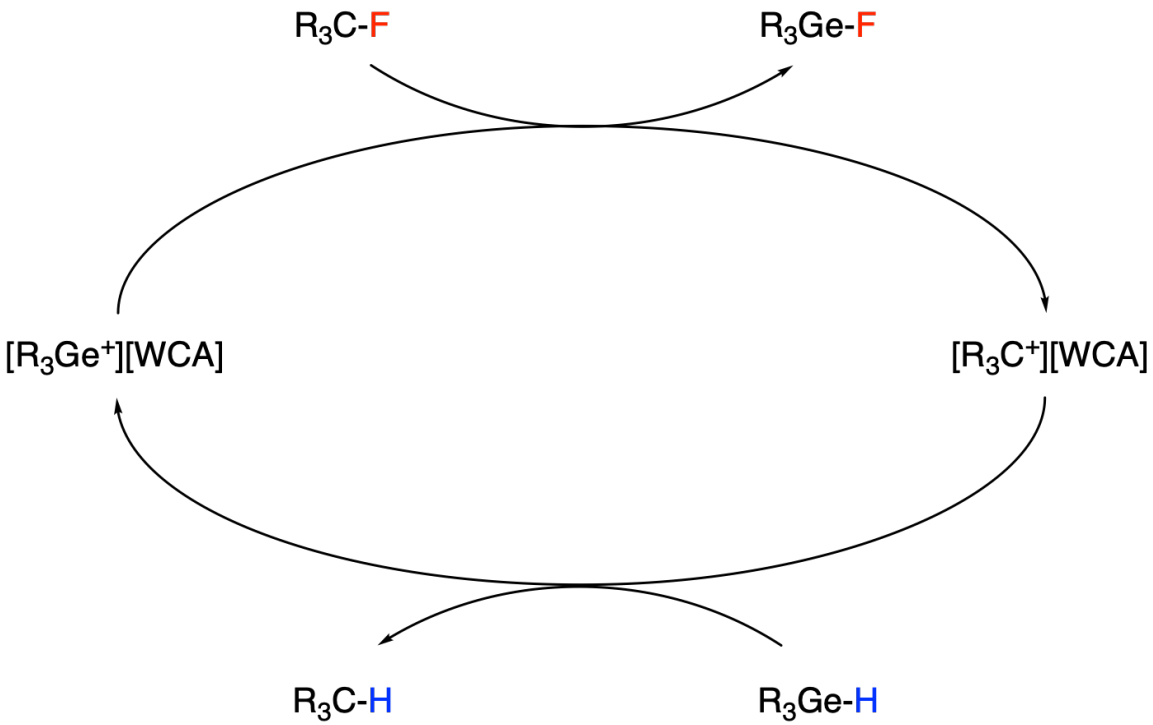

Scheme 3.11: A simplified mechanism of HDF by germyliums

There are many examples of main-group elements based HDF reactions. With respect to aliphatic C−F bonds, the pioneering work of Ozerov *et al.* is worthy of mention. By forming silylium ions from silicon hydrides such as Et_3SiH in solvents or under neat conditions aliphatic C−F-containing compounds can undergo HDF in high conversions. As discussed earlier, the key for a sustainable source of silylium ions is the WCA used in the reactions. Results show that even common WCAs such as $[B(C_6F_5)_4]^-$ are not suitable for stabilization of very electrophilic silylium ions, and a carborane WCA ($[HCB_{11}H_{11}]^-$) had to be used instead.[123]

The study by Stephan and coworkers shows that the C−F activation of alkyl fluorides can be achieved using Et_3SiH and 5% BCF. This approach features low temperatures and short reaction times.[124] In most reported HDF transformations, side-reactions between the Lewis acids and solvents can be observed. Another common side-reaction that results from the presence of carbocations is Friedel-Crafts reactions.[123]

3.1.5 Acyl Fluorides

Acyl fluorides are carboxylic acid derivatives that contain an F atom in place of the OH moiety. Acyl fluorides are more stable than acyl chlorides towards solvolysis and are easier to handle. The higher stability of acyl fluorides compared to acyl chlorides and anhydrides, and their higher reactivity compared to esters and amides, has made them valuable synthetic substrates in organic chemistry.[125]

Sakai *et al.* have recently reported that acyl fluorides can be reduced by Et_3SiH in the presence of a palladium catalyst, and Scheme 3.12 shows how the ligands affect the reduction process. When monodentate PCy_3 ligands were used, the reduction occurs without any decarbonylation to give the corresponding aldehydes. However, when a bidentate phosphine ligand such as $[Cy_2P(CH_2)_2PCy_2]$ is used a decarbonylative (over)reduction occurs to yield the corresponding alkanes.[126]

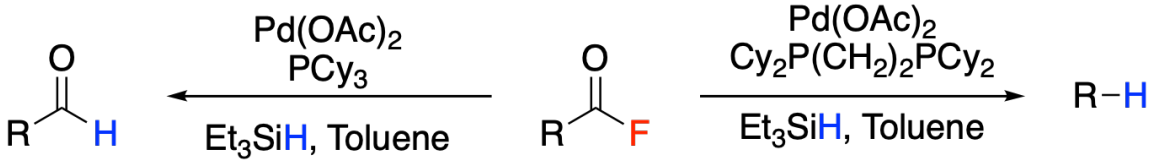

Scheme 3.12: Pd-Catalyzed reduction of acyl fluorides

The source of the observed selectivity is not fully clear. However, it is suggested that the difference lies in the Pd/P ratio. When a bidentate ligand is used the ratio is higher (e.g. 1:2) and there is an open coordination site present at the palladium center which favors decarbonylation and the formation of hydrocarbon products. When monodentate ligands are used the Pd/P ratio is lower (e.g. 1:3) and the absence of a vacant coordination site makes decarbonylation unfavorable and results in the aldehyde products. The selectivity also depends on the substrates and over-reduction reactions can affect the scope of this method.[126]

3.2 Results and Discussion

3.2.1 HDF Reactions of Benzotrifluorides

The initial studies to explore the potential of germylium ions in HDF reactions were conducted by reacting $[Ph_3Ge][B(C_6F_5)_4]$ **1** with benzotrifluorides, alkyl fluorides, and acyl fluorides using different solvents, temperatures, and reaction conditions.

Scheme 3.13 shows when 1,3-bis(trifluoromethyl)benzene is mixed with Ph_3GeH (3.1 equiv.) under neat conditions, a clear liquid results and upon the addition of catalytic amounts of $[Ph_3C][B(C_6F_5)_4]$ white solids start to form rapidly (within 1 minute).

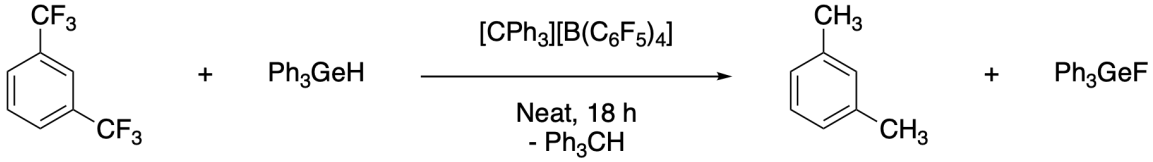

Scheme 3.13: HDF reaction of 1,3-bis(trifluoromethyl)benzene

The ^{19}F-NMR spectrum of the reaction mixture (Figure 3.5) shows signals that correspond to the fluorines of the starting hexafluorotoluene at -62.79 ppm signals for $[Ph_3C][B(C_6F_5)_4]$ at -131.82,-162.50 and -166.32 ppm , and Ph_3GeF at -202.29 ppm. The ^{1}H-NMR spectrum of the reaction mixture in Figure 3.6 shows a sharp signal at 2.10 ppm that matches with the methyl signals of *m*-xylene.[127] The signals for Ph_3CH and remaining Ph_3GeH also were present at 5.43 and 5.86 ppm, respectively. No signals in either the ^{1}H- or ^{19}F-NMR spectra of the reaction mixture indicated the formation of over-reduction products.

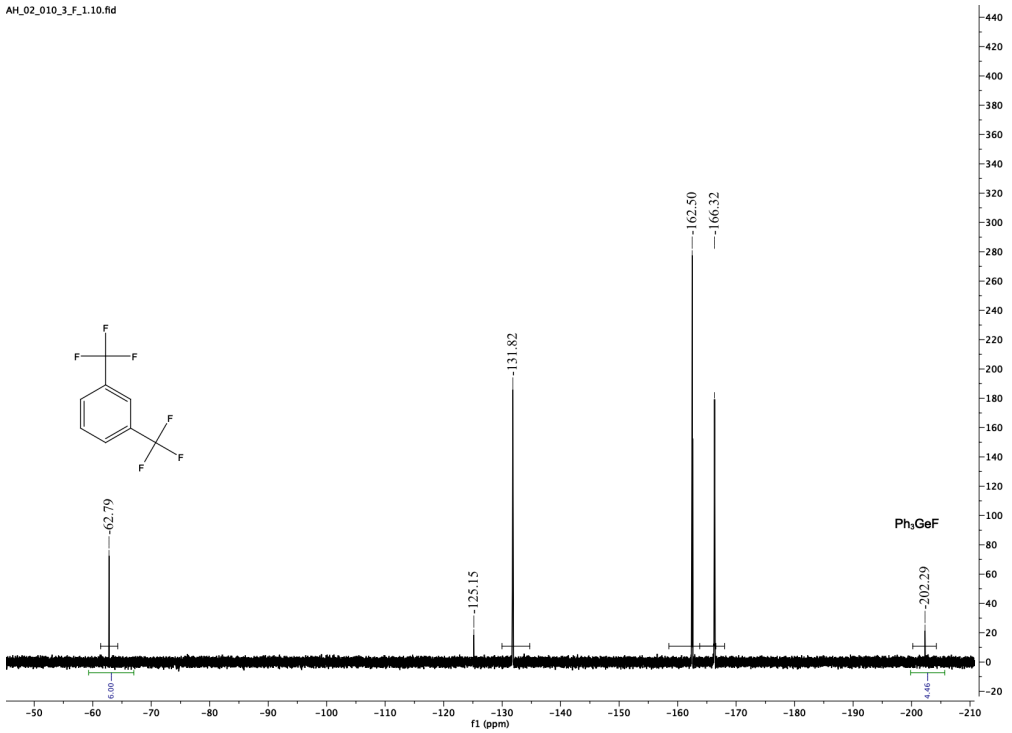

Figure 3.5: ^{19}F-NMR (376 MHz, C_6D_6) spectrum of the HDF reaction of 1,3-bis(trifluoromethyl)benzene

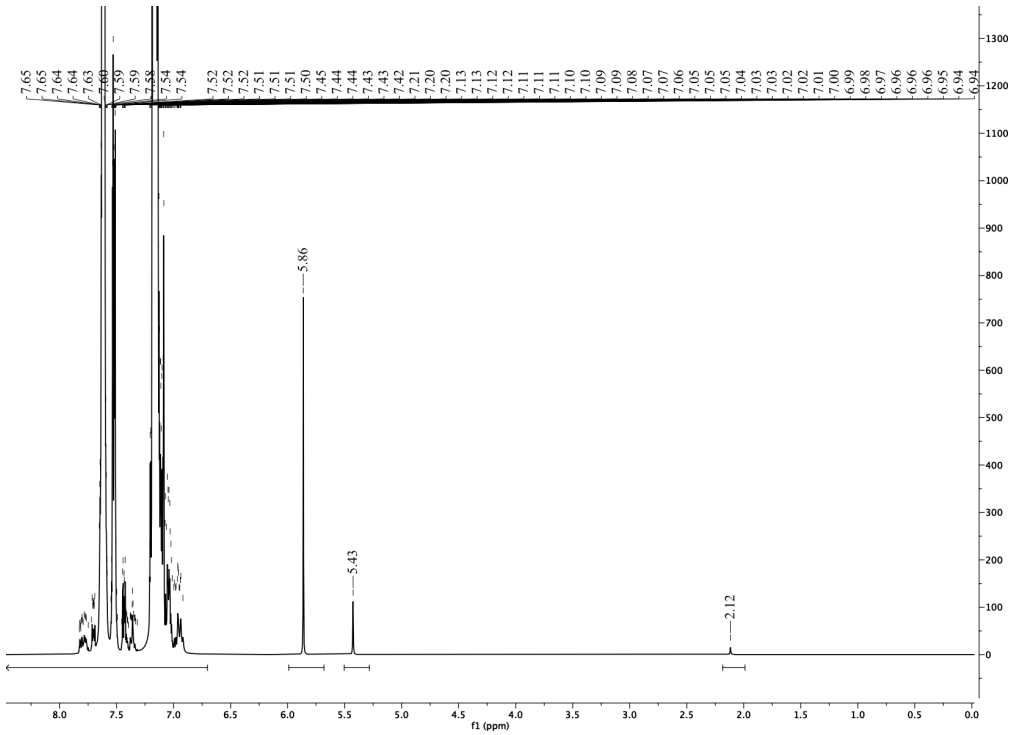

Figure 3.6: ^{1}H-NMR (400 MHz, C_6D_6) spectrum of the HDF reaction of 1,3-bis(trifluoromethyl)benzene

To better understand the identity of the products formed, GC-MS chromatograms of the reaction mixture were compared with those of authentic standard samples. Figure 3.7 shows the GC-MS traces of the standard *m*-xylene sample which has a retention time of 7 minutes and a peak at $m/z = 106$ in its mass spectrum.

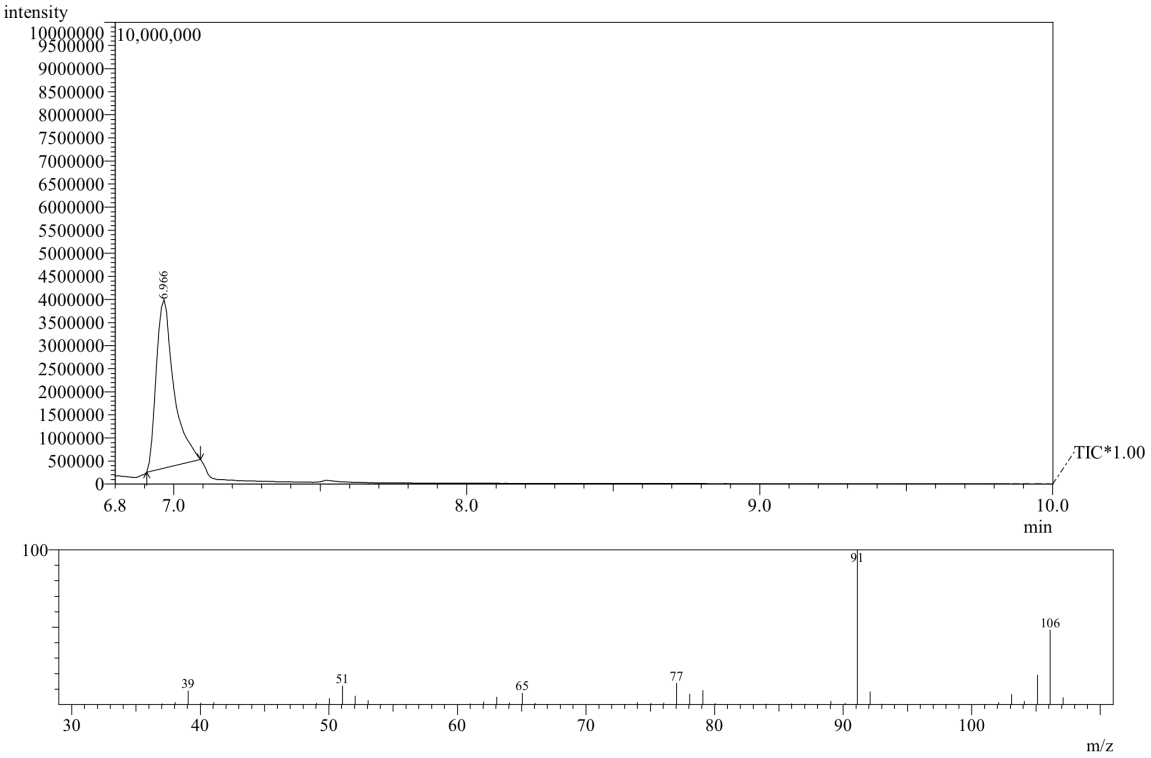

Figure 3.7: GC-MS trace of *m*-xylene

The chromatogram of the reaction mixture in Figure 3.8 shows a peak at 6.5 minutes with a peak at m/z =106 in its mass spectrum for the parent ion that corresponds to *m*-xylene. The results of the GC-MS experiments agree with the NMR results, as no signals indicating the formation of partial HDF products were observed. The conversion of the reactions were calculated by integrating the signal for Ph_3GeF versus those of starting materials in the ^{19}F-NMR spectrum of the reaction mixture. In the case of 1,3-bis(trifluoromethyl)benzene (Figure 3.5), the conversion was found to be 74% after letting the reaction stir for 18 hours in the presence of 3 mol% of $[Ph_3C][B(C_6F_5)_4]$.

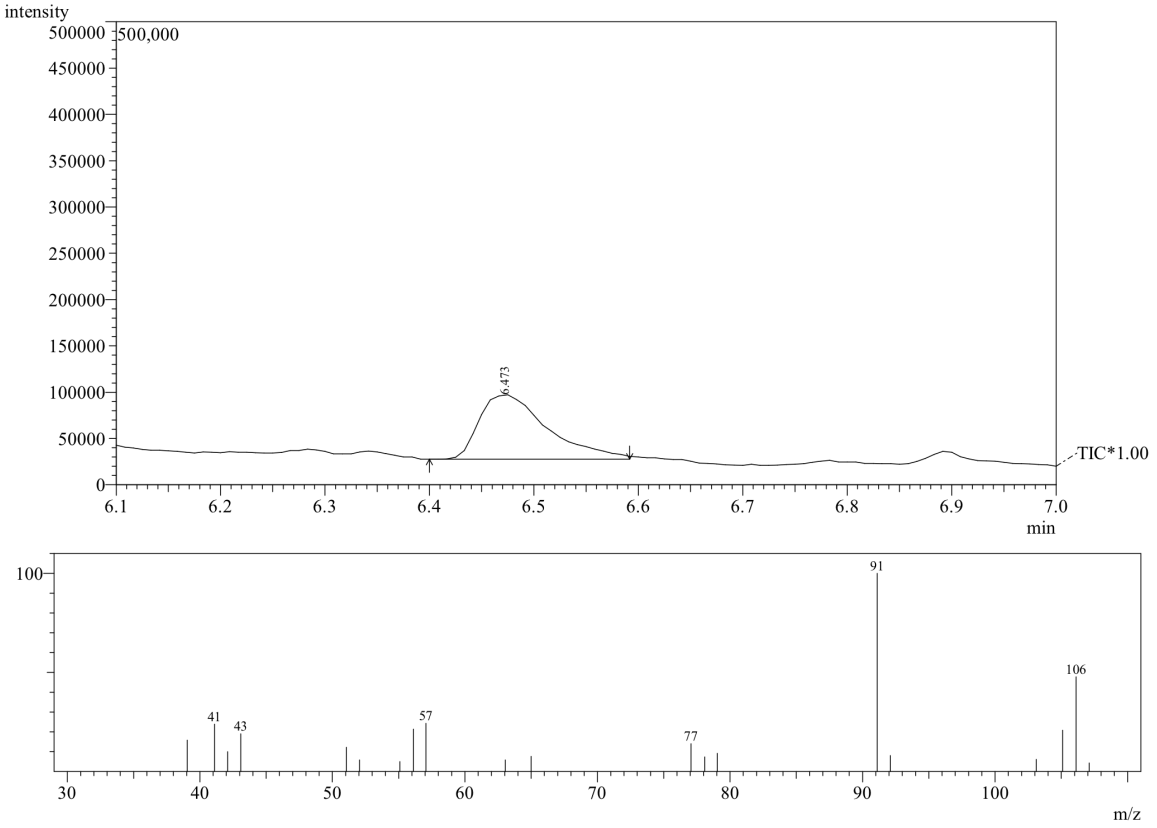

Figure 3.8: GC-MS trace of the HDF reaction of 1,3-bis(trifluoromethyl)benzene

Under the same conditions (Scheme 3.14), (trifluoromethyl)benzene reacts with Ph_3GeH and 3 mol% $[Ph_3C][B(C_6F_5)_4]$, and 56% of the benzotrifluoride is converted to products after 18 hours.

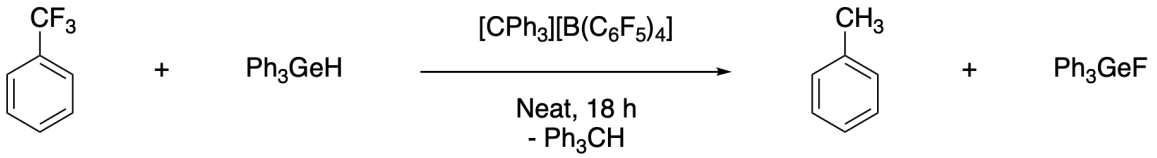

Scheme 3.14: HDF reaction of (trifluoromethyl)benzene

The ^{19}F-NMR spectrum of this reaction (Figure 3.9) shows a sharp signal at -202.4, corresponding to Ph_3GeF. Some of the starting material is unreacted probably due to solubility issues and the signal at -62.45 corresponding to (trifluoromethyl) -benzene remains. The signals for the $[Ph_3C][B(C_6F_5)_4]$ salt along with other unidentified side-products were present in the range of -130 to -170 ppm.

The ^{1}H-NMR spectrum of the reaction mixture, shown in Figure 3.10, indicates the formation of toluene which has a signal at 2.11 ppm. Unreacted germanium hydride along with Ph_3CH which is the side-product of the hydride transfer reaction, are present at 5.42 and 5.85 ppm, respectively. A standard sample of toluene was analyzed using GC-MS (Figure 3.11) and it shows a base peak for the $[M-H]^+$ ion with an $m/z = 91$ in its mass spectrum and it has a peak at $T_R = 8.2$ min in its GC trace. The GC-MS results for the reaction mixture (Figure 3.12) show the same characteristic signal at 8.2 minutes in the GC trace and a peak at $m/z = 91$ in the mass spectrum that indicates of the formation toluene.

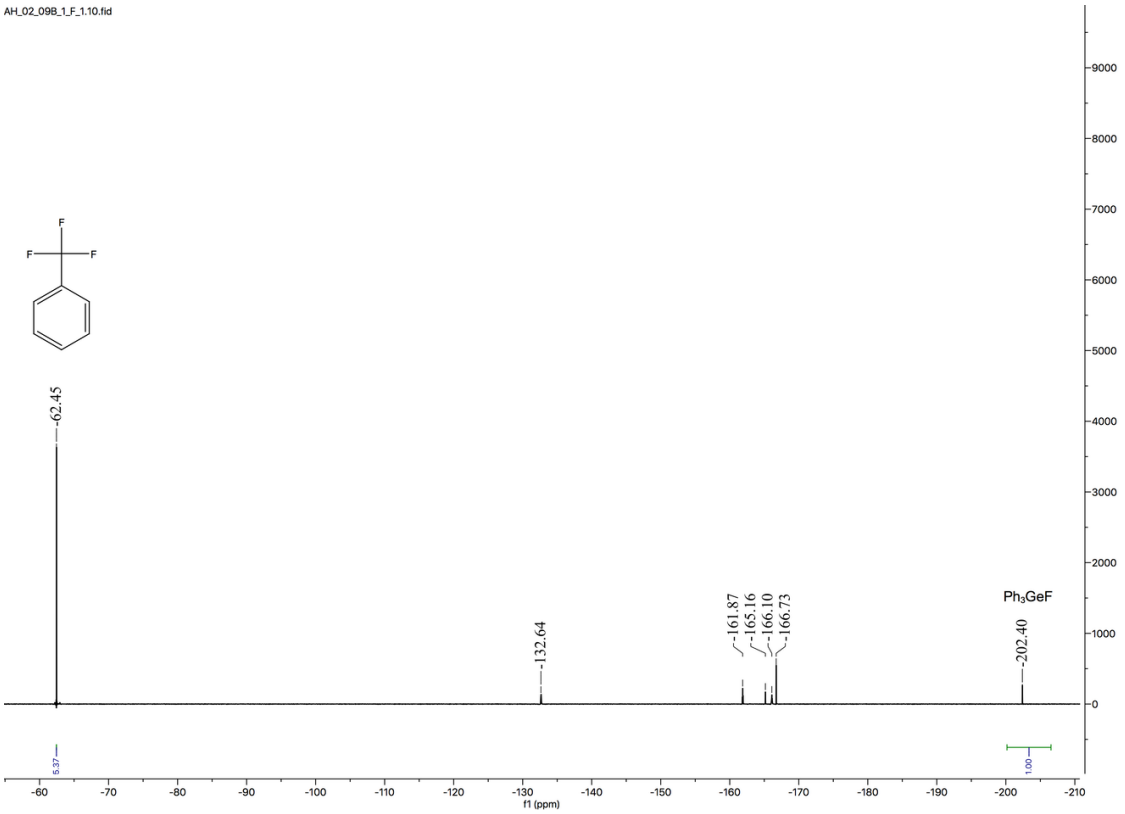

Figure 3.9: ^{19}F-NMR (376 MHz, C_6D_6) spectrum of the HDF reaction of (trifluoromethyl)benzene

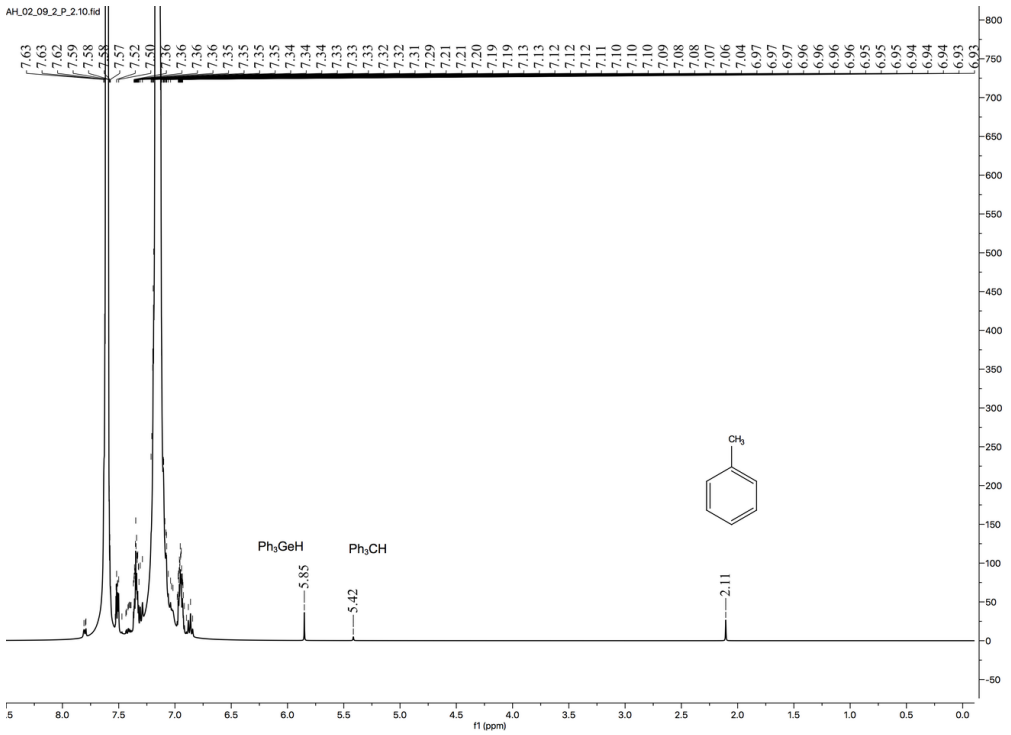

Figure 3.10: ^{1}H-NMR (400 MHz, C_6D_6) spectrum of the HDF reaction of (trifluoromethyl)benzene

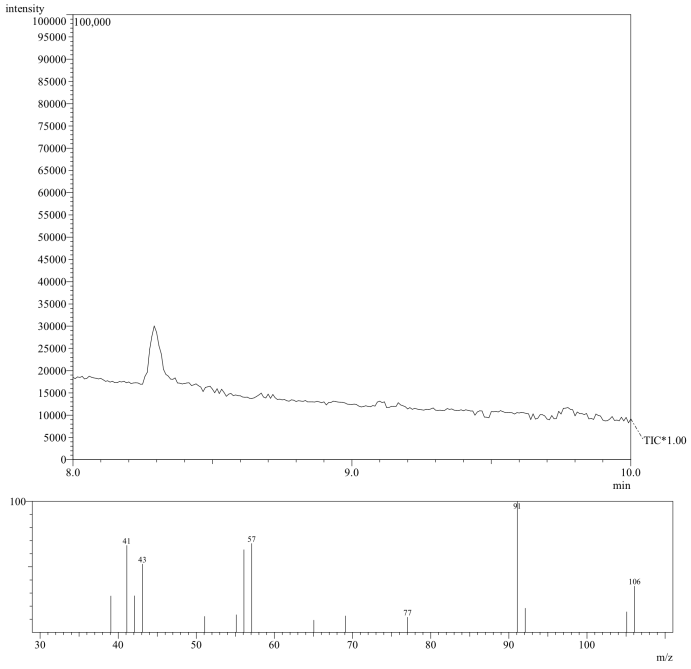

Figure 3.11: GC-MS trace of toluene

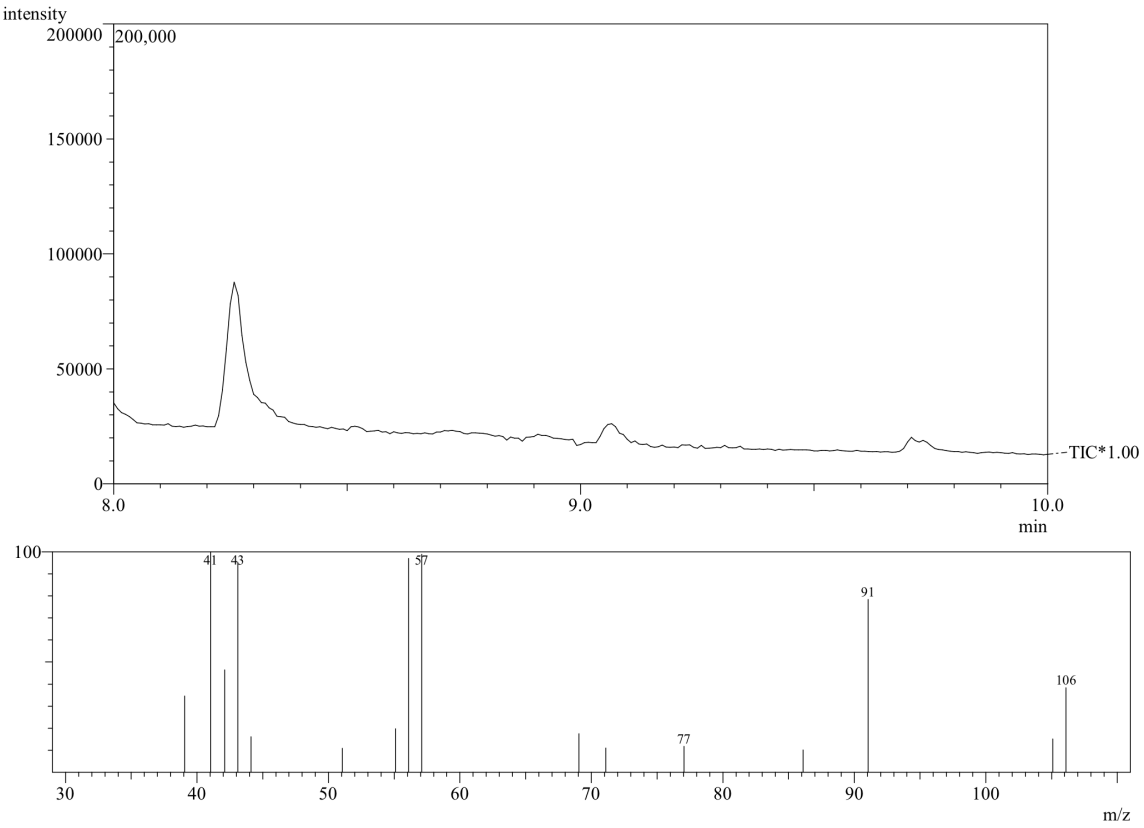

Figure 3.12: GC-MS trace of the HDF reaction of (trifluoromethyl)benzene

Different reaction conditions were applied to the benzotrifluoride substrates to gain more information about their HDF reactions. For example when 1,3-bis -(trifluoromethyl) benzene was reacted **1** in hexane, no conversion to products was detected. Trials using $^{i}Pr_3GeH$, in hexane were also unfruitful and did not result in any conversion. Other low-coordinating solvents used as well as neat conditions gave similar results. When 1,3-dichlorobenzene was used as the solvent, no conversion was observed in the (trifluoromethyl)benzene HDF reaction after a reaction time of 2 days.

In order to explore the effects of the presence of an electron-donating group on the carbocation intermediates that form in the HDF reactions with **1**, the HDF reaction of 3-(trifluoromethyl)aniline was conducted and no conversion to products was observed using neat conditions. It is theorized that the reason for this is that

the $-NH_2$ group acts as a Lewis base and quenches the reactivity of **1**. Scheme 3.15 shows how the reductive amination reaction using (trifluoromethyl)aniline and formaldehyde can yield *N,N*-dimethyl-3-(trifluoromethyl)aniline. The HDF reaction of *N,N*-dimethyl-3-(trifluoromethyl)aniline was performed under neat conditions at a higher temperature (40 °C), and this time, 80% conversion was observed after one hour. Figure 3.13 shows the signal for the remaining starting material and Ph_3GeF. The observed conversion highlights the fact that while the Lewis basicity of the amine group increases upon alkylation but steric limitations also play important role on the quenching the reactivity of **1**.

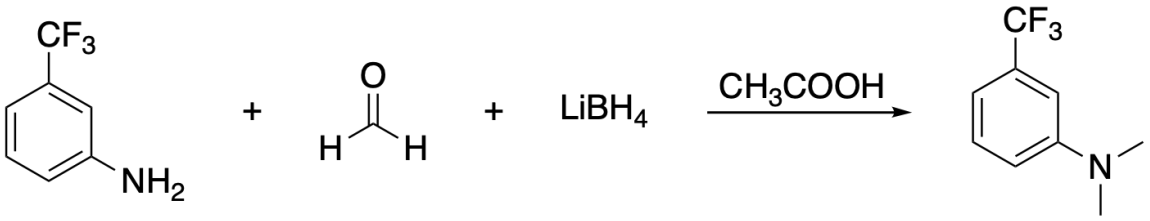

Scheme 3.15: Synthesis of *N,N*-dimethyl-3-(trifluoromethyl)aniline

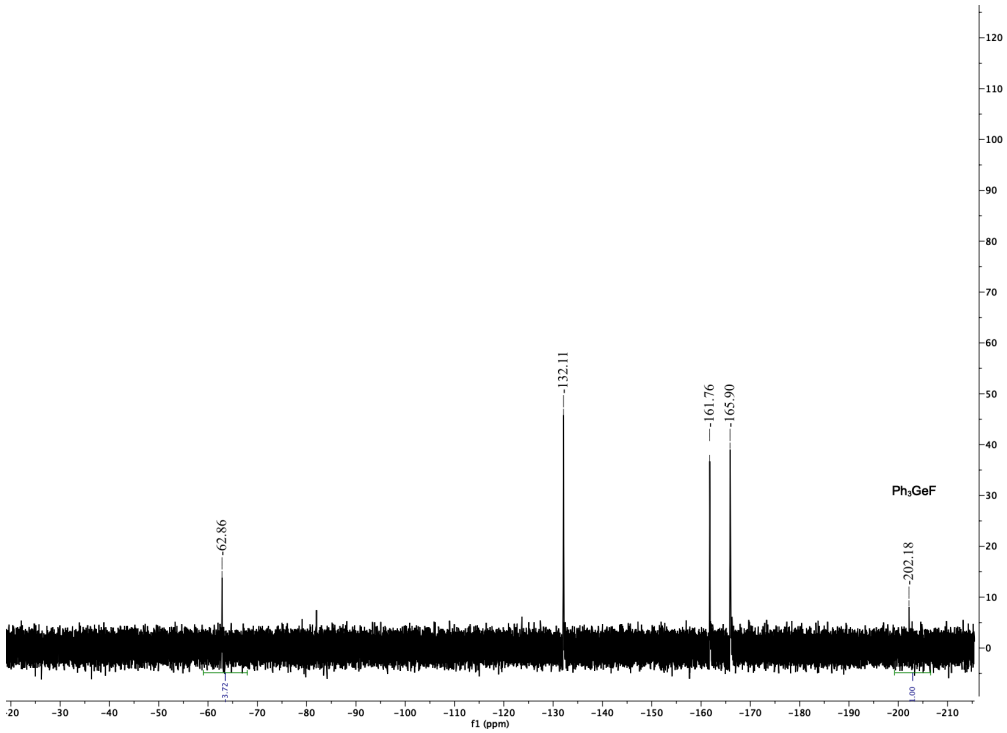

Figure 3.13: ^{19}F-NMR (376 MHz, C_6D_6) spectrum of the HDF of *N,N*-dimethyl-3-(trifluoromethyl)aniline

Benzotrifluorides containing electron-withdrawing groups showed no conversion in the HDF reactions using **1**. Octafluorotoluene did not result in the formation of any Ph_3GeF when reacted with **1** at room temperature, or at 45 °C under neat conditions, or in 1,3-dichlorobenzene solvent at 80 °C with a reaction time of 2 days.

3.2.2 HDF Reactions of Alkyl Fluorides

The HDF protocol using **1** was also evaluated using several alkyl fluoride substrates. Scheme 3.16 shows the reactions of 1-fluorooctane and 1-fluorocyclohexane with **1**. In both cases the reactions undergo an almost quantitative conversion. In case of 1-fluorooctane, it is postulated that the high Lewis acidity/fluorophilicity of **1** compensates for the initial formation of an unstable primary carbocation. Figures 3.14 and 3.15 show the ^{19}F-NMR and the ^{1}H-NMR spectra of the reaction mixture for the HDF reaction of 1-fluorooctane. The upfield signal at -217.59 matches with the signal found from the original sample of 1-fluorooctane and the signal of Ph_3GeF is observed at chemical shift of -201.80 ppm.

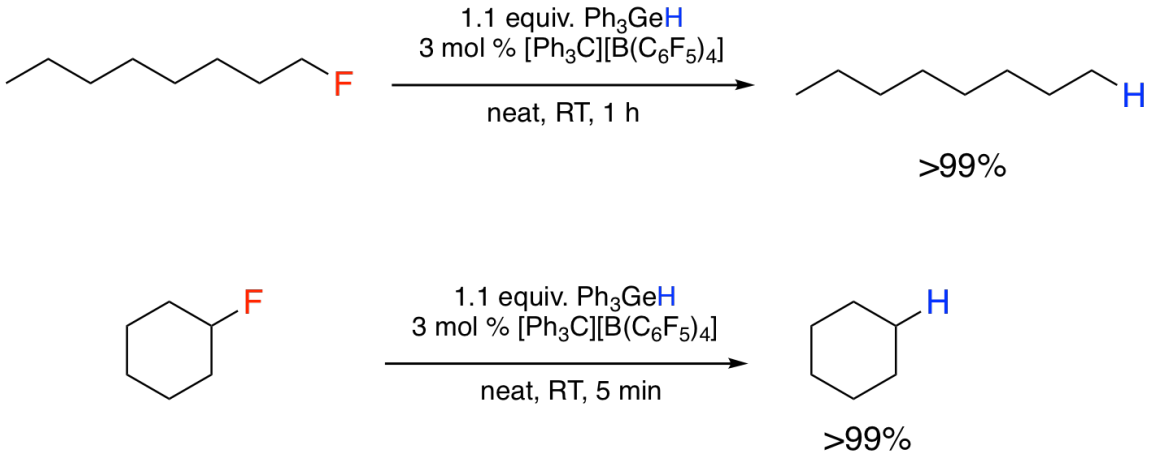

Scheme 3.16: HDF reactions of primary and secondary alkyl fluorides

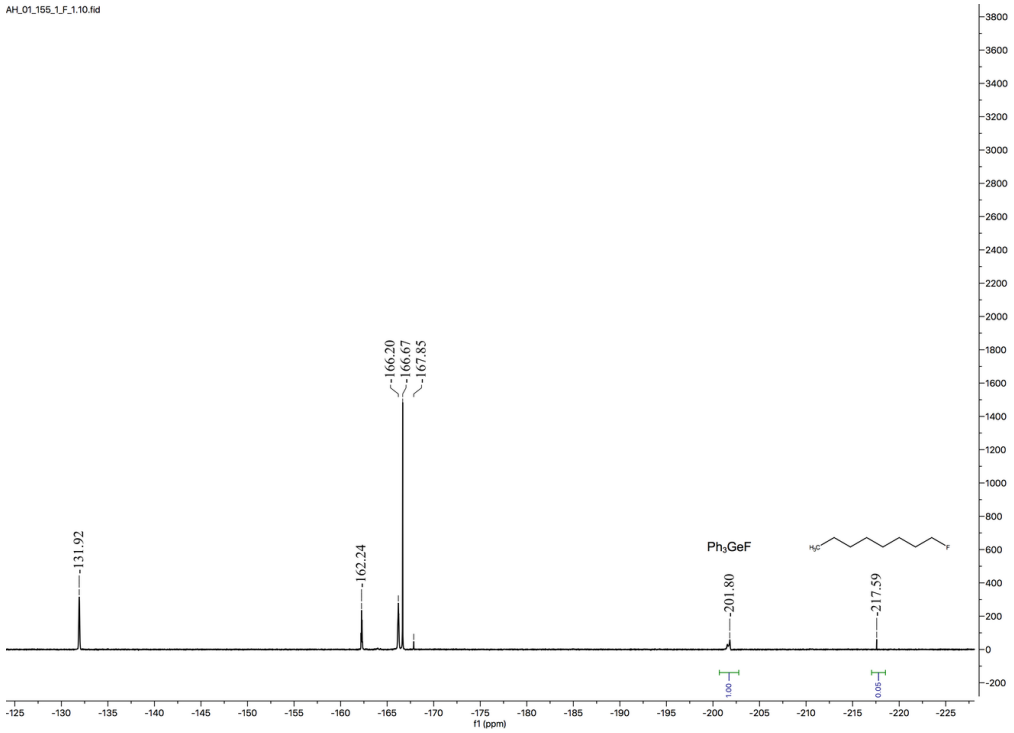

Figure 3.14: ^{19}F-NMR (376 MHz, C_6D_6) spectrum of the HDF reaction of 1-fluorooctane

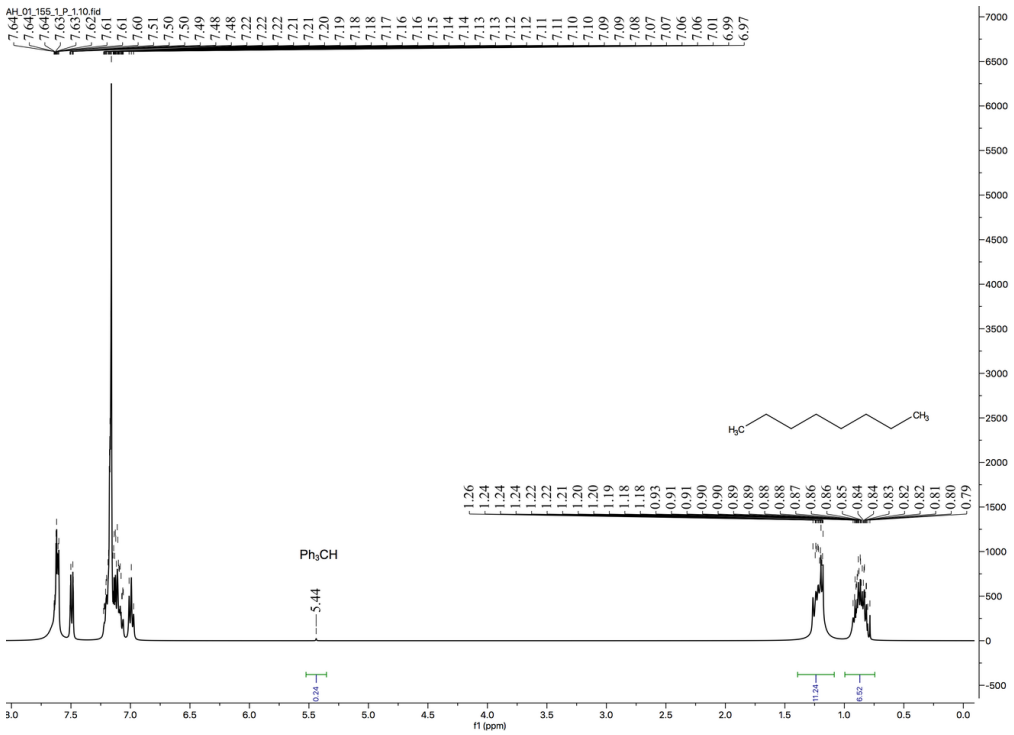

Figure 3.15: ^{1}H-NMR (400 MHz, C_6D_6) spectrum of the HDF reaction of 1-fluorooctane

In the ^{1}H-NMR spectrum for the HDF of 1-fluorooctane signals for aliphatic C−H bonds are observed in the range of 0.79-1.26 ppm and no hydride peak is observed at 5.80 ppm which indicates all the Ph_3GeH is consumed. Figure 3.16 shows the GC-MS trace of the standard 1-fluorooctane sample. The retention times and the fragmentation patterns observed in the GC-MS trace of the reaction mixture shown in Figure 3.17 matches with that of the standard sample, and the MS exhibits the characteristic fragmentation pattern of alkanes.

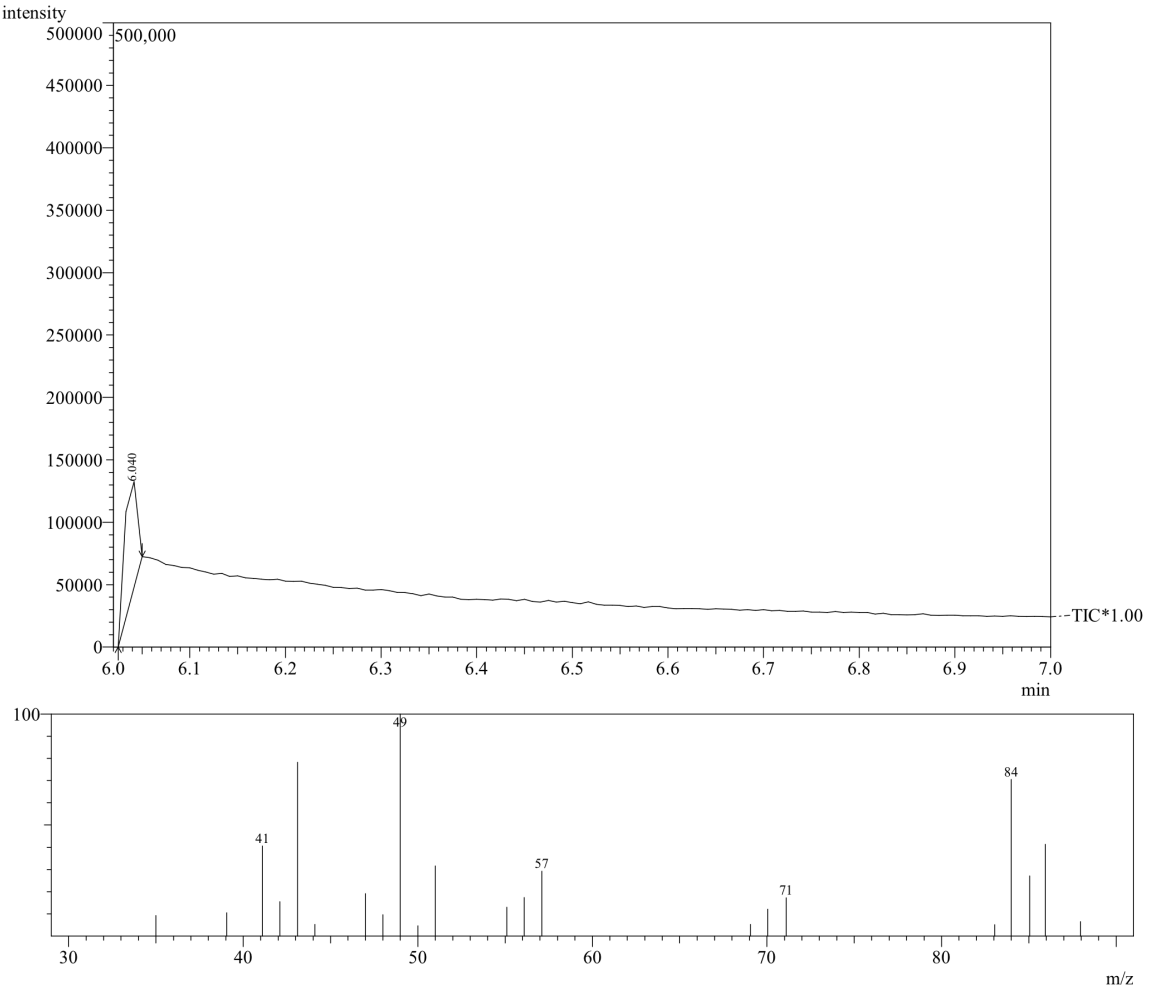

Figure 3.16: GC-MS trace of octane

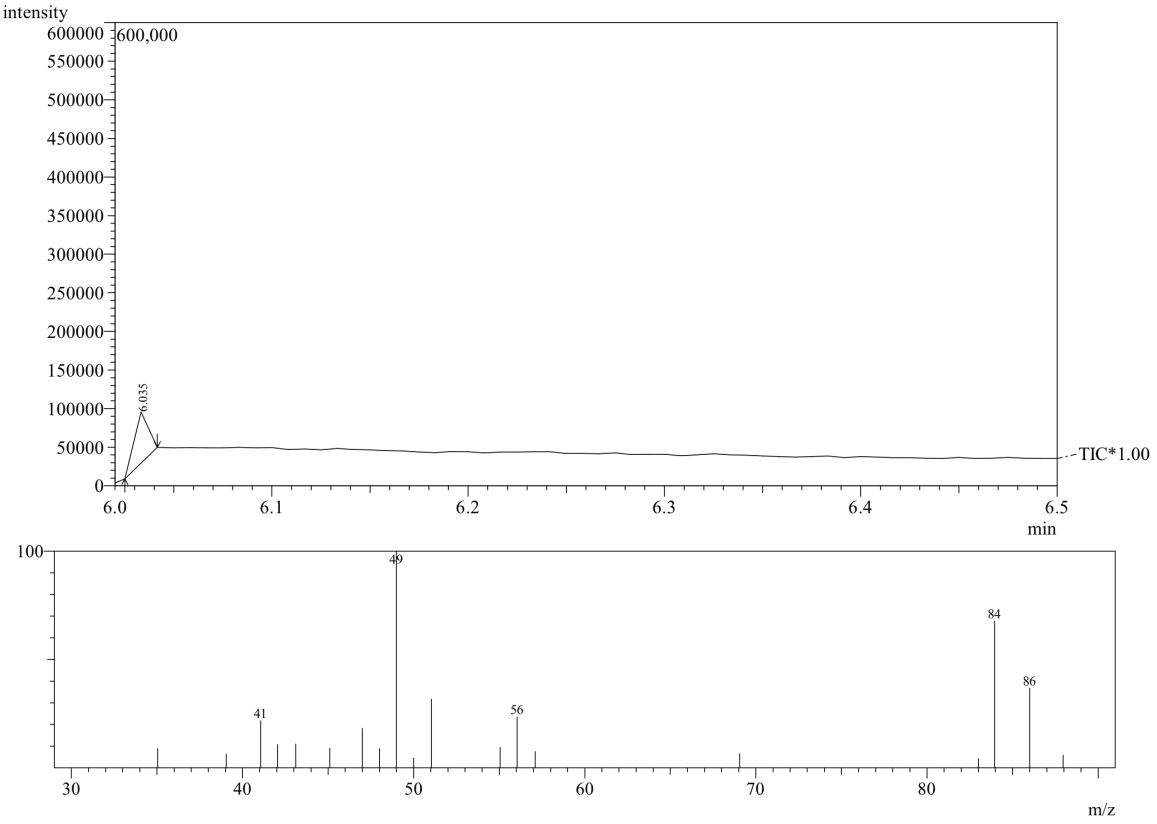

Figure 3.17: GC-MS trace of the HDF reaction of octane

The HDF reaction using **1** also proceeded cleanly using a secondary alkyl fluoride. The ^{19}F-NMR of the HDF reaction of 1-fluorocyclohexane (Figure 3.18) shows a full conversion of the starting material to cyclohexane. The sharp signal of Ph_3GeF was observed at -201.77 ppm along with the signals corresponding to $[B(C_6F_5)_4]^-$ anion. The ^{1}H-NMR spectrum of the reaction mixture (Figure 3.19) indicates the formation of cyclohexane by a sharp singlet signal at 1.39 ppm. The other signals observed in the reaction are due to remaining Ph_3GeH at 5.86 ppm and Ph_3CH at 5.43 ppm, and both also have respective signals in the aryl region.

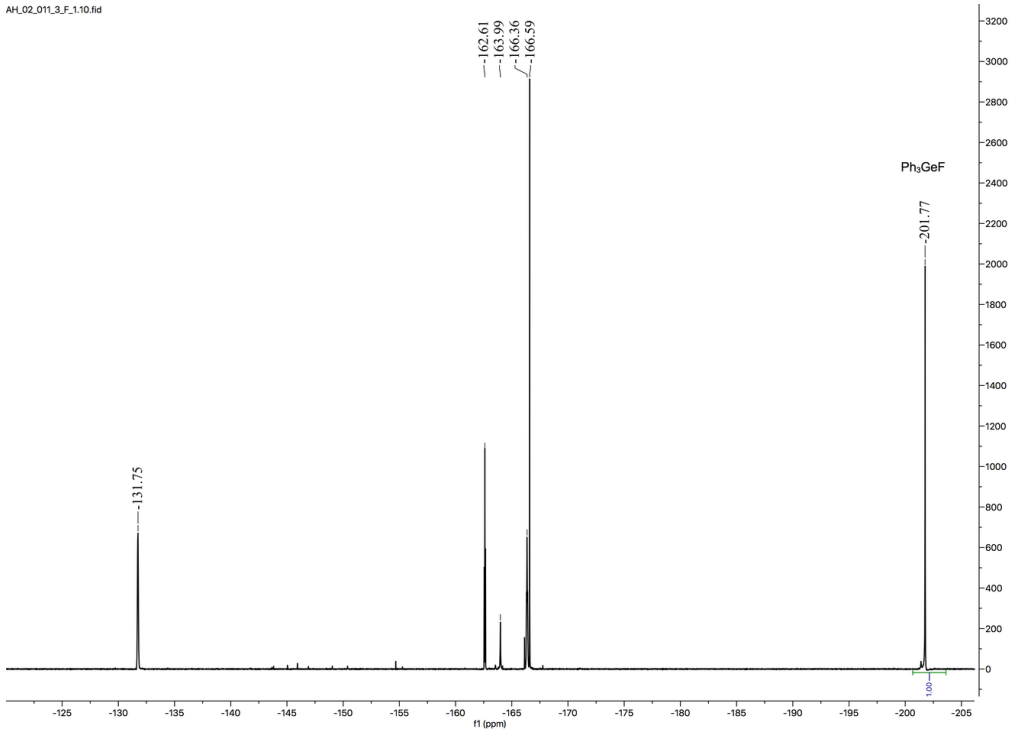

Figure 3.18: ^{19}F-NMR (376 MHz, C_6D_6) spectrum of the HDF reaction of 1-fluorocyclohexane

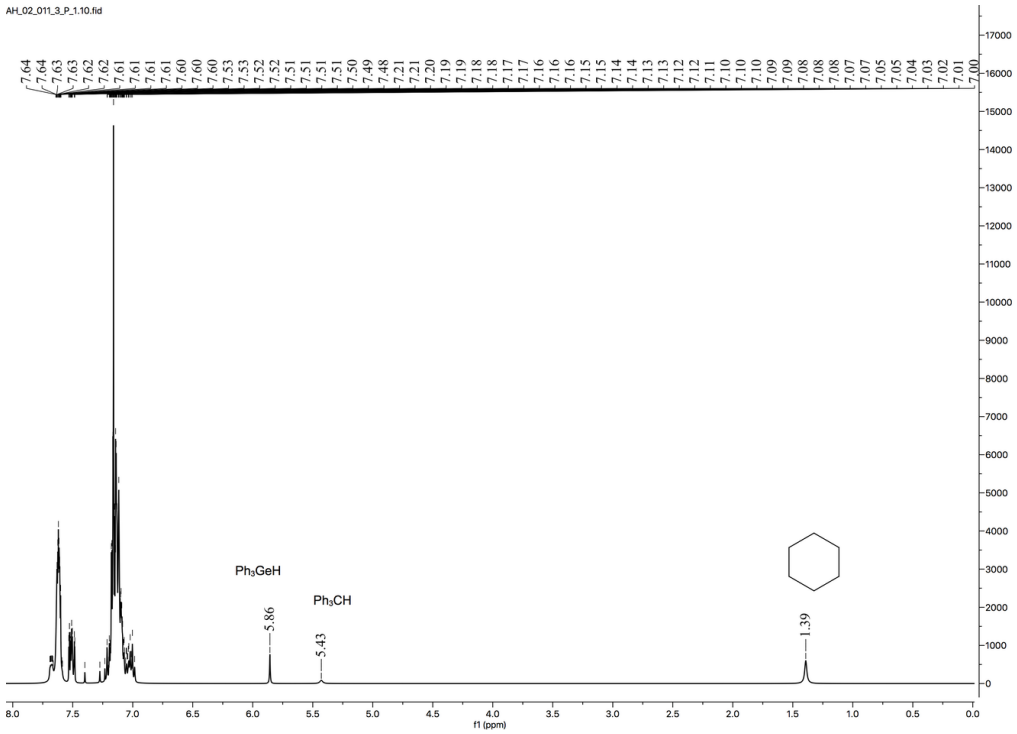

Figure 3.19: ^{1}H-NMR (400 MHz, C_6D_6) spectrum of the HDF reaction of 1-fluorocyclohexane

The GC-MS trace of the HDF reaction mixture of 1-fluorocyclohexane was compared with that of a standard sample of cyclohexane. In Figure 3.20, the chromatogram of cyclohexane exhibits a peak at 11 minutes and the MS exhibits a peak at $m/z = 84$. The GC trace of the reaction mixture in Figure 3.21 shows a peak with $T_R = 12$ minutes with mass spectrum matches that of the standard sample of cyclohexane.

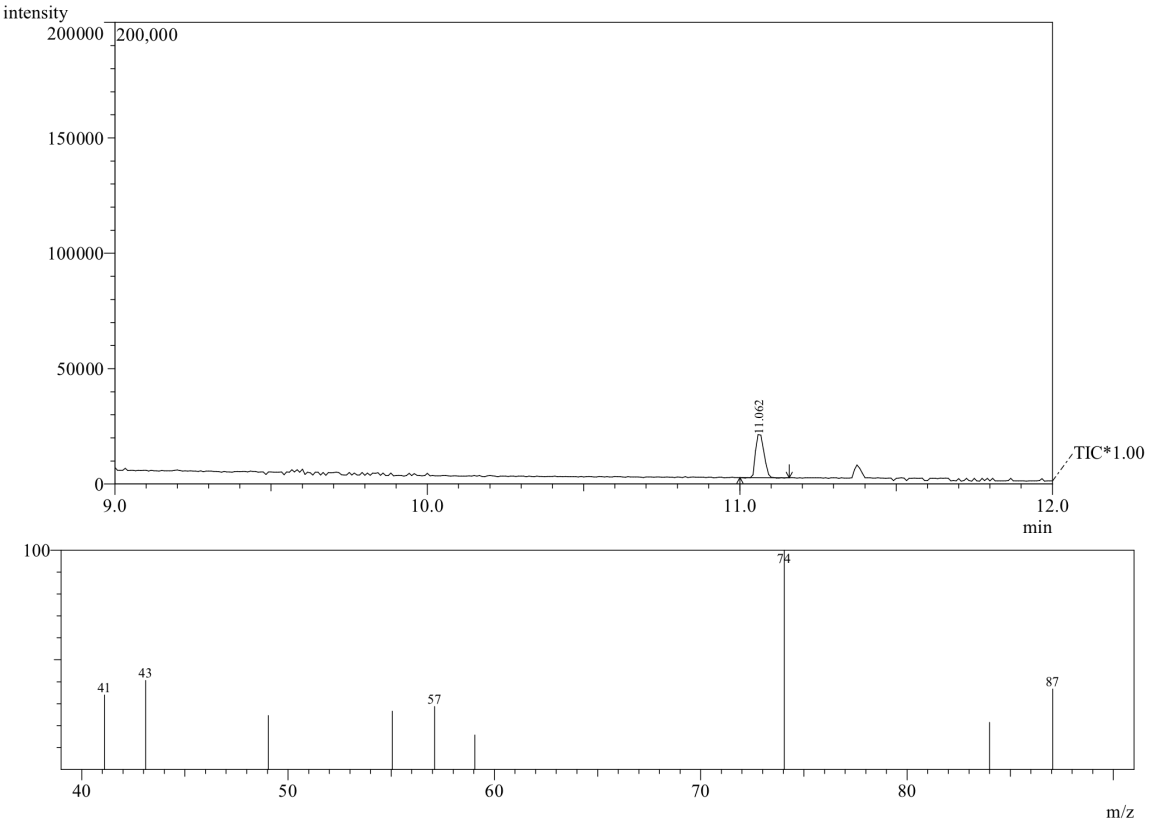

Figure 3.20: GC-MS trace of cycloxhexane

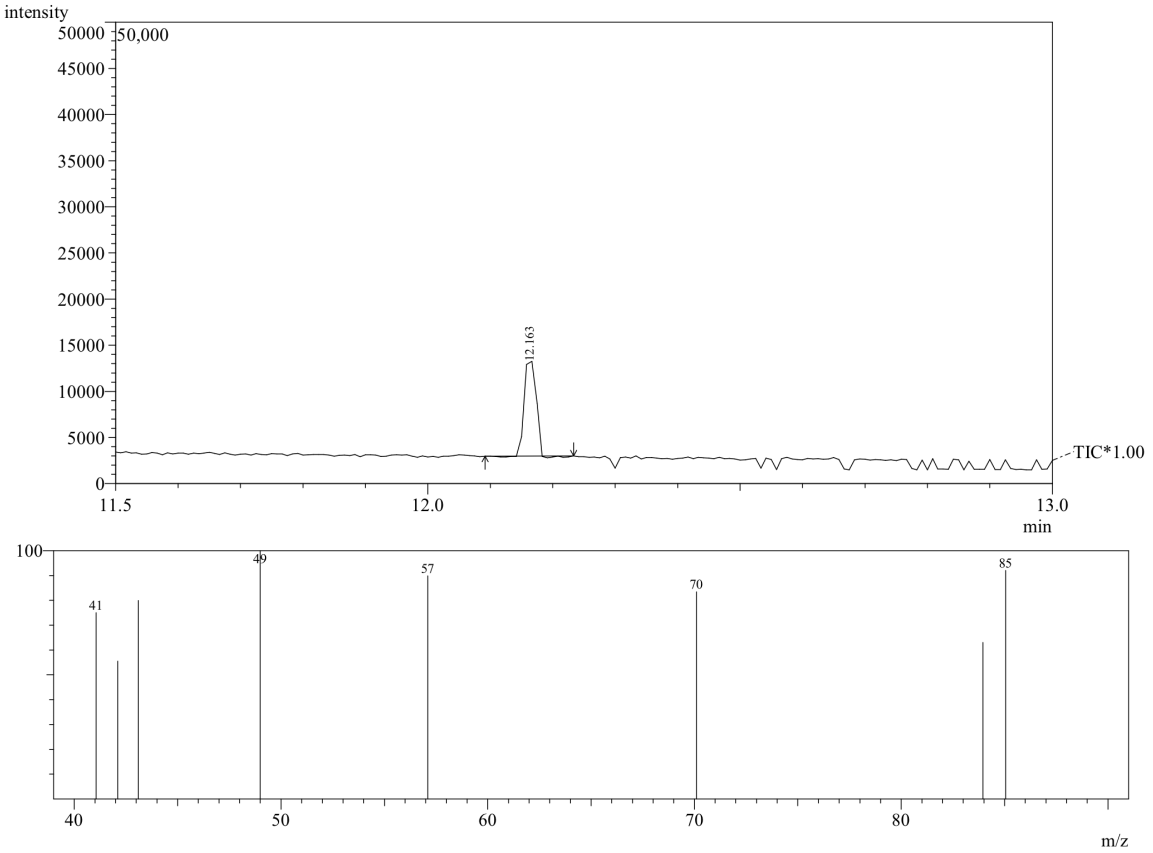

Figure 3.21: GC-MS trace of the HDF of reaction of 1-fluorocyclohexane

The HDF reactions of other alkyl fluorides were also attempted using **1**. The reaction of **1** with CH_2F_2 under neat conditions or in 1,3-dichlorobenzene at 80 °C with a reaction time of two days were unsuccessful. The HDF of HFIP was also tried by using **1**, but no conversion was observed. The ability of **1** to function in HDF reactions in the presence of a Lewis base compound emphasizes the strong sensitivity of the Lewis acidity of **1**, rendering the reaction to be very functional group intolerant. The HDF of **1** with Ph_3SiF was also attempted and did not result in any hydrodefluorination. This reactivity was expected since the silylium ions are more unstable compared to germylium ions and their formation is thermodynamically unfavorable.

3.2.3 HDF Reactions of Acyl Fluorides

Benzoyl fluoride can also be converted to benzaldehyde without any decarbonylative over-reduction to benzene using **1** as the Lewis acid to abstract the fluorine atom. The reaction can be monitored by ^{1}H-NMR spectroscopy because the signal of by-product Ph_3CH at 5.44 ppm in C_6D_6 is distinctive and indicative of the hydride transfer reaction between Ph_3GeH and $[CPh_3][B(C_6F_5)_4]$. When $[Ph_3Ge][B(C_6F_5)_4]$ **1** is formed, the signal for benzoyl fluoride in the ^{19}F-NMR spectrum of the reaction mixture at 17.9 ppm, starts to disappear and the signal for Ph_3GeF at -202.4 starts to become visible and increases in intensity as the reaction proceeds.

Scheme 3.17 shows that when benzoyl fluoride is mixed with 1.1 equivalents of Ph_3GeH and 3 mol% of $[CPh_3][B(C_6F_5)_4]$ and the reaction mixture is stirred at room temperature for 18 hours in a glove box, a sharp signal at -202.38 appears in the ^{19}F-NMR spectrum which confirms the formation of Ph_3GeF, while the peak corresponding to benzoyl fluoride at 17.9 ppm completely disappears (Figure 3.22).

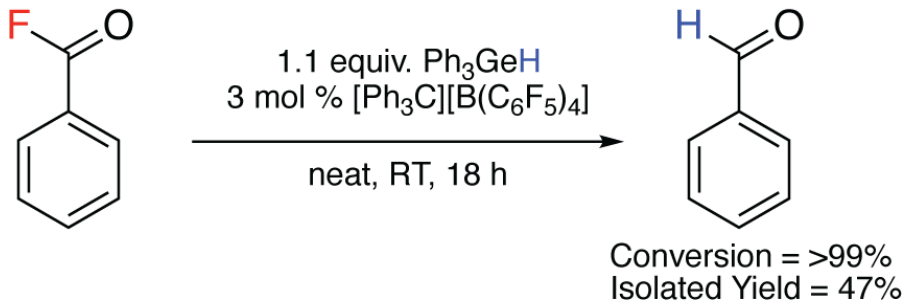

Scheme 3.17: The HDF reaction of benzoyl fluoride

The crude ^{1}H-NMR spectrum of the reaction mixture shows a signal at 5.44 ppm corresponding to Ph_3CH. After work-up, the ^{1}H-NMR spectrum of the product (Figure 3.23) shows a singlet peak at 9.69 ppm that indicates benzaldehyde has been formed in the reaction.

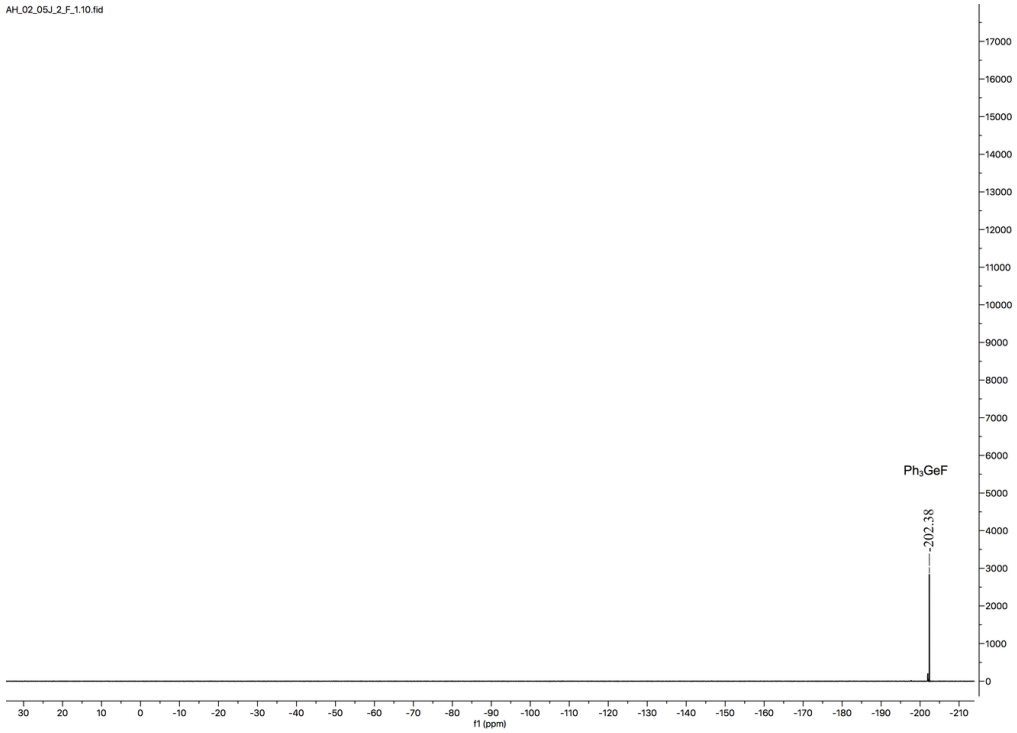

Figure 3.22: ^{19}F-NMR (376 MHz, C_6D_6) spectrum of the HDF of benzoyl fluoride

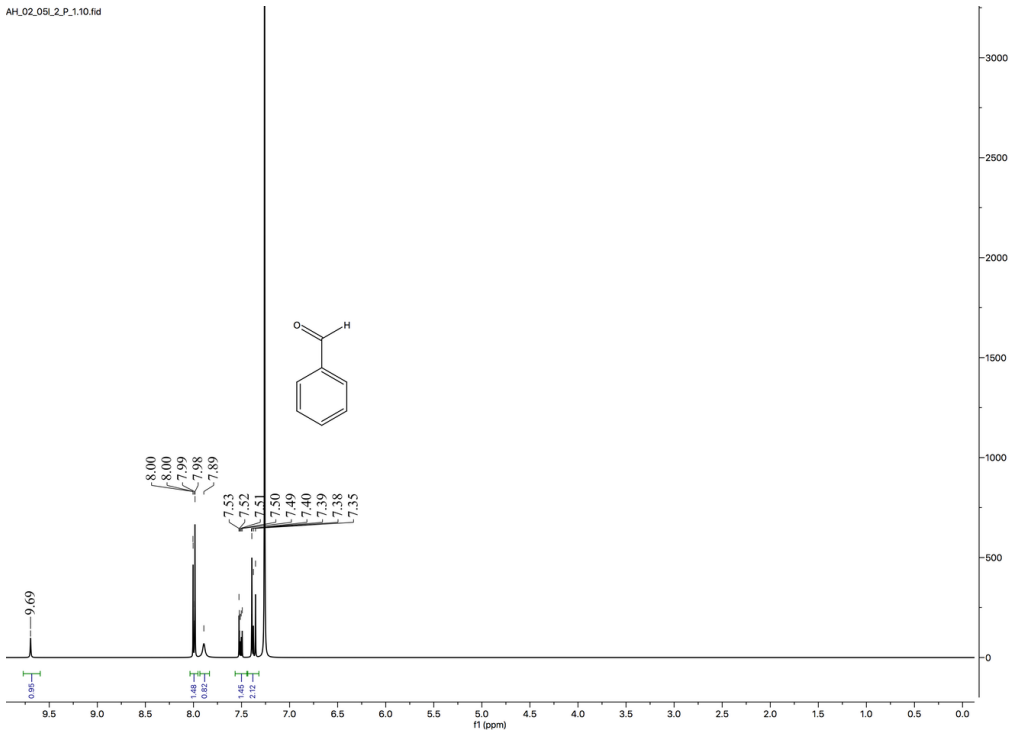

Figure 3.23: ^{1}H-NMR (400 MHz, $CDCl_3$) spectrum of benzaldehyde as the product of the HDF of benzoyl fluoride

The reaction was also monitored by GC-MS. The GC trace of the reaction mixture (Figure 3.24) shows a peak at 6.95 minutes with a corresponding peak at $m/z = 105.00$ in the MS that is due to the parent acylium ion $PhCO^+$. The fragmentation pattern and the retention time in the GC chromatogram of the reaction mixture was found to be identical to the GC-MS data for the standard sample of benzaldehyde (Figure 3.25).

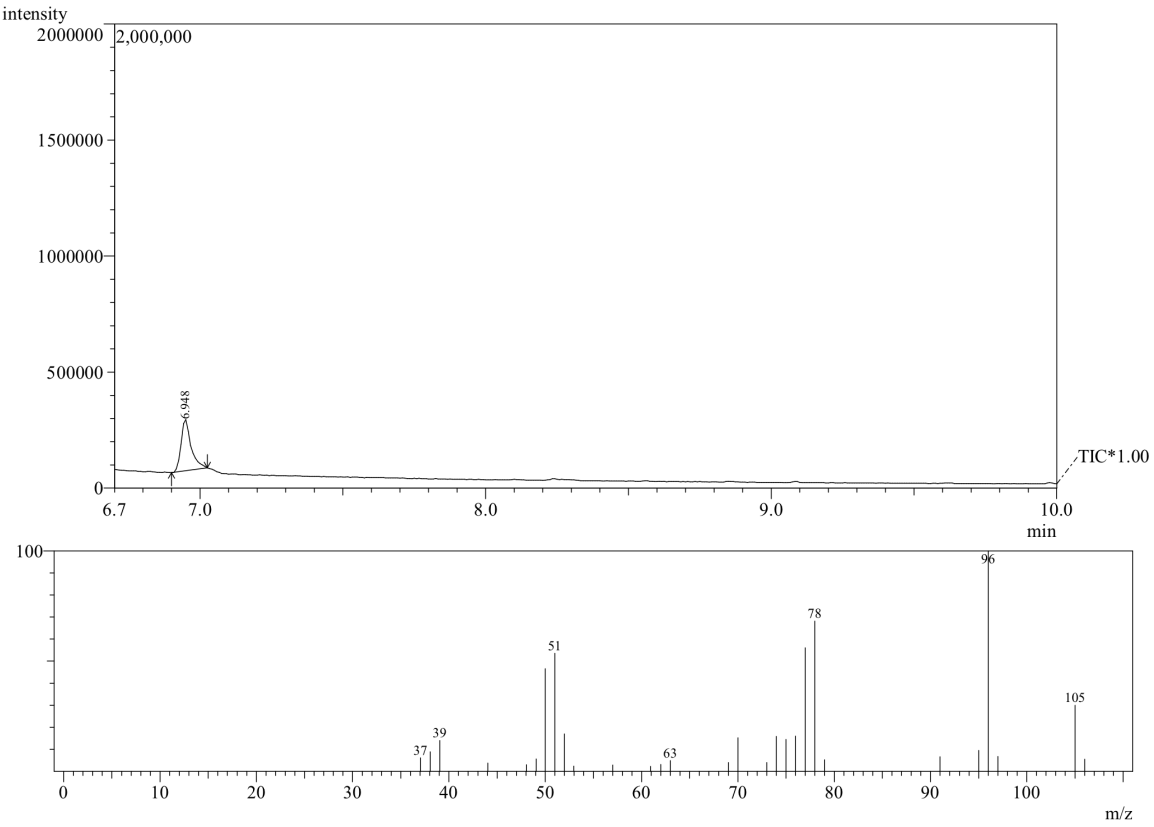

Figure 3.24: GC-MS trace of the HDF reaction of benzoyl fluoride

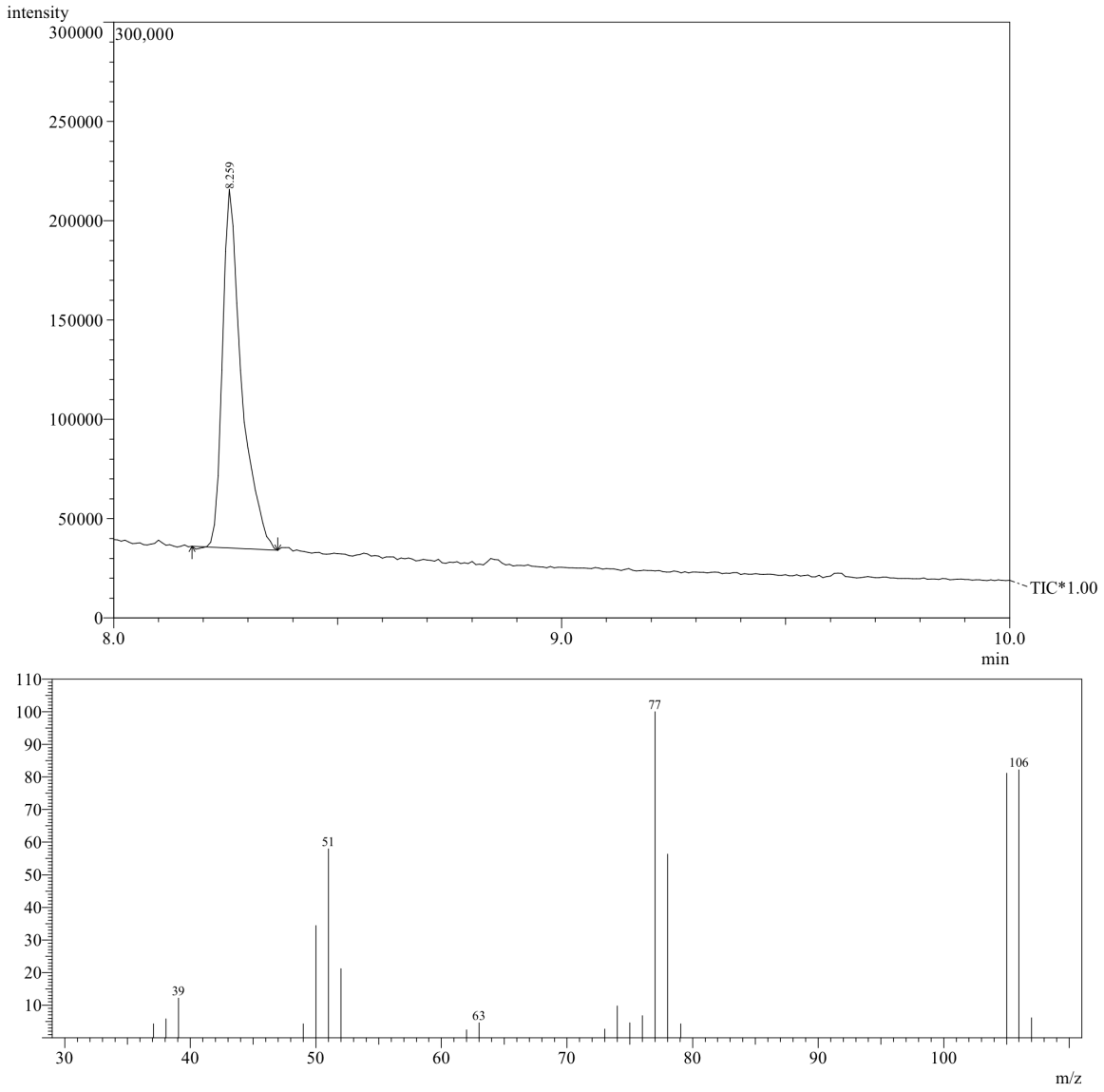

Figure 3.25: GC-MS trace of benzaldehyde

Ozerov *et al.* have reported HDF reactions using silylium ions that are generated from silanes. In their studies, they have used $[Et_3Si][HCB_{11}H_5Cl_6]$ as the catalyst. A very good WCA, here the carborane, was required for a successful reaction and the $[B(C_6F_5)_4]^-$ anion was shown to be unstable when paired with the very reactive silylium ions.[123,128] When the reactions of $Ph_3SiH/[Ph_3C][B(C_6F_5)]$ with (trifluoromethyl)benzene and benzoyl fluoride were attempted, highly exothermic reactions occurred which yielded toluene and benzaldehyde with only partial conversion to

the products. Unsurprisingly, when Ph_3CH was used as a potential reagent for F^- abstraction via formation of Ph_3C^+ instead of Ph_3GeH, no reaction was observed.

Stephan *et al.* have shown that BCF can activate C–F bonds catalytically and stoichiometrically.[124] It was previously discussed that BCF was able to generate silylium ions and germylium ions *in situ* from silicon and germanium hydrides. In order to see if similar reactivity could be observed, the HDF reactions of benzoyl fluoride or (trifluoromethyl)benzene with Ph_3GeH and a catalytic amount of BCF were attempted. In the case of (trifluoromethyl)benzene, no HDF was observed and the reason for this is likely that an *in situ* formed germylium is not Lewis acidic enough to activate relatively inert benzotrifluorides. However, the HDF of benzoyl fluoride did occur under these conditions but the observed conversion was only 18% after 18 hours.

Scheme 3.18 indicates that **1** is also able to abstract fluorine from aliphatic acyl fluorides and convert them to aldehydes. When the HDF reaction mixture of pentanoyl fluoride was stirred at room temperature under neat conditions for 18 hours, the NMR spectra were acquired in CD_2Cl_2 solvent because of the poor solubility of the aldehyde product in benzene. The ^{19}F-NMR spectrum of the reaction mixture (Figure 3.26) indicated the formation of Ph_3GeF by the presence of signal at -201.79 ppm, and the peak for pentanoyl fluoride at 45.1 ppm was absent.

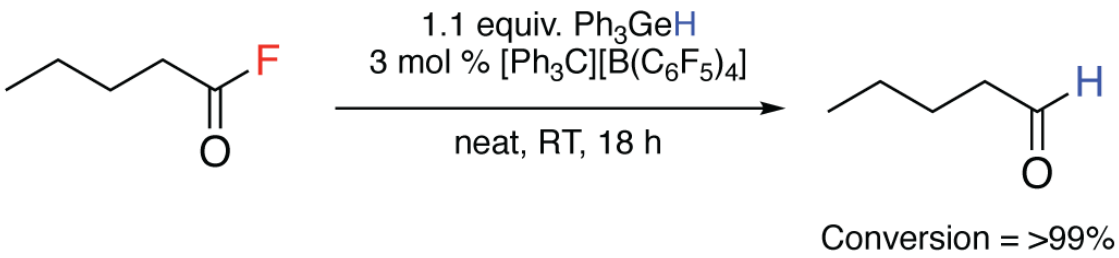

Scheme 3.18: The HDF of pentanoyl fluoride

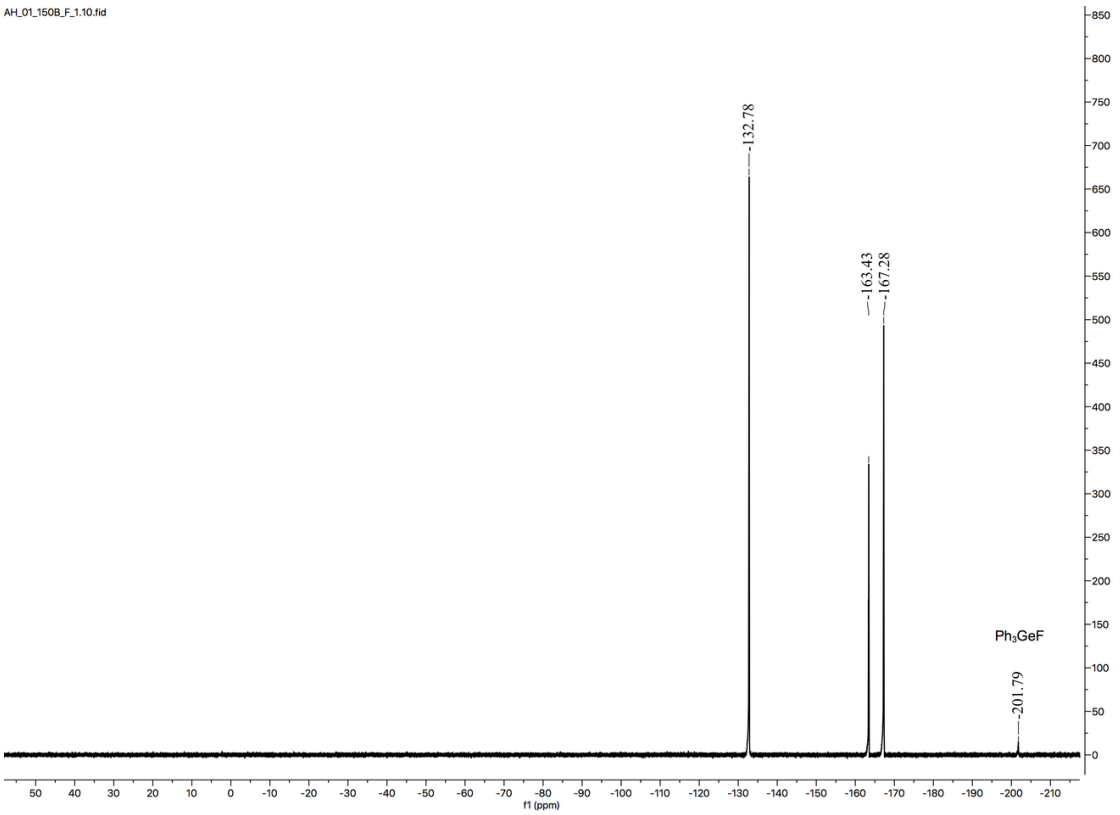

Figure 3.26: ^{19}F-NMR (376 MHz, CD_2Cl_2) spectrum of the HDF of pentanoyl fluoride

The ^{1}H-NMR spectrum of the reaction mixture (Figure 3.27) after work-up exhibited a signal at 9.11 ppm which indicated the formation of pentanal. The observed signal for pentanoic acid is attributed to the oxidation of the formed aldehyde. This was further verified using GC-MS (Figure 3.28) in which the GC peak at $T_R = 12.18$ minutes which has a peak at $m/z = 85.10$ in its MS that corresponds to the aliphatic acylium ion $C_5H_9O^+$. This data matches with the GC-MS data of the authentic sample of pentanal (Figure 3.29).

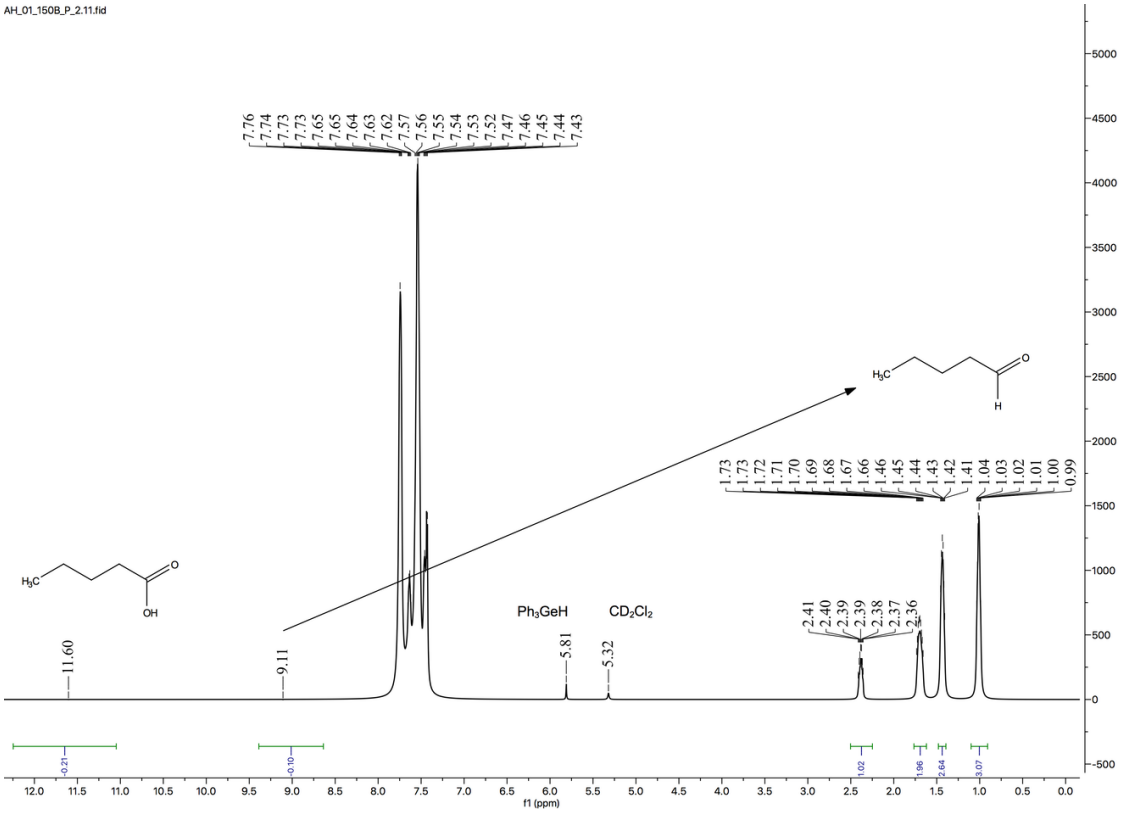

Figure 3.27: ^{1}H-NMR (400 MHz, CD_2Cl_2) spectrum of pentanal as the product of the HDF of pentanoyl fluoride

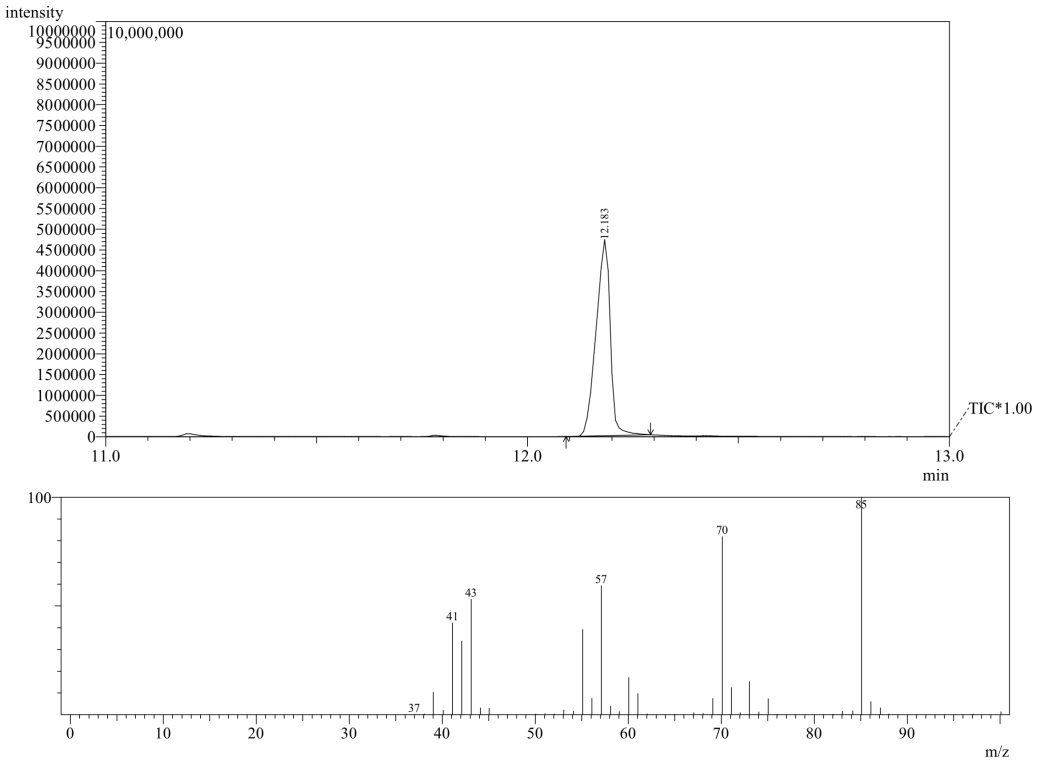

Figure 3.28: GC-MS trace of the HDF reaction of pentanoyl fluoride

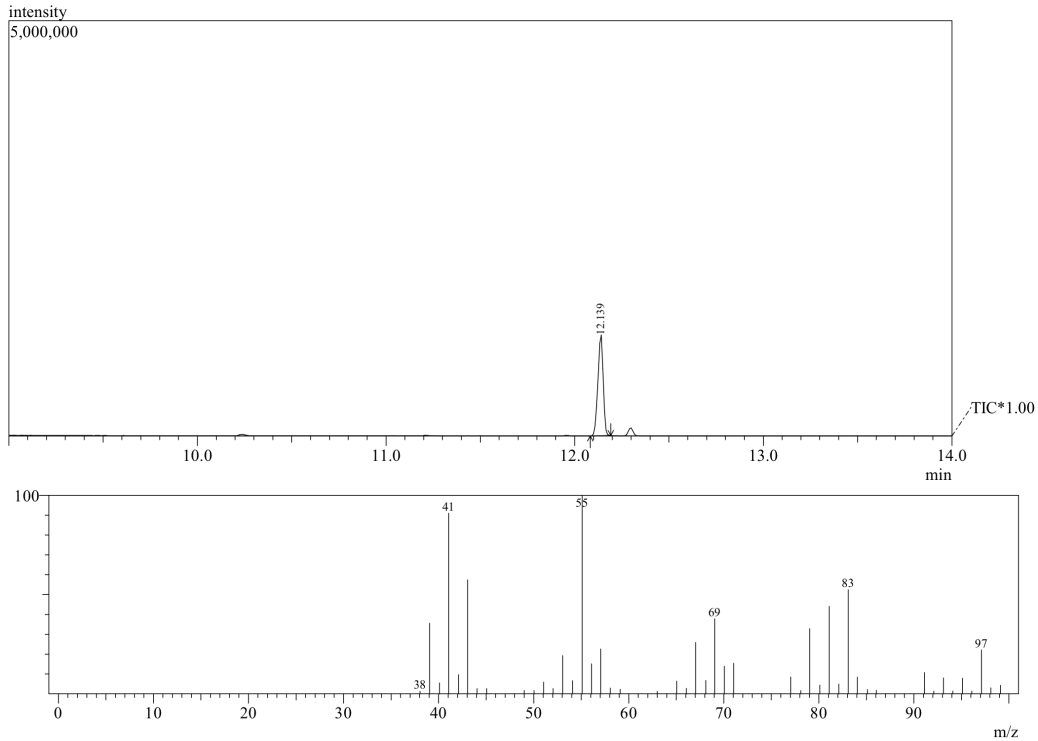

Figure 3.29: GC-MS trace of pentanal

3.2.4 Proposed Mechanism of HDF by $[Ph_3Ge][B(C_6F_5)_4]$ 1

The proposed mechanism of the HDF by **1** is based on the notion that **1** is the actual catalyst in the HDF reactions, since Ph_3GeH cannot perform the HDF reactions alone. When a mixture of benzoyl fluoride and Ph_3GeH were mixed for 24 hours without the addition of $[CPh_3][B(C_6F_5)_4]$, no defluorination or the formation of benzaldehyde was observed. As shown in Scheme 3.19 for the HDF of benzoyl fluoride, it is proposed that after tritylium cation $[Ph_3C]^+$ abstracts a hydride from Ph_3GeH, **1** is generated. Our ongoing research, along with recent studies regarding silylium ions and other germylium ions strongly suggest that **1** coexists as adducts and complexed germylium ion during the reaction.[86,129]

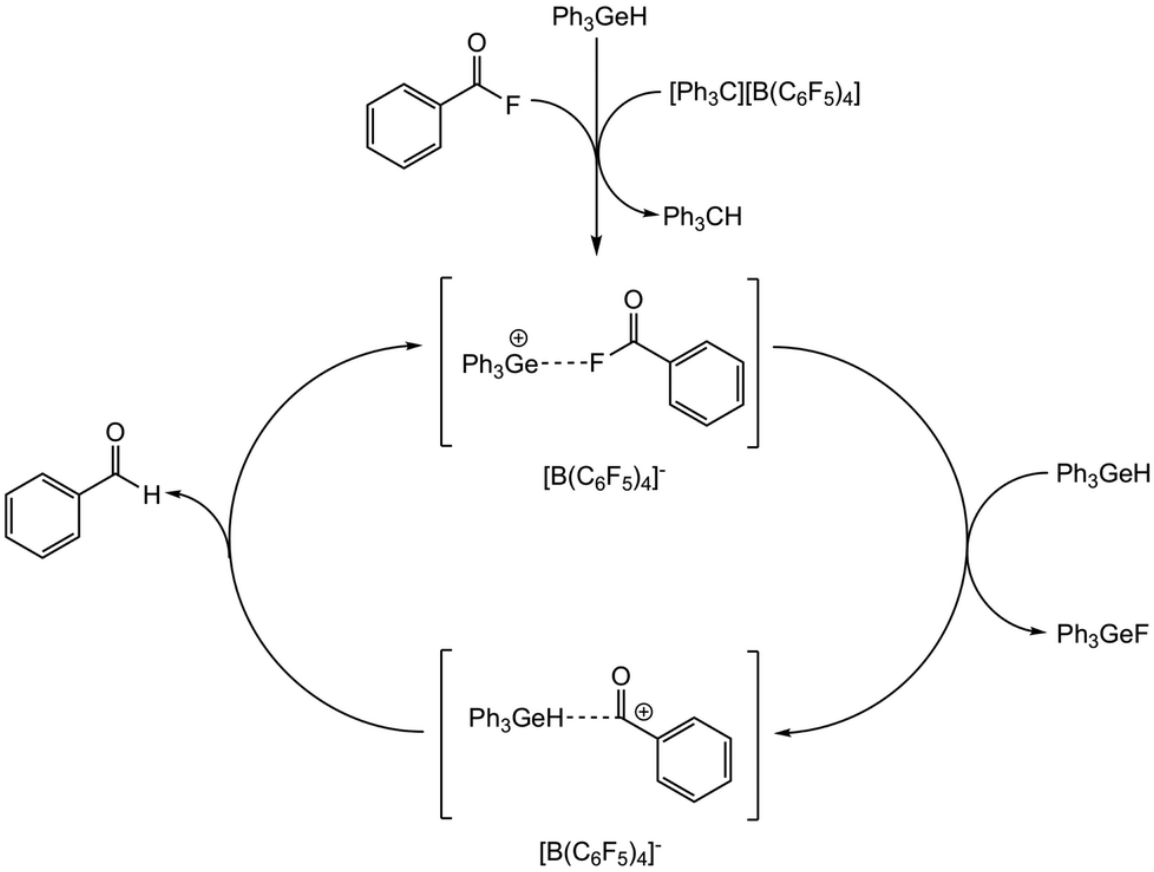

Scheme 3.19: Proposed reaction mechanism for the HDF of benzoyl fluoride

It is very likely that **1** interacts with any species that are even slightly Lewis basic. It is proposed that **1** interacts with benzoyl fluoride and this interaction is not

exclusive with the fluorine atom but can also occur with the C=O group of benzoyl fluoride or, as discussed previously (in Figure 3.4), with the remaining Ph_3GeH. The coordinated germylium ion **1** then abstracts a fluorine to form Ph_3GeF and a very reactive acylium ion that is stabilized by the $[B(C_6F_5)_4]^-$ ion as its WCA. The benzoyl cation then abstracts a hydride from Ph_3GeH to form benzaldehyde and regenerate **1**.

Figure 3.30 shows the DFT-calculated structure of the LUMO of Ph_3Ge^+ in the gas-phase with no interactions with other substituents. This structure essentially is a trigonal planar cation, in which the positive charge is localized in the empty $4p$ orbital of germanium and is delocalized onto the phenyl rings as well. The calculated Ge−C bond distance with an average value of 198.9 pm is longer than previously reported values by Schnepf *et al.* at 191.2 pm.[105]

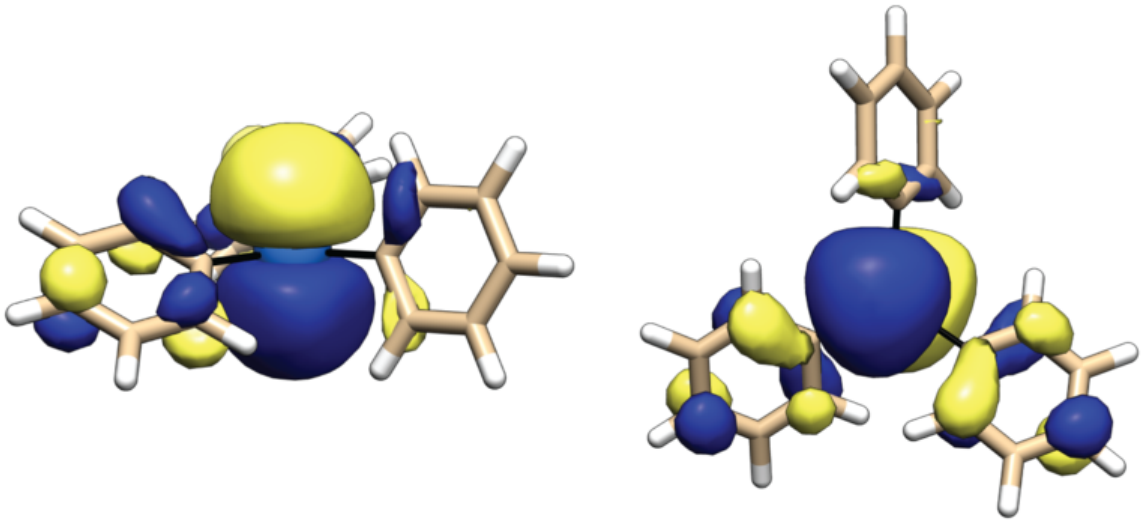

Figure 3.30: Gas-phase DFT-calculated structure/LUMO of Ph_3Ge^+

When the structure of **1** is calculated accounting for the presence of the $[B(C_6F_5)_4]^-$ WCA, the germylium ion Ph_3Ge^+ does not retain its ideal trigonal planar structure and shows some degree of pyramidalization. In Figure 3.31, it is shown that one the fluorines on $[B(C_6F_5)_4]^-$ anion interacts with the positive charge on germanium and causes the hybridization of germanium resulting to deviate from a perfect sp^2

hybridization. The experimental examples of such effects were discussed in detail earlier in this chapter (Figure 3.3).

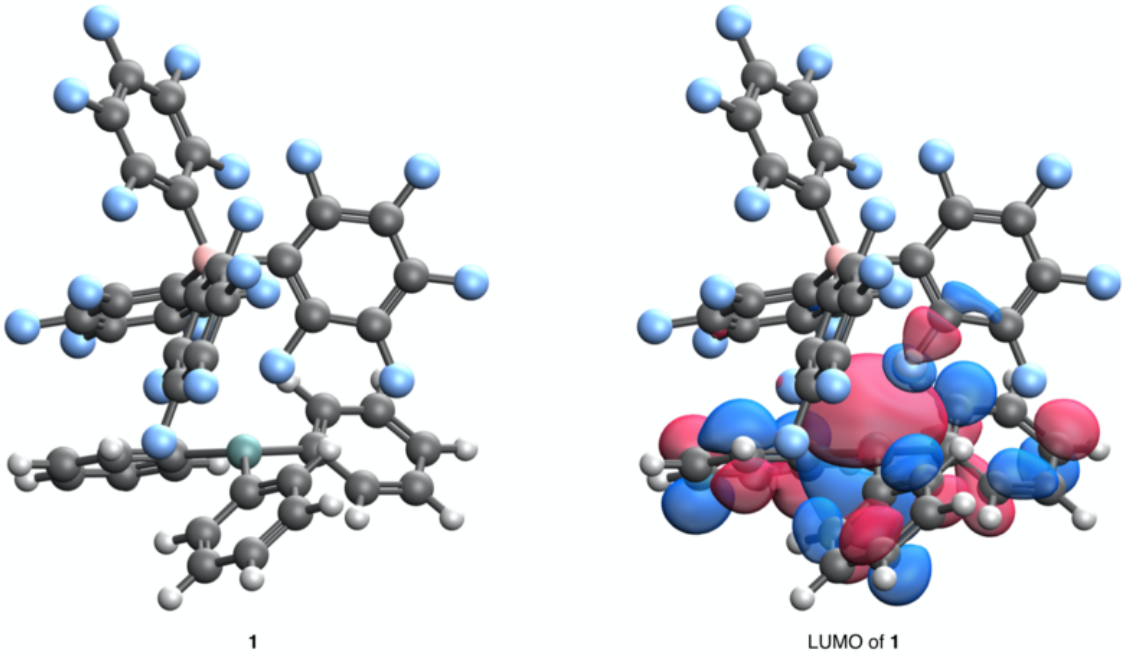

Figure 3.31: DFT-calculated structure and LUMO of **1**

3.3 Conclusions

In this chapter, the HDF of acyl fluorides and aliphatic C–F containing compounds by $[Ph_3Ge][B(C_6F_5)_4]$ **1** was discussed. In the case of acyl fluorides, the advantage over reported methods is that the HDF reactions selectively proceed without any over-reduction through decarbonylative pathways. No transition-metal catalyst is required and the method is sustainable since the Ph_3GeF formed as the product can be easily recovered by chromatography or recrystallization and subsequently reconverted to Ph_3GeH using $LiAlH_4$. The mechanism of the HDF reaction by **1** is proposed to proceed via an ionic Lewis acidic mechanism in which **1** is the actual catalyst of the HDF reactions and Ph_3GeH can be considered to be the pre-catalyst and $[CPh_3][B(C_6F_5)_4]$ to be the initiator. Rudimentary DFT calculations show that the LUMO of Ph_3Ge^+ is mainly composed of the $4p$ orbital on germanium. Further investigation regarding

the mechanism of the reaction using experimental and computational chemistry is still ongoing and will be discussed in the following chapters.

3.4 Experimental

3.4.1 General Considerations

All manipulations were carried using standard Schlenk procedures, syringe, and glovebox techniques. The reagents benzoyl fluoride, pentanoyl fluoride, 1-fluorooctane, 1-fluorocyclohexane, 1,1,1-trifluoromethyltoluene, and 1,3-bis(trifluoromethyl)xylene were purchased from Alfa Aesar. The reagents triphenylgermanium hydride and $[Ph_3C][B(C_6F_5)_4]$ were purchased from Aldrich and were used without further purification. All NMR solvents were dried over activated molecular sieves and non-deuterated solvents were purified using a Glass Contour Solvent Purification System. NMR spectra were recorded using a Bruker Avance III 400 MHz spectrometer. GC/MS data were acquired using a Shimadzu QP2010 instrument.The computing for this project was performed at the OSU High Performance Computing Center at Oklahoma State University supported in part by the National Science Foundation Grant OCI-1126330. Some of the molecular graphics were made using UCSF ChimeraX, developed by the Resource for Biocomputing, Visualization, and Informatics at the University of California, San Francisco, with support from NIH R01-GM129325 and P41-GM103311. Orbital plots were built using IQmol 2.12 visualization packages. DFT calculations were performed using Gaussian 09. The calculated LUMOs of Ph_3Ge^+ and **1** were calculated at B3LYP level of theory using a 6-31G(d) basis set. For the latter, parametrization using Grimm's dispersion correction (DFT-D3) was also included.[130–133]

3.4.2 Experimental Procedure for the HDF Reaction of 1,3-Bis(trifluoromethyl)benzene

To a 20 mL glass vial equipped with a stir bar, 1,3-bis(trifluoromethyl)xylene (0.080 g, 0.37 mmol) was added to Ph_3GeH (0.695 g, 2.28 mmol, 6.1 equiv.) using a pipette, resulting in the formation of a liquid mixture. $[Ph_3C][B(C_6F_5)_4]$ (0.010 g, 0.011 mmol) was added to the mixture and a white solid formed. The reaction mixture was stirred in the glove box for 18 hours. An aliquot of the reaction mixture was filtered through Celite and analyzed by ^1H and ^{19}F-NMR spectroscopy in C_6D_6. The conversion (74%) was calculated by integrating the signals for Ph_3GeF versus 1,3-bis(trifluoromethyl)xylene in ^{19}F-NMR spectrum. An aliquot of the reaction mixture was filtered through Celite and was analyzed by GC-MS in hexane.

3.4.2.1 In Hexane

In a 20 mL glass vial, 1,3-bis(trifluoromethyl)xylene (0.211 g, 0.986 mmol) and Ph_3GeH (1.83 g, 6.00 mmol) were mixed in hexane (15 mL). To this mixture $[Ph_3C][B(C_6F_5)_4]$ (0.0273 g, 0.0296 mmol) was added and the reaction mixture was stirred at room temperature for 18 hours in the glove box. The reaction mixture was filtered through Celite and hexane was removed *in vacuo*. The resulting clear liquid was analyzed by ^1H and ^{19}F-NMR spectroscopy in C_6D_6 and in hexane by GC-MS.

3.4.3 Experimental Procedure for the HDF Reaction of (Trifluoromethyl)benzene

To a 20 mL glass vial equipped with a stir bar, (trifluoromethyl)benzene (0.060 g, 0.41mmol) was added to Ph_3GeH (0.388 g, 1.27 mmol) using a pipette, resulting in the formation of a liquid mixture. $[Ph_3C][B(C_6F_5)_4]$ (0.011 g, 0.012 mmol) was added to the mixture and a white solid formed. The reaction mixture was stirred in the glove box for 18 hours. An aliquot of the reaction mixture was filtered through Celite

and was analyzed by ^{1}H and ^{19}F-NMR spectroscopy in C_6D_6. The conversion (74%) was calculated by integrating the signals for Ph_3GeF versus (trifluoromethyl)benzene in ^{19}F-NMR spectrum. An aliquot of the reaction mixture was filtered through Celite and was analyzed by GC-MS in hexane.

3.4.3.1 With BCF

To a 20 mL glass vial equipped with a stir bar, (trifluoromethyl)benzene (0.100 g, 0.684 mmol) was added to Ph_3GeH (0.647 g, 2.12 mmol) using a pipette, resulting in the formation of a liquid mixture. BCF (0.011 g, 0.021 mmol) was added to the mixture and reaction mixture was stirred in the glove box for 18 hours. An aliquot of the reaction mixture was was analyzed by ^{19}F-NMR spectroscopy in C_6D_6. No Ph_3GeF formation was observed.

3.4.3.2 With Ph_3SiH

In a 20 mL glass vial, (trifluoromethyl)benzene (0.110 g, 0.752 mmol) and Ph_3SiH (0.607 g, 2.33 mmol) were mixed. To this mixture $[Ph_3C][B(C_6F_5)_4]$ (0.03 g, 0.022 mmol) was added and the reaction mixture immediately became exothermic. After that the reaction was stirred at room temperature for 18 hours in the glove box. An aliquot of the reaction mixture was filtered through Celite and was analyzed by ^{19}F-NMR spectroscopy in C_6D_6.

3.4.3.3 In Hexane

In a 20 mL glass vial, (trifluoromethyl)benzene (0.187 g, 1.28 mmol) and Ph_3GeH (1.20 g, 3.97 mmol) were mixed in hexane (15 mL). To this mixture $[Ph_3C][B(C_6F_5)_4]$ (0.0351 g, 0.0381 mmol) was added and the reaction mixture was stirred at room temperature for 18 hours in the glove box. The reaction mixture was filtered through Celite and hexane was removed *in vacuo*. The resulting clear liquid was analyzed by

^{1}H and ^{19}F-NMR spectroscopy in C_6D_6 and in hexane by GC-MS.

3.4.4 Experimental Procedure for the Synthesis of *N,N*-dimethyl-3-(trifluoromethyl)aniline

N,N-dimethyl-3-(trifluoromethyl)aniline was synthesized based on the procedure of reference.[134] In a Schlenk flask 3-(trifluoromethyl)aniline (2.00 g, 12.41 mmol), formaldehyde (2.01 g, 67.03 mmol), and $LiBH_4$ (33.51 mL, 2 M solution in THF, 67.03 mmol) were mixed. Glacial acetic acid (4.03 g, 67.03 mmol) was added to the mixture dropwise at room temperature. The mixture was stirred at 55 °C overnight. The reaction mixture was partitioned between saturated aqueous sodium bicarbonate and Et_2O. The aqueous layer was extracted with Et_2O and organic layers were merged and washed with water and brine and then were are dried over $MgSO_4$. The solvent was removed by distillation. The resulting residue was further purified by column chromatography eluted with 5% EtOAc-Hexane to 10% EtOAc-Hexane using an alumina column (R_F=0.2). ^{1}H-NMR (400 MHz, $CDCl_3$) δ 7.36 (s, 1H), 6.86 – 6.70 (m, 3H), 2.87 (s, 6H). ^{19}F-NMR (376 MHz, $CDCl_3$) δ -62.92.

3.4.5 Experimental Procedure for the HDF Reaction of *N,N*-dimethyl-3-(trifluoromethyl)aniline

In a 20 mL glass vial equipped with a stir bar, *N,N*-dimethyl-3-(trifluoromethyl)aniline (0.040 g, 0.211 mmol) was added to Ph_3GeH (0.199 g, 0.655 mmol) using a pipette, resulting in the formation of a liquid mixture. $[Ph_3C][B(C_6F_5)_4]$ (0.017 g, 0.019 mmol) was added to the mixture and a white solid formed. The reaction mixture was stirred in the glove box for 1 hour. An aliquot of the reaction mixture was filtered through Celite and was analyzed by ^{1}H and ^{19}F-NMR spectroscopy in C_6D_6. The conversion (80%) was calculated by integrating the signals for Ph_3GeF versus *N,N*-dimethyl-3-(trifluoromethyl)aniline in ^{19}F-NMR spectrum.

3.4.6 Experimental Procedure for the HDF Reaction of 1-Fluorooctane

In a 20 mL glass vial equipped with a stir bar, 1-fluorooctane (0.110 g, 0.833 mmol) was added to Ph_3GeH (0.270 g, 0.886 mmol) using a pipette, resulting in the formation of a liquid solution. $[Ph_3C][B(C_6F_5)_4]$ (0.020 g, 0.022 mmol) was added to the mixture and a white solid formed. The reaction mixture was stirred in the glove box for 1 hour. An aliquot of the reaction mixture was filtered through Celite and was analyzed by ^1H and ^{19}F-NMR spectroscopy in C_6D_6. The conversion (>99%) was calculated by integrating the signals for Ph_3GeF versus 1-fluorooctane in ^{19}F-NMR spectrum. An aliquot of the reaction mixture was filtered through Celite and was analyzed by GC-MS in CH_2Cl_2.

3.4.6.1 In Hexane

In a 20 mL glass vial, 1-fluorooctane (0.650 g, 4.92 mmol) and Ph_3GeH (1.65 g, 5.41 mmol) were mixed in hexane (15 mL). To this mixture $[Ph_3C][B(C_6F_5)_4]$ (0.136 g, 0.147 mmol) was added and the reaction was stirred at room temperature for 18 hours in the glove box. The reaction mixture was filtered through Celite and hexane was removed *in vacuo*. The resulting clear liquid was analyzed by ^1H and ^{19}F-NMR spectroscopy in C_6D_6 and in hexane by GC-MS.

3.4.7 Experimental Procedure for the HDF Reaction of 1-Fluorocyclohexane

In a 20 mL glass vial equipped with a stir bar, 1-fluorocyclohexane (0.100 g, 0.978 mmol) was added to Ph_3GeH (0.328 g, 1.08 mmol) using a pipette, resulting in the formation of a liquid solution. $[Ph_3C][B(C_6F_5)_4]$ (0.027 g, 0.029 mmol) was added to the mixture and a white solid formed. The reaction mixture was stirred in the glove box for 5 minutes. An aliquot of the reaction mixture was filtered through Celite and was analyzed by ^1H and ^{19}F-NMR spectroscopy in C_6D_6. The conversion (>99%)

was calculated by integrating the signals for Ph_3GeF versus 1-fluorocyclohexane in ^{19}F-NMR spectrum. An aliquot of the reaction mixture was filtered through Celite and was analyzed by GC-MS in CH_2Cl_2.

3.4.7.1 In Hexane

In a 20 mL glass vial, 1-fluorocyclohexane (0.477 g, 4.67 mmol) and Ph_3GeH (1.57 g, 5.14 mmol) were mixed in hexane (15 mL). To this mixture $[Ph_3C][B(C_6F_5)_4]$ (0.136 g, 0.129 mmol) was added and the reaction was stirred at room temperature for 18 hours in the glove box. The reaction mixture was filtered through Celite and hexane was removed *in vacuo*. The resulting clear liquid was analyzed by ^{1}H and ^{19}F-NMR spectroscopy in C_6D_6 and in hexane by GC-MS.

3.4.8 Experimental Procedure for the HDF Reaction of Benzoyl Fluoride

In a 20 mL glass vial equipped with a stir bar, benzoyl fluoride (0.200 g, 1.62 mmol) was added to Ph_3GeH (0.545 g, 1.79 mmol) using a pipette, resulting in the formation of a liquid mixture. $[Ph_3C][B(C_6F_5)_4]$ (0.045 g, 0.049 mmol) was added to the mixture and a yellow solution formed. The reaction mixture was stirred in the glove box for 18 hours. An aliquot of the reaction mixture was analyzed by ^{1}H and ^{19}F-NMR spectroscopy in C_6D_6. The conversion (>99%) was calculated by integrating the signals for Ph_3GeF versus benzoyl fluoride in ^{19}F-NMR spectrum. An aliquot of the reaction mixture was filtered through Celite and was analyzed by GC-MS in CH_2Cl_2.

3.4.8.1 Isolated Yield

In a Schlenk flask, Ph_3GeH (0.811 g, 2.66 mmol) treated with and benzoyl fluoride (0.300 g, 2.42 mmol) was added to it by a pipette, resulting in the formation of a yellow liquid solution. The mixture was stirred at room temperature for 18 hours in the glove box. The reaction mixture was taken up in benzene and then benzaldehyde

was extracted with water to leave behind Ph_3GeF and Ph_3CH by-products. Benzaldehyde was then extracted from by extraction using Et_2O. Ether layer was dried over magnesium sulfate and was removed *in vacuo* to yield a clear liquid which was identified by ^1H and ^{19}F-NMR spectroscopy in $CDCl_3$ to be pure benzaldehyde (0.121 g 46.8%)

3.4.8.2 In Hexane

In a 20 mL glass vial, benzoyl fluoride (0.243 g, 1.96 mmol) and Ph_3GeH (0.657 g, 2.16 mmol) were mixed in hexane (10 mL). To this mixture, $[Ph_3C][B(C_6F_5)_4]$ (0.054 g, 0.059 mmol) was added and the reaction mixture was stirred at room temperature for 18 hours in the glove box. The reaction mixture was filtered through Celite and hexane was removed *in vacuo*. The resulting pale yellow liquid was analyzed by ^1H and ^{19}F-NMR spectroscopy in C_6D_6 and in hexane by GC-MS.

3.4.8.3 With Ph_3SiH

In a 20 mL glass vial, benzoyl fluoride (0.321 g, 2.59 mmol) and Ph_3SiH (0.741 g, 2.85 mmol) were mixed. To this mixture $[Ph_3C][B(C_6F_5)_4]$ 0.079 g, 0.086 mmol) was added and the reaction mixture and the reaction mixture immediately became exothermic. After that the reaction was stirred at room temperature for 18 hours in the glove box. An aliquot of the reaction mixture was filtered through Celite and was analyzed by ^{19}F-NMR spectroscopy in C_6D_6.

3.4.8.4 With BCF

In a 20 mL glass vial equipped with a stir bar, benzoyl fluoride (0.120 g, 0.967 mmol) was added to Ph_3GeH (0.324 g, 1.06 mmol) using a pipette, resulting in the formation of a liquid mixture. BCF (0.015 g, 0.029 mmol) was added to the mixture and formed a yellow liquid. The reaction mixture was stirred in the glove box for 18 hours. An

aliquot of the reaction mixture was was analyzed by ^{19}F-NMR spectroscopy in C_6D_6. The conversion (18%) was calculated by integrating the signals for Ph_3GeF versus benzoyl fluoride in ^{19}F-NMR spectrum.

3.4.9 Experimental Procedure for the HDF Reaction of Pentanoyl Fluoride

In a 20 mL glass vial equipped with a stir bar, pentanoyl fluoride (0.100 g, 0.960 mmol) was added to Ph_3GeH (0.322 g, 1.06 mmol) using a pipette, resulting in the formation of a liquid mixture. $[Ph_3C][B(C_6F_5)_4]$ (0.026 g, 0.029 mmol) was added to the mixture to give a yellow solution. The reaction mixture was stirred in the glove box for 18 hours. An aliquot of the reaction mixture was filtered through Celite and was analyzed by ^{1}H and ^{19}F-NMR spectroscopy in CD_2Cl_2. The conversion (>99%) was calculated by integrating the signals for Ph_3GeF versus pentanoyl fluoride in ^{19}F-NMR spectrum. An aliquot of the reaction mixture was filtered through Celite and was analyzed by GC-MS in CH_2Cl_2.

3.4.9.1 In Hexane

In a 20 mL glass vial, pentanoyl fluoride (0.481 g, 4.62 mmol) and Ph_3GeH (1.55 g, 5.09 mmol) were mixed in hexane (15 mL). To this mixture $[Ph_3C][B(C_6F_5)_4]$ (0.127 g, 0.138 mmol) was added and the reaction mixture was stirred at room temperature for 18 hours in the glove box. The reaction mixture was filtered through Celite and hexane was removed *in vacuo*. The resulting clear liquid was analyzed by ^{1}H and ^{19}F-NMR spectroscopy in CD_2Cl_2 and in hexane by GC-MS.

3.4.10 Computational Results

Table 3.1: Optimized Coordinates for Ph_3Ge^+ in Gas-Phase

C	2.95044	-3.56875	-0.09602
C	1.70352	-3.75975	0.36399
C	0.79837	-2.77308	0.26918
C	1.14156	-1.59921	-0.28058
C	2.38623	-1.40951	-0.74133
C	3.2934	-2.39385	-0.64784
H	4.31869	-2.23513	-1.02402
H	2.64861	-0.43863	-1.19198
Ge	-0.05797	-0.02838	-0.05715
C	-2.02975	-0.28594	-0.03554
C	-2.76649	0.15758	-1.06337
C	-4.10544	0.08453	-1.00668
C	-4.70149	-0.43432	0.07865
C	-3.96086	-0.88225	1.10547
C	-2.62216	-0.80678	1.04806
H	-1.99635	-1.16714	1.88067
H	-4.4525	-1.31177	1.99529
H	-5.80278	-0.49544	0.12513
H	-4.71563	0.4493	-1.85095
H	-2.25695	0.57933	-1.94549
C	0.71715	1.78272	0.22122
C	0.15335	2.84166	-0.37815
C	0.79124	4.02203	-0.39508
C	1.99432	4.14158	0.18917
C	2.55736	3.08181	0.79188
C	1.91657	1.90295	0.80876
H	2.3633	1.02336	1.30105
H	3.54459	3.17955	1.27541
H	2.51825	5.11304	0.17552
H	0.32897	4.89454	-0.88901
H	-0.83467	2.72635	-0.85287
H	-0.23062	-2.91294	0.63973
H	1.42255	-4.7254	0.81925
H	3.69561	-4.37937	-0.0198
H	1.42255	-4.7254	0.81925
H	3.69561	-4.37937	-0.0198

Table 3.2: Optimized Coordinates for **1** in Gas-Phase

C	-2.44373	1.92683	0.3973	C	2.06004	2.27245	-5.72064
C	-1.72914	1.37513	-0.66831	H	0.96536	-0.92424	-5.2069
C	-0.35332	1.49376	-0.52796	H	0.72559	-0.8156	-7.65894
C	0.31405	2.1171	0.51241	H	1.33364	1.25989	-8.88398
C	-0.44542	2.67537	1.53639	H	2.18189	3.24039	-7.63743
C	-1.83233	2.57668	1.47431	H	2.41674	3.14635	-5.18384
B	-2.31355	0.50199	-1.94963	C	2.81013	-0.5499	-2.45556
C	-1.75362	-1.00798	-1.57484	C	2.86271	-0.79012	-1.07054
C	-2.24447	-1.6464	-0.42943	C	3.40882	-1.97826	-0.58698
C	-1.76418	-2.85788	0.05735	C	3.92174	-2.92955	-1.47724
C	-0.719	-3.49415	-0.60973	C	3.88939	-2.69275	-2.85421
C	-0.17973	-2.89481	-1.74042	C	3.33188	-1.51004	-3.341
C	-0.70238	-1.68234	-2.18613	H	2.4715	-0.05424	-0.3756
F	-3.24008	-1.06528	0.2757	H	3.43043	-2.1654	0.48318
F	-2.28778	-3.41787	1.16125	H	4.33746	-3.85822	-1.09568
F	-0.22959	-4.66137	-0.15866	H	4.28109	-3.43178	-3.54741
F	0.83985	-3.4865	-2.39406	H	3.28631	-1.34508	-4.41398
F	-0.08026	-1.15519	-3.27938	F	-0.55081	4.16275	-5.03797
F	0.45246	0.90393	-1.49614	F	-1.16794	2.66993	-7.25763
F	1.66233	2.15123	0.56159	F	-2.11527	0.12288	-6.94147
F	0.15517	3.28239	2.57147	F	-2.56049	-0.86375	-4.48464
F	-2.572	3.09753	2.46516	Ge	2.11506	1.06033	-3.17115
F	-3.78568	1.85166	0.45021	C	2.69098	2.67907	-2.37357
C	-3.94602	0.58412	-2.13393	C	3.82017	2.63046	-1.53531
C	-4.55634	1.83694	-2.25174	C	4.29323	3.78977	-0.92047
C	-5.91186	2.02904	-2.49049	C	3.6367	5.00658	-1.13171
C	-6.73492	0.91632	-2.64729	C	2.51289	5.06512	-1.96456
C	-6.17723	-0.35474	-2.56634	C	2.0448	3.90881	-2.58871
C	-4.80925	-0.49637	-2.32494	H	4.31832	1.68343	-1.34494
F	-3.79934	2.95669	-2.12993	H	5.16375	3.74157	-0.27212
F	-6.43333	3.26665	-2.5773	H	3.99673	5.90866	-0.64395
F	-8.04791	1.07091	-2.88193	H	1.99885	6.00857	-2.12611
F	-6.95947	-1.43668	-2.73311	H	1.17269	3.96943	-3.22971
F	-4.353	-1.76952	-2.2949	C	1.71244	1.10049	-5.01719
C	-1.78851	1.10395	-3.4047	C	1.2398	-0.01691	-5.73041
C	-1.28669	2.38634	-3.63157	C	1.11252	0.04288	-7.11791
C	-1.06721	2.92259	-4.90126	C	1.45442	1.21204	-7.80538
C	-1.35958	2.16915	-6.0269	C	1.929	2.32715	-7.10677
C	-1.85858	0.87948	-5.85962	C	-2.05291	0.38437	-4.57593
F	-1.00238	3.22715	-2.60403				

CHAPTER IV

Direct Amidation of Acid Fluorides Using Germylamines

4.1 Introduction - Amidation of Acyl Fluorides

In Chapter III, it was shown that germylium ions are strong Lewis acids that have high fluorine ion affinities and therefore can act as catalysts in HDF reactions. The main issues that often diminish the Lewis acidity of germyliums are that they are heavily influenced by the coordinating properties of their WCAs, solvent, and other even slightly Lewis basic species that might be present. Germanium amines R_3Ge-NR_2 are accessible and diverse reagents that have been mainly used in our group for hydrogermolysis reactions to make oligogermanes. However, their reactivity in other transformations is still unexplored. The uncanny resemblance of germanium amines to borderline germylium ions $[R_3Ge][NR_2]$ that contains a very poor WCA, led us to examine the reactivity of these species as Lewis acids in the amidation reactions of acyl fluorides.

4.1.1 Amide Bonds

Amide bonds are one the key functional groups that exist in nature and are found in proteins, synthetic compounds and about 25% of pharmaceuticals.[135] An amide bond can be formed directly by reacting a carboxylic acid and an amine. However, this approach poses several limitations. The resulting ammonium caboxylate salt often needs to be dehydrated at high temperatures (140-210 °C) to yield the desired amide product.

A more conventional approach to access amides is by converting the carboxylic acid into a more reactive derivative such as an ester, acyl halide, or anhydride using stoichiometric coupling reagents. Although widely used, this method has its own disadvantages. The stoichiomeric use of coupling reagents to make the carbonyl of the carboxylic acid more electrophilic is wasteful to the degree that "Amide formation avoiding poor atom economy reagents" is rated to be the top priority by the ACS green chemistry institute and also by pharmaceutical companies.[136]

Alternative synthetic methods to prepare amides rely on using "surrogates" for the carboxylic acid or the amine. Alcohols and esters have been reported as the sources for the acyl component along with amines, amides, and azides for the amine source.[137] The common feature in these approaches is that the oxygen source should be oxidized to form a more electrophilic species than the carboxylic acid, such as an aldehyde or an ester, and the nitrogen source should be reduced to an amine to enable the amide formation, usually in the presence of a transition metal.

Main-group Lewis acids that are mainly boron-compounds are used as catalysts or reagents for amide bond formation. Different boron species such as boric acid ($B(OH)_3$), boronic acids ($ArB(OH)_2$), and borinic acids ($Ar_2B(OH)$) facilitate amide formation by converting the carboxylic acid into a an ester-like intermediate that is more reactive.[138–143] Another transition-metal free amidation protocol was introduced by Hevia *et al.* As shown in Scheme 4.1, using lithium amides ($LiNR_2$), esters and amides can be converted to amides in a very fast reaction in the presence of air.[144] The key component of this method seems to be the solvent 2-MeTHF that provides full solubility for the lithium reagents. The solvent 2-MeTHF also favors the formation of more reactive monomeric lithium species that can rapidly add across the C=O bond of esters. As seen in Scheme 4.1, the reported yields are moderate to high but the presence of α-C−H moiety might play a role in the lower yields for aliphatic amides **1b-c**.

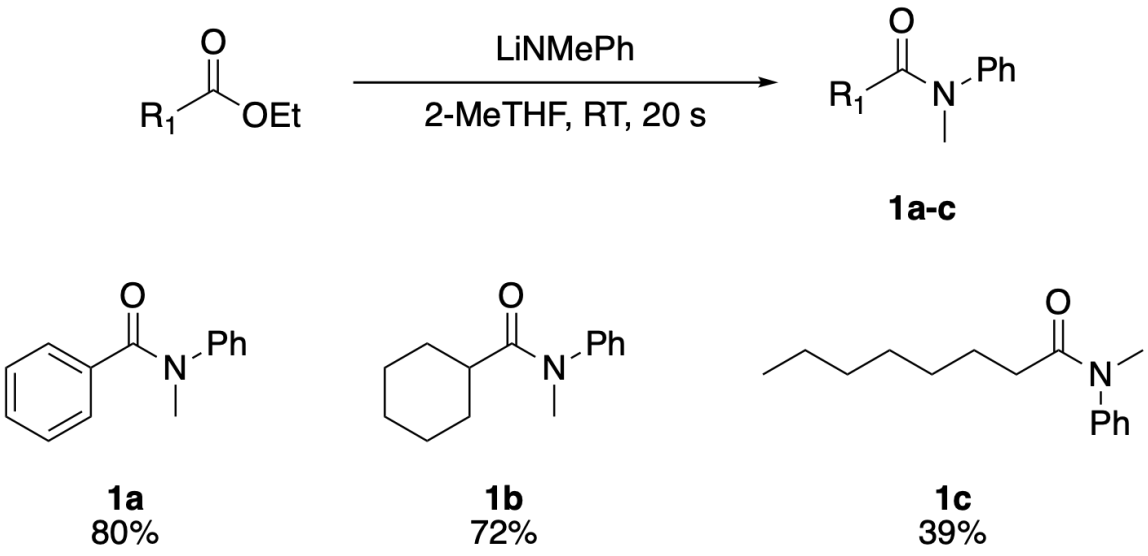

Scheme 4.1: Addition of LiNMePh to various ester to form amides

In all amidation methods the nitrogen source should somehow attack the carbon of a carbonyl and act as a nucelophile. Transition-metal based methods proceed based on providing proximity between the reactants and so act as the catalyst for the reaction. More electron-donating substituents can increase the nucelophilicity of nitrogen but bulky groups hinder their reactivity thus accessing amides with bulky groups on nitrogen is a synthetic challenge. The examples in which a tertiary amine is used for amidation reactions are almost nonexistent. The only example of such a reaction is in the case of strained aziridines that can react with acyl chlorides or fluorides to form amides (Scheme 4.2).[145] The release of strain from the 3-membered aziridine ring is the driving force behind this reaction. This reaction is suggested to proceed first by quaternization of nitrogen followed by attack of the halide to the aziridine ring.[146]

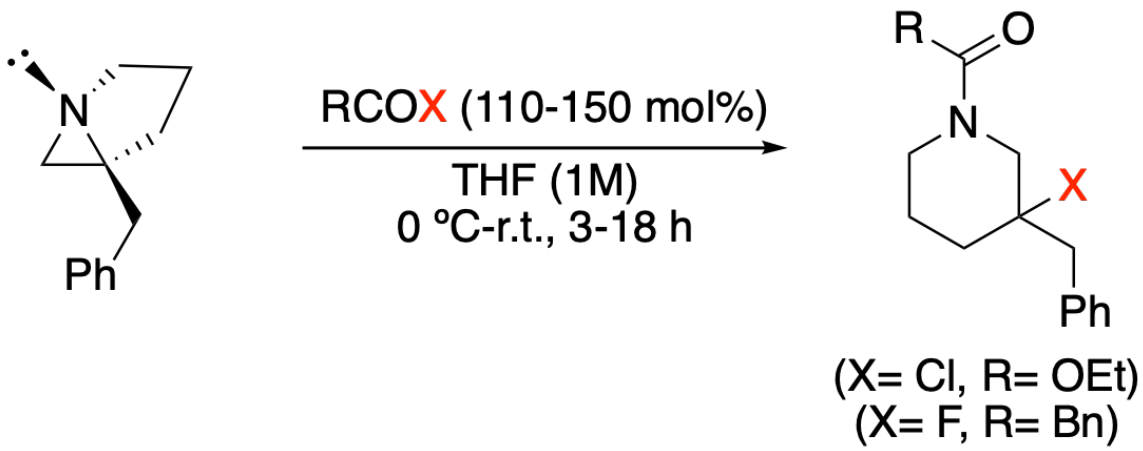

Scheme 4.2: Reaction of an aziridine with acyl halides

Reports of amide formation where group 14 amines act as the nitrogen source are scarce. The only reported example involves reaction of N-silylamines and acyl fluorides to form amides in yields higher than other preparative methods for acyl fluorides that contain heterocycles. The activation of amines is carried out by silylation using BSA (bis(trimethylsilyl)acetamide). In Scheme 4.3, the second step that leads to amidation is technically a desilylation with the formation of a strong Si−F bond as the driving force.[147]

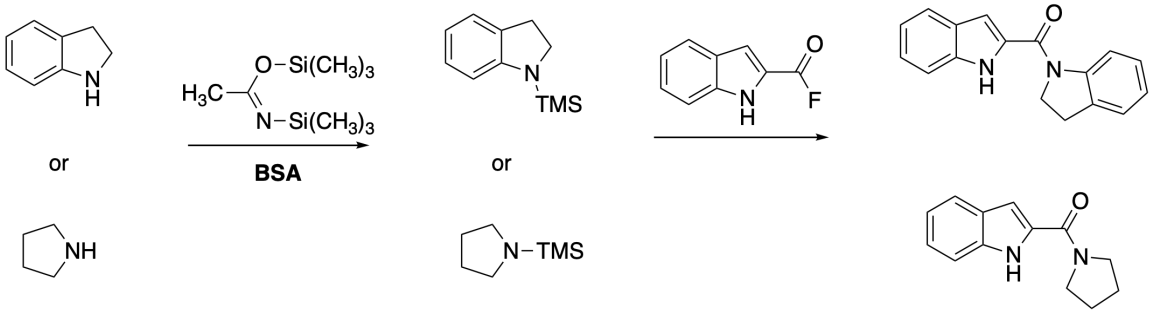

Scheme 4.3: Amide formation by N-silylamines

4.1.2 Germyl Amines

Germyl amines with the general formula of $R_3Ge{-}NR'_2$ are the heavier analogues of tertiary amines in group 14. These compounds are typically synthesized from halogermanes $R_3Ge{-}X$ (X = Cl, Br) and by reacting them with lithium amides

($LiNR'_2$). Due to reasons that will be discussed later in this chapter, there are no reports of the X-ray solid-state structure of any of these compounds.

Early attempts at describing the bonding of heavier group 14 amines was described in the work by Yoder *et al.* where ^{13}C-H coupling constant data obtained by NMR was used to evaluate the extent of pπ-dπ interactions in the series $(CH_3)_3M{-}NMe_2$ (M = C, Si, Ge, Sn). Table 4.1 summarizes the results of this study for one example of a group 14 amine. The observed trend is attributed to the presence of a π-interaction in the M–N bond that decreases in the order of Si > C ≈ Ge > Sn.[148]

Table 4.1: ^{13}C-H coupling constants in $(CH_3)_3M{-}NMe_2$ (M = C, Si, Ge, Sn)

M	^{13}C-H Coupling Constant (Hz)
C	131.4
Si	132.2
Ge	131.4
Sn	130.2

A concise description of bonding in germyl amines is still missing in the literature as there is very little systematic work in this area. X-ray crystallography data and detailed quantum calculations have helped shed some light on the nature of bonding in nitrogen containing germanium clusters. Figure 4.1 shows two examples of germanium compounds that contain Ge–N bonds. In spiropentadiene **2a**, the Ge–N bond lengths range from 1.885(5) to 1.930(5) Å.[149] In cluster **2b**, the Ge–N bond length is slightly shorter with an average value of 1.860(4) Å. Quantum calculations indicate Mayer bond orders for the Ge–N bonds of 0.89 and 0.90, indicating some degree of Ge=N double bond character which arises from the negative hyperconjugation of nitrogen lone pairs to the σ^*-orbitals of the Ge–Ge bonds.[150]

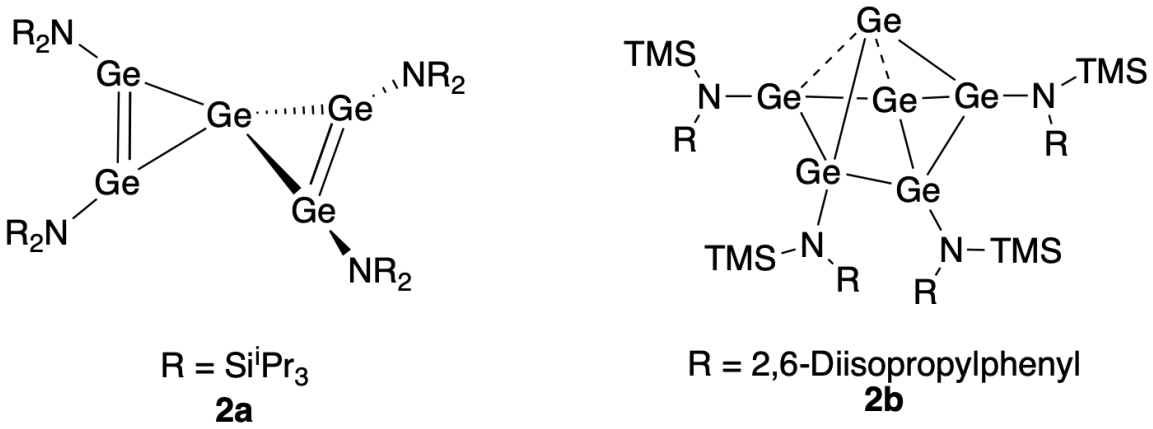

Figure 4.1: Amido-substituted germanium clusters

4.2 Results and Discussion

4.2.1 Lewis Acidity of Germyl Amines

As discussed in Chapter III by utilizing the Lewis acidity of germylium ions, HDF reactions of acyl fluorides and alkyl fluorides can be achieved in which a fluorine atom is replaced by a hydrogen. The described process is heavily influenced by the WCA used as it can affect the nature of the positive charge on germanium dramatically. The first descriptions of germyl amines led us to look at them as germylium ions with a very bad WCA (e.g. NMe_2) that could act as masked germyliums. In order to test this hypothesis, the Gutmann-Beckett method [32,33] was used with Et_3PO as a sensitive probe with a solution of **3a** (Ph_3GeNMe_2). Figure 4.2 shows the ^{31}P-NMR spectrum of the mixture of these two reagents. The new signal that is downfield by 6.4 ppm from the resonance of free Et_3PO indicates that the germanium atom in **3a** is slightly Lewis acidic.

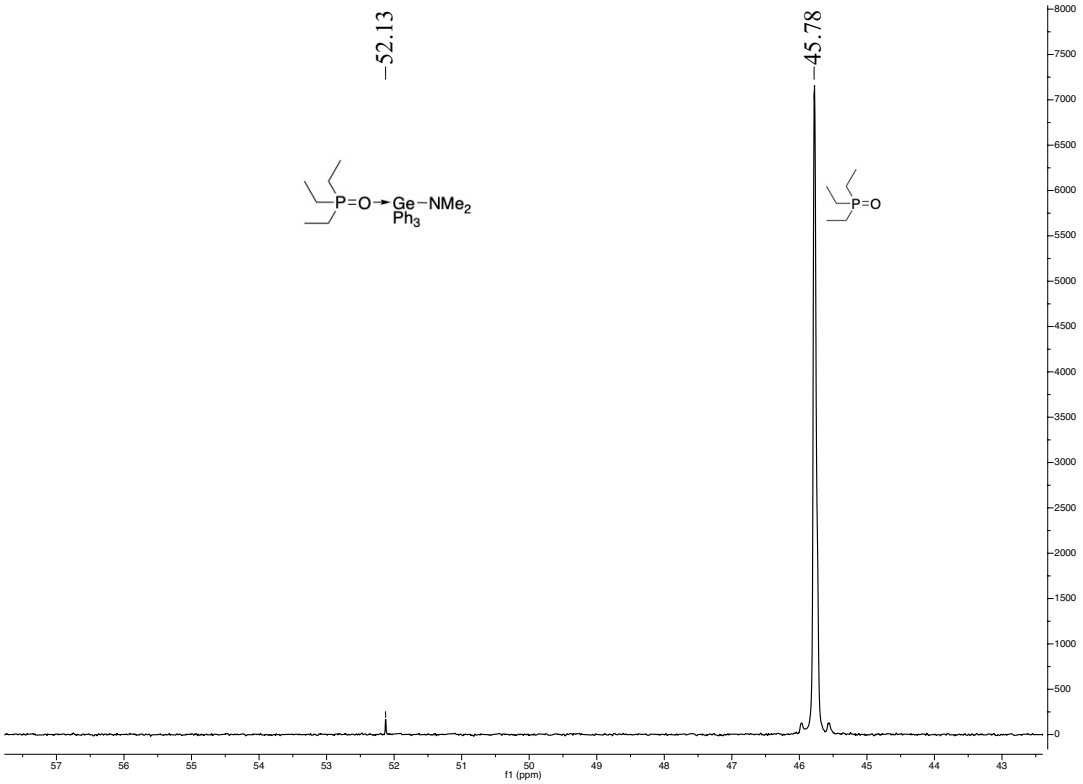

Figure 4.2: ^{31}P-NMR (162 MHz, C_6D_6) spectrum of the mixture of **3a** and Et_3PO

Figure 4.3 shows the ^{1}H-NMR spectrum of the mixture. The signals for Et_3PO do not change significantly. However a new signal in the amide region appears at 2.20 ppm which is slightly upfield compared to the signal of $-NMe_2$ in free **3a** at 2.75 ppm. This shielding effect can be attributed to the formation of a pentacoordinated germanate intermediate.

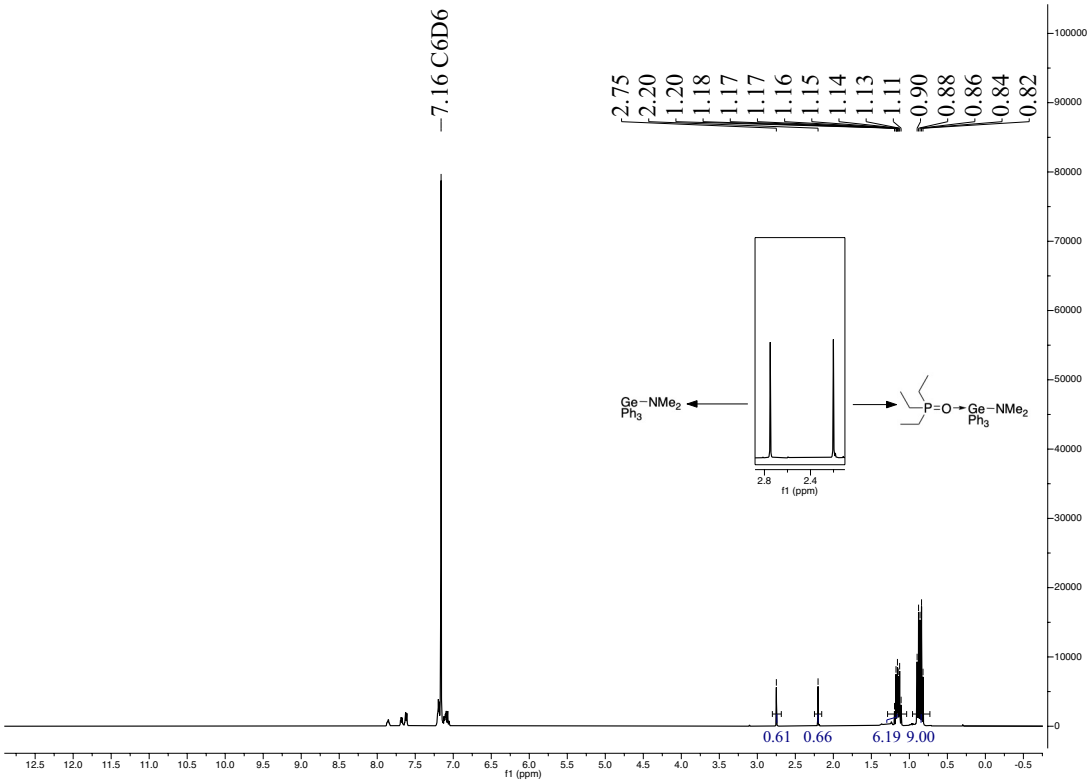

Figure 4.3: ^{1}H-NMR (400 MHz, C_6D_6) spectrum of **3a** and Et_3PO

In another attempt to gain more insight about the bonding in **3a**, a variable-temperature ^{1}H-NMR study was conducted in toluene-d_8. The hypothesis was that if there is a pπ-dπ donation from nitrogen to germanium *d*-orbitals it should be more noticeable in affecting the ^{13}C-^{1}H coupling constant at lower temperatures. Figure 4.4 illustrates the stacked ^{13}C-NMR of **3a** at 25 °C (bottom-red) and at -45 °C (top-blue). Both spectra show a quartet of quartets pattern with coupling constants of 132.3 and 5.3 Hz that do not vary with the changes in temperature. The observed splitting pattern suggests that there is hindered rotation of the Ge−N bond in **3a** that causes the difference signals for the two methyl groups.

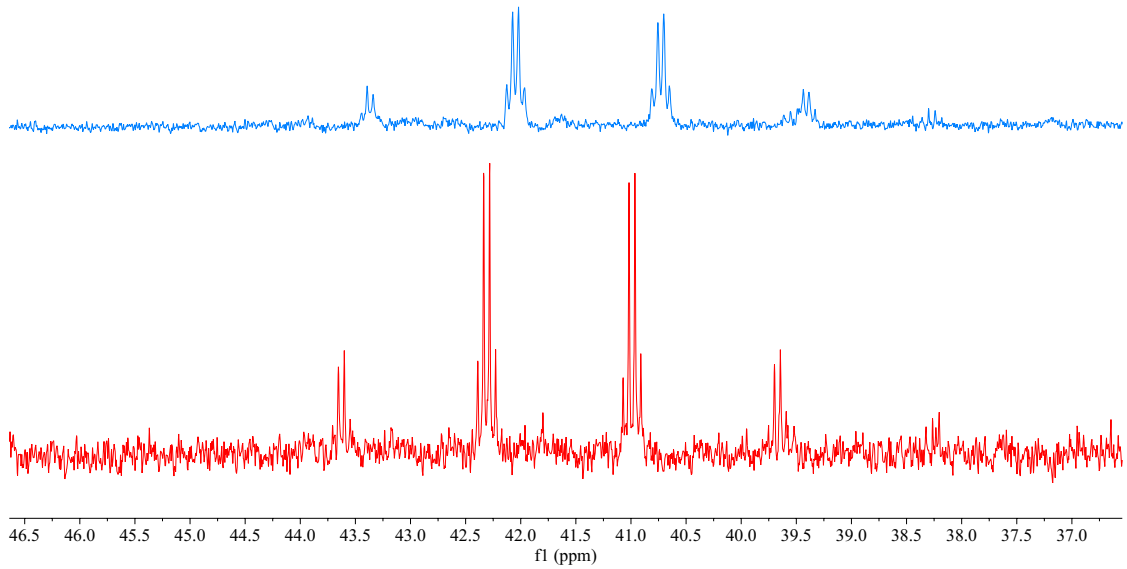

Figure 4.4: Variable-temperature ^{13}C-NMR (101 MHz, C_6D_6) spectrum of **3a** (top: -45 °C, bottom: 25 °C)

Fluoride ion affinity is a reliable quantitative measure for assessing the Lewis acidity. The FIA of a series of germyl amines **3a-e** in Figure 4.5 as well as several other germanium compounds were calculated using isodesmic reactions that are anchored to a COF_2/COF_3^- reference system that has an accurate experimental value (ΔH = 208.8 kJ.mol^{-1}) and will treat the calculations for "naked" fluoride ion.[151]

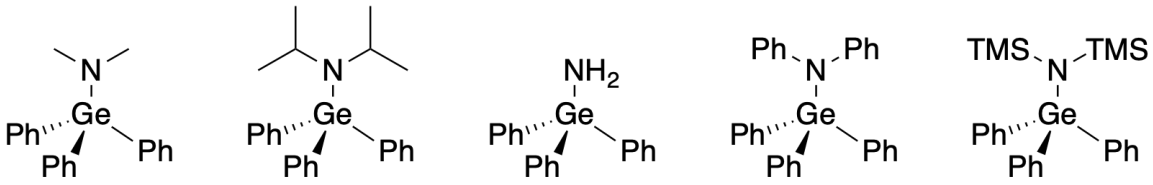

3a **3b** **3c** **3d** **3e**

Figure 4.5: List of studied germyl amines

Table 4.2 summarizes the results from the FIA calculations. The studied germyl amines (**3a-e**) have FIAs around 200 kJ.mol^{-1} which are similar to that of $GePh_4$ (188 kJ.mol^{-1}). This similarity is expected given the structural similarities of these two types of compounds. The FIA of germyl amines is comparable to other main-group Lewis acids with close FIAs such as: $B(OH)_3$ (190 kJ.mol^{-1}), BMe_3 (248 kJ.mol^{-1}), $Si(OH)_4$ (223 kJ.mol^{-1}), $SiPh_4$ (149 kJ.mol^{-1}), PH_5 (186 kJ.mol^{-1}), $Sn(NH_2)_4$ (240 kJ.mol^{-1}), and SbH_5 (219 kJ.mol^{-1}).[151] The calculated FIA values for **3a-e** subtly change with the steric and electronic properties of the substituents on nitrogen. Base on their larger thermal corrections in enthalpy calculations, large TMS groups in **3e**, and phenyl groups in **3d** have more degrees of freedom. The volume strain causes the Ge−N bond to be more polarized (*vide infra*) and thus increases the Lewis acidity in **3d-e** compared to other germyl amines.

Table 4.2: Calculated FIA of **3a-e**

	FIA (kJ.mol^{-1})
Ph_3GeNMe_2 **3a**	210
$Ph_3GeN^iPr_2$ **3b**	202
Ph_3GeNH_2 **3c**	206
Ph_3GeNPh_2 **3d**	217
$Ph_3GeN(SiMe_3)_2$ **3e**	225

Table 4.3 summarizes the calculated FIAs of several germanium compounds. Compounds **3a-e** are not as Lewis acidic as GeF_4 and $GeCl_4$ but are stronger Lewis acids compared to germane and $GePh_4$ and $GeMe_4$. However the trend of the Lewis acidity of these species increases down the group 14.[151]

Table 4.3: Calculated FIA of germanium compounds

	Calculated FIA (kJ.mol^{-1})	Reported FIA (kJ.mol^{-1})†
GeH_4	111	112
$GeMe_4$	107	101
$GePh_4$	188	86
$GeCl_4$	314	323
GeF_4	353	355

† Values from Ref.[151]

The FIA calculations indicate that the presence of the $-NR_2$ substituent versus hydrogen, alkyl or aryl substituents signficantly increases the Lewis acidity/fluorophilicity of the germanium atom in **3a-e**.

The FIA of **3a** was also investigated experimentally by reacting it with TASF ($[(Me_2N)_3S][Me_3SiF_2]$), which is a strong fluorine source. When one equivalent of TASF was reacted with **3a**, three signals were observed in the ^{19}F-NMR spectrum of the reaction mixture. The signals at -157.1 and 202.4 ppm are for Me_3SiF and Ph_3GeF respectively.[94,152] Another signal at -125.0 ppm is in the range of other reported pentavalent fluorogermanates such as $[Ph_3GeF_2]$ and $[PhMe_2GeF_2]$ which have reported chemical shift values at -118.9 and -126.4 ppm, respectively.[59,153] Therefore the signal, at -125.0 ppm is assigned to the $[Ph_3Ge(F)NMe_2]^-$ anion. When **3a** was reacted with excess amounts of benzoyl fluoride, ^{19}F-NMR spectrum of the reaction mixture did not indicate the formation of $[Ph_3Ge(F)NMe_2]^-$ anion.

4.2.2 NBO Analysis

NBO analysis breaks down the total electron density into localized contributions from individual atoms and gives a valuable, and easy-to-interpret picture of bonding. NBO results in Table 4.4, point to a polarized distribution of the electrons in the Ge−N bonds of **3a-e**. In **3a**, calculated occupancy indicates that electron density is distributed 79.3 % on nitrogen and 20.7 % on germanium. The distribution of electron occupancy on the nitrogen atom in Ph_3Ge-NR_2 increases in the order of R = Me < ^{i}Pr < $SiMe_3$, suggesting that the inductive effects of the substituents affects the electron density in the Ge−N bond.

The Wiberg Bond Index calculated from NBO analysis in Table 4.4 shows a decrease in the Ge−N bond order in **3a-e**, as the bulkiness of the substituents on nitrogen decreases. The WBI decreases in Ph_3GeNR_2, in the order of R: NH_2 > Me > ^{i}Pr > TMS > Ph, indicating bulkier groups cause a slight weakening of the Ge−N

bond.

Table 4.4: WBI and occupancy for Ge−N bond in **3a-e**

	WBI (Ge−N)	Occupancy (N−Ge %)
Ph_3GeNH_2 **3c**	0.751	77.6/22.4
Ph_3GeNMe_2 **3a**	0.6734	79.3/20.7
$Ph_3GeN^iPr_2$ **3b**	0.6487	80.2/19.8
Ph_3GeNPh_2 **3d**	0.5385	81.0/19.0
$Ph_3GeN(SiMe_3)_2$ **3e**	0.6167	85.0/15.0

4.2.3 Reaction of Ph_3GeNMe_2 with Benzotrifluoride

The potential of Ph_3GeNMe_2 for C−F activation was initially explored by reacting it with benzotrifluorides. In initial attempts, the reaction did not show any conversion but when the Lewis acid $B(C_6F_5)_3$ was also added to the reaction, to our surprise, conversion was observed as indicated by the formation of Ph_3GeF.

The similar recent study by Young *et al.* suggests an FLP-mediated pathway for the observed process. In their suggested mechanism $B(C_6F_5)_3$ abstracts a fluorine from NaF to form a borate intermediate $[Na][F(B(C_6F_5)_3]$. This intermediate when reacted with strong Lewis acid silyl amide (Me_3SiNTf_2) will transfer a F^- ion to the trimethylsilyl amide.[154] To evaluate the pathway $[Na][F(B(C_6F_5)_3]$ was synthesized based on the reaction in Scheme 4.4. The formation of $[F(B(C_6F_5)_3]^-$ was confirmed by the presence of a broad singlet signal in ^{19}F-NMR spectrum of the reaction mixture (Figure 4.6) at -190.01 ppm.[154] When FBCF was reacted with Ph_3GeNMe_2, the signal for Ph_3GeF emerged in the ^{19}F-NMR spectrum of the reaction mixture (Figure 4.7) suggesting that Ph_3GeNMe_2 is Lewis acidic enough to abstract a fluorine.

$$NaF + B(C_6F_5)_3 \xrightarrow{CHCl_3,\ RT} Na[FB(C_6F_5)_3]$$

Scheme 4.4: Synthesis of F-(BCF)

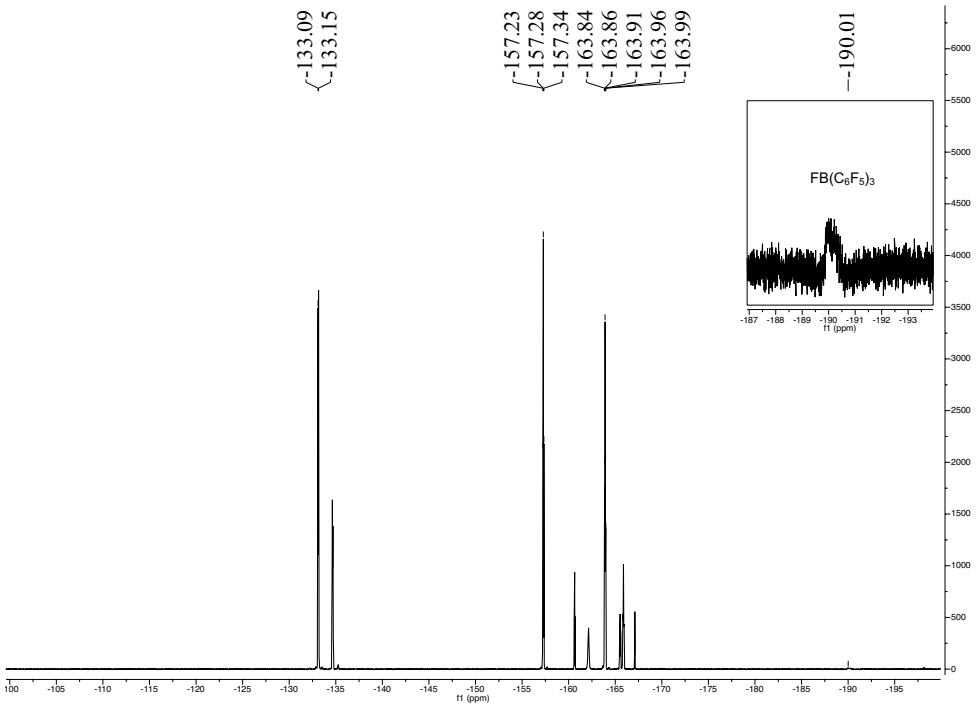

Figure 4.6: ^{19}F-NMR (376 MHz, $(CD_3)_2S{=}O$) spectrum of the reaction mixture of F−BCF

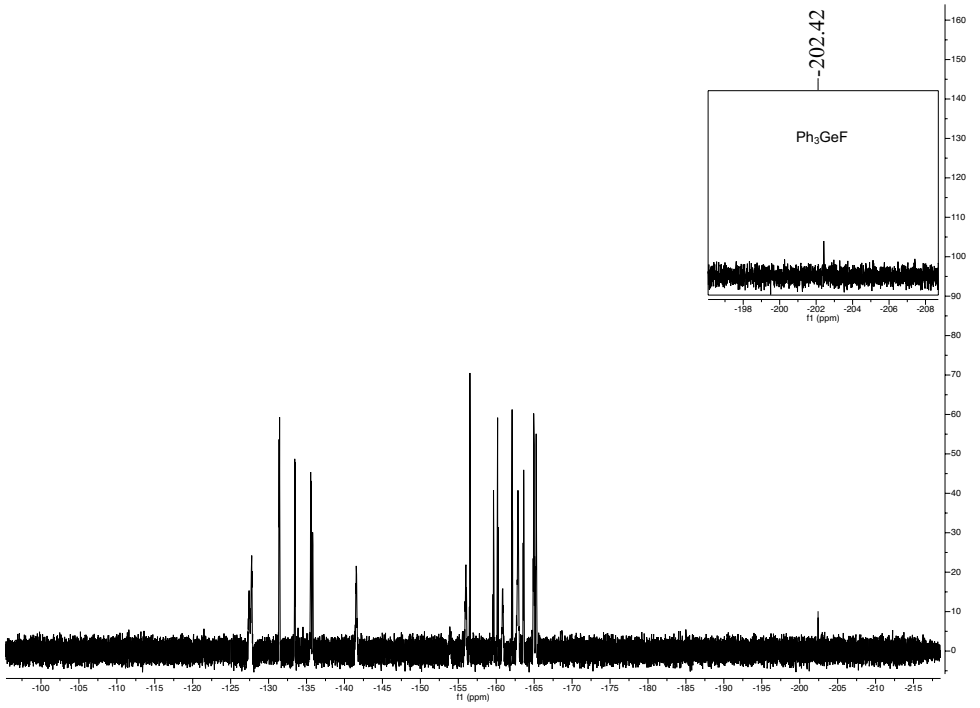

Figure 4.7: ^{19}F-NMR (376 MHz, C_6D_6) spectrum of the reaction of FBCF and **3a**

The complicated ^{19}F-NMR of reaction mixtures, the need to have BCF in the reaction, and observing conversion only with Ph$-$CF$_3$ and not fluorocyclohexane all point to the fact that a clean transformation such as a direct C$-$F amination is not probable. This led to focus on the C$-$F bonds in acyl fluorides.

4.2.4 Reaction of 3a, 3b, 3e with Acyl Fluorides

Tertiary and hindered amides are important motifs and can be are hard to prepare. The steric hindrance will cause a disruption in the conjugation in the amide and thus makes it more electrophilic. This is especially important in the selectivity of reactions involving compounds containing tertiary amides. Added to this, hindered amines, which are precursors to this type of amides, are less reactive in amidation reactions. It was anticipated that germyl amines would be suitable reagents for the formation of tertiary amides via reaction with acyl fluorides.

As shown in Chapter III, when Ph$_3$GeH was reacted with a Ph$_3$C$^+$ Lewis acid, the germylium [Ph$_3$Ge$^+$][WCA] was formed that is capable of HDF of acyl fluorides and organofluorines. However, this cation is extremely sensitive to even slightly basic species. Consequently the addition of [Ph$_3$Ge$^+$][WCA] to a mixture of an acyl fluoride and an amine is not a feasible method of amidation.

When **3a, 3b**, and **3e** was added to a solution of acyl fluorides (**4a-f**) (Scheme 4.5) in benzene, followed by refluxing for 6 hours, NMR (^{1}H, ^{19}F, and ^{13}C NMR) showed an almost quantitative conversion (99%) of the acyl fluorides to amides (**5a-f**) and Ph$_3$GeF.

Unlike common work-up procedures for amides, the purification of reaction mixture could be carried out with a straightforward wash on a silica column. After the reaction is completed, the mixture in benzene was passed through a silica column. The products **5a-f** stuck to the top of the column and were then washed out using chloroform or ethyl acetate. The benzene fraction contained Ph$_3$GeF which could be

converted back to the starting material using $LiNR_2$.

The identities of the pure amides (**5a-f**) were confirmed by NMR, GC, and HRAM-MS (Table 4.5). For the HRAM-MS experiments, the samples were injected in water and were analyzed in positive ion mode. There is a strong agreement between the calculated masses and the experimental values, with the exception of **5c**. When this amide was analyzed in THF/acetic acid, the intensity of its signal increased.

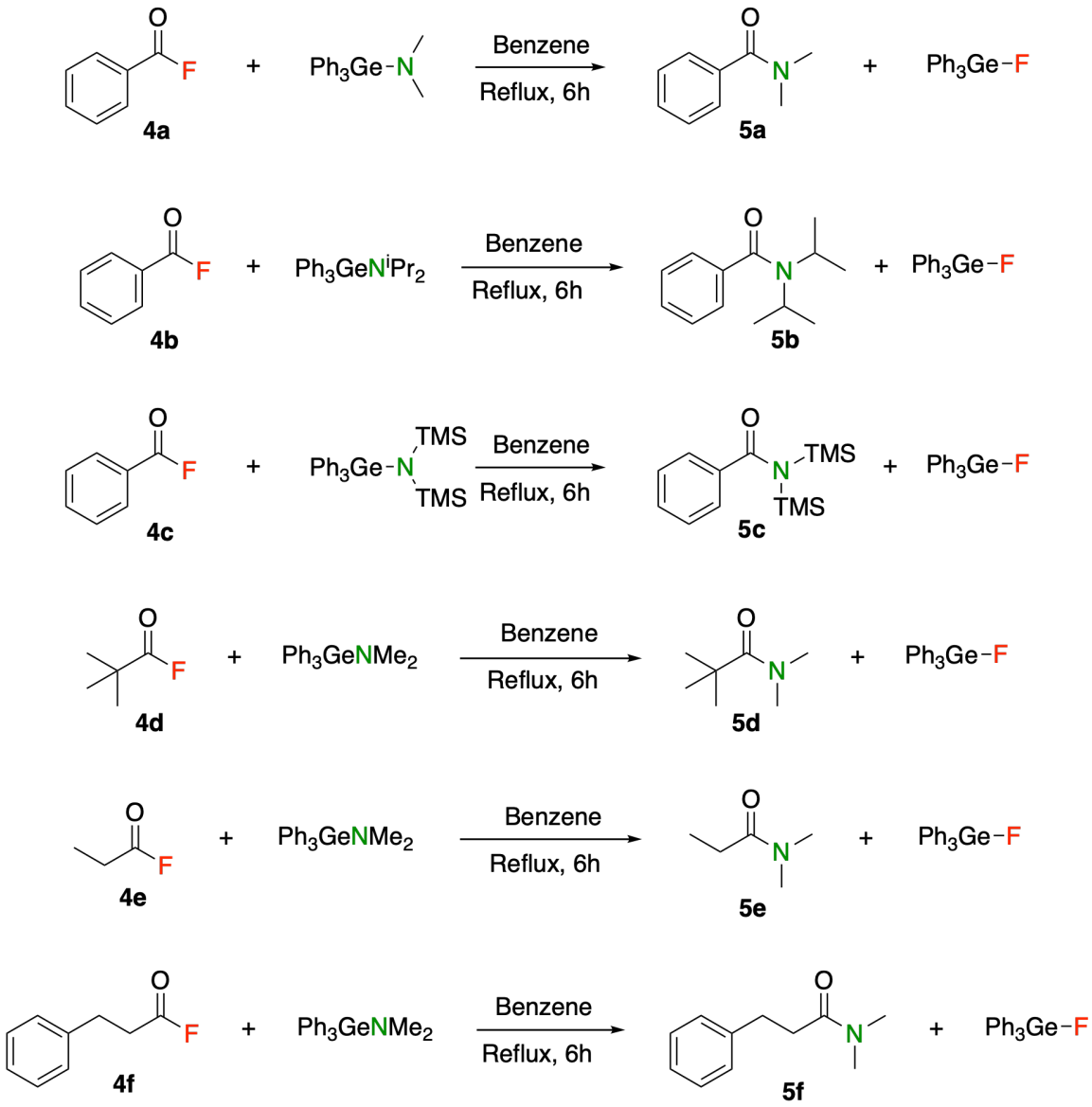

Scheme 4.5: Amidation of acyl fluorides by **3a, 3b,** and **3e**

Table 4.5: HRAM-MS data for **5a-f**

Compound	Experimental m/z	Theoretical m/z	Δ (ppm)
5a	150.0914	150.0913	0.67
5b	206.1539	206.1539	0.05[†]
5c	266.1364	266.1391	10.15
5c[‡]	266.1414	255.1391	8.64
5d	130.1225	130.1226	0.77
5e	102.0914	102.0913	0.98
5f	178.1221	178.1226	2.81

[†] Error calculated using the fifth decimal place of the m/z values.
[‡] Injected in THF/acetic acid

The *in situ* formation of benzoyl fluoride was described by Prakash and coworkers and its one-pot reaction with **3a** was also possible.[155] Scheme 4.6 shows when TBAF was added to a solution of benzoic acid, PPh_3, and *N*-bromosuccinimide in benzene, it resulted in the formation of benzoyl fluoride, which was further confirmed by the appearance of a signal at 18.1 ppm in the ^{19}F-NMR spectrum of the mixture. The other side-products formed in this step included HF, Ph_3PF_2, and Ph_3PO. The subsequent addition of **3a** to the mixture resulted in the formation of **5a** with an isolated yield of 50%.

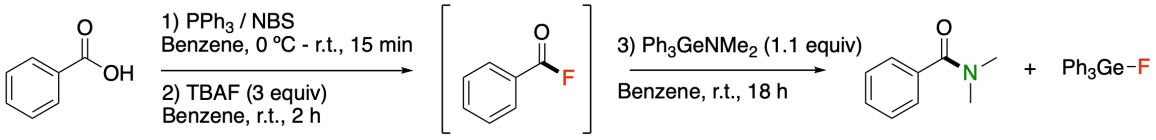

Scheme 4.6: One-pot amidation of benzoic acid with **3a**

To gain more insight into the amidation reaction pathway, kinetic studies of the reaction was carried out. Furthermore, to help explain the results, the energy of the proposed intermediates and transition-state study was explored by DFT calculations. Unlike the original assumption that germyl amines are masked germylium ions and react with acyl fluorides in a dissociative manner, both experimental and computational results point to an associative mechanism namely a "σ-bond metathesis" pathway.

A kinetic analysis was conducted by monitoring the rate of consumption of benzoyl fluoride versus time using its signal in the ^{19}F-NMR spectrum, at room temperature. Figure 4.8-top, shows that the concentration of benzoyl fluoride with time displays an exponential decay. Having a non-zero reaction order suggests an associative pathway. When fitted to first (Figure 4.8-middle), and second order reactions (Figure 4.8-bottom), it was found that the reaction between **4a** and **3a** was second-order in benzoyl fluoride.

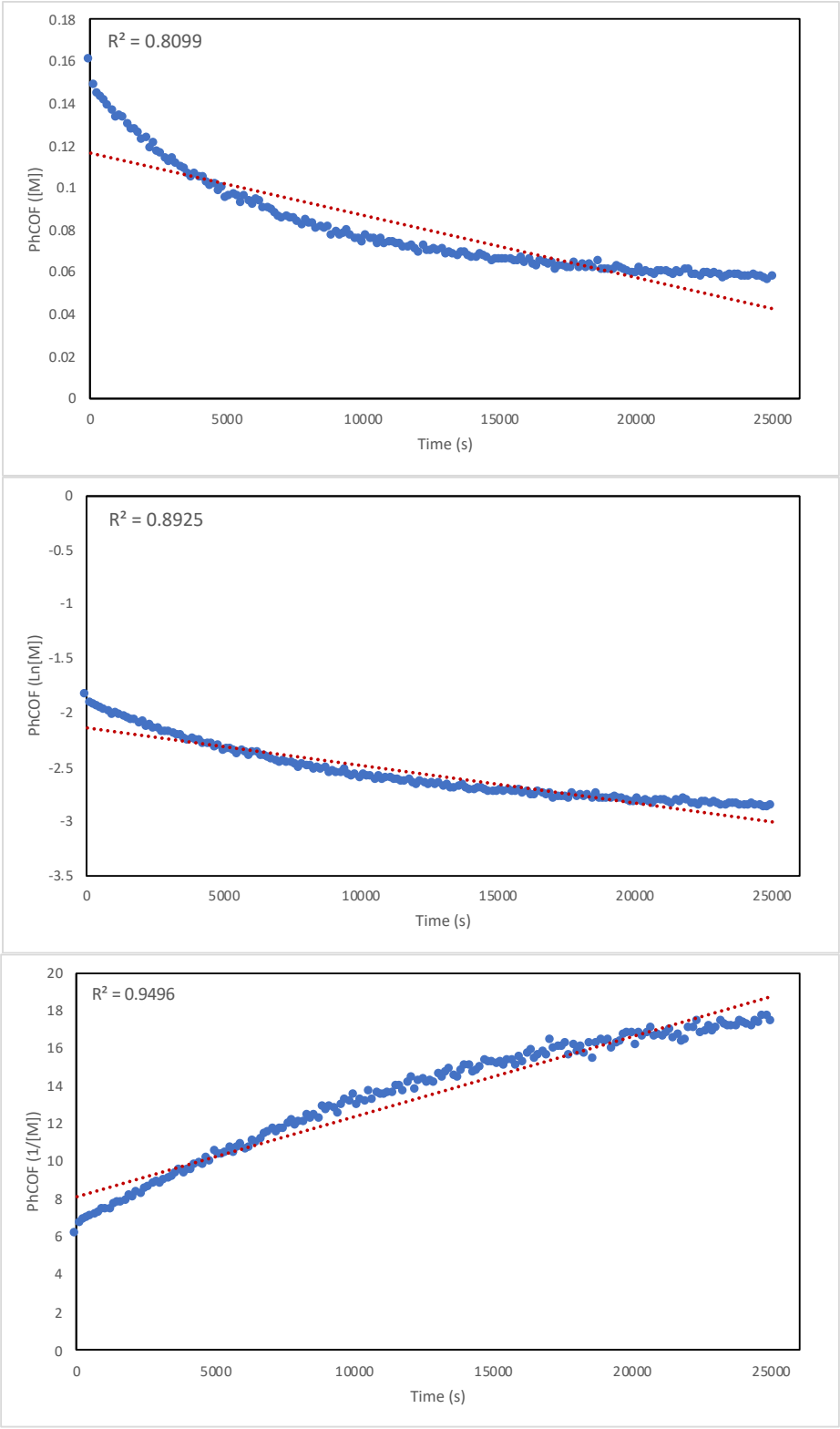

Figure 4.8: Kinetics analysis plots and linear fit analysis of [PhCOF] versus time (top), ln[PhCOF] versus time (middle), and 1/[PhCOF] versus time (bottom)

Figure 4.9 shows the calculated energy profile of the amidation reaction of benzoyl fluoride with **3a**. The calculated energy for a dissociative pathway involving a germylium ion to form intermediate **I_2** was found to be very unfavorable at +733.35 kJ.mol^{-1}. This high energy was confirmed experimentally as the charge separation for this intermediate was not stabilized in benzene, a low dielectric solvent.

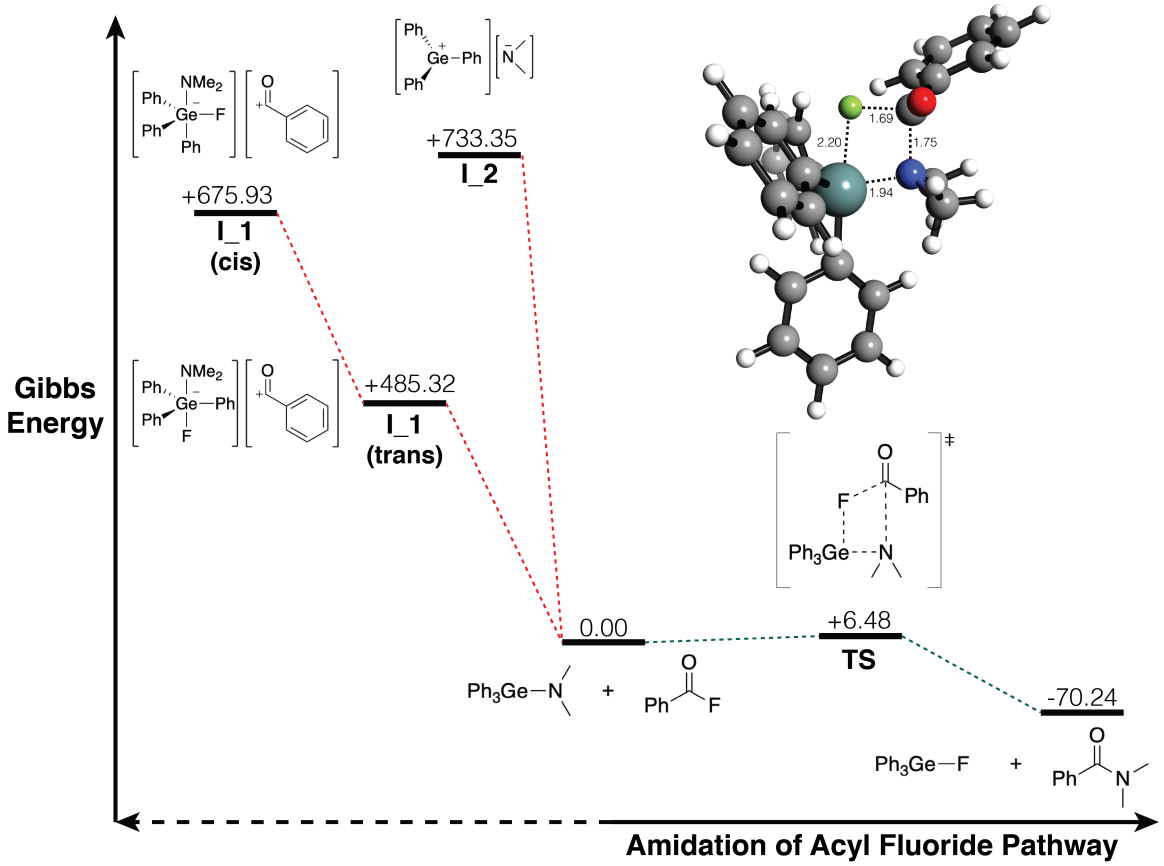

Figure 4.9: Energy profile of the amidation reaction of benzoyl fluoride and **3a**. Values in energy are in kJ.mol^{-1}. Bond distances are reported in Angstroms Å.

The other proposed intermediate that is not observed in the ^{19}F-NMR spectrum of the reaction is hypervalent penta-coordinated germanate **I_1**. The initial search for the transition state was focused on this intermediate but it was not successful. In **I_1** the fluorine atom can approach the germanium from the opposite side of $-NMe_2$, or the same side to form **I_1_trans** and **I_1_cis**, respectively. Both of these intermediates were also studied by FIA calculations and **I_1_trans** proved more stable, however both

of them were thermodynamically unfavorable compared to the calculated transition state.

The lowest energy transition state was found to be that in a "σ-bond metathesis" pathway. A low energy (6.48 kJ.mol^{-1}) transition state **TS** consists of the concerted coordination of the fluorine atom of **4a** to the germanium atom in **3a**, coordination of the nitrogen atom of **3a** to the carbon atom of **4a**, and elongation in C−F and Ge−N bond lengths. The nature of the transition state was further confirmed by IRC calculations showing a declining energy landscape in both the forward and reverse directions of the vibrational mode of the **TS**. The greater decrease in the forward direction is supportive of the reaction being exothermic and products being more thermodynamically stable than the reactants.

4.3 Conclusions

The results in this chapter clearly demonstrate that the germyl amines Ph_3GeNR_2 are effective reagents for the direct amidation of acyl fluorides. The kinetic and DFT data suggest that these compounds do not react similar to a "masked germylium" ion and they rather react with acyl fluorides by a "σ-bond metathesis" that is a concerted pathway and does not involve the formation of intermediates.

4.4 Experimental

4.4.1 General Considerations

The compounds benzoyl fluoride, pivaloyl chloride, propionyl chloride, 3-phenyl -propionyl chloride were purchased from TCI America and were used without purification. The reagents N-bromosuccinimide, triphenylphosphine, benzoic acid, lithium diisopropylamide, triphenylgermanium chloride, and tetrabutylammonium fluoride were purchased from Sigma Aldrich and used without further purification. Ph_3GeNMe_2 was prepared using the literature procedures.[45,156] GC/MS data were acquired using

a Shimadzu QP2010 GC/MS and HRAM-MS were collected using a Thermo Fisher Q Exactive Hybrid Quadrupole Orbitrap mass spectrometer.

All calculations including the optimization and frequency calculations of the structures and FIA analyses were carried out by Gaussian 09, Rev. C.01.[157] All geometries were fully optimized to a local minima and were confirmed by performing frequency calculations and not having imaginary frequencies. A D3(0) empirical dispersion correction was also applied in all the calculations.[131] All structures except for FIA calculations were optimized at B3LYP level with cc-pVTZ as the basis set. NBO analysis and Wiberg Bond Indices were calculated using the keyword *BNDIDX*.[158]

The Lewis acidity of germyl amines was evaluated by FIA analysis in the gas phase at the M06-2X level of theory with a Def2-TZVPP basis set.[159,160] The FIA values were determined by isodesmic reactions anchored to the COF_2/COF_3^- system.[151] For the fluorinated germanate anions ($Ph_3Ge(F)NR_2^-$) with trigonal bipyramidal geometry both *cis* and *trans* geometries were calculated and the one with lower energy was considered for the FIA values.

4.4.2 Procedures for the Synthesis of Acyl Fluorides

4.4.2.1 Pivaloyl Fluoride

Pivaloyl chloride (2.00 g, 16.6 mmol, 1 equiv.) was dissolved in dichloromethane in a screw-cap vial. Sodium fluoride NaF (1.04 g, 24.9 mmol, 1.5 equiv) was slowly added to the solution and the mixture was stirred overnight at room temperature. The reaction mixture was then filtered through Celite and the solvent was removed by distillation to yield pivaloyl fluoride (0.98 g, 57 %). ^{1}H-NMR ($CDCl_3$) δ 1.27 (s, 9H, $-C(CH_3)_3$) ppm. ^{13}C-NMR (C_6D_6) δ 173.7 (C=O), 26.8 ($-C(CH_3)_3$), 25.5 ($-C(CH_3)_3$) ppm. ^{19}F-NMR ($CDCl_3$) δ 25.3 (COF) ppm. The NMR spectra are consistent with the literature data.[161]

4.4.2.2 Propionyl Fluoride

Propionyl chloride (2.00 g, 21.6 mmol, 1 equiv.) was dissolved in dichloromethane in a screw-cap vial. Sodium fluoride (1.36 g, 32.4 mmol, 1.5 equiv.) was slowly added to the solution and the mixture was stirred overnight at room temperature. The reaction mixture was then filtered through Celite and the solvent was removed by distillation to yield propionyl fluoride (1.02 g, 62 %). ^{1}H-NMR (C_6D_6) δ 2.12 (q, J = 8.1 Hz, 2H, $-CH_2CH_3$), 0.62 (t, J = 8.1 Hz, 3H, $-CH_2CH_3$) ppm. ^{13}C-NMR (C_6D_6) δ 174.1 (C=O), 40.6 ($-CH_2CH_3$), 9.2 ($-CH_2CH_3$) ppm. ^{19}F-NMR (C_6D_6) δ 42.8 (COF) ppm.

4.4.2.3 3-Phenylpropionyl Fluoride

On the bench-top,3-Phenylpropionyl chloride (2.00 g, 11.9 mmol, 1 equiv.) was dissolved in dichloromethane in a screw-cap vial. Sodium fluoride NaF (0.747 g, 17.8 mmol, 1.5 equiv) was slowly added to the solution and the mixture was stirred overnight at room temperature. The reaction mixture was then filtered through Celite and the solvent was removed by distillation to yield propionyl fluoride(1.19 g, 66 %). ^{1}H-NMR (C_6D_6) δ 2.12 (q, J = 8.1 Hz, 2H, $-CH_2CH_3$), 0.62 (t, J = 8.1 Hz, 3H $-CH_2CH_3$) ppm. ^{13}C-NMR (C_6D_6) δ 174.1 (C=O), 40.6 ($-CH_2CH_3$), 9.2 ($-CH_2CH_3$) ppm. ^{19}F-NMR (C_6D_6) δ 42.8 (COF) ppm.

4.4.3 Procedure for the Synthesis of Germyl Amines

4.4.3.1 *N,N*- Diisopropyltriphenylgermylamine 3b

In a Schlenk flask, triphenyl germanium chloride (2.79 g, 8.22 mmol, 1 equiv) was dissolved in benzene. Lithium diisopropylamide (1.06 g, 4.93 mL (2M solution in THF), 9.86 mmol, 1.2 equiv) was slowly added to the Schlenk flask using a cannula at room temperature. The reaction mixture was stirred overnight, after which, fresh benzene was poured into to the flask and the mixture was filtered through Celite.

Volatiles were then removed in vacuo to yield yellowish solids of *N,N*-diisopropyltriphenylgermanamine (2.89 g, 87 %).

4.4.3.2 *N,N*- Bis(trimethylsilyl)triphenylgermylamine 3e

In a Schlenk flask, triphenyl germanium chloride (0.50 g, 1.47 mmol, 1 equiv) was dissolved in benzene. Lithium bis(trimethylsilyl)amide (0.295 g, 1.77 mmol, 1.2 equiv) was slowly added to the Schlenk flask using a cannula at room temperature. The reaction mixture was stirred overnight, after which, fresh benzene was poured into to the flask and the mixture was filtered through Celite. Volatiles were then removed in vacuo to yield of *N,N*- bis(trimethylsilyl)triphenylgermylamine as a solid (0.512 g, 75 %). ^{1}H-NMR (C_6D_6) δ 7.68 (d, $J = 7.6$ Hz, 6H, *o*-C_6H_5), 7.22 – 7.17 (m, 9H, *m*-C_6H_5 and *p*-C_6H_5), 0.23 (s, 18 H, $-Si(CH_3)_3$) ppm. ^{13}C-NMR (C_6D_6) δ 135.3 (ipso-C_6H_5), 134.5 (*o*-C_6H_5), 130.6 (*m*-C_6H_5), 128.9 (*p*-C_6H_5), 5.3 ($-Si(CH_3)_3$) ppm. ^{29}Si-NMR (C_6D_6) δ – 111.3 ($-Si(CH_3)_3$) ppm. HRAM-MS: Calcd. $m/z = 466.1436$ ($M + H^+$). Found: 466.1431 ($M + H^+$).

4.4.4 Amidation Reactions

4.4.4.1 5a

In a Schlenk flask, benzoyl fluoride (200 mg, 1.61 mmol, 1 equiv) was dissolved in benzene. *N,N*-dimethyltriphenylgermanamine (616 mg, 1.77 mmol, 1.1 equiv) was slowly added to the mixture. The mixture was refluxed for 18 hours. Solvent was removed in vacuo and yellow oil was purified using a silica column (then EtOAc) to result pure *N,N*-dimethylbanzamide as a white solid. ^{1}H-NMR (400 MHz, $CDCl_3$) δ 7.52 – 7.32 (m, 5H $-C_6H_5$), 3.13 (s, 3H, $-N(CH_3)_2$), 2.99 (s, 3H, $-N(CH_3)_2$) ppm. ^{13}C-NMR (100.6 MHz, $CDCl_3$) δ 171.8 (C=O), 137.7 (ipso-C_6H_5), 134.5 (*o*-C_6H_5), 129.5 (*m*-C_6H_5), 128.1 (*p*-C_6H_5), 39.7 ($-N(CH_3)_2$), 35.5 ($-N(CH_3)_2$) ppm. Spectral data were in accord with published data.[162]

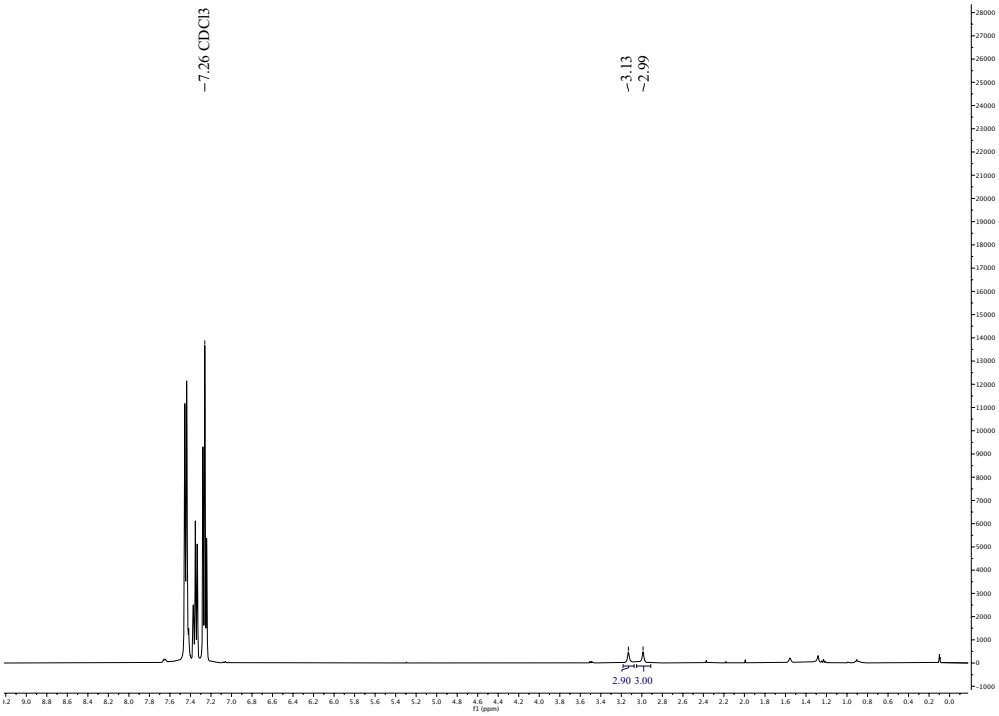

Figure 4.10: ^{1}H-NMR (400 MHz, $CDCl_3$) spectrum of **5a**

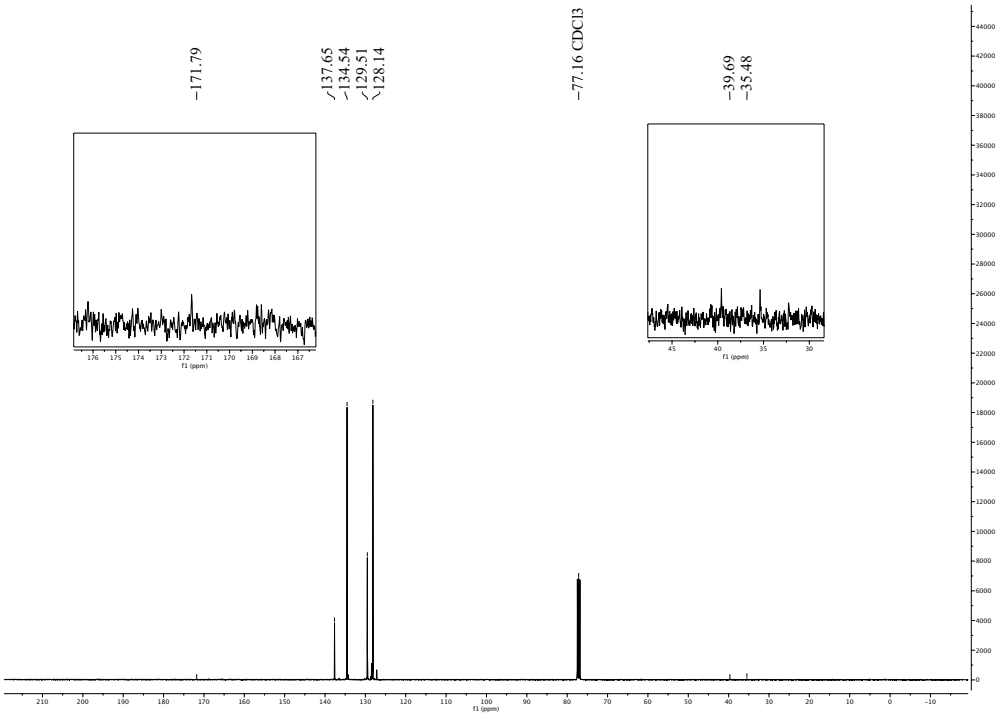

Figure 4.11: ^{13}C-NMR (101 MHz, $CDCl_3$) spectrum of **5a**

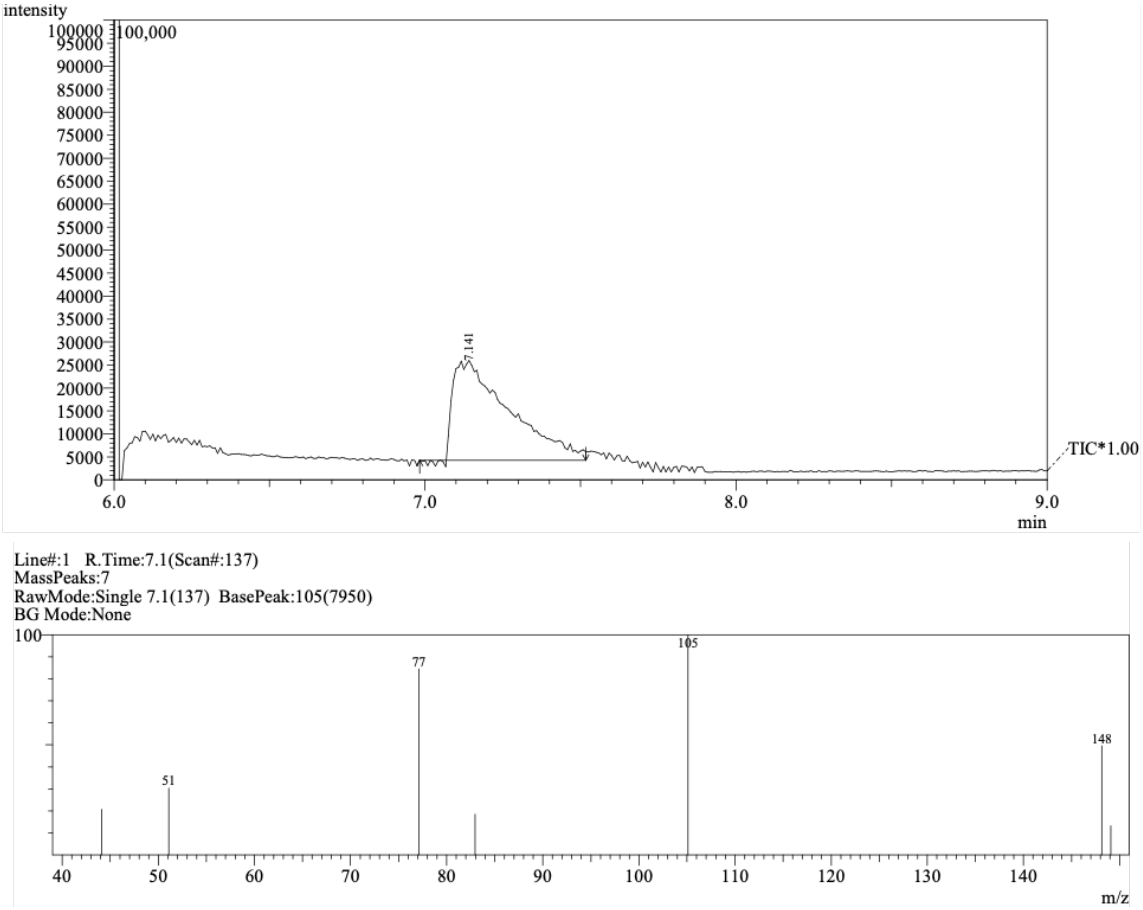

Figure 4.12: GC-MS trace of **5a**

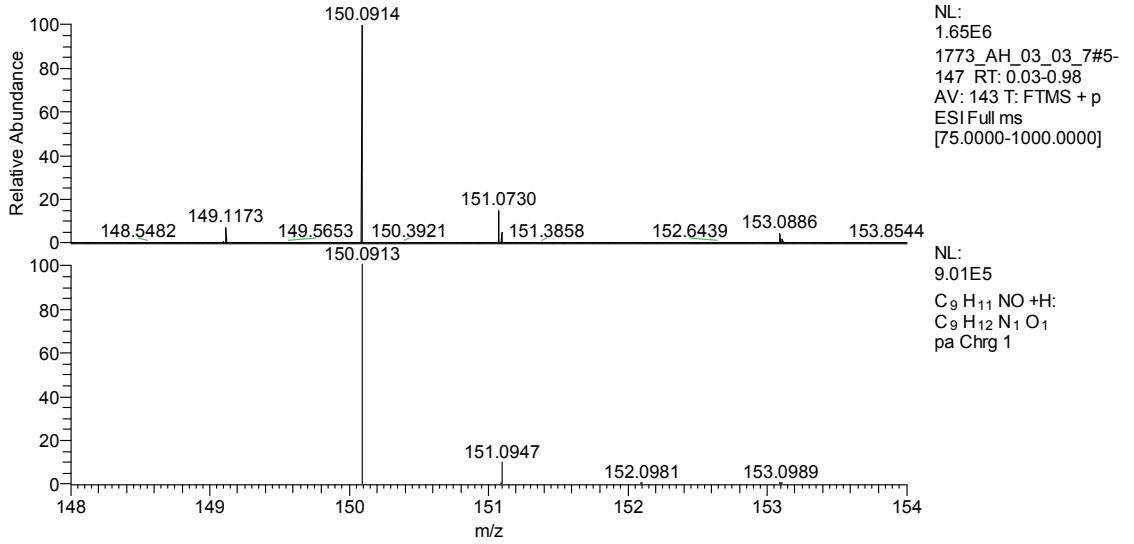

Figure 4.13: HRAM-MS of **5a** in water. (Top, experimental spectrum; bottom, calculated spectrum)

4.4.4.2 5b

In a Schlenk flask, benzoyl fluoride (100 mg, 0.805 mmol, 1 equiv) was dissolved in benzene. *N,N*-Diisopropyltriphenylgermanamine (358 mg, 0.886 mmol, 1.1 equiv) was slowly added to the mixture. The mixture was refluxed for 18 hours. Reaction mixture was filtered through Celite and the solvent was removed in vacuo. The residue was purified using a silica plug by first washing with benzene and then chloroform, to yield *N,N*-Diisopropylbenzamide as white crystals. ^{1}H-NMR (C_6D_6) δ 7.85 – 7.65 (m, 5H, $-C_6H_5$), 4.54 – 4.13 (m, 2H, $-CH(CH_3)_2$), 1.11 – 0.86 (m, 12H, $-CH(CH_3)_2$) ppm. ^{13}C-NMR (C_6D_6) δ 169.5 (C=O), 135.7 (ipso-C_6H_5), 135.72 (*o*-C_6H_5), 131.0 (*m*-C_6H_5), 129.4 (*p*-C_6H_5), 42.0 ($-CH(CH_3)_2$), 22.63 42.0 ($-CH(CH_3)_2$) ppm. Spectral data were in accord with published data.[163]

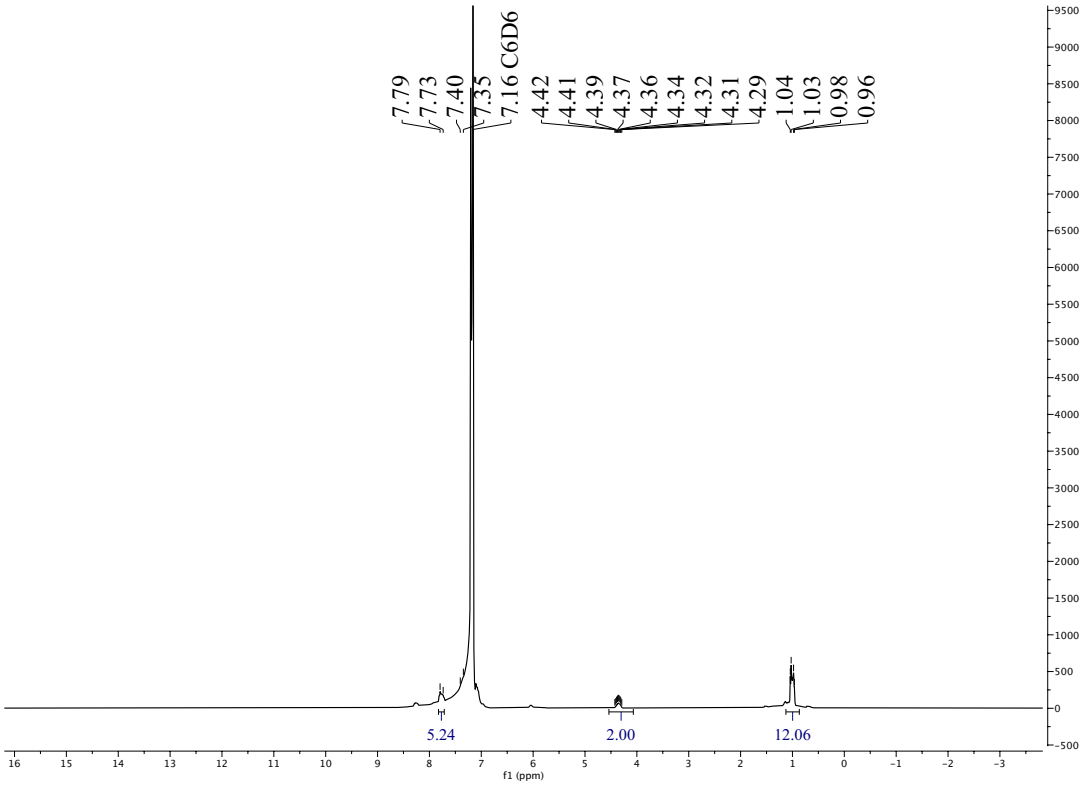

Figure 4.14: ^{1}H-NMR (400 MHz, C_6D_6) spectrum of **5b**

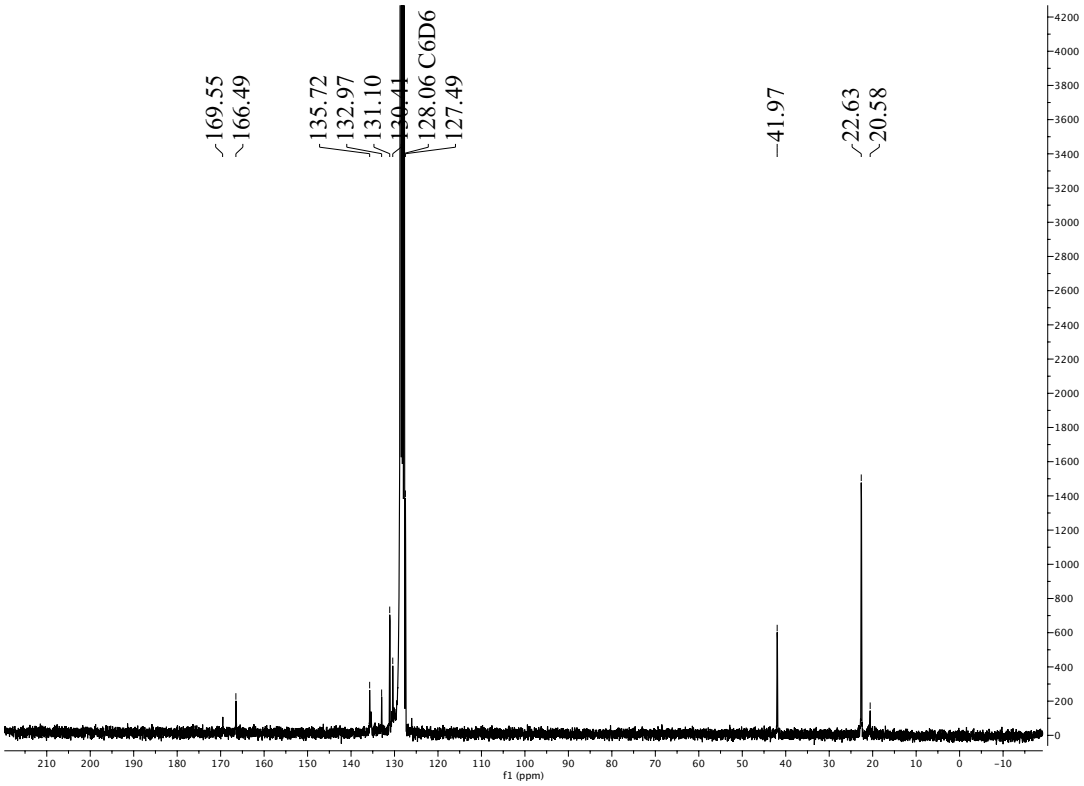

Figure 4.15: ^{13}C-NMR (101 MHz, C_6D_6) spectrum of **5b**

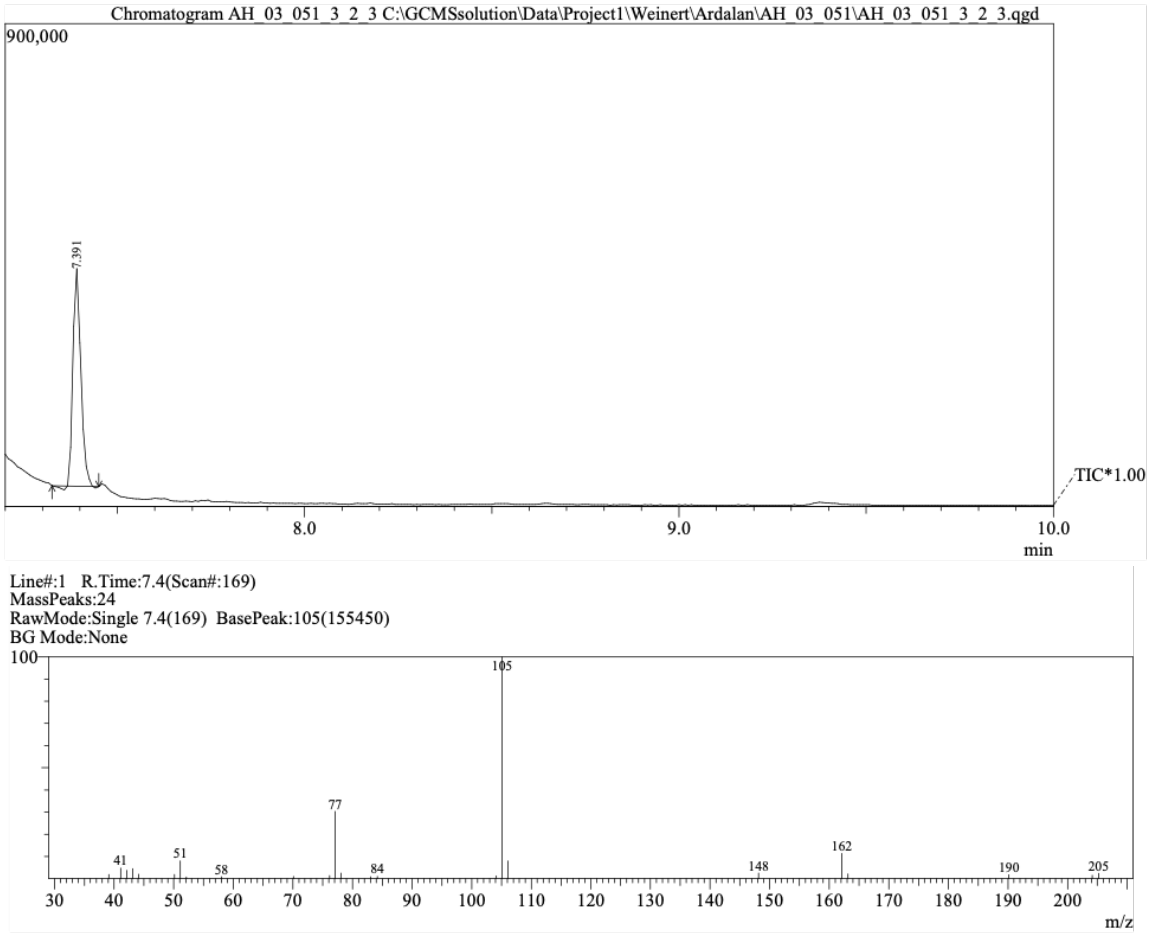

Figure 4.16: GC-MS trace of **5b**

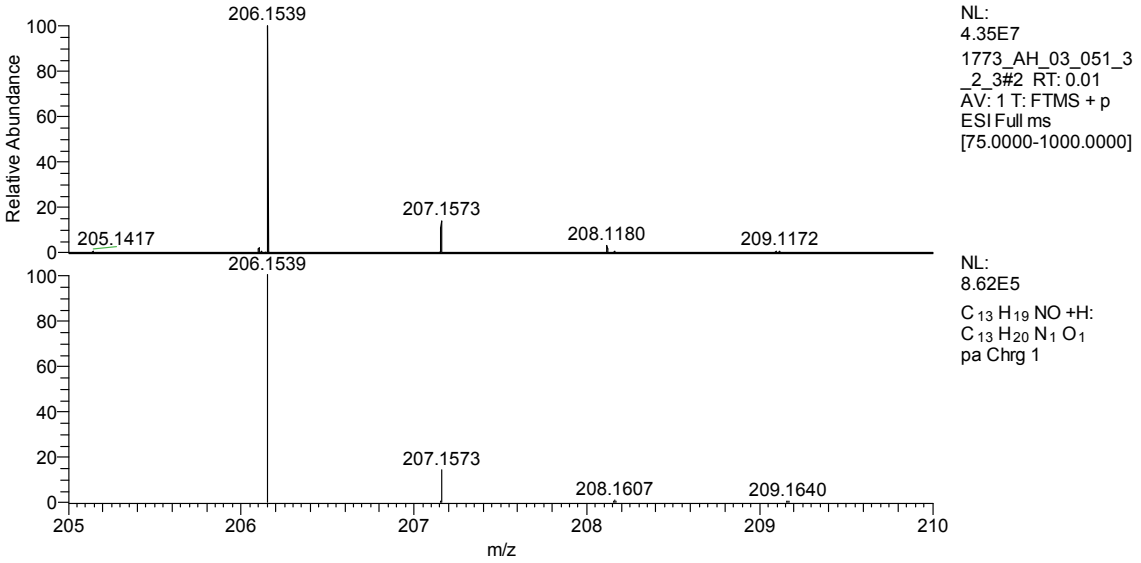

Figure 4.17: HRAM-MS of **5b** in water. (Top, experimental spectrum; bottom, calculated spectrum)

4.4.4.3 5c

In a Schlenk flask, benzoyl fluoride (80 mg, 0.644 mmol, 1 equiv) was dissolved in benzene. *N,N*-Bis(trimethylsilyl)triphenylgermanamine (300 mg, 0.644 mmol, 1 equiv) was slowly added to the mixture. The mixture was refluxed for 18 hours. Reaction mixture was passed through a silica plug and was washed with benzene and then chloroform to yield pure *N,N*-bis(trimethylsilyl)benzamide. ^{1}H-NMR (C_6D_6) δ 8.05 – 7.19 (m, 5H, $-C_6H_5$), 0.21 (s, 18H, $-N(Si(CH_3)_3)_2$) ppm. ^{13}C-NMR (C_6D_6) δ 168.5 (C=O), 135.3 (ipso-C_6H_5), 134.5 (*o*-C_6H_5), 130.6 (*m*-C_6H_5), 128.9 (*p*-C_6H_5), 2.95 (– $N(Si(CH_3)_3)_2$) ppm. Spectral data were in accord with published data.[164]

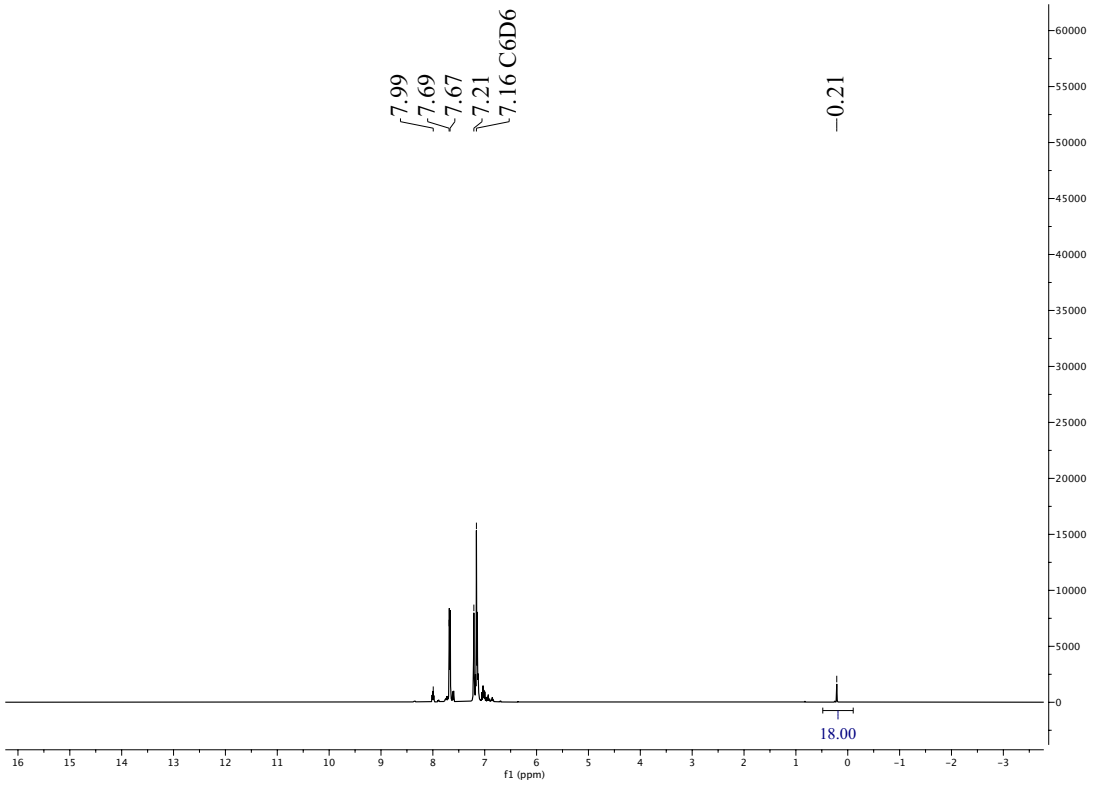

Figure 4.18: ^{1}H-NMR (400 MHz, C_6D_6) spectrum of **5c**

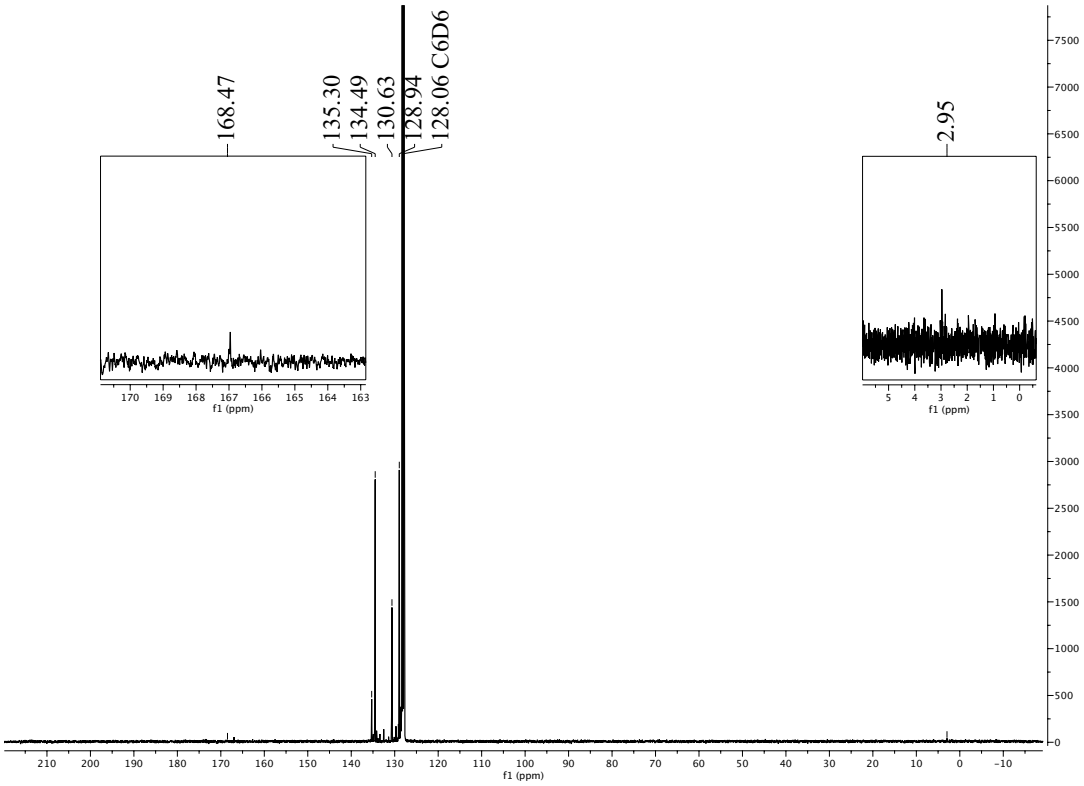

Figure 4.19: ^{13}C-NMR (101 MHz, C_6D_6) spectrum of **5c**

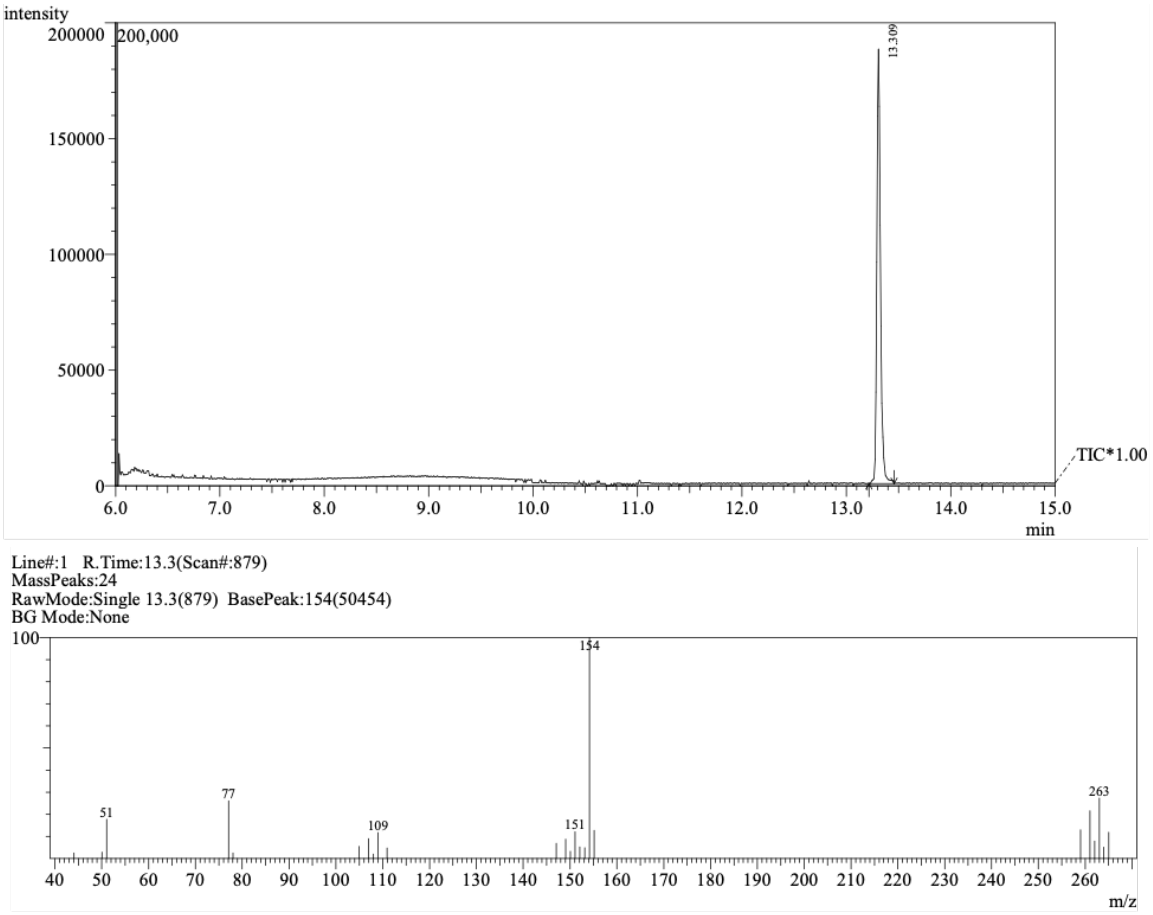

Figure 4.20: GC-MS trace of **5c**

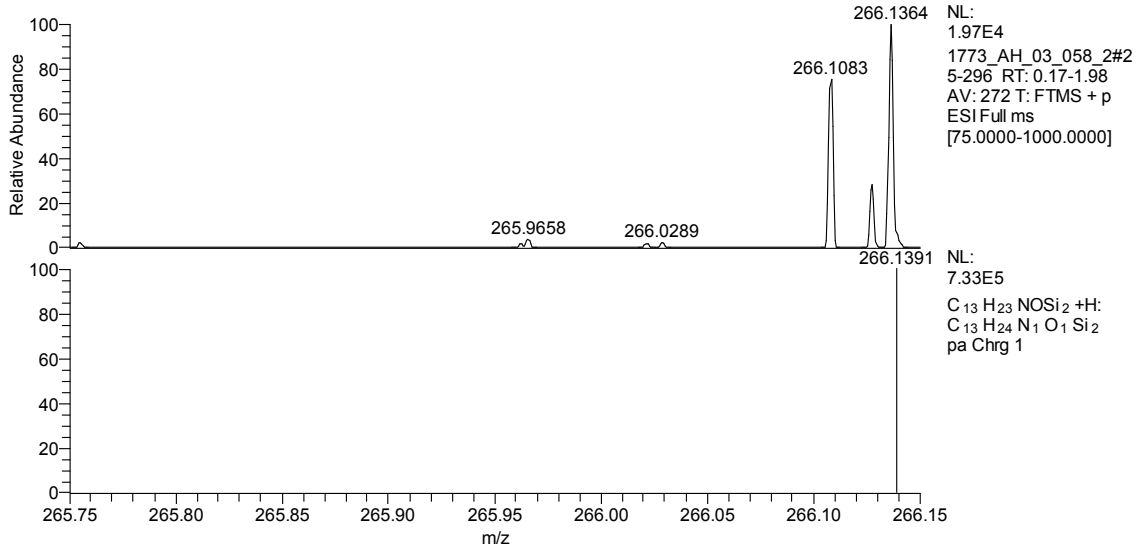

Figure 4.21: HRAM-MS of **5c** in water. (Top, experimental spectrum; bottom, calculated spectrum)

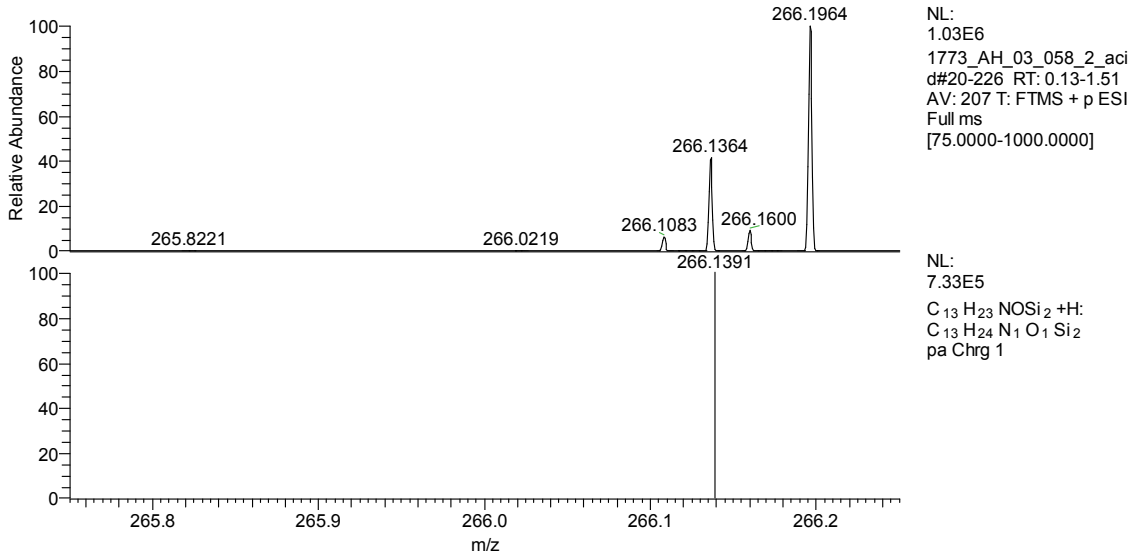

Figure 4.22: HRAM-MS of **5c** in water with added acetic acid. (Top, experimental spectrum; bottom, calculated spectrum)

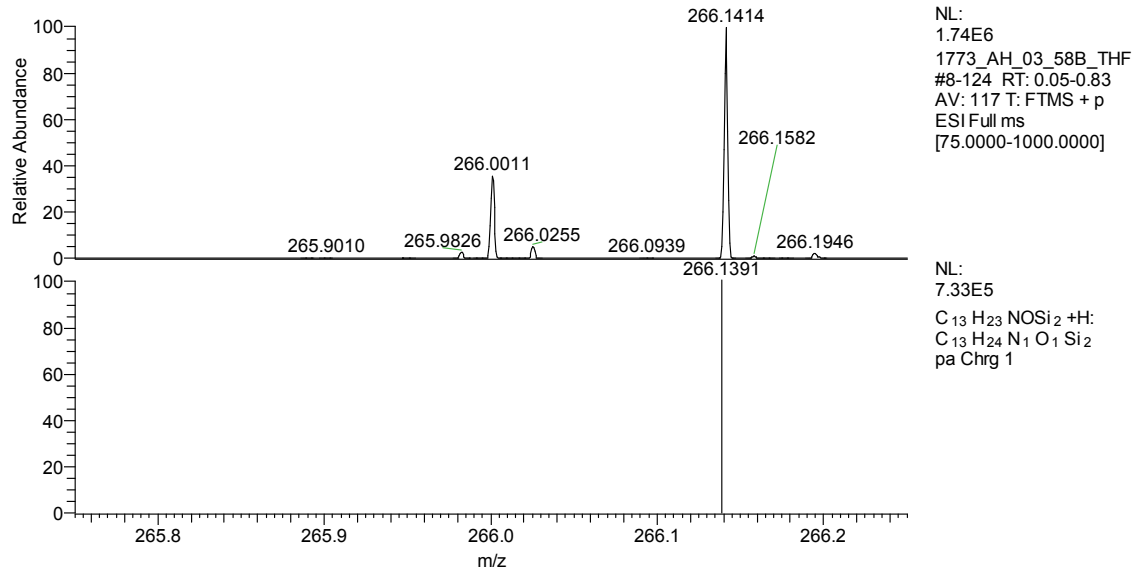

Figure 4.23: HRAM-MS of **5c** in THF. (Top, experimental spectrum; bottom, calculated spectrum)

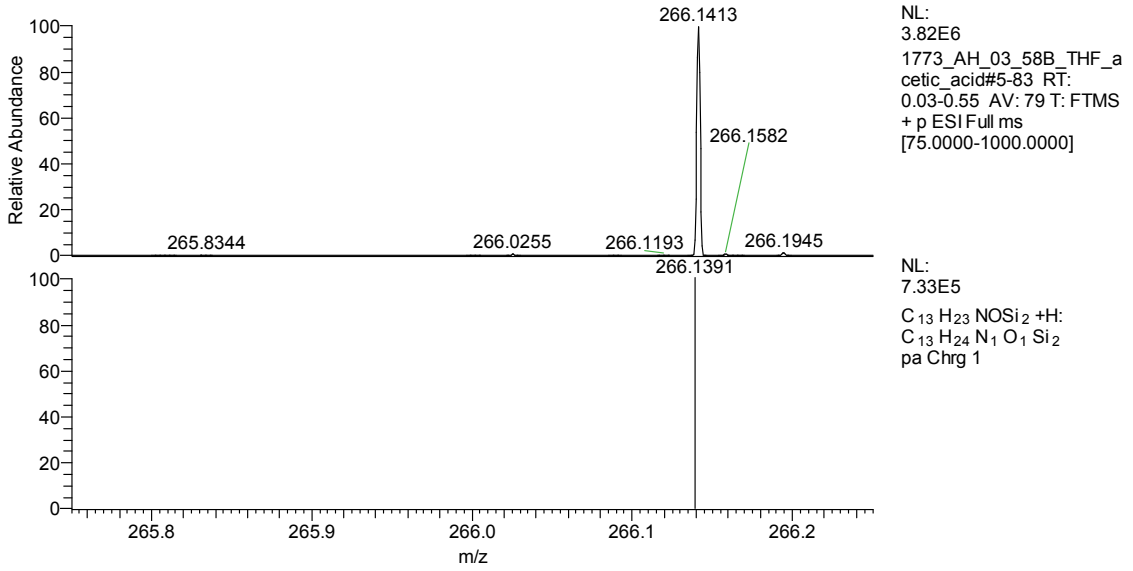

Figure 4.24: HRAM-MS of **5c** in THF with added acetic acid. (Top, experimental spectrum; bottom, calculated spectrum)

4.4.4.4 5d

In a Schlenk flask, pivaloyl fluoride (200 mg, 1.92 mmol, 1 equiv) was dissolved in benzene. *N,N*-Dimethyltriphenylgermanamine (735 mg, 2.11 mmol, 1.1 equiv) was slowly added to the mixture. The mixture was refluxed for 18 hours. Reaction mixture was passed through a silica plug and was washed with benzene and then ethyl acetate to yield pure *N,N*-dimethylpivalamide as a clear oil. ^{1}H-NMR (C_6D_6) δ 2.59 (s, 6H, $-N(CH_3)_2$), 1.16 (s, 9H, $-C(CH_3)_3$) ppm. ^{13}C-NMR (C_6D_6) δ 176.5 (C=O), 38.6 ($-C(CH_3)_3$), 37.9 ($-N(CH_3)_2$), 28.4 ($-C(CH_3)_3$) ppm. Spectral data were in accord with published data.[165]

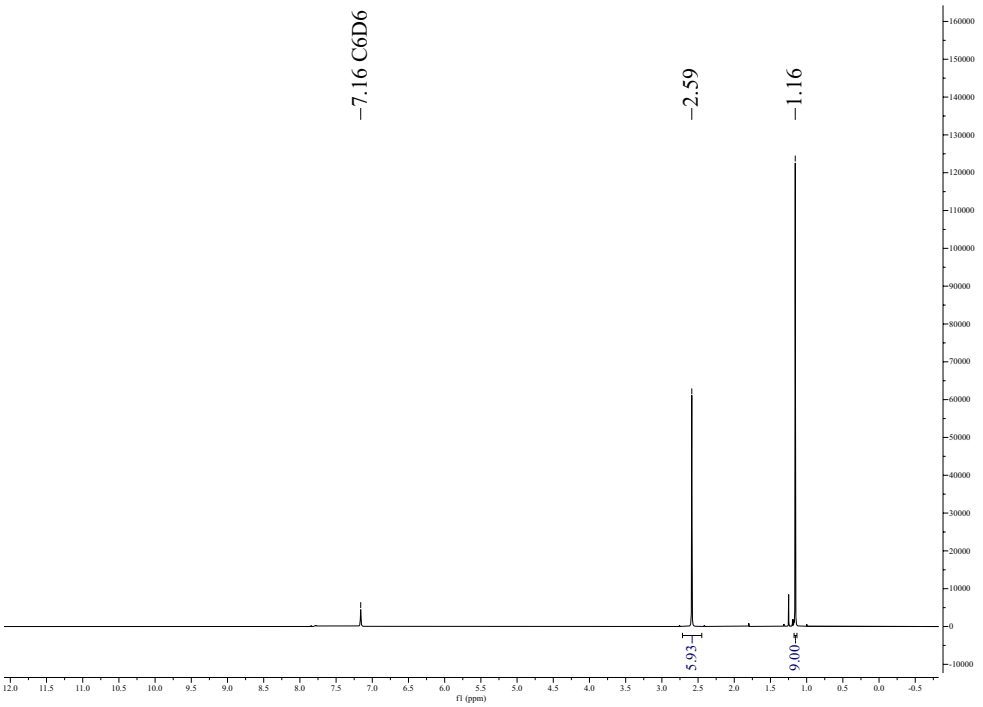

Figure 4.25: ^{1}H-NMR (400 MHz, C_6D_6) spectrum of **5d**

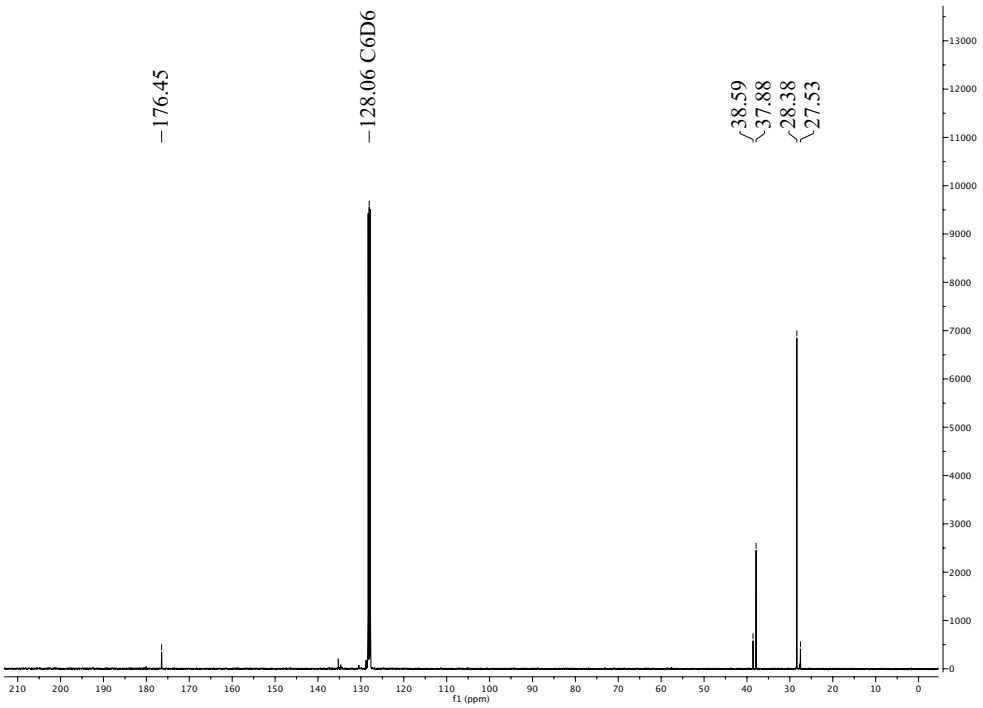

Figure 4.26: ^{13}C-NMR (101 MHz, C_6D_6) spectrum of **5d**

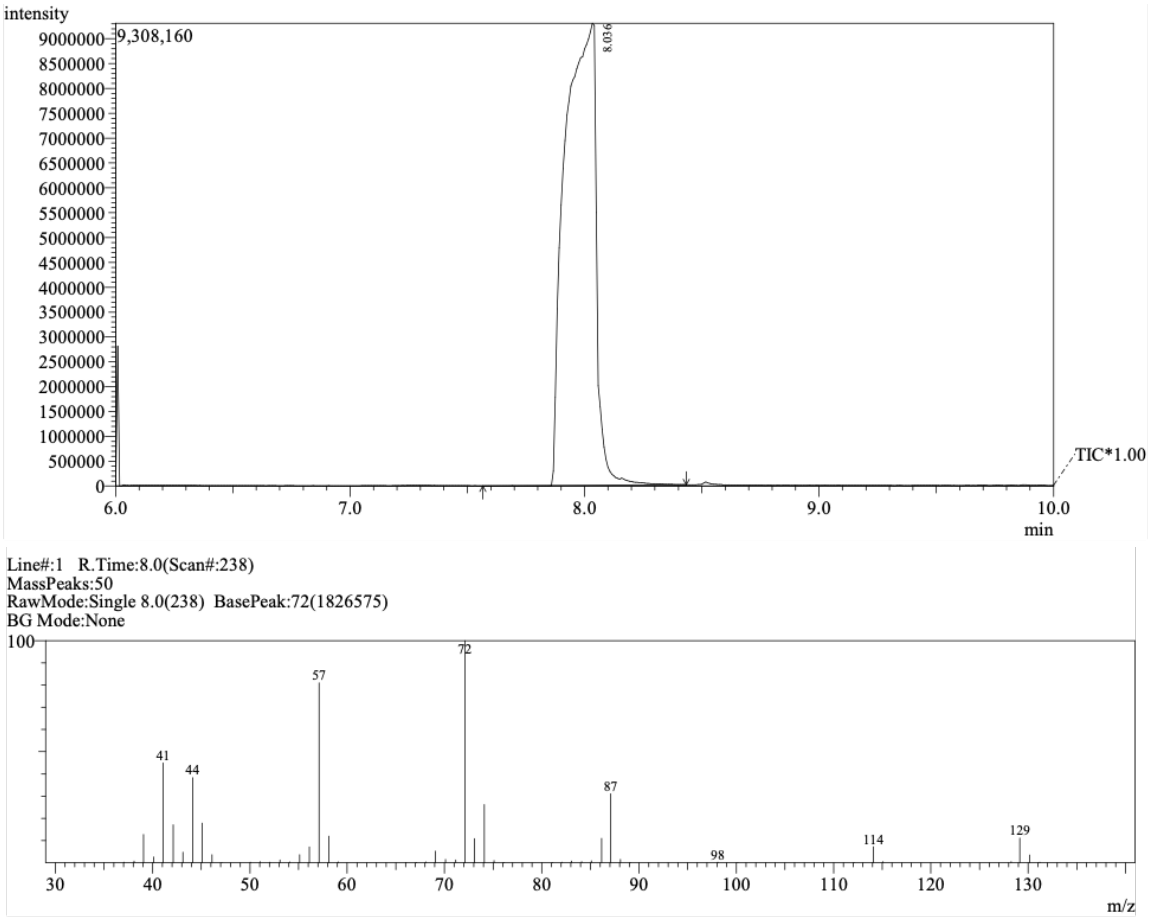

Figure 4.27: GC-MS trace of **5d**

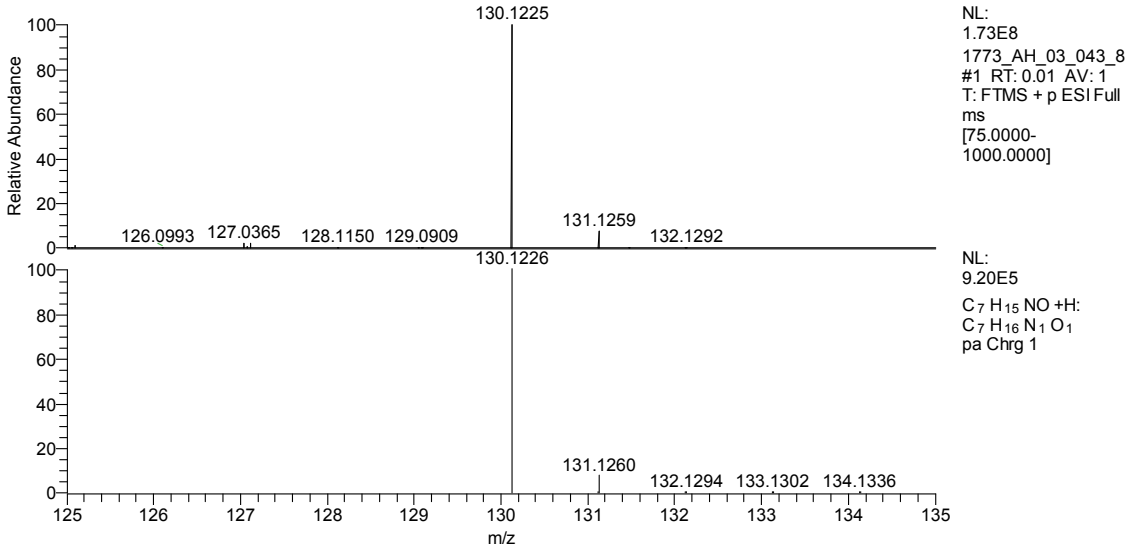

Figure 4.28: HRAM-MS of **5d** in water. (Top, experimental spectrum; bottom, calculated spectrum)

4.4.4.5 5e

In a Schlenk flask, propionyl fluoride (160 mg, 2.10 mmol, 1 equiv) was dissolved in benzene. *N,N*-Dimethyltriphenylgermanamine (805 mg, 2.31 mmol, 1.1 equiv) was slowly added to the mixture. The mixture was refluxed for 18 hours. Reaction mixture was passed through a silica plug and was washed with benzene and then chloroform to yield pure *N,N*-dimethylpropionamide as a clear oil. ^{1}H-NMR (C_6D_6) δ 2.66 (s, 3H, $-N(CH_3)_2$), 2.14 (s, 3H, $-N(CH_3)_2$), 1.83 (q, J = 7.4 Hz, 2H, $-CH_2CH_3$), 1.12 (t, J = 7.4 Hz, 3H, $-CH_2CH_3$) ppm. ^{13}C-NMR (C_6D_6) δ 172.4 (C=O), 36.1 ($-N(CH_3)_2$), 34.9 ($-N(CH_3)_2$), 26.4 ($-CH_2CH_3$), 9.6 ($-CH_2CH_3$) ppm. Spectral data were in accord with published data.[166]

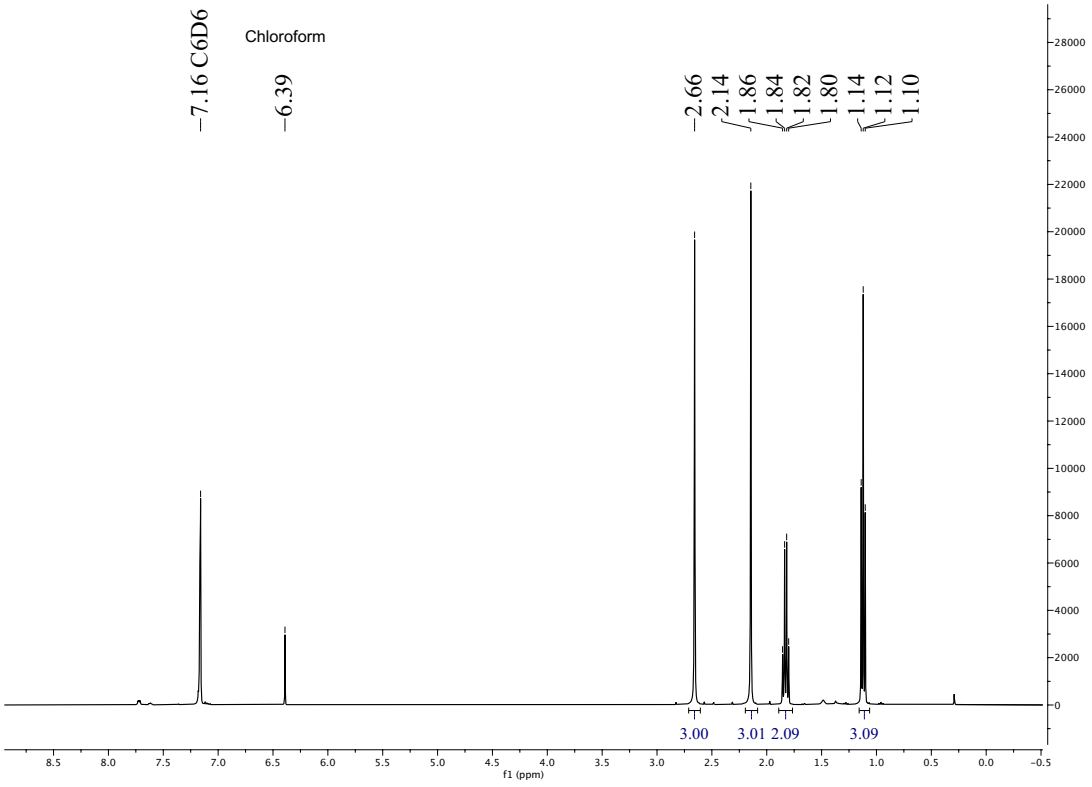

Figure 4.29: ^{1}H-NMR (400 MHz, C_6D_6) spectrum of **5e**

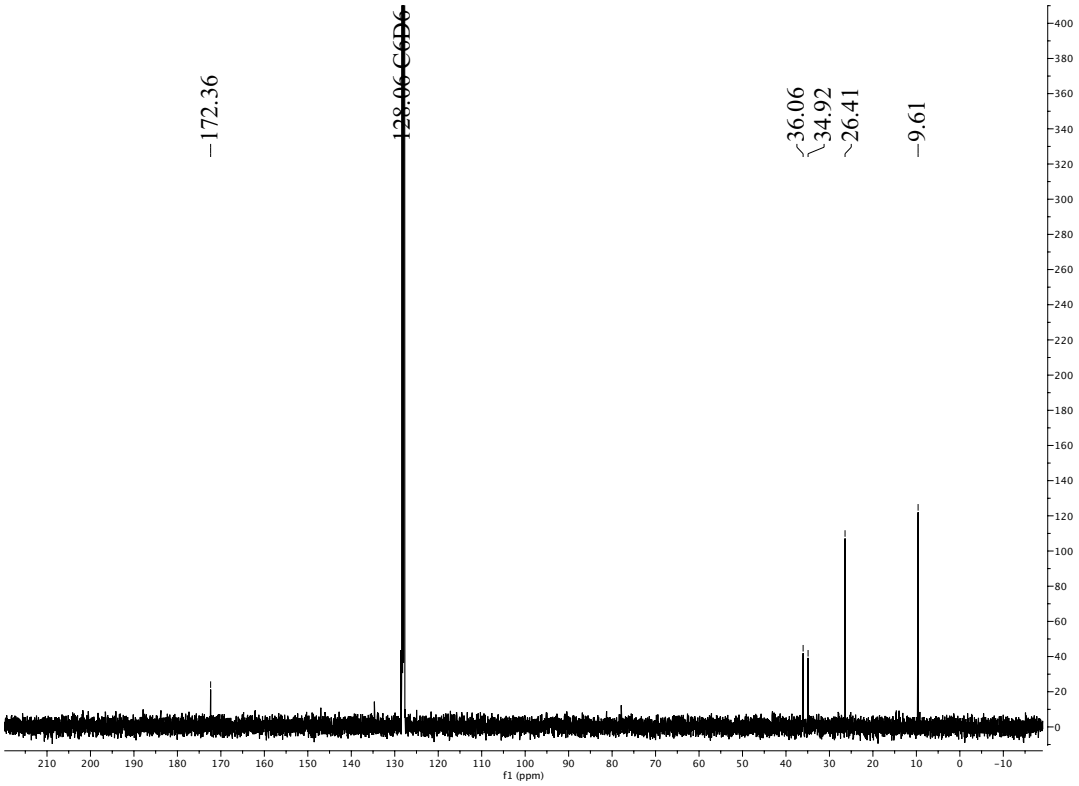

Figure 4.30: ^{13}C-NMR (101 MHz, C_6D_6) spectrum of **5e**

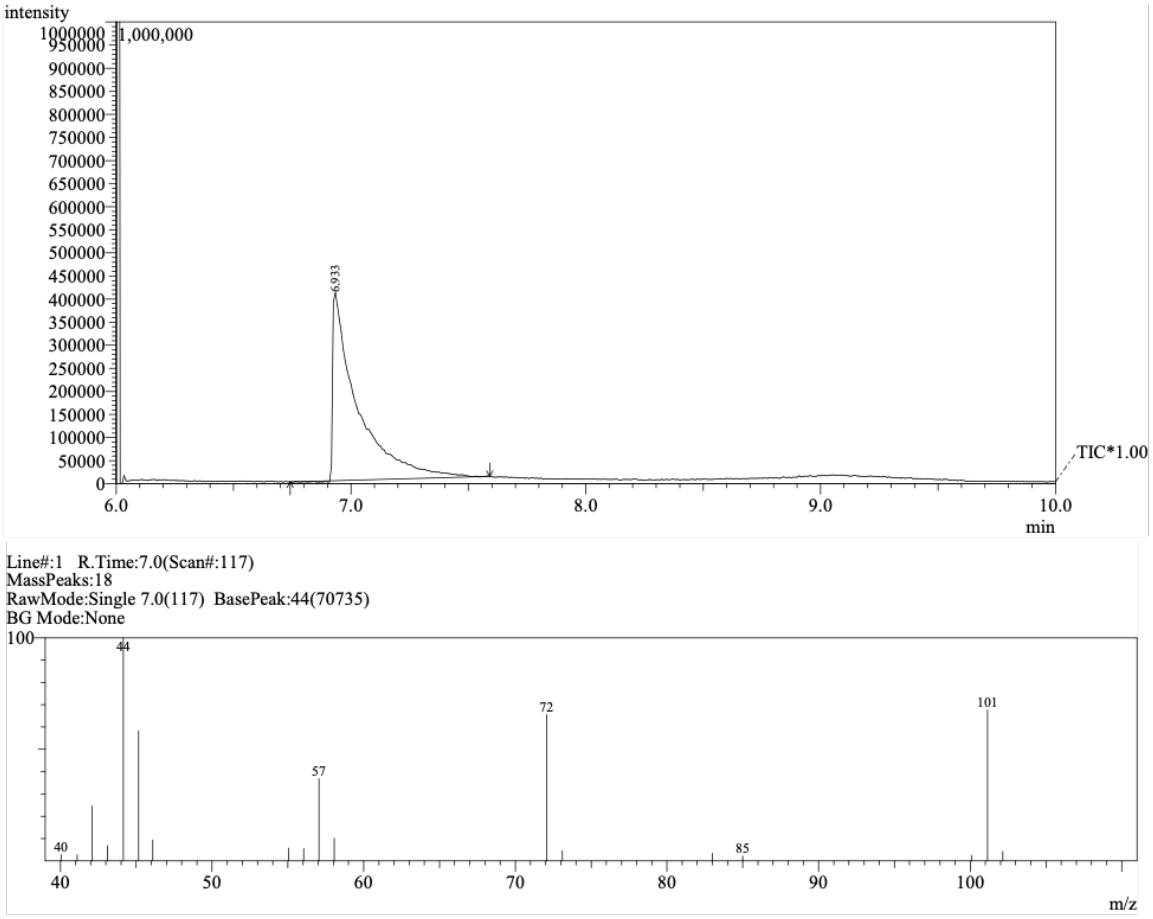

Figure 4.31: GC-MS trace of **5e**

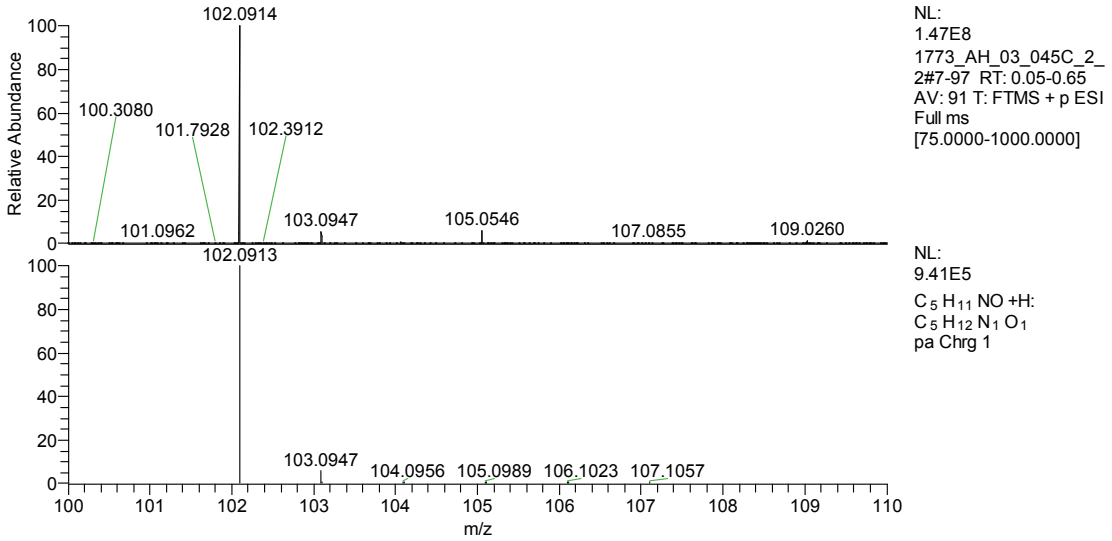

Figure 4.32: HRAM-MS of **5e** in water. (Top, experimental spectrum; bottom, calculated spectrum)

4.4.4.6 5f

In a Schlenk flask, 3-phenylpropanoyl fluoride (80 mg, 0.525 mmol, 1 equiv) was dissolved in benzene. *N,N*-Dimethyl-triphenylgermanamine (182 mg, 0.525 mmol, 1 equiv) was slowly added to the mixture. The mixture was refluxed for 18 hours. Reaction mixture was passed through a silica plug and was washed with benzene and then chloroform to yield pure *N,N*-dimethyl-3-phenylpropanamide as a clear solid. ^{1}H-NMR (C_6D_6) δ 7.10 – 6.99 (m, 5H, $-C_6H_5$), 3.00 (t, J = 7.8 Hz, 2H, $PhCH_2(CH_2)C(O)$-), 2.60 (s, 3H, $-N(CH_3)_2$), 2.18 (t, J = 7.8 Hz, 2H, $Ph(CH_2)CH_2C(O)^-$)), 2.00 (s, 3H, $-N(CH_3)_2$) ppm. ^{13}C-NMR (C_6D_6) δ 171.5 (C=O), 142.3 (ipso-C6H5), 128.9 (o-C_6H_5), 128.7 (m-C_6H_5), 126.3 (p-C_6H_5), 36.2 ($PhCH_2CH_2C(O)$), 35.9 ($PhCH_2$ -$CH_2C(O)$), 35.4 ($-N(CH_3)_2$), 31.7 ($-N(CH_3)_2$) ppm. Spectral data were in accord with published data.[167]

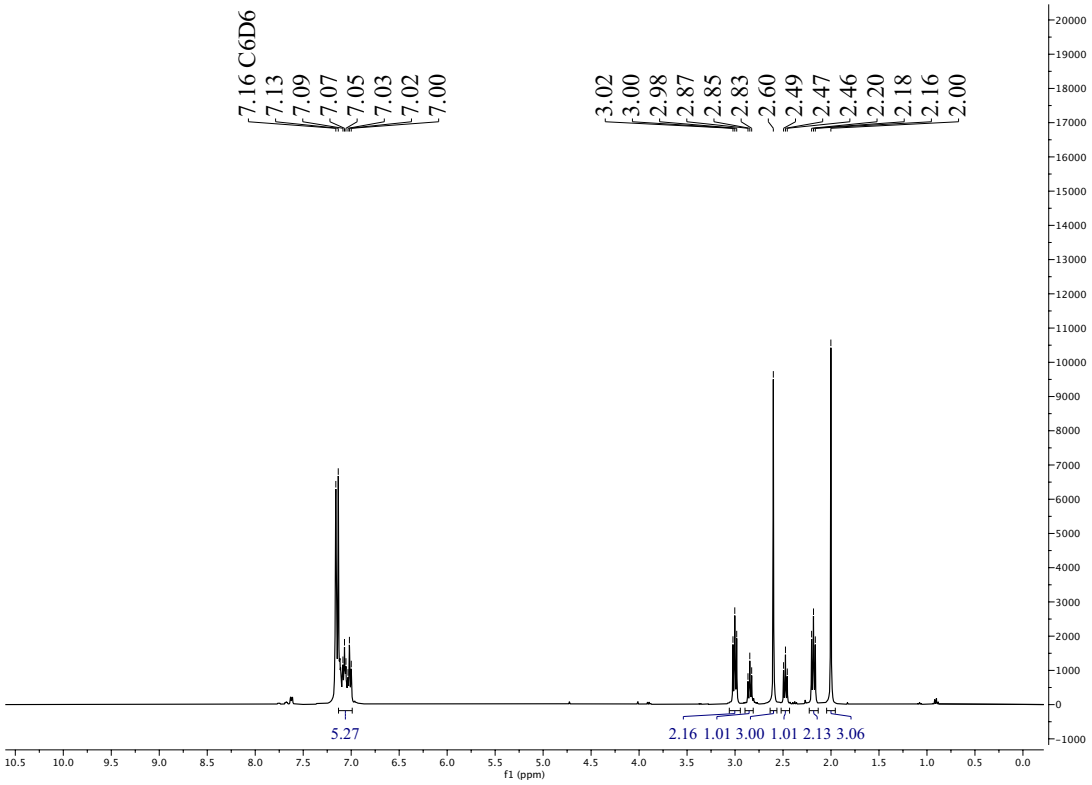

Figure 4.33: ^{1}H-NMR (400 MHz, C_6D_6) spectrum of **5f**

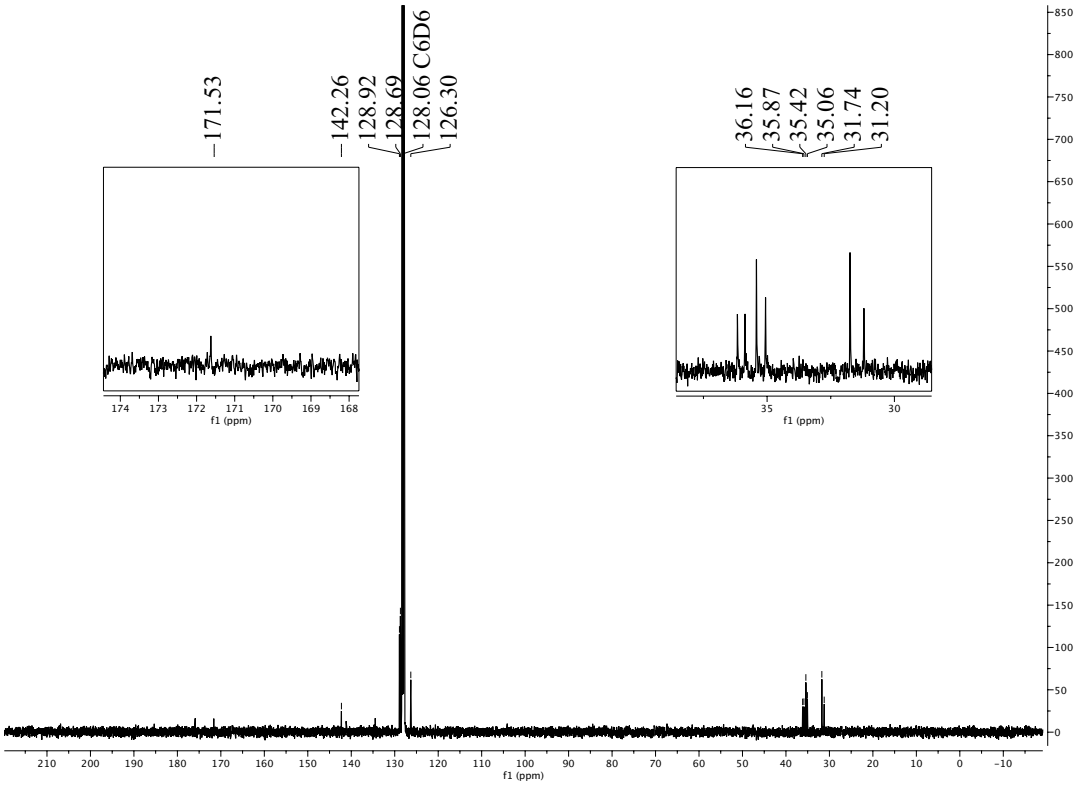

Figure 4.34: ^{13}C-NMR (101 MHz, C_6D_6) spectrum of **5f**

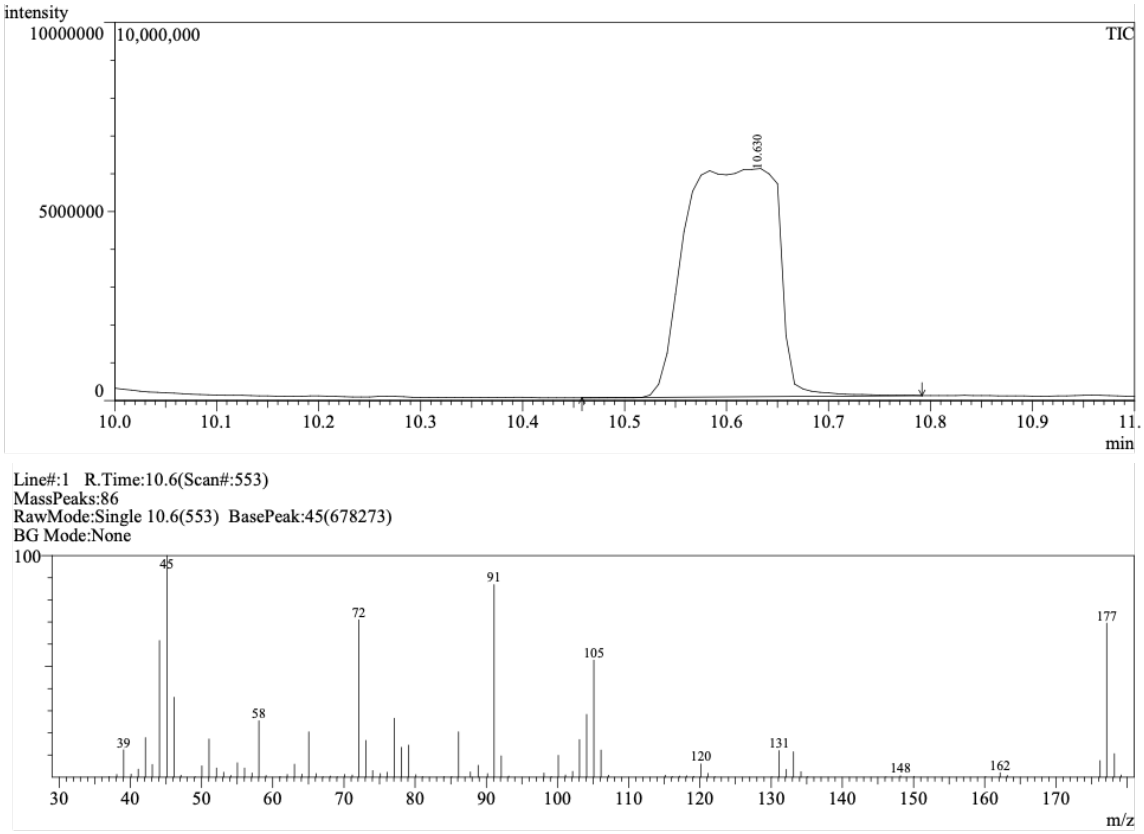

Figure 4.35: GC-MS trace of **5f**

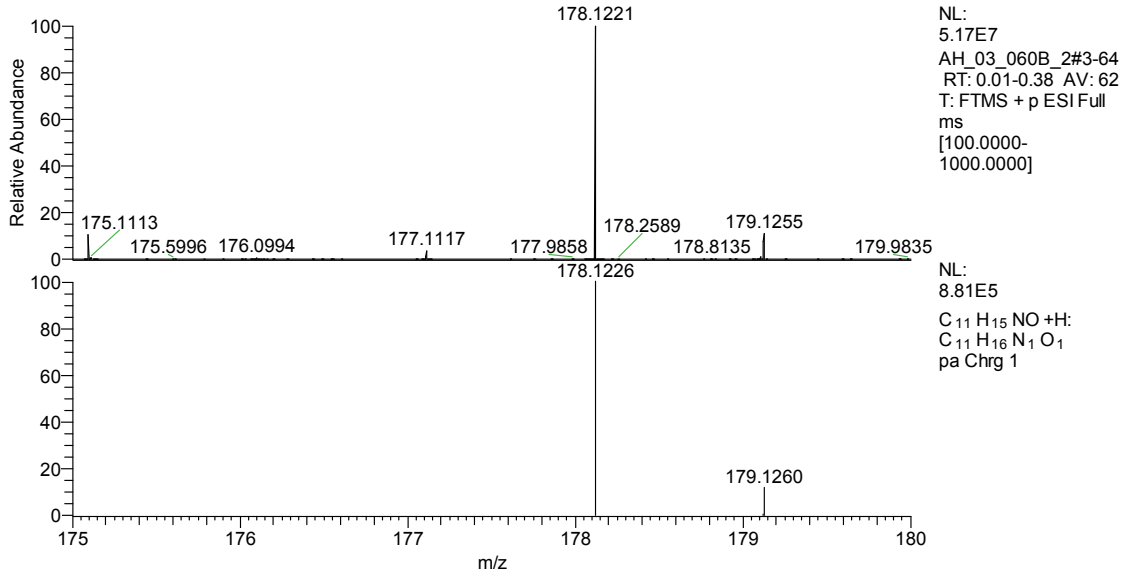

Figure 4.36: HRAM-MS of **5f** in water. (Top, experimental spectrum; bottom, calculated spectrum)

4.4.5 Procedure for the One-pot Amidation of Benzoic Acid to 5a

Note: Hydrogen fluoride (HF) is formed in this reaction. This is a toxic, poisonous, and corrosive compound and needs to be handled with extreme care.

On the bench-top, in a screw-cap vial equiped with an stir bar, benzoic acid (200 mg, 1.64 mmol, 1 equiv) was dissolved in benzene (10 mL) and triphenylphosphine (1.29 g, 4.91 mmol, 3 equiv) was added to the mixture. While the vial was cooled in an ice bath, *N*-bromosuccinimide (612 mg, 3.44 mmol, 2.1 equiv) was slowly added to the reaction mixture. After the addition of NBS the ice bath was removed and the mixture was stirred for 15 minutes. TBAF (1.28 g, 4.91 mmol, 3 equiv) was then added to the mixture and the reaction was stirred for a further 2 h. **3a** (616.89 mg, 1.77 mmol, 1.1 equiv) was slowly added to the mixture and the reaction mixture was stirred for 18 h. After this time, the vial was opened and benzene (10 mL) benzene was used to dilute the mixture. The solution was washed with aqueous sodium bicarbonate (3 × 10 mL), water (3 × 10 mL). The organic layer was dried over $MgSO_4$ and the benzene solution was passed through a silica column. The column was then washed with chloroform (25 mL). Chloroform was removal in vacuo to yield *N,N*- dimethylbenzamide (**5a**, 0.060 g, 50 %).

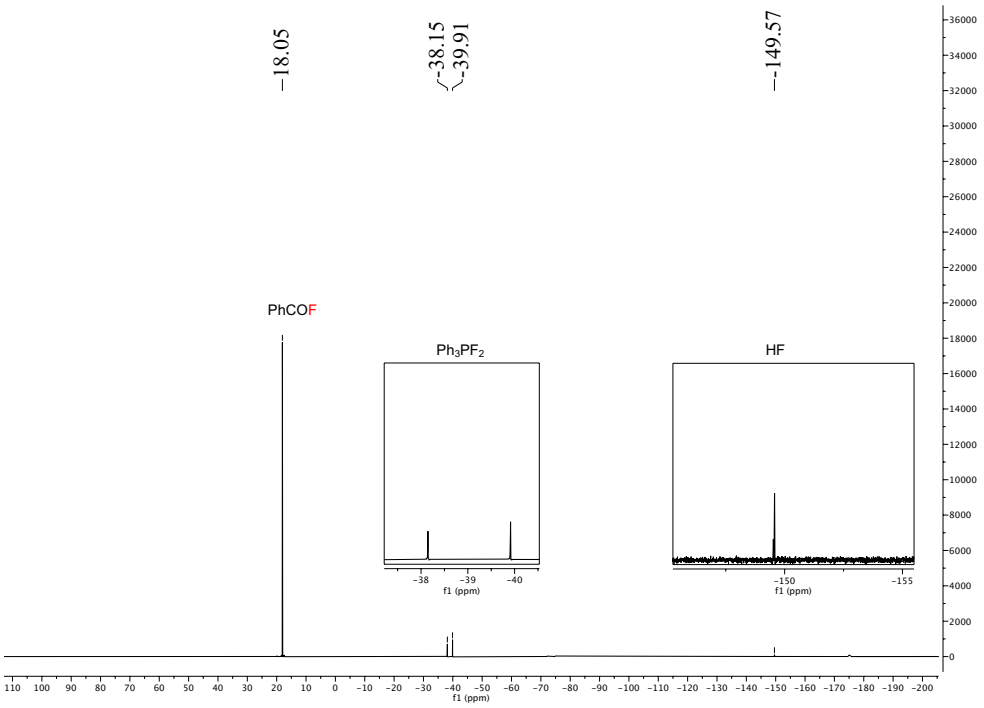

Figure 4.37: ^{19}F-NMR (376 MHz, C_6D_6) spectrum of the mixture after the addition of PPh_3/NBS and TBAF

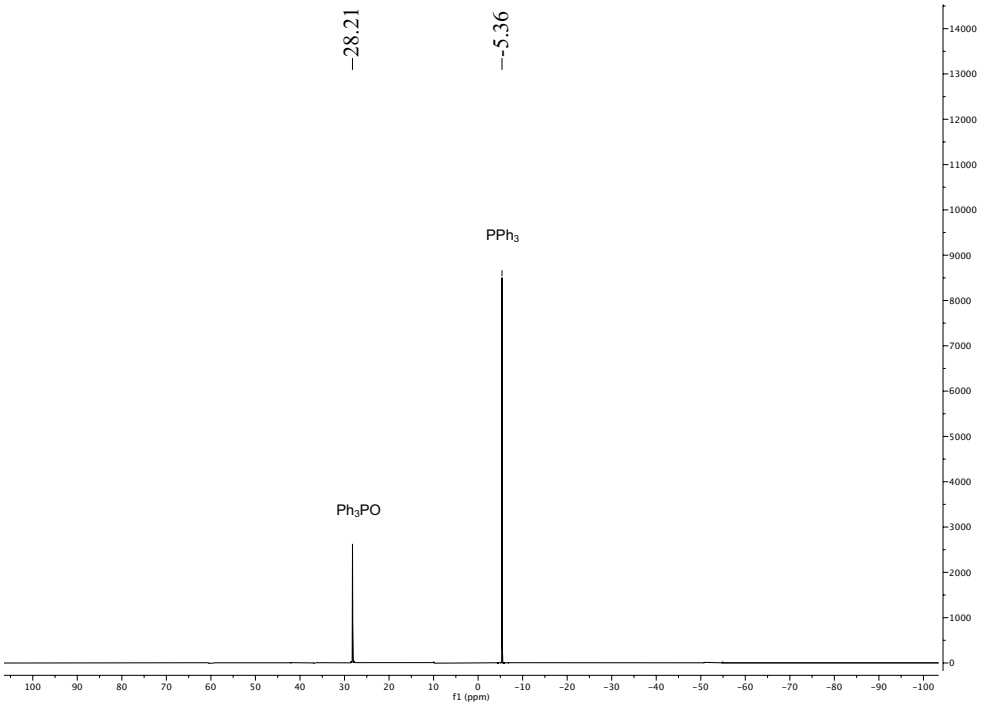

Figure 4.38: ^{31}P-NMR (162 MHz, C_6D_6) spectrum the mixture after the addition of PPh_3/NBS and TBAF

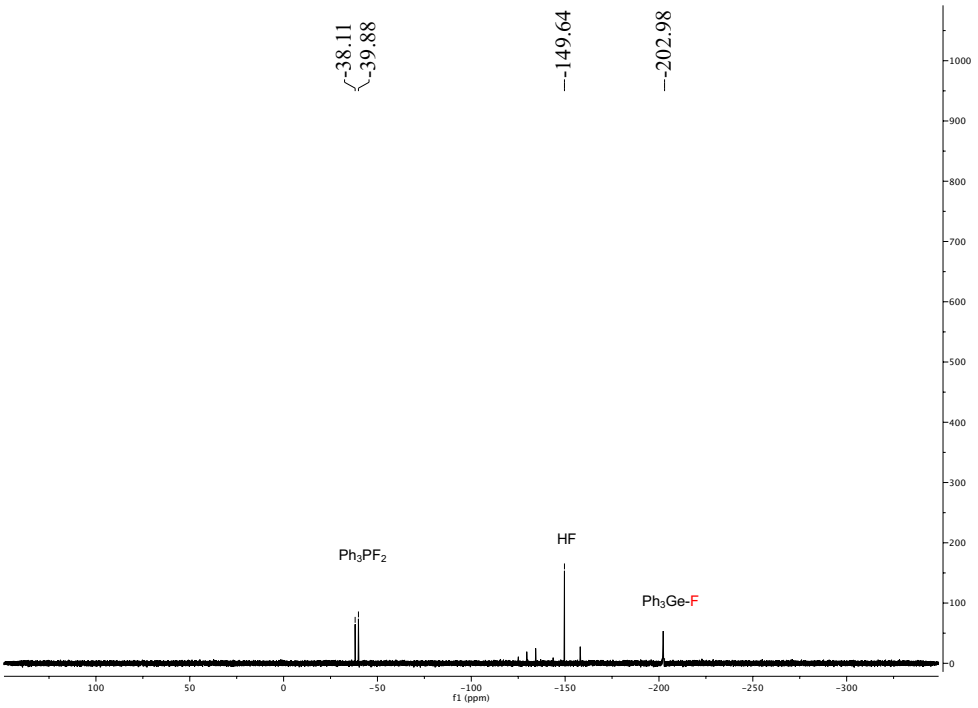

Figure 4.39: ^{19}F-NMR (376 MHz, C_6D_6) spectrum of the mixture after the addition **3a** to the mixture

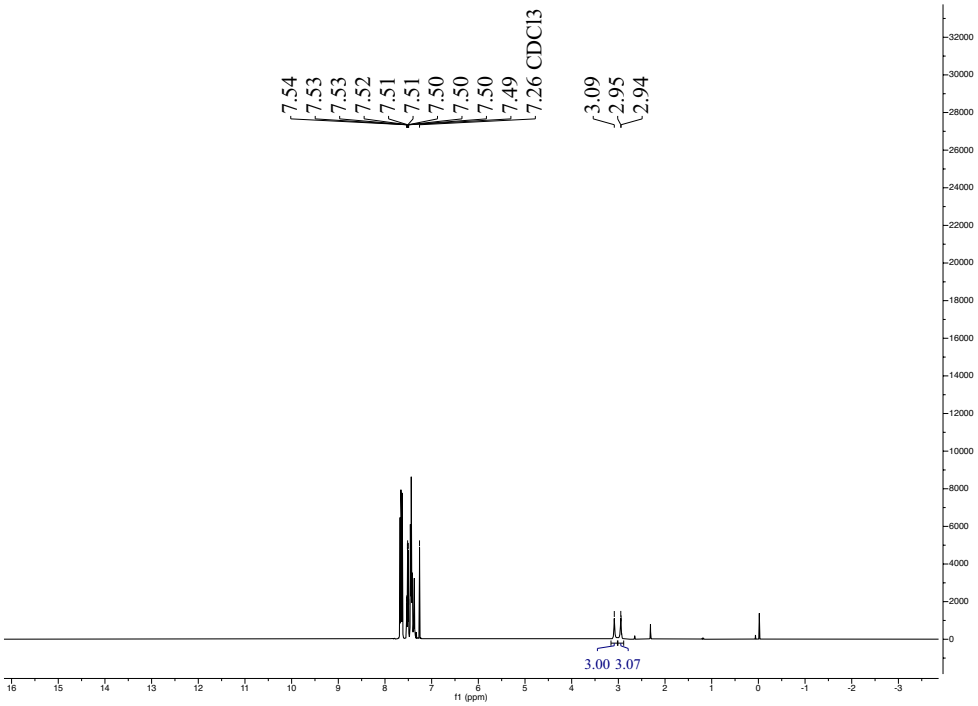

Figure 4.40: ^{1}H-NMR (400 MHz, $CDCl_3$) spectrum of the isolated **5a**

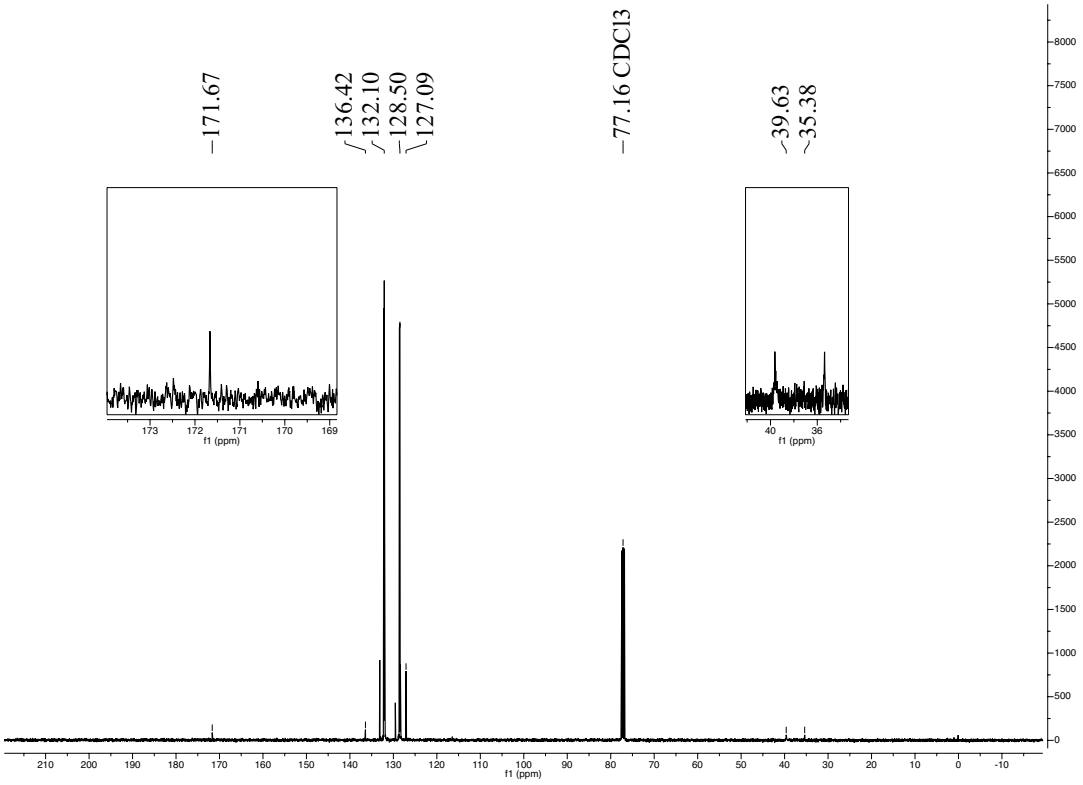

Figure 4.41: ^{13}C-NMR (101 MHz, $CDCl_3$) spectrum of the isolated **5a**

4.4.6 Experimental Investigation of The FIA of 3a

4.4.6.1 With TASF

In the glovebox, Ph_3GeNMe_2 (40 mg, 0.114 mmol, 1 equiv.) **3a** was dissolved in benzene in a screw-cap vial. TASF (31.66 mg, 0.114 mmol, 1 equiv.) was slowly added to the solution and the mixture was stirred for 1 hour. After that, an aliquot of the reaction was analyzed by ^{19}F-NMR spectroscopy.

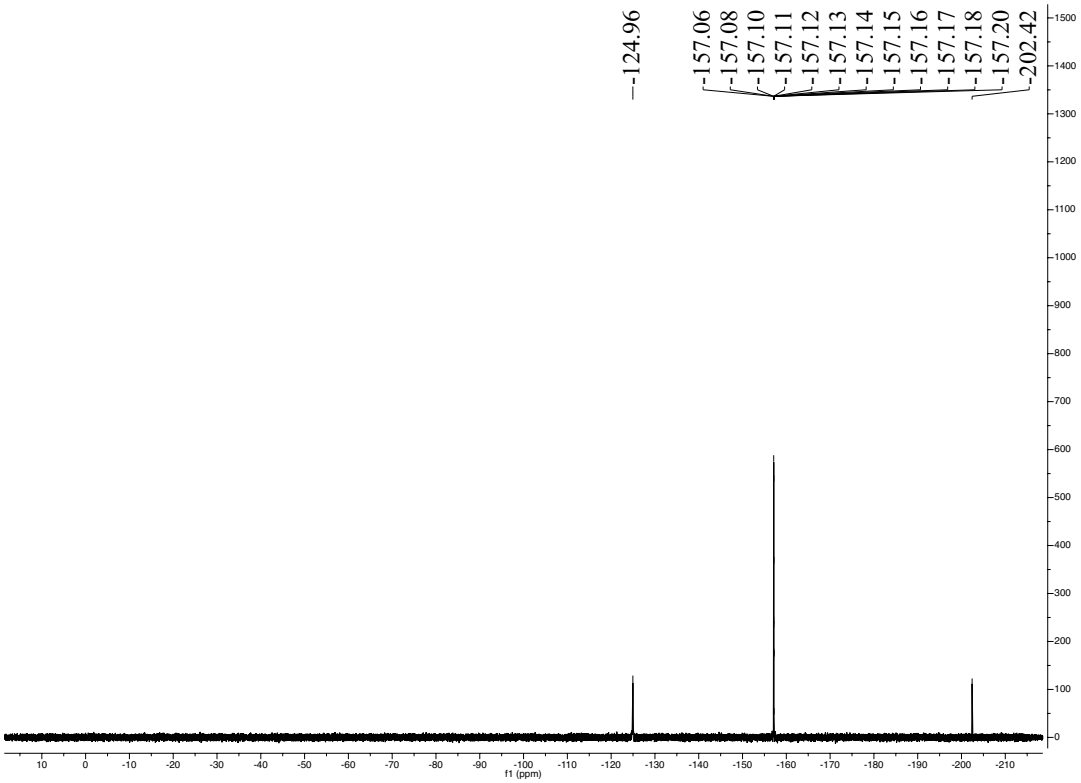

Figure 4.42: ^{19}F-NMR (376 MHz, C_6D_6) spectrum of the reaction of **3a** with TASF

4.4.6.2 With Excess Benzoyl Fluoride

In the glovebox, Ph_3GeNMe_2 (30 mg, 0.08 mmol, 1 equiv.) **3a** was dissolved in benzene in a screw-cap vial. Benzoyl fluoride (53.49 mg, 0.431 mmol, 5 equiv.) was slowly added to the solution and the mixture was stirred for 1 hour. After that, an aliquot of the reaction was analyzed by ^{19}F-NMR spectroscopy.

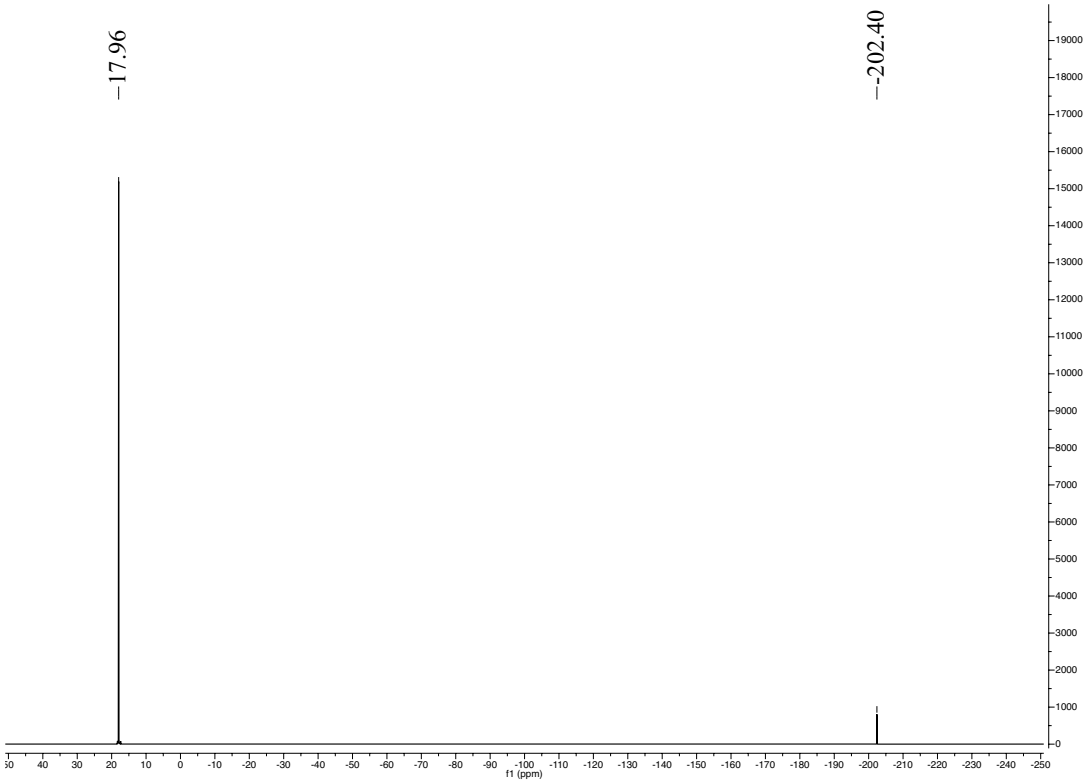

Figure 4.43: ^{19}F-NMR (376 MHz, C_6D_6) spectrum of the reaction of **3a** with excess benzoyl fluoride

4.4.7 The Procedure For The Kinetic Analysis

In an NMR tube with a septum, was placed 0.1 mL (0.161 M solution in benzene) of **3a**. To this solution 0.1 mL (0.161 M solution in benzene) of fluorobenzene was added as an internal standard. The initial concentration of benzoyl fluoride was determined by recording the ^{19}F-NMR spectrum. An equimolar amount of the benzoyl fluoride solution in benzene (0.1 mL, 0.161 M) was added to the NMR tube and spectra were recorded at the intervals of 140 seconds.

4.4.8 FIA Calculations Data

Table 4.6: FIA calculations data

	Electronic Energy (Hartree) (Def2-TZVPP/ D3(0))	Thermal Correction (Hartree) to Enthalpy	Enthalpy (Hartree) (298.15 K, 1 atm)	FIA (kJ/mol)
COF_2	-313.049	0.019	-313.031	-
$[COF_2]^-$	-412.987	0.021	-412.966	-
GeH_4	-2079.377	0.034	-2079.343	111
$GeMe_4$	-2236.661	0.158	-2236.503	107
$GePh_4$	-3003.630	0.384	-3003.246	188
$GeCl_4$	-3917.994	0.014	-3917.980	314
GeF_4	-2476.603	0.017	-2476.586	353
Ph_3GeNMe_2	-2906.559	0.377	-2906.181	210
$Ph_3GeN^iPr_2$	-3063.829	0.498	-3063.331	202
Ph_3GeNH_2	-2827.953	0.319	-2827.635	206
Ph_3GeNPh_2	-3290.068	0.489	-3289.579	217
$Ph_3GeN(SiMe_3)_2$	-3645.377	0.538	-3644.839	225

4.4.9 IRC Calculation of the Transition State

Table 4.7: Summary of reaction path following

Reaction Coordinate	Energy	Step
-1	-0.00002	-0.00092
Transition State	0.00000	0.00000
+1	-0.00028	0.01693

4.4.10 Cartesian Coordinates and Energies of Calculated Structures

Table 4.8: xyz coordinates for Ph_3GeNH_2

Electronic energy (B3LYP/cc-pVTZ) = -2828.3266201 Hartree
Thermal correction to enthalpy = 0.316581 Hartree
Thermal correction to Gibbs free energy = 0.247609 Hartree

N	0.01700	0.51500	2.49800
Ge	0.00600	0.10400	0.68600
C	-1.61200	0.95900	-0.00500
C	-2.21700	2.00000	0.70500
C	-3.35700	2.62800	0.21200
C	-3.90400	2.22500	-1.00200
C	-3.30900	1.19200	-1.72100
C	-2.17300	0.56400	-1.22300
C	1.67500	0.85800	-0.00300
C	2.33400	1.86700	0.70500
C	3.51000	2.42600	0.21500
C	4.03900	1.98600	-0.99400
C	3.39100	0.98500	-1.71000
C	2.21800	0.42500	-1.21500
C	-0.05700	-1.81000	0.23800
C	-1.28300	-2.47000	0.10400
C	-1.33400	-3.83200	-0.17600
C	-0.15600	-4.55700	-0.32700
C	1.07100	-3.91400	-0.19700
C	1.11800	-2.55200	0.08300
H	-0.81400	0.21500	2.99300
H	0.82400	0.16000	2.99600
H	-1.78800	2.31900	1.64700
H	-3.81600	3.43100	0.77300
H	-4.78900	2.71400	-1.38700
H	-3.73200	0.87600	-2.66600
H	-1.72400	-0.24600	-1.78500
H	1.91900	2.21400	1.64400
H	4.01200	3.20600	0.77500
H	4.95300	2.42200	-1.37600
H	3.80000	0.64000	-2.65100
H	1.72600	-0.36000	-1.77600
H	-2.20600	-1.91400	0.20900
H	-2.29200	-4.32700	-0.27800
H	-0.19400	-5.61500	-0.54700
H	1.99100	-4.47300	-0.31600
H	2.07900	-2.06100	0.17300

Table 4.9: xyz coordinates for $[Ph_3Ge(F)-NH_2]^-$

Electronic energy (M06-2X/Def2-TZVPP/D3(0)) = -2927.890 Hartree
Thermal correction to enthalpy = 0.321 Hartree

Ge	0.112	-0.283	0.997
N	-0.013	0.324	2.762
H	0.321	1.267	2.902
H	0.442	-0.308	3.405
C	1.854	-0.359	0.015
C	2.627	0.781	-0.205
C	3.847	0.717	-0.87
C	4.311	-0.501	-1.352
C	3.554	-1.649	-1.15
C	2.347	-1.575	-0.463
H	1.775	-2.475	-0.271
H	3.91	-2.603	-1.521
H	5.255	-0.555	-1.881
H	4.431	1.618	-1.02
H	2.258	1.74	0.139
C	-1.407	-1.179	0.037
C	-1.377	-2.557	-0.206
C	-2.389	-3.194	-0.915
C	-3.477	-2.469	-1.386
C	-3.536	-1.103	-1.145
C	-2.508	-0.47	-0.453
H	-2.568	0.599	-0.295
H	-4.38	-0.524	-1.501
H	-4.271	-2.964	-1.933
H	-2.333	-4.262	-1.095
H	-0.55	-3.133	0.187
C	-0.393	1.604	0.246
C	-0.186	1.883	-1.109
C	-0.627	3.059	-1.703
C	-1.302	4.009	-0.942
C	-1.53	3.76	0.405
C	-1.082	2.572	0.98
H	-1.303	2.38	2.025
H	-2.065	4.487	1.005
H	-1.651	4.929	-1.396
H	-0.449	3.237	-2.757
H	0.332	1.149	-1.719
F	0.553	-1.974	1.755

Table 4.10: xyz coordinates for Ph_3GeN^iPr

Electronic energy (B3LYP/cc-pVTZ) = -3064.3020135 Hartree
Thermal correction to enthalpy = 0.493556 Hartree
Thermal correction to Gibbs free energy = 0.408673 Hartree

C	-2.627	-0.177	-2.678	H	-4.714	-0.009	1.667
C	-1.134	-0.532	-2.61	H	-2.74	0.853	0.474
N	-0.339	0.348	-1.741	H	0.76	2.095	-1.67
Ge	0.07	-0.084	0.017	H	-0.863	1.695	-4.21
C	1.602	-1.312	0.04	H	0.842	1.261	-4.009
C	2.328	-1.545	-1.129	H	0.327	2.951	-3.864
C	3.467	-2.344	-1.117	H	-2.219	2.505	-2.14
C	3.898	-2.922	0.073	H	-0.987	3.741	-1.862
C	3.192	-2.69	1.249	H	-1.398	2.606	-0.575
C	2.057	-1.885	1.232	H	-1.452	-2.219	-1.269
C	0.67	1.54	0.946	H	0.06	-2.305	-2.185
C	-0.154	2.225	1.841	H	-1.488	-2.619	-2.983
C	0.297	3.369	2.493	H	3.528	-3.131	2.179
C	1.583	3.844	2.259	H	1.529	-1.698	2.159
C	2.42	3.165	1.378	H	-1.154	1.861	2.039
C	1.966	2.02	0.733	H	-0.355	3.888	3.185
C	-1.482	-0.821	0.966	H	1.934	4.733	2.765
C	-1.439	-2.055	1.62	H	3.425	3.523	1.2
C	-2.557	-2.548	2.287	H	2.63	1.49	0.061
C	-3.737	-1.812	2.309	H	-2.507	-3.508	2.785
C	-3.796	-0.583	1.659	H	-4.606	-2.196	2.826
C	-2.677	-0.096	0.993				
C	-0.162	1.755	-2.145				
C	0.048	1.918	-3.651				
C	-1.266	2.705	-1.653				
C	-0.986	-2.007	-2.232				
H	-2.786	0.809	-3.11				
H	-3.065	-0.196	-1.679				
H	-3.155	-0.904	-3.301				
H	-0.732	-0.434	-3.623				
H	1.99	-1.093	-2.053				
H	4.018	-2.514	-2.033				
H	4.782	-3.546	0.085				

Table 4.11: xyz coordinates for $[Ph_3Ge(F)-N^iPr_2]^-$

Electronic energy (M06-2X/Def2-TZVPP/D3(0)) = -3163.763 Hartree

Thermal correction to enthalpy = 0.499 Hartree

Ge	-0.069	-0.234	-0.257	C	-4.451	1.294	-1.603
N	0.206	-1.63	0.981	C	-3.959	1.613	-0.345
C	1.358	-2.485	0.721	C	-2.691	1.187	0.036
C	2.108	-2.745	2.028	H	-2.318	1.466	1.013
H	2.992	-3.367	1.86	H	-4.56	2.198	0.342
H	2.413	-1.795	2.471	H	-5.436	1.627	-1.906
H	1.457	-3.263	2.739	H	-4.04	0.285	-3.452
C	1.052	-3.805	0.012	H	-1.819	-0.519	-2.729
H	1.98	-4.357	-0.157	C	0.198	1.263	1.17
H	0.395	-4.426	0.629	C	0.045	2.605	0.808
H	0.564	-3.6	-0.939	C	0.384	3.646	1.663
H	2.034	-1.926	0.066	C	0.897	3.365	2.926
C	-0.949	-2.288	1.568	C	1.064	2.042	3.311
H	-0.588	-3.144	2.151	C	0.719	1.012	2.438
C	-1.657	-1.34	2.533	H	0.871	-0.021	2.728
H	-0.992	-1.041	3.344	H	1.47	1.813	4.29
H	-1.963	-0.437	2.002	H	1.166	4.171	3.598
H	-2.552	-1.811	2.948	H	0.255	4.675	1.348
C	-1.967	-2.817	0.548	H	-0.347	2.839	-0.179
H	-1.482	-3.415	-0.219	F	-0.267	-1.593	-1.615
H	-2.735	-3.41	1.057				
H	-2.454	-1.98	0.043				
C	1.565	0.344	-1.257				
C	2.647	0.943	-0.607				
C	3.793	1.32	-1.298				
C	3.869	1.133	-2.672				
C	2.8	0.551	-3.341				
C	1.671	0.149	-2.637				
H	0.858	-0.345	-3.153				
H	2.849	0.4	-4.414				
H	4.755	1.436	-3.217				
H	4.622	1.77	-0.765				
H	2.593	1.125	0.461				
C	-1.889	0.418	-0.81				
C	-2.409	0.103	-2.07				
C	-3.667	0.541	-2.467				

Table 4.12: xyz coordinates for Ph_3GeNMe_2

Electronic energy (B3LYP/cc-pVTZ) = -2906.9678599 Hartree
Thermal correction to enthalpy = 0.376362 Hartree
Thermal correction to Gibbs free energy = 0.299628 Hartree

C	0.701	0.791	3.057	H	3.238	-1.798	-3.014
N	-0.206	-0.008	2.256	H	1.425	-0.354	-2.213
Ge	-0.05	-0.014	0.414	H	-0.996	-1.913	-1.801
C	1.408	-1.168	-0.216	H	-3.197	-2.593	-2.64
C	2.021	-2.088	0.635	H	-5.259	-1.721	-1.587
C	3.057	-2.898	0.183	H	-5.097	-0.159	0.327
C	3.495	-2.8	-1.132	H	-2.893	0.525	1.179
C	2.897	-1.884	-1.991	H	-1.713	2.38	-0.503
C	1.865	-1.074	-1.534	H	-1.19	4.664	-1.213
C	-1.779	-0.624	-0.26	H	1.16	5.432	-1.321
C	-1.885	-1.511	-1.333	H	2.99	3.879	-0.708
C	-3.131	-1.903	-1.809	H	2.479	1.589	0.002
C	-4.29	-1.415	-1.217	H	-1.31	-0.889	3.815
C	-4.199	-0.536	-0.143	H	0.066	-1.866	3.291
C	-2.952	-0.146	0.331	H	-1.375	-1.752	2.28
C	0.342	1.81	-0.181				
C	-0.679	2.695	-0.533				
C	-0.387	3.992	-0.941				
C	0.933	4.423	-1.003				
C	1.96	3.551	-0.659				
C	1.665	2.255	-0.254				
C	-0.721	-1.181	2.938				
H	0.936	1.726	2.55				
H	1.653	0.287	3.287				
H	0.231	1.048	4.012				
H	1.701	-2.178	1.664				
H	3.522	-3.605	0.857				
H	4.3	-3.429	-1.485				

Table 4.13: xyz coordinates for $[Ph_3Ge(F)-NMe_2]^-$

Electronic energy (M06-2X/Def2-TZVPP/D3(0)) = -3006.498 Hartree

Thermal correction to enthalpy = 0.381 Hartree

C	-0.692	-0.679	-2.747	C	-4.787	-0.71	0.21
N	0.087	0.072	-1.804	C	-3.973	-1.463	1.048
Ge	-0.021	-0.088	0.177	C	-2.595	-1.283	1.029
C	1.3	-1.599	0.305	H	-1.968	-1.838	1.716
C	1.642	-2.357	-0.816	H	-4.416	-2.184	1.726
C	2.558	-3.402	-0.743	H	-5.863	-0.841	0.23
C	3.174	-3.703	0.463	H	-4.837	0.816	-1.299
C	2.854	-2.959	1.591	H	-2.383	1.076	-1.37
C	1.923	-1.93	1.512	C	1.301	0.533	-2.416
H	1.652	-1.375	2.4	H	1.108	1.257	-3.229
H	3.328	-3.186	2.54	H	1.889	-0.288	-2.868
H	3.894	-4.511	0.524	H	1.949	1.029	-1.691
H	2.792	-3.978	-1.632	H	-1.523	-1.195	-2.263
H	1.181	-2.128	-1.768	H	-0.096	-1.448	-3.276
C	0.604	1.792	0.461	H	-1.121	-0.039	-3.54
C	1.284	2.144	1.628	F	-0.161	-0.221	2.086
C	1.696	3.45	1.863				
C	1.41	4.448	0.94				
C	0.718	4.124	-0.219				
C	0.332	2.809	-0.455				
H	-0.182	2.556	-1.376				
H	0.483	4.896	-0.944				
H	1.719	5.471	1.125				
H	2.231	3.693	2.774				
H	1.469	1.378	2.37				
C	-1.994	-0.375	0.156				
C	-2.829	0.37	-0.677				
C	-4.21	0.217	-0.648				

Table 4.14: xyz coordinates for Ph_3GeNPh_2

Electronic energy (B3LYP/cc-pVTZ) = -3290.6036593 Hartree
Thermal correction to enthalpy = 0.488011 Hartree
Thermal correction to Gibbs free energy = 0.396819 Hartree

C	-1.697	-1.22	-0.602	C	-4.057	-1.572	-0.182
Ge	0.071	-0.628	0.009	C	-4.225	-2.05	-1.477
C	0.309	-1.194	1.878	C	-3.133	-2.12	-2.334
C	0.011	-2.51	2.246	C	-1.878	-1.709	-1.897
C	0.161	-2.935	3.561	H	-0.356	-3.211	1.506
C	0.606	-2.045	4.532	H	-0.074	-3.957	3.828
C	0.897	-0.732	4.183	H	0.721	-2.373	5.557
C	0.75	-0.311	2.866	H	1.239	-0.034	4.936
C	1.462	-1.332	-1.186	H	0.983	0.714	2.611
C	2.186	-2.478	-0.856	H	2.018	-2.974	0.092
C	3.141	-2.991	-1.728	H	3.696	-3.88	-1.456
C	3.385	-2.361	-2.942	H	4.13	-2.758	-3.619
C	2.674	-1.216	-3.281				
C	1.72	-0.706	-2.408				
N	0.102	1.258	-0.096				
C	-1.165	1.924	-0.121				
C	-1.725	2.413	1.059				
C	-2.97	3.026	1.047				
C	-3.673	3.156	-0.146				
C	-3.12	2.673	-1.326				
C	-1.871	2.065	-1.314				
C	1.263	2.044	-0.022				
C	2.506	1.486	0.321				
C	3.652	2.265	0.369				
C	3.605	3.625	0.089				
C	2.38	4.191	-0.243				
C	1.227	3.421	-0.303				
C	-2.802	-1.164	0.252				

Table 4.15: xyz coordinates for $[Ph_3Ge(F)-NPh_2]^-$

Electronic energy (M06-2X/Def2-TZVPP/D3(0)) = -3390.010 Hartree

Thermal correction to enthalpy = 0.493 Hartree

Ge	0.288	-0.506	-0.411	H	4.041	-2.717	-3.107
C	-1.165	-1.865	-0.253	H	5.811	-2.396	-1.403
C	-2.101	-1.81	0.78	H	5.26	-1.238	0.719
C	-3.151	-2.716	0.853	H	2.981	-0.451	1.14
C	-3.27	-3.72	-0.098	N	-0.422	1.314	-0.548
C	-2.344	-3.797	-1.13	C	-1.833	1.381	-0.548
C	-1.313	-2.868	-1.212	C	-2.523	2.002	0.497
H	-0.621	-2.903	-2.044	C	-3.909	2.001	0.531
H	-2.433	-4.575	-1.88	C	-4.634	1.367	-0.471
H	-4.083	-4.434	-0.04	C	-3.956	0.744	-1.509
H	-3.877	-2.637	1.654	C	-2.569	0.755	-1.556
H	-2.016	-1.038	1.537	H	-2.023	0.256	-2.347
C	0.534	-0.332	1.652	H	-4.508	0.238	-2.291
C	0.783	-1.515	2.359	H	-5.717	1.353	-0.437
C	0.929	-1.54	3.738	H	-4.424	2.481	1.355
C	0.829	-0.359	4.467	H	-1.955	2.479	1.287
C	0.583	0.829	3.796	C	0.321	2.468	-0.541
C	0.437	0.834	2.409	C	1.718	2.42	-0.355
H	0.253	1.782	1.916	C	2.485	3.569	-0.349
H	0.505	1.758	4.35	C	1.911	4.823	-0.527
H	0.941	-0.369	5.545	C	0.538	4.887	-0.726
H	1.118	-2.478	4.248	C	-0.246	3.745	-0.737
H	0.863	-2.451	1.811	H	-1.308	3.834	-0.915
C	2.183	-1.112	-0.744	H	0.06	5.848	-0.885
C	3.199	-0.945	0.2	H	2.516	5.72	-0.519
C	4.494	-1.392	-0.032	H	3.555	3.479	-0.2
C	4.804	-2.039	-1.22	H	2.205	1.465	-0.216
C	3.81	-2.219	-2.173	F	0.046	-0.581	-2.283
C	2.522	-1.752	-1.94				
H	1.762	-1.863	-2.702				

Table 4.16: xyz coordinates for $Ph_3GeN(SiMe_3)_2$

Electronic energy (B3LYP/cc-pVTZ) = -3645.9211497 Hartree
Thermal correction to enthalpy = 0.534600 Hartree
Thermal correction to Gibbs free energy = 0.435890 Hartree

C	-2.886	-1.066	0.83	H	-2.212	-1.274	1.662
Si	-2.636	0.656	0.1	H	1.146	2.877	1.188
N	-0.945	0.976	-0.288	H	-0.438	3.551	1.577
Si	-0.421	2.598	-0.73	H	0.679	4.453	0.543
C	0.31	3.453	0.786	H	1.859	2.416	-1.81
C	0.841	2.625	-2.133	H	0.824	3.623	-2.584
C	-1.871	3.626	-1.379	H	0.583	1.906	-2.914
Ge	0.302	-0.375	0.047	H	-2.75	3.642	-0.737
C	0.479	-0.647	1.979	H	-2.18	3.273	-2.365
C	1.303	-1.656	2.486	H	-1.522	4.657	-1.495
C	1.461	-1.827	3.858	H	1.839	-2.309	1.808
C	0.804	-0.979	4.744	H	2.098	-2.616	4.234
C	-0.004	0.042	4.253	H	0.927	-1.108	5.811
C	-0.163	0.204	2.88	H	-0.508	0.712	4.938
C	-0.296	-1.969	-0.918	H	-0.786	1.002	2.503
C	-0.828	-1.819	-2.201	H	-0.924	-0.828	-2.626
C	-1.262	-2.923	-2.927	H	-1.676	-2.79	-3.918
C	-1.17	-4.197	-2.375	H	-1.511	-5.058	-2.935
C	-0.643	-4.36	-1.097	H	-0.576	-5.348	-0.661
C	-0.208	-3.252	-0.376	H	0.181	-3.391	0.625
C	2.087	0.095	-0.606	H	2.652	1.128	1.192
C	2.958	0.837	0.195	H	4.875	1.79	0.357
C	4.214	1.207	-0.272	H	5.596	1.113	-1.914
C	4.62	0.825	-1.547	H	4.091	-0.246	-3.332
C	3.773	0.062	-2.345	H	1.861	-0.892	-2.502
C	2.515	-0.301	-1.874	H	-3.351	0.055	-2.198
C	-3.718	0.756	-1.443	H	-3.742	1.752	-1.885
C	-3.258	1.875	1.411	H	-4.745	0.471	-1.197
H	-2.768	-1.856	0.089	H	-2.912	1.571	2.402
H	-3.91	-1.112	1.215	H	-4.352	1.881	1.435
				H	-2.924	2.899	1.245

Table 4.17: xyz coordinates for $[Ph_3Ge(F)-N(SiMe_3)_2]^-$

Electronic energy (M06-2X/Def2-TZVPP/D3(0)) = -3745.318 Hartree

Thermal correction to enthalpy = 0.537 Hartree

C	-3.082	-0.65	0.23	C	-0.885	1.828	-0.978
Si	-1.856	-0.316	1.627	C	-0.826	2.739	0.076
N	-0.22	-0.064	1.147	C	-1.465	3.973	0.009
Si	0.978	-0.018	2.372	C	-2.211	4.309	-1.111
C	1.742	-1.712	2.73	C	-2.289	3.414	-2.17
H	2.271	-2.108	1.861	C	-1.616	2.2	-2.11
H	0.97	-2.433	3.016	H	-1.638	1.529	-2.958
H	2.459	-1.64	3.552	H	-2.865	3.668	-3.052
C	2.414	1.18	2.116	H	-2.725	5.262	-1.161
H	3.216	0.779	1.496	H	-1.392	4.664	0.841
H	2.829	1.413	3.101	H	-0.286	2.47	0.976
H	2.083	2.117	1.662	C	2.071	0.212	-0.873
C	0.317	0.569	4.058	C	2.862	-0.91	-0.636
H	-0.584	0.07	4.413	C	4.249	-0.826	-0.633
H	0.114	1.643	4.03	C	4.871	0.39	-0.881
H	1.106	0.406	4.798	C	4.097	1.512	-1.153
Ge	0.103	0.09	-0.933	C	2.712	1.417	-1.155
C	-0.541	-1.775	-1.236	H	2.117	2.298	-1.375
C	-1.173	-2.124	-2.431	H	4.576	2.462	-1.36
C	-1.643	-3.413	-2.648	H	5.952	0.462	-0.872
C	-1.456	-4.398	-1.686	H	4.845	-1.71	-0.437
C	-0.794	-4.081	-0.509	H	2.389	-1.87	-0.454
C	-0.353	-2.781	-0.287	C	-2.644	1.159	2.517
H	0.126	-2.537	0.654	H	-2.845	1.954	1.795
H	-0.631	-4.842	0.246	H	-2.033	1.578	3.316
H	-1.819	-5.405	-1.856	H	-3.602	0.852	2.948
H	-2.152	-3.652	-3.575	C	-2.053	-1.826	2.759
H	-1.287	-1.37	-3.198	H	-1.817	-2.735	2.199
				H	-3.09	-1.905	3.097
				H	-1.413	-1.801	3.642
				H	-3.002	0.063	-0.593
				H	-4.082	-0.541	0.661
				H	-2.995	-1.657	-0.179
				F	0.214	0.257	-2.819

Table 4.18: xyz coordinates for I_1_trans

Electronic energy (B3LYP/cc-pVTZ) = -3006.9232602 Hartree
Thermal correction to enthalpy = 0.376228 Hartree
Thermal correction to Gibbs free energy = 0.300258 Hartree

Ge	0.013	0	-0.155	H	3.474	-3.377	1.5
N	-0.052	0	1.885	H	3.202	-4.947	-0.402
C	-0.642	1.173	2.492	H	1.569	-4.427	-2.194
H	-0.235	2.086	2.054	H	0.256	-2.325	-2.098
H	-0.437	1.2	3.576	C	-1.969	0.005	-0.264
H	-1.744	1.213	2.379	C	-2.696	-1.189	-0.268
C	-0.648	-1.17	2.491	C	-4.088	-1.191	-0.283
H	-0.247	-2.085	2.052	C	-4.789	0.011	-0.29
H	-1.75	-1.204	2.378	C	-4.083	1.21	-0.281
H	-0.443	-1.199	3.575	C	-2.69	1.202	-0.266
C	1.066	1.69	-0.222	H	-2.157	2.145	-0.26
C	1.991	1.998	0.78	H	-4.617	2.154	-0.286
C	2.771	3.15	0.715	H	-5.873	0.014	-0.302
C	2.626	4.031	-0.352	H	-4.627	-2.132	-0.289
C	1.707	3.741	-1.357	H	-2.166	-2.135	-0.263
C	0.947	2.576	-1.297	F	-0.015	-0.001	-2.099
H	0.269	2.322	-2.1				
H	1.592	4.418	-2.196				
H	3.226	4.932	-0.403				
H	3.487	3.363	1.501				
H	2.076	1.327	1.625				
C	1.058	-1.695	-0.222				
C	0.933	-2.581	-1.296				
C	1.688	-3.75	-1.355				
C	2.606	-4.043	-0.351				
C	2.757	-3.162	0.715				
C	1.983	-2.007	0.779				
H	2.072	-1.335	1.624				

Table 4.19: xyz coordinates for I_1_cis

Electronic energy (B3LYP/cc-pVTZ) = -3006.8512808 Hartree
Thermal correction to enthalpy = 0.377136 Hartree
Thermal correction to Gibbs free energy = 0.300880 Hartree

Ge	-0.023	-0.388	0.57	H	1.356	-2.975	-0.293
N	-0.005	0.113	2.403	H	3.487	-3.587	-1.394
C	0.44	-0.85	3.389	H	5.147	-1.826	-1.947
H	-0.32	-1.614	3.619	H	4.629	0.544	-1.418
H	0.693	-0.325	4.323	H	2.48	1.14	-0.399
H	1.324	-1.377	3.031	C	-1.775	-0.725	-0.368
C	-1.188	0.808	2.859	C	-2.065	-1.963	-0.951
H	-1.5	1.554	2.126	C	-3.281	-2.198	-1.588
H	-0.982	1.335	3.805	C	-4.255	-1.204	-1.627
H	-2.045	0.134	3.043	C	-3.995	0.028	-1.035
F	-0.151	-2.258	1.123	C	-2.763	0.262	-0.427
C	0.075	1.622	-0.053	H	-2.562	1.236	-0.001
C	0.566	2.648	0.763	H	-4.746	0.809	-1.053
C	0.75	3.947	0.29	H	-5.207	-1.388	-2.112
C	0.45	4.257	-1.033	H	-3.475	-3.163	-2.043
C	-0.034	3.255	-1.87	H	-1.332	-2.753	-0.876
C	-0.216	1.965	-1.379				
H	-0.598	1.202	-2.048				
H	-0.27	3.48	-2.905				
H	0.594	5.264	-1.408				
H	1.132	4.717	0.952				
H	0.816	2.408	1.789				
C	1.741	-0.874	-0.278				
C	2.692	0.1	-0.603				
C	3.911	-0.236	-1.188				
C	4.203	-1.562	-1.483				
C	3.271	-2.548	-1.173				
C	2.063	-2.207	-0.57				

Table 4.20: xyz coordinates for I_2

Electronic energy (B3LYP/cc-pVTZ) = -2772.0387109 Hartree
Thermal correction to enthalpy = 0.290462 Hartree
Thermal correction to Gibbs free energy = 0.227236 Hartree

Ge	-0.001	0	-0.002	C	-2.371	1.558	-0.467
C	0.649	-1.783	-0.001	H	-1.697	2.318	-0.839
C	-0.163	-2.832	-0.467	H	-4.124	2.731	-0.838
C	0.318	-4.132	-0.468	H	-5.676	1	0.002
C	1.603	-4.398	0.003	H	-4.808	-1.158	0.84
C	2.414	-3.366	0.472	H	-2.385	-1.598	0.838
C	1.945	-2.061	0.466				
H	2.576	-1.264	0.836				
H	3.407	-3.582	0.84				
H	1.973	-5.413	0.005				
H	-0.302	-4.937	-0.835				
H	-1.158	-2.629	-0.839				
C	1.22	1.454	-0.002				
C	0.815	2.715	0.468				
C	1.713	3.772	0.474				
C	3.01	3.584	0.002				
C	3.419	2.34	-0.472				
C	2.533	1.274	-0.47				
H	2.853	0.31	-0.843				
H	4.426	2.204	-0.84				
H	3.706	4.412	0.004				
H	1.405	4.74	0.845				
H	-0.189	2.864	0.841				
C	-1.87	0.33	0				
C	-2.76	-0.653	0.467				
C	-4.124	-0.406	0.471				
C	-4.611	0.812	0.001				
C	-3.738	1.791	-0.47				

Table 4.21: xyz coordinates for Ph_3GeF

Electronic energy (B3LYP/cc-pVTZ) = -2872.2539408 Hartree
Thermal correction to enthalpy = 0.292980 Hartree
Thermal correction to Gibbs free energy = 0.225926 Hartree

Ge	0	0	0.615	C	-3.932	-2.296	-0.712
F	0	0	2.38	C	-3.025	-2.906	0.151
C	0	1.87	0.08	C	-1.876	-2.23	0.543
C	-0.993	2.74	0.543	H	-1.178	-2.71	1.217
C	-1.004	4.073	0.151	H	-3.216	-3.906	0.518
C	-0.022	4.553	-0.712	H	-4.826	-2.822	-1.017
C	0.97	3.698	-1.18	H	-4.391	-0.532	-1.849
C	0.98	2.363	-0.785	H	-2.354	0.67	-1.149
H	1.757	1.703	-1.149				
H	1.735	4.069	-1.849				
H	-0.031	5.591	-1.017				
H	-1.775	4.738	0.518				
H	-1.758	2.376	1.217				
C	1.619	-0.935	0.08				
C	1.557	-2.03	-0.785				
C	2.718	-2.689	-1.18				
C	3.954	-2.257	-0.712				
C	4.029	-1.167	0.151				
C	2.869	-0.51	0.543				
H	2.936	0.335	1.217				
H	4.991	-0.832	0.518				
H	4.857	-2.769	-1.017				
H	2.656	-3.537	-1.849				
H	0.596	-2.374	-1.149				
C	-1.619	-0.935	0.08				
C	-2.537	-0.333	-0.785				
C	-3.687	-1.009	-1.18				

Table 4.22: xyz coordinates for PhCOF

Electronic energy (B3LYP/cc-pVTZ) = -445.011398 Hartree
Thermal correction to enthalpy = 0.110357 Hartree
Thermal correction to Gibbs free energy = 0.070515 Hartree

C	-1.704	0.139	0
F	-2.305	-1.085	0
C	-0.232	0.04	0
C	0.501	1.231	0
C	1.887	1.189	0
C	2.545	-0.039	0
C	1.818	-1.225	0
C	0.43	-1.19	0
H	-0.143	-2.105	0
H	2.332	-2.176	0
H	3.627	-0.071	0
H	2.455	2.109	0
H	-0.031	2.171	0
O	-2.37	1.121	0

Table 4.23: xyz coordinates for $PhCONMe_2$

Electronic energy (B3LYP/cc-pVTZ) = -479.7379706 Hartree
Thermal correction to enthalpy = 0.194639 Hartree
Thermal correction to Gibbs free energy = 0.146513 Hartree

C	3.353	0.04	-0.173
N	1.962	-0.31	0.07
C	1.759	-1.496	0.885
H	0.721	-1.59	1.181
H	2.054	-2.399	0.344
H	2.369	-1.434	1.792
C	1.001	0.629	-0.206
C	-0.446	0.234	-0.083
C	-1.32	1.129	0.534
C	-2.678	0.852	0.6
C	-3.183	-0.308	0.021
C	-2.322	-1.191	-0.621
C	-0.959	-0.925	-0.666
H	-0.294	-1.611	-1.175
H	-2.711	-2.084	-1.091
H	-4.243	-0.518	0.061
H	-3.346	1.546	1.092
H	-0.924	2.046	0.948
O	1.286	1.757	-0.585
H	3.85	0.36	0.748
H	3.882	-0.831	-0.564
H	3.396	0.852	-0.89

Table 4.24: xyz coordinates for TS

Electronic energy (B3LYP/cc-pVTZ) = -3351.9491717 Hartree
Thermal correction to enthalpy = 0.485718 Hartree
Thermal correction to Gibbs free energy = 0.401086 Hartree

Ph_3GeNMe_2							
Ge	-0.658	0.019	0.051	H	-2.636	-4.91	2.469
N	0.677	-0.318	-1.321	H	-3.407	-4.221	0.208
C	1.261	0.937	-1.917	H	-2.607	-2.097	-0.771
H	0.501	1.425	-2.537	C	-0.27	1.629	1.072
H	2.124	0.668	-2.532	C	0.622	1.626	2.158
H	1.576	1.616	-1.133	C	0.874	2.785	2.892
C	0.149	-1.19	-2.431	C	0.258	3.986	2.532
H	0.072	-2.199	-2.03	C	-0.603	4.017	1.433
H	0.863	-1.195	-3.26	C	-0.866	2.847	0.718
H	-0.818	-0.818	-2.776	H	-1.55	2.88	-0.12
C	-2.258	0.589	-0.966	H	-1.077	4.946	1.138
C	-2.288	1.18	-2.233	H	0.454	4.89	3.098
C	-3.481	1.617	-2.816	H	1.558	2.753	3.733
C	-4.688	1.454	-2.137	H	1.15	0.71	2.386
C	-4.688	0.861	-0.871	PhCOF			
C	-3.49	0.44	-0.298	F	1.235	-0.633	0.986
H	-3.506	-0.015	0.687	C	1.846	-1.293	-0.452
H	-5.618	0.727	-0.33	C	3.213	-0.688	-0.463
H	-5.618	1.787	-2.584	C	4.171	-1.369	-1.217
H	-3.462	2.084	-3.795	C	5.457	-0.847	-1.352
H	-1.362	1.331	-2.783	C	5.786	0.359	-0.728
C	-1.316	-1.607	0.873	C	4.836	1.021	0.057
C	-2.235	-2.415	0.197	C	3.55	0.5	0.194
C	-2.703	-3.604	0.756	H	2.836	0.964	0.865
C	-2.272	-3.989	2.027	H	5.104	1.93	0.581
C	-1.365	-3.185	2.723	H	6.785	0.767	-0.829
C	-0.877	-2.019	2.137	H.	6.198	-1.377	-1.939
H	-0.136	-1.43	2.657	H	3.884	-2.307	-1.677
H	-1.022	-3.479	3.708	O	1.648	-2.493	-0.63

References

[1] Weeks, M. E.; Leicester, H. *J. Chem. Educ* **1956**, 820–823.

[2] Shriver, D.; Atkins, P.; Langford, C. H. Inorganic Chemistry; W. H. 1990.

[3] Siekierski, S.; Burgess, J. *Concise Chemistry of the Elements*; Elsevier, 2002.

[4] Roewe, K. D.; Rheingold, A. L.; Weinert, C. S. *Chemical Communications* **2013**, *49*, 8380–8382.

[5] Teng, F.-Z.; Dauphas, N.; Watkins, J. M. *Reviews in Mineralogy and Geochemistry* **2017**, *82*, 1–26.

[6] Mason, J. *Multinuclear Nmr*; Springer Science & Business Media, 2012.

[7] Rochow, E. G.; Abel, E. W. *The Chemistry of Germanium, Tin and Lead*; Elsevier, 2014; Vol. 14.

[8] Morgan, G. T.; Drew, H. D. K. *Journal of the Chemical Society, Transactions* **1925**, *127*, 1760–1768.

[9] Roller, S.; Simon, D.; Dräger, M. *Journal of Organometallic Chemistry* **1986**, *301*, 27–40.

[10] Kraus, C. A.; Brown, C. L. *Journal of the American Chemical Society* **1930**, *52*, 4031–4035.

[11] Bulten, E.; Noltes, J. *Tetrahedron Letters* **1967**, *8*, 1443–1447.

[12] Castel, A.; Riviere, P.; Saintroch, B.; Satge, J.; Malrieu, J. *Journal of Organometallic Chemistry* **1983**, *247*, 149–160.

[13] Krygowski, T. M.; Stęń, B. T. *Chemical Reviews* **2005**, *105*, 3482–3512.

[14] Sita, L. R. *Accounts of Chemical Research* **1994**, *27*, 191–197.

[15] Diaz, A.; Miller, R. *Journal of the Electrochemical Society* **1985**, *132*, 834.

[16] Gilman, H.; Atwell, W. H.; Schwebke, G. L. *Journal of Organometallic Chemistry* **1964**, *2*, 369–371.

[17] Miller, R. D.; Michl, J. *Chemical Reviews* **1989**, *89*, 1359–1410.

[18] Lombos, B.; Sauvageau, P.; Sandorfy, C. *Chemical Physics Letters* **1967**, *1*, 42–43.

[19] Roewe, K. D.; Golen, J. A.; Rheingold, A. L.; Weinert, C. S. *Canadian Journal of Chemistry* **2014**, *92*, 533–541.

[20] Komanduri, S. P.; Shumaker, F. A.; Roewe, K. D.; Wolf, M.; Uhlig, F.; Moore, C. E.; Rheingold, A. L.; Weinert, C. S. *Organometallics* **2016**, *35*, 3240–3247.

[21] Amadoruge, M. L.; Golen, J. A.; Rheingold, A. L.; Weinert, C. S. *Organometallics* **2008**, *27*, 1979–1984.

[22] Zeigler, J. *Synthetic Metals* **1989**, *28*, 581–591.

[23] Balaji, V.; Michl, J. *Polyhedron* **1991**, *10*, 1265–1284.

[24] Amadoruge, M. L.; Gardinier, J. R.; Weinert, C. S. *Organometallics* **2008**, *27*, 3753–3760.

[25] Shumaker, F. A. Synthetic and Physical Properties of Long-Chain Linear and Branched Oligogermanes. Ph.D. thesis, Oklahoma State University, 2019.

[26] Tsuji, H.; Fukazawa, A.; Yamaguchi, S.; Toshimitsu, A.; Tamao, K. *Organometallics* **2004**, *23*, 3375–3377.

[27] Mallesha, H.; Tsuji, H.; Tamao, K. *Organometallics* **2004**, *23*, 1639–1642.

[28] Fukazawa, A.; Tsuji, H.; Tamao, K. *Journal of the American Chemical Society* **2006**, *128*, 6800–6801.

[29] Tsuji, H.; Terada, M.; Toshimitsu, A.; Tamao, K. *Journal of the American Chemical Society* **2003**, *125*, 7486–7487.

[30] Tamao, K.; Tsuji, H.; Terada, M.; Asahara, M.; Yamaguchi, S.; Toshimitsu, A. *Angewandte Chemie* **2000**, *112*, 3425–3428.

[31] Komanduri, S. P.; Shumaker, F. A.; Hallenbeck, S. A.; Knight, C. J.; Yoder, C. H.; Buckwalter, B. A.; Dufresne, C. P.; Fernandez, E. J.; Kaffel, C. A.; Nazareno, R. E.; Neu, M.; Reeves, G.; Rivard, J. T.; Shackelford, L. J.; Weinert, C. S. *Journal of Organometallic Chemistry* **2017**, *848*, 104–113.

[32] Samanamu, C. R.; Amadoruge, M. L.; Schrick, A. C.; Chen, C.; Golen, J. A.; Rheingold, A. L.; Materer, N. F.; Weinert, C. S. *Organometallics* **2012**, *31*, 4374–4385.

[33] Roller, S.; Simon, D.; Dräger, M. *Journal of Organometallic Chemistry* **1986**, *301*, 27–40.

[34] Hlina, J.; Zitz, R.; Wagner, H.; Stella, F.; Baumgartner, J.; Marschner, C. *Inorganica Chimica Acta* **2014**, *422*, 120–133.

[35] Hlina, J.; Baumgartner, J.; Marschner, C. *Organometallics* **2010**, *29*, 5289–5295.

[36] Amadoruge, M. L.; Yoder, C. H.; Conneywerdy, J. H.; Heroux, K.; Rheingold, A. L.; Weinert, C. S. *Organometallics* **2009**, *28*, 3067–3073.

[37] Glockling, F.; Hooton, K. A. *Journal of the Chemical Society (Resumed)* **1963**, 1849.

[38] Bulten, E. J.; Noltes, J. *Journal of Organometallic Chemistry* **1971**, *29*, 409–417.

[39] Wagner, H.; Baumgartner, J.; Muller, T.; Marschner, C. *Journal of the American Chemical Society* **2009**, *131*, 5022–5023.

[40] Fischer, R.; Frank, D.; Gaderbauer, W.; Kayser, C.; Mechtler, C.; Baumgartner, J.; Marschner, C. *Organometallics* **2003**, *22*, 3723–3731.

[41] Creemers, H.; Noltes, J. *Journal of Organometallic Chemistry* **1967**, *7*, 237–247.

[42] Creemers, H.; Verbeek, F.; Noltes, J. *Journal of Organometallic Chemistry* **1967**, *8*, 469–477.

[43] Creemers, H. M. J. C.; Noltes, J. G. *Recueil des Travaux Chimiques des Pays-Bas* **2010**, *84*, 590–593.

[44] Bochkarev, M.; Vyazankin, N.; Bochkarev, L.; Razuvaev, G. *Journal of Organometallic Chemistry* **1976**, *110*, 149–157.

[45] Subashi, E.; Rheingold, A. L.; Weinert, C. S. *Organometallics* **2006**, *25*, 3211–3219.

[46] Samanamu, C. R.; Amadoruge, M. L.; Weinert, C. S.; Golen, J. A.; Rheingold, A. L. *Phosphorus, Sulfur, and Silicon and the Related Elements* **2011**, *186*, 1389–1395.

[47] Sukegawa, J.; Schubert, C.; Zhu, X.; Tsuji, H.; Guldi, D. M.; Nakamura, E. *Nature Chemistry* **2014**, *6*, 899–905.

[48] Tsuji, H.; Nakamura, E. *Accounts of Chemical Research* **2019**, *52*, 2939–2949.

[49] Shirakawa, H. *Reviews of Modern Physics* **2001**, *73*, 713–718.

[50] Davidson, R.; Al-Owaedi, O. A.; Milan, D. C.; Zeng, Q.; Tory, J.; Hartl, F.; Higgins, S. J.; Nichols, R. J.; Lambert, C. J.; Low, P. J. *Inorganic Chemistry* **2016**, *55*, 2691–2700.

[51] Tanaka, Y.; Ohmura, K.; Fujii, S.; Tada, T.; Kiguchi, M.; Akita, M. *Inorganic Chemistry* **2020**,

[52] Samanamu, C. R.; Amadoruge, M. L.; Yoder, C. H.; Golen, J. A.; Moore, C. E.; Rheingold, A. L.; Materer, N. F.; Weinert, C. S. *Organometallics* **2011**, *30*, 1046–1058.

[53] Parkanyi, L.; Kalman, A.; Sharma, S.; Nolen, D. M.; Pannell, K. H. *Inorganic Chemistry* **1994**, *33*, 180–182.

[54] McGrady, G. S.; Odlyha, M.; Prince, P. D.; Steed, J. W. *CrystEngComm* **2002**, *4*, 271–276.

[55] Kaim, W.; Schwederski, B.; KLEIN, A. **1995**,

[56] Davies, C. J. E.; Page, M. J.; Ellul, C. E.; Mahon, M. F.; Whittlesey, M. K. *Chemical Communications* **2010**, *46*, 5151.

[57] Fang, H.; Jing, H.; Zhang, A.; Ge, H.; Yao, Z.; Brothers, P. J.; Fu, X. *Journal of the American Chemical Society* **2016**, *138*, 7705–7710.

[58] Prince, P. D.; McGrady, G. S.; Steed, J. W. *New Journal of Chemistry* **2002**, *26*, 457–461.

[59] Pitteloud, J.-P.; Zhang, Z.-T.; Liang, Y.; Cabrera, L.; Wnuk, S. F. *The Journal of Organic Chemistry* **2010**, *75*, 8199–8212.

[60] Wang, X.; Peng, Y.; Olmstead, M. M.; Hope, H.; Power, P. P. *Journal of the American Chemical Society* **2010**, *132*, 13150–13151.

[61] Tacke, R.; Heermann, J.; Pülm, M. *Zeitschrift für Naturforschung B* **1998**, *53*, 535–539.

[62] Samuel, P. P.; Singh, A. P.; Sarish, S. P.; Matussek, J.; Objartel, I.; Roesky, H. W.; Stalke, D. *Inorganic Chemistry* **2013**, *52*, 1544–1549.

[63] Pelzer, S.; Neumann, B.; Stammler, H.-G.; Ignat'ev, N.; Hoge, B. *Chemistry - A European Journal* **2016**, *22*, 16460–16466.

[64] Ovchinnkov, Y. E.; Struchkov, Y. T.; Baukov, Y. I.; Shipov, A. G.; Bylikin, S. Y. *Russian Chemical Bulletin* **1994**, *43*, 1351–1355.

[65] Ovchinnikov, Y. E.; Pogozhikh, S. A.; Khrustalev, V. N.; Bylikin, S. Y.; Negrebetsky, V. V.; Shipov, A. G.; Baukov, Y. I. *Russian Chemical Bulletin* **2000**, *49*, 1775–1781.

[66] Kameo, H.; Kawamoto, T.; Sakaki, S.; Bourissou, D.; Nakazawa, H. *Organometallics* **2014**, *33*, 6557–6567.

[67] Kameo, H.; Kawamoto, T.; Bourissou, D.; Sakaki, S.; Nakazawa, H. *Organometallics* **2015**, *34*, 1440–1448.

[68] Kameo, H.; Ikeda, K.; Bourissou, D.; Sakaki, S.; Takemoto, S.; Nakazawa, H.; Matsuzaka, H. *Organometallics* **2016**, *35*, 713–719.

[69] Brown, Z. D.; Erickson, J. D.; Fettinger, J. C.; Power, P. P. *Organometallics* **2013**, *32*, 617–622.

[70] Brauer, D.; Wilke, J.; Eujen, R. *Journal of Organometallic Chemistry* **1986**, *316*, 261–269.

[71] Allan, C. J.; Reinhold, C. R. W.; Pavelka, L. C.; Baines, K. M. *Organometallics* **2011**, *30*, 3010–3017.

[72] Sugiyama, Y.; Matsumoto, T.; Yamamoto, H.; Nishikawa, M.; Kinoshita, M.; Takei, T.; Mori, W.; Takeuchi, Y. *Tetrahedron* **2003**, *59*, 8689–8696.

[73] Rupar, P. A.; Jennings, M. C.; Baines, K. M. *Organometallics* **2008**, *27*, 5043–5051.

[74] Ouhsaine, F.; Andre, E.; Sotiropoulos, J. M.; Escudie, J.; Ranaivonjatovo, H.; Gornitzka, H.; Saffon, N.; Miqueu, K.; Lazraq, M. *Organometallics* **2010**, *29*, 2566–2578.

[75] Nemes, G.; Escudié, J.; Silaghi-Dumitrescu, I.; Ranaivonjatovo, H.; Silaghi-Dumitrescu, L.; Gornitzka, H. *Organometallics* **2007**, *26*, 5136–5139.

[76] Iwanaga, K.; Kobayashi, J.; Kawashima, T.; Takagi, N.; Nagase, S. *Organometallics* **2006**, *25*, 3388–3393.

[77] Cabeza, J. A.; García-Álvarez, P.; Pérez-Carreño, E.; Polo, D. *Inorganic Chemistry* **2014**, *53*, 8735–8741.

[78] Brauer, D. J.; Bürger, H.; Eujen, R. *Angewandte Chemie International Edition in English* **1980**, *19*, 836–837.

[79] Böttcher, T.; Bassil, B. S.; Röschenthaler, G.-V. *Inorganic Chemistry* **2012**, *51*, 763–765.

[80] Bonnefille, E.; Mazières, S.; Bibal, C.; Saffon, N.; Gornitzka, H.; Couret, C. *European Journal of Inorganic Chemistry* **2008**, *2008*, 4242–4247.

[81] Bartlett, P. D.; Condon, F. E.; Schneider, A. *Journal of the American Chemical Society* **1944**, *66*, 1531–1539.

[82] Krossing, I. *Chemistry–A European Journal* **2001**, *7*, 490–502.

[83] Krossing, I.; Brands, H.; Feuerhake, R.; Koenig, S. *Journal of Fluorine Chemistry* **2001**, *112*, 83–90.

[84] Schenk, C.; Drost, C.; Schnepf, A. *Dalton Transactions* **2009**, 773–776.

[85] Hayatifar, A.; Borrego, A.; Bosek, D.; Czarnecki, M.; Derocher, G.; Kuplicki, A.; Lytle, E.; Padilla, J.; Paroly, C.; Tubay, G.; Vyletel, J.; Weinert, C. S. *Chemical Communications* **2019**, *55*, 10852–10855.

[86] Talavera, M.; Meißner, G.; Rachor, S. G.; Braun, T. *Chemical Communications* **2020**, *56*, 4452–4455.

[87] Albers, L.; Meshgi, M. A.; Baumgartner, J.; Marschner, C.; Müller, T. *Organometallics* **2015**, *34*, 3756–3763.

[88] Parks, D. J.; Blackwell, J. M.; Piers, W. E. *The Journal of Organic Chemistry* **2000**, *65*, 3090–3098.

[89] Weinert, C. S. *ISRN Spectroscopy* **2012**, *2012*, 1–18.

[90] Riedmiller, F.; Wegner, G. L.; Jockisch, A.; Schmidbaur, H. *Organometallics* **1999**, *18*, 4317–4324.

[91] Wilkins, A. L.; Watkinson, P. J.; Mackay, K. M. *Journal of the Chemical Society, Dalton Transactions* **1987**, 2365.

[92] Meiboom, S.; Gill, D. *Review of Scientific Instruments* **1958**, *29*, 688–691.

[93] Carr, H. Y.; Purcell, E. M. *Physical Review* **1954**, *94*, 630.

[94] Hayatifar, A.; Shumaker, F. A.; Komanduri, S. P.; Hallenbeck, S. A.; Rheingold, A. L.; Weinert, C. S. *Organometallics* **2018**, *37*, 1852–1859.

[95] Frisch, M. J.; Nielsen, A. B. *Gaussian 03 Programmer's Reference*; Gaussian, 2003.

[96] Becke, A. D. *The Journal of Chemical Physics* **1993**, *98*, 5648–5652.

[97] Lee, C.; Yang, W.; Parr, R. G. *Physical Review B* **1988**, *37*, 785–789.

[98] Francl, M. M.; Pietro, W. J.; Hehre, W. J.; Binkley, J. S.; Gordon, M. S.; DeFrees, D. J.; Pople, J. A. *The Journal of Chemical Physics* **1982**, *77*, 3654–3665.

[99] Olah, G. A. *The Journal of organic chemistry* **2001**, *66*, 5943–5957.

[100] Harvey, D.; Horning, M.; Vouros, P. *Organic Mass Spectrometry* **1971**, *5*, 599–604.

[101] Muller, T. *Advances in Organometallic Chemistry* **2005**, *53*, 155.

[102] Engesser, T. A.; Lichtenthaler, M. R.; Schleep, M.; Krossing, I. *Chemical Society Reviews* **2016**, *45*, 789–899.

[103] Sekiguchi, A.; Tsukamoto, M.; Ichinohe, M. *Science* **1997**, *275*, 60–61.

[104] Sekiguchi, A.; Fukawa, T.; Lee, V. Y.; Nakamoto, M.; Ichinohe, M. *Angewandte Chemie* **2003**, *115*, 1175–1177.

[105] Schenk, C.; Drost, C.; Schnepf, A. *Dalton Trans.* **2009**, 773–776.

[106] Ishida, Y.; Sekiguchi, A.; Kabe, Y. *Journal of the American Chemical Society* **2003**, *125*, 11468–11469.

[107] Müller, T.; Bauch, C.; Ostermeier, M.; Bolte, M.; Auner, N. *Journal of the American Chemical Society* **2003**, *125*, 2158–2168.

[108] Wright, J. H.; Mueck, G. W.; Tham, F. S.; Reed, C. A. *Organometallics* **2010**, *29*, 4066–4070.

[109] Zharov, I.; Weng, T.-C.; Orendt, A. M.; Barich, D. H.; Penner-Hahn, J.; Grant, D. M.; Havlas, Z.; Michl, J. *Journal of the American Chemical Society* **2004**, *126*, 12033–12046.

[110] Kordts, N.; Borner, C.; Panisch, R.; Saak, W.; Müller, T. *Organometallics* **2014**, *33*, 1492–1498.

[111] Diab, F.; Aicher, F. S. W.; Sindlinger, C. P.; Eichele, K.; Schubert, H.; Wesemann, L. *Chemistry – A European Journal* **2019**, *25*, 4426–4434.

[112] Strauss, S. H. *Chemical reviews* **1993**, *93*, 927–942.

[113] Jenkins, H. D. B.; Roobottom, H. K.; Passmore, J.; Glasser, L. *Inorganic Chemistry* **1999**, *38*, 3609–3620.

[114] Rosenthal, M. R. *Journal of Chemical Education* **1973**, *50*, 331.

[115] Sekiguchi, A.; Fukawa, T.; Nakamoto, M.; Lee, V. Y.; Ichinohe, M. *Journal of the American Chemical Society* **2002**, *124*, 9865–9869.

[116] Sekiguchi, A.; Fukaya, N.; Ichinohe, M.; Ishida, Y. *European Journal of Inorganic Chemistry* **2000**, *2000*, 1155–1159.

[117] Fang, H.; Jing, H.; Zhang, A.; Ge, H.; Yao, Z.; Brothers, P. J.; Fu, X. *Journal of the American Chemical Society* **2016**, *138*, 7705–7710.

[118] Lambert, J. B.; Kuhlamann, B. *Journal of the Chemical Society, Chemical Communications* **1992**, 931.

[119] Schwier, T.; Gevorgyan, V. *Organic Letters* **2005**, *7*, 5191–5194.

[120] Jing, H.; Ge, H.; Li, C.; Jin, Y.; Wang, Z.; Du, C.; Fu, X.; Fang, H. *Organometallics* **2019**, *38*, 2412–2416.

[121] Kuehnel, M. F.; Lentz, D.; Braun, T. *Angewandte Chemie International Edition* **2013**, *52*, 3328–3348.

[122] Stahl, T.; Klare, H. F. T.; Oestreich, M. *ACS Catalysis* **2013**, *3*, 1578–1587.

[123] Douvris, C.; Nagaraja, C. M.; Chen, C.-H.; Foxman, B. M.; Ozerov, O. V. *Journal of the American Chemical Society* **2010**, *132*, 4946–4953.

[124] Caputo, C. B.; Stephan, D. W. *Organometallics* **2011**, *31*, 27–30.

[125] Ogiwara, Y.; Sakai, N. *Angewandte Chemie International Edition* **2020**, *59*, 574–594.

[126] Ogiwara, Y.; Sakurai, Y.; Hattori, H.; Sakai, N. *Organic Letters* **2018**, *20*, 4204–4208.

[127] Prechtl, M. H. G.; Hölscher, M.; Ben-David, Y.; Theyssen, N.; Milstein, D.; Leitner, W. *European Journal of Inorganic Chemistry* **2008**, *2008*, 3493–3500.

[128] Douvris, C.; Ozerov, O. V. *Science* **2008**, *321*, 1188–1190.

[129] Omann, L.; Pudasaini, B.; Irran, E.; Klare, H. F. T.; Baik, M.-H.; Oestreich, M. *Chemical Science* **2018**, *9*, 5600–5607.

[130] Frisch, M.; Clemente, F. *Scalmani, V. Barone, B. Mennucci, GA Petersson, H. Nakatsuji, M. Caricato, X. Li, HP Hratchian, AF Izmaylov, J. Bloino, G. Zhe*

[131] Grimme, S.; Antony, J.; Ehrlich, S.; Krieg, H. *The Journal of Chemical Physics* **2010**, *132*, 154104.

[132] Gilbert, A. IQmol Molecular Viewer. 2012.

[133] Goddard, T. D.; Huang, C. C.; Meng, E. C.; Pettersen, E. F.; Couch, G. S.; Morris, J. H.; Ferrin, T. E. *Protein Science* **2017**, *27*, 14–25.

[134] Reed, H.; Paul, T. R.; Chain, W. J. *The Journal of Organic Chemistry* **2018**, *83*, 11359–11368.

[135] Ghose, A. K.; Viswanadhan, V. N.; Wendoloski, J. J. *Journal of Combinatorial Chemistry* **1999**, *1*, 55–68.

[136] Constable, D. J.; Dunn, P. J.; Hayler, J. D.; Humphrey, G. R.; Leazer Jr, J. L.; Linderman, R. J.; Lorenz, K.; Manley, J.; Pearlman, B. A.; Wells, A., et al. *Green Chemistry* **2007**, *9*, 411–420.

[137] de Figueiredo, R. M.; Suppo, J.-S.; Campagne, J.-M. *Chemical Reviews* **2016**, *116*, 12029–12122.

[138] Marcelli, T. *Angewandte Chemie* **2010**, *122*, 6992–6995.

[139] Tam, E. K. W.; Liu, L. Y.; Chen, A., et al. *European Journal of Organic Chemistry* **2015**, *2015*, 1100–1107.

[140] Gernigon, N.; Zheng, H.; Hall, D. G. *Tetrahedron Letters* **2013**, *54*, 4475–4478.

[141] Al-Zoubi, R. M.; Marion, O.; Hall, D. G. *Angewandte Chemie International Edition* **2008**, *47*, 2876–2879.

[142] Arnold, K.; Batsanov, A. S.; Davies, B.; Whiting, A. *Green Chemistry* **2008**, *10*, 124–134.

[143] Ishihara, K.; Ohara, S.; Yamamoto, H. *The Journal of Organic Chemistry* **1996**, *61*, 4196–4197.

[144] Fairley, M.; Bole, L. J.; Mulks, F. F.; Main, L.; Kennedy, A. R.; O'Hara, C. T.; García-Alvarez, J.; Hevia, E. *Chemical Science* **2020**, *11*, 6500–6509.

[145] Farndon, J. J.; Young, T. A.; Bower, J. F. *Journal of the American Chemical Society* **2018**, *140*, 17846–17850.

[146] Nagata, W.; Hirai, S.; Kawata, K.; Aoki, T. *Journal of the American Chemical Society* **1967**, *89*, 5045–5046.

[147] Rajeswari, S.; Jones, R. J.; Cava, M. P. *Tetrahedron Letters* **1987**, *28*, 5099–5102.

[148] Mack, J.; Yoder, C. H. *Inorganic Chemistry* **1969**, *8*, 278–281.

[149] Guo, C.; Zhang, C.; Sun, Z.; Zhao, X.; Zhou, Q.; Hoffmann, M. R. *Chemical Engineering Journal* **2019**, *360*, 1101–1110.

[150] Helmer, J.; Hepp, A.; Lips, F. *Dalton Transactions* **2020**, *49*, 11843–11850.

[151] Erdmann, P.; Leitner, J.; Schwarz, J.; Greb, L. *ChemPhysChem* **2020**, *21*, 987–994.

[152] Suvorov, B. A. *Russian Journal of General Chemistry* **2006**, *76*, 1401–1406.

[153] Makosza, M.; Bujok, R. *Synlett* **2004**, 0371–0373.

[154] Mandal, D.; Gupta, R.; Jaiswal, A. K.; Young, R. D. *Journal of the American Chemical Society* **2020**, *142*, 2572–2578.

[155] Munoz, S. B.; Dang, H.; Ispizua-Rodriguez, X.; Mathew, T.; Prakash, G. K. S. *Organic Letters* **2019**, *21*, 1659–1663.

[156] Rivière, P.; Rivière-baudet, M.; Couret, C.; Satgé, J. *Synthesis and Reactivity in Inorganic and Metal-Organic Chemistry* **1974**, *4*, 295–307.

[157] Frisch, M. J., et al. Gaussian 09 Revision E.01. Gaussian Inc. Wallingford CT 2009.

[158] E. D. Glendening, J. E. C., A. E. Reed; Weinhold, F. *Theoretical Chemistry Institute and Department of Chemistry, University of Wisconsin, Madison, WI* **2018**,

[159] Weigend, F.; Ahlrichs, R. *Physical Chemistry Chemical Physics* **2005**, *7*, 3297.

[160] Zhao, Y.; Truhlar, D. G. *Theoretical Chemistry Accounts* **2007**, *120*, 215–241.

[161] Tordeux, M.; Wakselman, C. *Synthetic Communications* **1982**, *12*, 513–520.

[162] Kumagai, T.; Anki, T.; Ebi, T.; Konishi, A.; Matsumoto, K.; Kurata, H.; Kubo, T.; Katsumoto, K.; Kitamura, C.; Kawase, T. *Tetrahedron* **2010**, *66*, 8968–8973.

[163] Talukdar, R. *New Journal of Chemistry* **2020**, *44*, 5303–5308.

[164] Voronkov, M. G.; Tsyrendorzhieva, I. P.; Lis, A. V.; Grinberg, E. E.; Shatokhina, V. A.; Rakhlin, V. I. *Russian Journal of Organic Chemistry* **2013**, *49*, 147–150.

[165] Clayden, J.; Watson, D. W.; Chambers, M. *Tetrahedron* **2005**, *61*, 3195–3203.

[166] Wu, X.; Cruz, F. A.; Lu, A.; Dong, V. M. *Journal of the American Chemical Society* **2018**, *140*, 10126–10130.

[167] Molander, G. A.; Jean-Gérard, L. *The Journal of Organic Chemistry* **2009**, *74*, 5446–5450.

VITA

Ardalan Hayatifar

Candidate for the Degree of

Doctor of Philosophy

Dissertation: THE EXPLORATION OF LEWIS ACIDITY AND FLUOROPHILICITY OF GERMANIUM COMPOUNDS AND THEIR APPLICATIONS IN C-F BOND ACTIVATION

Major Field: Chemistry

Biographical:

Education:

Received a Doctor of Philosophy in Chemistry at Oklahoma State University, Stillwater, Oklahoma, USA in 2021.

Received a Masters of Science in Nano-Chemistry at Iran University of Science and Technology, Tehran, Iran in 2015.

Received a Bachelors of Science in Chemistry at Shahid Beheshti University, Tehran, Iran in 2013.

Publications:

• *Direct Amidation of Acid Fluorides Using Germanium Amides*
Hayatifar, A.; Elifritz, E.; Bloom M.; , Pixley, K.; Fennell. C.; Weinert, C.S.* *Dalton Transactions* **2021**, 50, 4490-4493.

• *Transition Metal-Free Hydrodefluorination of Acid Fluorides and Organofluorines by Ph_3GeH Promoted by Catalytic $[CPh_3][B(C_6F_5)_4]$*
Hayatifar, A.; Borrego, A.; Bosek, D.; Czarnecki, M.; Derocher, G.; Kuplicki, A.; Lytle, E.; Padilla, J.; Paroly, C.; Tubay, G.; Vyletel, J.; Weinert, C.S.* *Chemical Communications* **2019**, 55, 73, 10852-10855.

• *Synthesis of the Elusive Branched Fluoro-oligogermane $(Ph_3Ge)_3GeF$: A Structural, Spectroscopic, Electrochemical, and Computational Study*
Hayatifar, A.; Shumaker, F.A.; Komanduri, S.P.; Hallenbeck, S.A.; Rheingold, A.L.; Weinert, C.S.* *Organometallics* **2018**, 37, 12, 1852-1859, 917.